EXPERIMENTAL STUDIES ON PARTIAL SUBSTITUTION OF DIESEL WITH BIOETHANOL (DERIVED FROM MADHUCA INDICA FLOWERS) USING DIFFERENT TECHNIQUES

A THESIS

Submitted by

DULARI HANSDAH

(Roll No: 511ME105)

In Partial Fulfillment of the Requirement for the Degree of

DOCTOR OF PHILOSOPHY

DEPARTMENT OF MECHANICAL ENGINEERING

NATIONAL INSTITUTE OF TECHNOLOGY

ROURKELA-769008 (INDIA)

NOVEMBER 2015

EXPERIMENTAL STUDIES ON PARTIAL SUBSTITUTION OF DIESEL WITH BIOETHANOL (DERIVED FROM MADHUCA INDICA FLOWERS) USING DIFFERENT TECHNIQUES

A THESIS

Submitted by

DULARI HANSDAH

(Roll No: 511ME105)

In Partial Fulfillment of the Requirement for the Degree of

DOCTOR OF PHILOSOPHY

UNDER THE SUPERVISION OF

PROF. S. MURUGAN

DEPARTMENT OF MECHANICAL ENGINEERING

NATIONAL INSTITUTE OF TECHNOLOGY

ROURKELA-769008 (INDIA)

NOVEMBER 2015

Department of Mechanical Engineering
National Institute of Technology Rourkela
Rourkela-769008

CERTIFICATE

This is to certify that the thesis entitled "**Experimental studies on partial substitution of diesel with bioethanol (derived from Madhuca Indica flowers) using different techniques**" being submitted by **Mrs. Dulari Hansdah** for the award of Ph.D. degree is a record of bona fide research and was carried out by her in the Department of Mechanical Engineering, National Institute of Technology, Rourkela, under my supervision. It is also certified that to the best of my knowledge the work reported here in, does not form a part of any other thesis or dissertation on the basis of which a degree or award was conferred on an earlier occasion for this or any other candidate.

NIT Rourkela
Date:

(Prof. S. Murugan)
Supervisor
Associate Professor
Department of Mechanical Engineering
National Institute of Technology
Rourkela- 769008

ACKNOWLEDGEMENT

Completion of work with a lot of hurdles put off all joys of life, because it brings the real ecstasy in the life. This may not happen without a continuous support of my supervisor. I would like to take the opportunity to express my humble gratitude and deep regards to my supervisor, Prof. S. Murugan, Associate Professor, Department of Mechanical Engineering, for his flawless guidance, monitoring and continuous motivation for the completion of the thesis. The regular counselling, and lessons for life given by him shall help me to proceed properly in a long journey of my life.

I would like to express my heartfelt respect to Prof. S.K. Sarangi, Director, NIT Rourkela for his indirect support by providing a good ambience and necessary facilities for carrying out the research.

I express my sincere thanks to Prof. S.S. Mohapatra, HOD, Department of Mechanical Engineering, NIT Rourkela for providing me the necessary facilities in the department. I take this opportunity to express my deep sense of gratitude to the members of my Doctoral Scrutiny Committee members, Prof. K.P. Maity (Chairman), Prof. R.K. Sahoo and Prof. A.K. Satapathy, Department of Mechanical Engineering, and Prof. R.K. Singh, Department of Chemical Engineering, for their constant encouragement and valuable suggestions while carrying out my research.

My grateful thanks are also extended to Prof. R. Jayabalan, Department of Life Science, for his suggestions and helping hand to carry out my research work in their Lab, to Ms. Indira Dash, who supported me during experimentation.

My completion of research work could not have been accomplished without the support of my research colleagues, Mr. R. Prakash, Mrs. Pritinika Behera, Mr. Debabrata Barik, Mr. Arun Kumar Wamankar, Mr. Harishankar Bendu, Mrs. Kapura Tudu and Mr. Abhishek Sharma. I express my appreciation for their in debt help and useful ideas related to the improvement and completion of the research work.

I am also thankful to Mr. N.P. Barik, Mr. Ramakrishna Mandal, Mr. N.K. Bisoi and Mr. L.K. Mahanta for their timely help and cooperation in completing the experimental work.

Finally, I wish to give my profound love and care to my beloved daughter Ms. Manvika Shrikirti for her indirect involvement in completion of my work. I am deeply regretted, not to give her childhood happiness which was the precious period of her life. I also thank my almighty, husband, parents, uncle, aunty, father in law and mother in law for their constant encouragement and devotion of their countless times for keeping my child during my hectic schedule of work.

Last but not the least, there may be many who remain unacknowledged in this humble note of gratitude and there are none who remain unappreciated.

(Dulari Hansdah)

ABSTRACT

Use of renewable energy from biomass sources for CI engines can greatly reduce the air pollution, and dependency on the import of crude oil in a country. In the recent days, the use of ethanol for automotive power applications has gained more importance, as it can be used in both SI and CI engines and reduce the greenhouse gas (GHG) emissions. Different feedstocks have been explored for production of ethanol in a large quantity. In this research study, bioethanol from the Madhuca Indica flowers as an alternative fuel for compression ignition (CI) engines has been proposed. As a first step of the research study, bioethanol obtained from the Madhuca Indica flowers was characterized for its suitability as an alternative fuel for CI engines. For this purpose, the presence of group compounds in bioethanol were identified by using the Fourier transform infrared spectroscopy (FTIR) and Gas chromatograph-mass spectrometer (GC-MS), and analysed. Also, the physico-chemical properties of bioethanol were determined and compared with those of the diesel properties. Seven modules of work have been carried out in this research work to establish the results of using bioethanol as an alternative fuel in a CI engine. For this purpose, a single cylinder, four stroke, air cooled, DI diesel engine was used for this investigation. Bioethanol has a low cetane number and thus it cannot be directly used in CI engines. Therefore, initially in the first four modules, bioethanol was used with diesel in the engine by adopting four techniques viz. i) in the form of emulsion, ii) addition of an ignition improver to an optimum bioethanol-diesel emulsion, iii) bioethanol-DEE dual fuel mode, and iv) diesel-bioethanol dual fuel mode (fumigation). The experimental results of the combustion, performance and emissions of the engine run on bioethanol in these techniques were evaluated, and compared with those of diesel operation in the same engine.

In the first module of work, bioethanol was emulsified with diesel in a step of 5% to 15% by volume with the help of a surfactant Span 80. The stability of the emulsion was checked for 15 days under normal atmospheric conditions. The bioethanol-diesel emulsion was designated as BMDE5, BMDE10 and BMDE15, where the numeric values were the volume percentages of bioethanol. Up to 15% bioethanol in the emulsion was used for the experimental investigation by considering the miscibility, minimum calorific value and cetane number of fuel which would not affect the performance and combustion parameters of the engine. The experiments were carried out with the three different bioethanol-diesel emulsions in the diesel engine and results were compared with the diesel data. The results

indicated that the ignition delay of engine run on the bioethanol-diesel emulsions was found to be longer by about 1 to 2 °CA than that of the diesel operation at full load. The maximum cylinder pressure of the engine run on the bioethanol-diesel emulsions was higher by about 2% to 3% than that of diesel at full load. The BMDE15 emulsion gave a better performance and emission than that of BMDE5, BMDE10 and diesel. The useful work and brake specific energy consumption (BSEC) for BMDE15 was observed to be higher by about 6% and 27% respectively, at full load. The nitric oxide (NO), smoke and carbon monoxide (CO) emissions were observed to be lower with a maximum reduction of 24%, 21% and 6% respectively, compared to those of diesel at full load. But, a marginal increase of hydrocarbon (HC) emission was observed, with the BMDE15 operation than that of diesel operation.

In order to reduce the ignition delay of the engine run on the optimum bioethanol-diesel emulsion (BMDE15), an ignition improver diethyl ether (DEE) was added to it in a step of 0.5% by volume and designated as DED1%, DED1.5%, DED2% and DED2.5%. The higher percentage of DEE was considered up to 2.5% for its vapour lock problem. The DED1.5% was considered to be an optimum blend which lowered the noisy operation and ignition delay of the diesel engine. At full load, the ignition delay of engine operated with DED1.5% was reduced by about 1°CA. The maximum cylinder pressure and BSEC were observed to increase by about 1.2% and 4% respectively, compared to that of diesel, at full load. The NO and smoke emissions were lower by about 11.3% and 13.7% respectively, compared to that of diesel at full load.

Further, as a third technique, bioethanol was directly used in the diesel engine with the help of an ignition improver. DEE with a flow rate of 60 g/h, 120 g/h, 180 g/h and 240 g/h was injected at 10cm distance of the intake manifold of the engine. The necessary arrangement was made for DEE injection. The upper and lower limits of the DEE flow rate were considered by the audible knocking and misfire of the engine. The bioethanol operation with the 180 g/h flow rate of DEE exhibited a shorter ignition delay, and higher cylinder pressure compared to those of 60 g/h, 120 g/h, 240 g/h flow rate of DEE and diesel at full load. The NO and smoke emissions were found to be lower by about 22.2% and 16.6% respectively, compared to those of diesel at full load.

In the fourth technique, bioethanol was fumigated at different flow rates viz., 0.24 kg/h, 0.48 kg/h, 0.96 kg/h and 1.22 kg/h with the help of electronically controlled injector at the intake

manifold of the engine, whereas diesel was injected into the cylinder as a pilot fuel. The results revealed that, bioethanol fumigation at the flow rate of 0.48 kg/h and the equivalence ratio of 0.88 gave an increase in thermal efficiency of about 3% than that of diesel. At full load, the ignition delay was found to be longer by about 3 °CA and the maximum cylinder pressure was increased by about 2.1% compared to that diesel. The volumetric efficiency and brake specific fuel consumption (BSFC) was found to be lower by about 6% and 5.2% respectively, than those of diesel at full load. The NO and smoke emissions were observed to be lower by about 24.2% and 5.5% respectively, than those of diesel operation at full load.

The BMDE15 emulsion was chosen as the best among all the above mentioned techniques in terms of performance and emission point of view, when bioethanol was used with diesel. The spray pattern of the BMDE15 emulsion was studied with the help of a MATLAB programme in the fifth module of the work. Also the experimental results were validated with the help of the MATLAB programme and compared with those of diesel. From the analysis, it was proved that the spray profile of BMDE15 was found to be better compared to that of diesel at full load. The deviation between the simulated and experimental results of cylinder peak pressure, NO and smoke emissions for BMDE15 was found to be 3%, 5% and 4% respectively at full load.

Bioethanol has a poor lubricity in comparison with diesel that resulted in a power drop. In the sixth module, to improve the lubricity property of BMDE15, bioethanol was added with the volume percentage of 5% in each step up to 15%. The BEBDD10 blend improved the lubricity of the fuel without much affecting the performance and emissions of the engine. The power output of the engine run on BEBDD10 was found to be increased by about 2% compared to that of the BMDE15 operation at full load. The NO and smoke emissions were observed to be lower by about 4% and 21% compared to that of diesel at full load.

In the last module of the work, a short term endurance test was carried out; when the engine was run on both the BMDE15 and BEBDD10 fuel for 100 h. The carbon deposits, engine wear and change in the lubricating oil properties were analysed in both the cases. The decrease in the carbon deposit on the cylinder head, piston crown and nozzle tip were measured by about 40%, 38% and 25% respectively, with the BEBDD10 operation in comparison with the diesel operation. The wear in the fuel injection pump components such as plunger, pump barrel, pinion, and spring were found to be lower by about 0.4%, 0.32%,

1.7% and 1.5% respectively, with the BEBDD10 blend in comparison with BMDE15. With the BEBDD10 operation, the amount of metal debris such as Zn, Fe, Cu, Mn, Al, Pb, Ni and Cr were observed to be lower by about 13.6%, 24.5%, 25.7%, 14.6%, 11.7%, 17.3%, 15.1% and 36% respectively, compared to those of BMDE15. By overall comparison, it is concluded that the BEBDD10 operation seems to give better lubricating properties and lower material wear than those of diesel operation.

Key words: Bioethanol, Madhuca Indica flowers, Emulsion, DEE blending, DEE fumigation, bioethanol fumigation, MATLAB program, durability test

CONTENTS

Chapter No.	Title	Page No.
	Abstract	i
	List of Figures	xiii
	List of Tables	xviii
	Nomenclature	xix
Chapter 1	INTRODUCTION	1
1.1	General	1
	1.1.1 Power sector	2
	1.1.2 Transportation	3
	1.1.2.1 Land transportation	3
	1.1.2.2 Sea transportation	4
	1.1.2.3 Air transportation	4
	1.1.3 Agricultural Sector	6
	1.1.4 Industrial sector	6
	1.1.5 Commerce	6
1.2	Consequences of air pollution	7
	1.2.1 Greenhouse effect	7
	1.2.2 Loss of flora and fauna	7
	1.2.3 Desertification	8
	1.2.4 Melting of glaciers and Sea level rise	8
	1.2.5 Acid rain	8
	1.2.6 Human health	9
1.3	Alternative fuels	9
	1.3.1 Liquid biofuels for transportation	10
	1.3.1.1 Biodiesel	10
	1.3.1.2 Alcohols	10
	1.3.1.2.1 Methanol	11
	1.3.1.2.2 Ethanol/bioethanol	11
1.4	Benefits of liquid biofuels over petroleum fuels	12

1.5	Organisation of thesis	12
Chapter 2	LITERATURE REVIEW	14
2.1	General	14
2.2	Over view of ethanol/bioethanol production	14
	2.2.1 Sugar feedstock	15
	2.2.2 Starchy feedstocks	16
	2.2.3 Ethanol production from cellulosic materials	17
	2.2.3.1 Acid hydrolysis	18
	2.2.3.2 Enzymatic Hydrolysis	20
	2.2.3.3 Thermochemical conversion	21
	2.2.4 Ethanol production from lignocellulosic materials	21
2.3	Bioethanol from the Madhuca Indica flowers	25
2.4	Use of ethanol/bioethanol in CI engines	27
	2.4.1 Diesel-ethanol/bioethanol solutions and emulsions	28
	2.4.2 Use of cetane improvers	36
	2.4.3 Dual injection	39
	2.4.4 Fumigation	40
	2.4.5 Surface ignition	43
	2.4.6 Spark ignition	44
2.5	Bioethanol-biodiesel-diesel blends	44
2.6	Conclusion	47
2.7	Objectives of the study	47
Chapter 3	FUEL CHARACTERISATION	49
3.1	General	49
3.2	Bioethanol from the Madhuca Indica flowers	49
	3.2.1 Availability of feedstock	49
	3.2.2 Fermentation using *Saccharomyces cerevisiae*	50
3.3	Characterisation of bioethanol	52
	3.3.1 Identification of group compounds	

by FTIR 52
3.3.2 GC-MS Analysis 54
3.3.3 Ultimate analysis and fuel properties 55
3.4 Discussion of fuel properties 57
3.5 Production cost of one litre of bioethanol 58

Chapter 4 EXPERIMENTATION AND METHODOLOGY OF PRESENT WORK 59
4.1 General 59
4.2 Elementary work for investigation 59
4.3 Experimental setup 60
4.3.1 Test engine 61
4.3.2 Exhaust gas measurements 62
4.3.2.1 CO and CO_2 measurements 62
4.3.2.2 FID for HC measurement 63
4.3.2.3 Electrochemical principle for NO measurement 64
4.3.2.4 Diesel smoke measurement 66
4.3.3 Combustion parameters 68
4.4 Different methods of using bioethanol in diesel engine 72
4.4.1 Investigation on the bioethanol-diesel emulsions 72
4.4.2 Experimental test procedure 74
4.4.3 Investigations with the bioethanol diethyl-ether blends 74
4.4.4 Investigations with the bioethanol-DEE on dual fuel mode 75
4.4.5 Investigations with the use of bioethanol on fumigation 77
4.4.6 Mathematical modeling for validation 80
4.4.7 Investigation with the bioethanol-diesel-biodiesel blends 80
4.4.8 Comparative study of endurance test 81
4.5 Analysis and procedure 82
4.5.1 Performance parameters 82
4.5.1.1 Fuel consumption measurement 82
4.5.1.2 Air consumption measurement 82

4.5.1.3 Speed and EGT measurement 82
4.5.1.4 Brake specific energy consumption (BSEC) calculation 82
4.5.1.5 Thermal energy balance calculation 82
4.5.1.6 Global equivalence ratio 83
4.5.1.7 Bioethanol energy share 83
4.5.2 Emission measurements 84
4.5.3 Combustion parameter measurements 84
4.5.3.1 Ignition delay 84
4.5.3.2 Heat release rate analysis 84
4.5.3.3 Smoothing of P-θ curve 85
4.5.3.4 Rate of pressure rise 85
4.5.3.5 Combustion duration 85
4.5.3.6 Mass fraction burned 86
4.6 Uncertainty analysis 86

Chapter 5 MATHEMATICAL MODELLING 87
5.1 General 87
5.2 Spray formation model 87
5.2.1 Fuel injection process 88
5.2.2 Fuel jet break up point and initial angle 88
5.2.3 Fuel spray development 90
5.2.4 Fuel droplet evaporation 93
5.2.5 Calculation of Whitehouse-Way fuel preparation rate constant 93
5.3 General description of the model for combustion 93
5.3.1 Energy equations 94
5.3.2 Heat transfer model 95
5.3.3 Ignition delay 96
5.3.4 Wiebe's combustion model 96
5.3.5 Chemistry of combustion 97
5.3.6 Nitric oxide (NO) formation model 98

5.3.7 The net soot formation model 99

Chapter 6 RESULTS AND DISCUSSION 100

6.1 General 100

6.2 Results obtained from the engine fueled with the bioethanol-diesel emulsions 100

6.2.1 Combustion parameters 100

6.2.1.1 Pressure (P)-crank angle (θ) diagram 101

6.2.1.2 Ignition delay 102

6.2.1.3 Heat release rate (HRR) 102

6.2.1.4 Maximum cylinder pressure 103

6.2.1.5 Maximum rate of pressure rise 104

6.2.1.6 Combustion duration 105

6.2.2 Engine performance analysis 106

6.2.2.1 Brake specific energy consumption (BSEC) 106

6.2.2.2 Exhaust gas temperature (EGT) 107

6.2.2.3 Thermal energy balance 108

6.2.3 Emission analysis 109

6.2.3.1 Brake specific hydrocarbon emission (BSHC) 109

6.2.3.2 Brake specific carbon monoxide emission (BSCO) 110

6.2.3.3 Brake specific nitric oxide emission (BSNO) 111

6.2.3.4 Smoke emission 111

6.2.4 Summary 112

6.3 Investigation of bioethanol-diesel-DEE blends 114

6.3.1 Combustion parameters 114

6.3.1.1 P-θ diagram 114

6.3.1.2 Ignition delay 115

6.3.1.3 Heat release rate 116

6.3.1.4 Maximum cylinder pressure 117

6.3.1.5 Maximum rate of pressure rise 118

6.3.1.6 Combustion duration 119

6.3.2 Engine performance analysis 120

6.3.2.1 BSEC 120
6.3.2.2 EGT 120
6.3.2.3 Thermal energy balance 121
6.3.3 Emission analysis 122
6.3.3.1 BSHC emission 122
6.3.3.2 BSCO emission 123
6.3.3.3 BSNO emission 124
6.3.3.4 Smoke emission 125
6.3.4 Summary 126
6.4 Bioethanol operation with DEE fumigation 127
6.4.1 Combustion parameters 127
6.4.1.1 P-θ diagram 127
6.4.1.2 Ignition delay 128
6.4.1.3 Heat release rate 129
6.4.1.4 Maximum cylinder pressure 130
6.4.1.5 Maximum rate of pressure rise 131
6.4.1.6 Combustion duration 131
6.4.2 Engine performance analysis 132
6.4.2.1 Energy share 133
6.4.2.2 Brake specific fuel consumption (BSFC) 133
6.4.2.3 EGT 134
6.4.2.4 Volumetric efficiency 134
6.4.2.5 Thermal energy balance 135
6.4.3 Emission analysis 136
6.4.3.1 BSHC emission 136
6.4.3.2 BSCO emission 137
6.4.3.3 BSNO emission 138
6.4.3.4 Smoke emission 139
6.4.4 Summary 140
6.5 Diesel-bioethanol dual fuel mode 141
6.5.1 Combustion parameters 142
6.5.1.1 P-θ diagram 141

6.5.1.2 Ignition delay 142
6.5.1.3 Heat release rate 143
6.5.1.4 Maximum rate of pressure rise 144
6.5.1.5 Combustion duration 145
6.5.2 Engine performance analysis 145
6.5.2.1 BSFC 146
6.5.2.2 EGT 146
6.5.2.3 Volumetric efficiency 147
6.5.2.4 Thermal energy balance 148
6.5.3 Emission analysis 149
6.5.3.1 BSHC emission 149
6.5.3.2 BSCO emission 150
6.5.3.3 BSNO emission 151
6.5.3.4 Smoke emission 151
6.5.4 Summary 153
6.5.5 Comparison of the results obtained from four different techniques 153
6.6 Validation of experimental results of BMDE15 through mathematical modelling 155
6.6.1 Spray profile of diesel and BMDE15 155
6.6.2 Comparative study 155
6.6.2.1 Cylinder pressure 155
6.6.2.2 Ignition delay 157
6.6.2.3 NO emission 157
6.6.2.4 Smoke 158
6.6.3 Summary 159
6.7 Running the engine with bioethanol-biodiesel-diesel blends 161
6.7.1 Combustion parameters 161
6.7.1.1 P-θ diagram 161
6.7.1.2 Ignition delay 162
6.7.1.3 Heat release rate 163
6.7.1.4 Maximum cylinder pressure 164

	6.7.1.5 Combustion duration	164
	6.7.1.6 Maximum rate of pressure rise	165
	6.7.2 Performance analysis	166
	6.7.2.1 BSEC	166
	6.7.2.2 EGT	167
	6.7.2.3 Thermal energy balance	167
	6.7.3 Emission analysis	168
	6.7.3.1 BSHC emission	168
	6.7.3.2 BSCO emission	169
	6.7.3.3 BSNO emission	170
	6.7.3.4 Smoke emission	171
	6.7.4 Summary	172
6.8	Durability issues of a diesel engine run on BMDE15 and BEBDD10	173
	6.8.1 General	173
	6.8.2 Analysis of carbon deposits on different engine components	173
	6.8.2.1 Cylinder head and piston crown	173
	6.8.2.2 Fuel injector and its parts	175
	6.8.2.3 Components of the fuel injection pump	175
	6.8.2.4 Wear measurements	176
	6.8.2.5 Lubrication oil analysis	177
	6.8.3 Summary	180
Chapter 7	CONCLUSIONS AND SCOPE FOR FURTHER RESEARCH	181
	APPENDICES	184
	ANNEXURES	189
	REFERENCES	205
	BIODATA	217

LIST OF FIGURES

Figure No.	Caption	Page No.
1.1	Sector wise energy consumption	1
1.2	Use of fuels and energy in the transportation applications	5
1.3	Alternative fuels from different sources	9
2.1	Block diagram of fuel ethanol production from starchy materials	17
2.2	Ethanol production process from biomass	21
2.3	Block diagram of fuel ethanol production from lignocellulosic biomass	22
2.4	Percentage variations of performance parameters	31
2.5	Percentage variations of emission parameters	32
2.6	Percentage variations of performance parameters	33
2.7	Percentage variations of emissions parameters	33
3.1	Madhuca Indica tree	50
3.2	Madhuca Indica raw and dry flowers	50
3.3	Production process of bioethanol from the Madhuca Indica flowers	51
3.4	Steps involved in checking the purity of bioethanol	51
3.5	Photograph of Perkin Elmer RX 1	52
3.6	FTIR spectra of bioethanol and diesel	53
3.7	Perkin Elmer GC-MS instrument	54
4.1	Schematic diagram of the experimental setup	60
4.2	Photographic view of the experimental setup	61
4.3	NDIR principle for measuring the CO/CO_2 species in the exhaust	63
4.4	FID principles for HC measurement	63
4.5	Electrochemical principle for NO measurement	64
4.6	Photographic view of the exhaust gas analyzer	66
4.7	Principle of diesel smoke measurement	67
4.8	Photograph of the diesel smoke meter	67
4.9	Photographic view of Kistler pressure transducer	68
4.10	Pressure transducer mounted on the engine head	69

4.11	TDC position sensor	70
4.12	Photographic view of the mechanical agitator	72
4.13	Photographic view of the bioethanol-diesel emulsion samples	73
4.14	Experimental setup for bioethanol dual fuel mode	76
4.15	Arrangement used in this study for the fumigation of bioethanol	77
4.16	Block diagram representing the arrangement of fumigation technique	78
4.17	Flow chart of the fuel injection system	78
4.18	Experimental techniques used for bioethanol application in the diesel engine	80
4.19	Ternary diagram for the checking of stability	81
6.1	Variation of cylinder pressure with crank angle	101
6.2	Ignition delay for diesel and the bioethanol-diesel emulsions at different BMEP	102
6.3	Variation of the heat release rate for diesel and bioethanol-diesel emulsions at full load	103
6.4	Variation of the maximum pressure for diesel and the bioethanol-diesel emulsions at different BMEP	104
6.5	Variation of the maximum rate of pressure rise of bioethanol diesel emulsions and diesel with BMEP	105
6.6	Variation of combustion duration for diesel and the bioethanol-diesel emulsions at different BMEP	106
6.7	Variation of BSEC for diesel and the bioethanol-diesel emulsions at different BMEP	107
6.8	Variation of EGT for diesel and the bioethanol-diesel emulsions at different BMEP	107
6.9	Variation of thermal energy balance for diesel and the bioethanol-diesel emulsions at full load	108
6.10	Variation of BSHC for diesel and the bioethanol-diesel emulsions at different BMEP	109
6.11	Variation of BSCO for diesel and the bioethanol-diesel emulsions at different BMEP	110

6.12	Variation of BSNO for the diesel and the bioethanol-diesel emulsions at different BMEP	111
6.13	Variation of smoke density for the diesel and the bioethanol-diesel emulsions at different BMEP	112
6.14	Variation of cylinder pressure with crank angle	115
6.15	Variation of ignition delay with BMEP	116
6.16	Variation of heat release rate with crank angle	117
6.17	Variation of maximum cylinder pressure with BMEP	117
6.18	Variation of maximum rate of pressure rise with BMEP	118
6.19	Variation of combustion duration with BMEP	119
6.20	Variation of BSEC with BMEP	120
6.21	Variation of EGT with BMEP	121
6.22	Variation of thermal energy balance for diesel, BMDE15 and BMDE15-DEE blends at full load	122
6.23	Variation of BSHC emission with BMEP	123
6.24	Variation of BSCO emission with BMEP	124
6.25	Variation of BSNO emission with BMEP	125
6.26	Variation of smoke emission with BMEP	126
6.27	Variation of cylinder pressure with crank angle	127
6.28	Variation of ignition delay with BMEP for diesel and bioethanol operation with DEE fumigation	128
6.29	Variation of heat release rate with crank angle for diesel and bioethanol operation with DEE fumigation	129
6.30	Variation of maximum cylinder pressure with load for diesel and bioethanol operation with DEE fumigation	130
6.31	Variation of the maximum rate of pressure rise with BMEP for diesel and bioethanol operation with DEE fumigation	131
6.32	Variation of combustion duration with BMEP for diesel and bioethanol operation with DEE fumigation	132
6.33	Variation of BSFC with BMEP for diesel and bioethanol operation with DEE fumigation	133
6.34	Variation of EGT with BMEP for diesel and bioethanol operation	

	with DEE fumigation	134
6.35	Variation of volumetric efficiency with BMEP for diesel and bioethanol operation with DEE fumigation	135
6.36	Variation of thermal energy balance for diesel and bioethanol operation with DEE fumigation at full load	136
6.37	Variation of BSHC emission for sole bioethanol operation with DEE and diesel at different BMEP	137
6.38	Variation of BSCO emission for sole bioethanol operation with DEE and diesel at different BMEP	137
6.39	Variation of BSNO emission for sole bioethanol operation with DEE and diesel at different BMEP	138
6.40	Variation of smoke emission for sole bioethanol operation with DEE and diesel at different BMEP	139
6.41	Pressure crank angle diagram at full load	142
6.42	Variation in the ignition delay with the global equivalence ratio	143
6.43	Variation in the heat release rate with crank angle at BMEP	143
6.44	Variation in the maximum rate of pressure rise with the global equivalence ratio	144
6.45	Variation in the combustion duration with the global equivalence ratio	145
6.46	Variation in the BSFC with the global equivalence ratio	146
6.47	Variation in the EGT with the global equivalence ratio	147
6.48	Variation in the volumetric efficiency with the global equivalence ratio	147
6.49	Variation of thermal energy balance for diesel and bioethanol fumigation at full load	148
6.50	Variation in the BSHC emission with the global equivalence ratio	149
6.51	Variation in the BSCO emission with the global equivalence ratio	150
6.52	Variation in the BSNO emission with the global equivalence ratio	151
6.53	Variation in the smoke emission with the global equivalence ratio	152
6.54	Diesel spray	155
6.55	BMDE15 emulsion spray	155

6.56	Cylinder pressure with crank angle for diesel and BMDE15	156
6.57	Variation of ignition delay with load	157
6.58	Variation of BSNO emission with load	158
6.59	Variation of smoke with load	159
6.60	Variation of cylinder pressure with crank angle	161
6.61	Variation of ignition delay with BMEP	162
6.62	Variation of heat release rate with crank angle	163
6.63	Variation of maximum cylinder pressure with BMEP	164
6.64	Variation of combustion duration with BMEP	165
6.65	Variation of maximum rate of pressure rise with BMEP	165
6.66	Variation of BSEC with BMEP	166
6.67	Variation of EGT with BMEP	167
6.68	Variation of thermal energy balance for diesel, BMDE15 and bioethanol-biodiesel-diesel operation at full load	168
6.69	Variation of BSHC emission with BMEP	169
6.70	Variation of BSCO emission with BMEP	169
6.71	Variation of BSNO emission with BMEP	170
6.72	Variation of smoke emission with BMEP	171
6.73 a, b, and c	Photographic view of the cylinder head, piston crown, and injector tip	174
6.74 a, b, c, d	Photographic view of dismantled fuel injection pump components	176
6.75	Percent change in carbon content as function of lubricating oil usage	177
6.76a	Presence of Zn, Fe and Cu in the lubricating oil with time	178
6.76b	Presence of Mn, Al and Pb in the lubricating oil with time	179
6.76c	Presence of Ni and Cr in the lubricating oil with time	179

LIST OF TABLES

Table No.	Caption	Page No.
1.1	List of important diesel power plants in the world in 2014	2
1.2	List of diesel plants in India	3
1.3	Annual motor vehicles production by top 10 countries	5
2.1	World ethanol production in the year 2013	14
2.2	Different lignocellulosic materials and their composition	23
2.3	Ethanol yield from different sources	24
2.4	Various pretreatment methods for lignocellulosic biomass for ethanol/bioethanol production	25
2.5	Percentage variation in parameters	37
2.6	Percentage variation in parameters	38
3.1	Various bonds present in bioethanol	53
3.2	Various functional bonds, peak and wavelength of diesel	54
3.3	GC-MS results of bioethanol	55
3.4	Elemental analysis of bioethanol and diesel	55
3.5	Fuel properties of bioethanol obtained from the Madhuca Indica flowers and other feedstocks	56
3.6	Comparison of production cost of bioethanol	58
4.1	Properties of Surfactant Span-80	72
4.2	Properties of test fuels	73
4.3	Properties of DEE	75
4.4	Properties of test fuels	75
4.5	Properties of test fuels	81
5.1	Properties of diesel and BMDE15	94
6.1	Energy share of DEE in bioethanol operation	133
6.2	Comparison of all the results of four different techniques	154
6.3	Carbon deposits (wt%) on different parts of the engine with both the fuel	175
6.4	Wear (wt%) amount on different components of the fuel injection pump	176

NOMENCLATURE

English symbols

a_s	Speed of sound (m/s)
AF	mass ratio of air to liquid and evaporated fuel
C_p	specific heat capacity under constant pressure (J/kg K)
D	cylinder bore (m)
D_n	injector nozzle hole (each) diameter (m)
D_{SM}	Sauter mean diameter (m)
$\frac{d(mu)}{d\theta}$	rate of change of internal energy of the system of mass
$\frac{dQ_r}{d\theta}$	rate of heat release during combustion period, kJ/degree crank angle
$\frac{dQ_h}{d\theta}$	rate of heat transfer from gases to walls, kJ/degree crank angle
$\frac{dW}{d\theta}$	rate of mechanical work done by the system on the boundary
h	convective heat transfer coefficient (W/m^2K)
i	axial zone number
j	radial zone number
K_{bm}	bulk modulus of elasticity (Pa)
K_{ac}	Optical absorption co-efficient of the obscuring matter per unit length
$K_{pr(vap)}$	preparation (evaporation) constant
L_p	connecting pipe length (m)
m	mass (kg)
$\acute{m}_{finj}$	fuel injection rate per jet (kg/°CA)
N	engine rotational speed (rpm)
n	Number of soot particles per unit volume
N_{drop}	number of fuel droplets in a zone
P	pressure (Pa)
Qp	Volumetric product productivity
r	Energy share
R_{mol}	universal gas constant, 8314.3 J/kmol K

S	spray penetration (m)
T	absolute temperature (K)
u	spray velocity (m/s)
x	space cartesian coordinate (m)
X	Microbial biomass concentration
Yx/s	Ethanol yield
y	space cartesian coordinate (m)
z	number of nozzle holes (jets)
Δp	pressure difference (Pa)

Greek symbols

$\Delta\varphi$	computational step (^{o}CA)
$\Delta\varphi_{inj}$	duration of fuel injection (^{o}CA)
θ	initial spray angle (rad)
λ	Ratio of length of connecting road to stroke length
ρ	Density (kg/m^3)
φ	Crank angle (degree)
Φ	equivalence ratio (fuel to air)
ψ	Specific absorption per particle

Subscripts

a	air
br	spray break up
inj	injected, or at injection point
ign	ignition
max	maximum
mid	mid-zone
n	nozzle hole
tot	total
vap	evaporated fuel
z	zone

Abbreviations

A	Average projected area of each particle
AFEX	Ammonia fibre explosion
Al	Aluminium
aTDC	After top dead centre
ADC	Analog to digital converter
ASTM	American society for testing material
B	Bioethanol
Br	Bromine
B100	Biodiesel 100 percentage
BDC	Bottom dead centre
BMDE	Bioethanol-diesel emulsion
BSEC	Brake specific energy consumption
BSFC	Brake specific fuel consumption
BSHC	Brake specific hydrocarbon
BSCO	Brake specific carbon monoxide
BSNO	Brake specific nitric oxide
bTDC	Before top dead centre
C	Carbon
CI	Compression ignition
CNG	Compressed natural gas
CO_2	Carbon dioxide
CH_4	Methane
CFCs	Chlorofluorocarbons
Cl	Chlorine
C_2H_4	Ethylene
CN	Cetane number
Cr	Chromium
D	Diesel
DC	Direct current
DDT	Dichlorodiphenyltrichloroethane
DEE	Diethyl ether

DI	Direct injection
DME	Dimethyl ether
DAS	Data acquisition system
DA	Digital to analog
EC	External combustion
E	Ethanol
F^-	Fluoride
FFV	Flexible fuel vehicle
FTIR	Fourier transform infrared spectroscopy
FAME	Fatty acid methyl ester
FID	Flame ionisation detector
GHGs	Greenhouse gases
GC-MS	Gas chromatography and mass spectrometry
H	Hydrogen
Hg	Mercury
HCB	Hexachlorobenzene
HC	Hydrocarbon
HSU	Hatridge Smoke Units
IC	Internal combustion
IEA	International energy agency
IPCC	Inter-governmental panel on climate change
IDI	Indirect injection
kWh	kilowatt hour
kW	kilowatts
KOH	Potassium hydroxide
LPG	Liquefied petroleum gas
LNG	Liquefied natural gas
LHW	Liquid hot water
LTC	Low temperature combustion
MW	Mega watt
M	Methanol
MSW	Municipal solid waste

N	Nitrogen
N_2O	Nitrous oxide
NO_2	Nitrogen dioxide
NO_x	Oxides of nitrogen
NREL	National renewable energy laboratory
NDIR	Non-dispersive infrared
O	Oxygen
O_3	Ozone
PAN	Peroxyacetyl nitrate
PM	Particulate matter
Pb	Lead
PCBs	Polychlorinated biphenyls
ppm	Parts per million
ppr	Pulse per revolution
PC	Personal computer
PWM	Pulse width modulation
rpm	Revolution per minute
RME	Rapeseed methyl ester
RT	Retention time
S	Sulphur
SI	Spark ignition
SF_6	Sulfur hexafluoride
SO_2	Sulfur dioxide
SSCF	Simultaneous saccharification and co-fermentation
SHF	Separate hydrolysis and fermentation
TVA	Tennessee valley authority
TEGDN	Triethylene glycol dinitrate
THC	Total hydrocarbon
TEGN	TriEthyl Glycol Di-Nitrate
TDC	Top dead centre
USDA	United States Department of Agriculture
YENB	Yeast extract nutrient broth

Unit and description

bar	Unit of pressure
°C	Temperature in degree Celsius
^{o}CA	Crank angle in degree
cc	Cubic centimetre
cm	Centimetre
cSt	Centistoke
eV	Electron volt
°F	Temperature in degree Fahrenheit
g	Gram
gal/acre	Gallon/hectare
g kg^{-1}	Gram/kilogram
hp	Horse power
kg	kilogram
kHz	Kilo Hertz
kPa	Kilo Pascal
L	Litre
L/t	Litre/tonne
Lha	Litre-hectare
mm	Millimetre
m	Meter
m^3	Cubic meter
mg	Milligram
min	Minute
ml	Millilitre
mV	Millivolt
MJ	Mega joule
Nm	Newton-meter
v/v	Volume/volume
V	Voltage
wt %	Percentage by weight
%	Percentage

CHAPTER 1

INTRODUCTION

1.1 General

Energy is the backbone of the economic development of a country. The energy demand depends mainly upon the population and consumption. It is projected that the world energy consumption is expected to increase by about 40% by the year 2035 over the present. It is also predicted that only India and China will have an increased energy demand of 25% by the year 2035 due to an increase in their population [1]. Generally, the per capita energy consumption is the measure of the per capita income or prosperity of the nation. The per capita income in the USA is about 7032 kWh per year, whereas it was about 614 kWh in India in the year 2011 [2]. The population of the USA is 7% of that of the world, and it consumes approximately 32% of the total energy consumed in the world. But India, a fast developing country with 20% of the world's population consumes only 1% of the total energy consumed in the world. In developing countries, due to a greater development of education, health care, and social services, there is more demand for energy. The five major sectors, in which energy is consumed predominantly, are; (i) power generation, (ii) transportation, (iii) agriculture, (iv) commerce, and (v) households. Figure 1.1 shows the information on the sector wise energy consumption in the world during the year 2011-2012 [3].

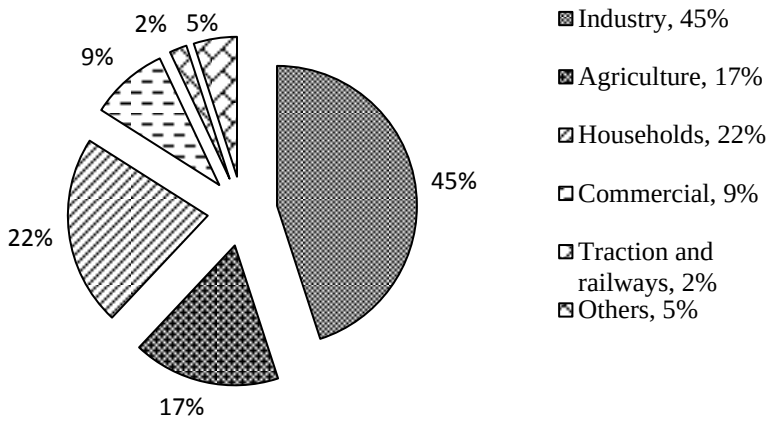

Fig. 1.1 Sector wise energy consumption

External combustion (EC) and internal combustion (IC) engines are mainly used for energy conversion in the power, transportation, industries, agriculture and commercial sectors, which are mainly run on fossil fuels. Electricity is mainly consumed in different applications in all

these sectors. However, the electricity is mainly generated from the combustion of fossil fuels in thermal power plants, followed by nuclear and hydro-electric power plants. The trend of energy consumption in each sector is discussed in the following subsections.

1.1.1 Power sector

Spark ignition (SI) and compression ignition (CI) engines are mainly used in small and medium capacity power plants, while gas turbines are used in higher capacity power plants. The SI and CI engines are primarily operated with conventional petroleum fuels, while gas turbines are operated with petroleum fuels, and industrial and municipal wastes of an organic nature. Diesel power plants with power ratings of 110, 220, 330, 440, and 735 kilowatts (kW) are used widely for small and medium power applications. Stationary diesel engines with a power rating of 2,200 kW are used in large power plants. Diesel power plants are used where sources such as coal and water are unavailable, which are used in steam power plants. A list of the important major diesel power plants in the world is given in Table 1.1.

Table 1.1 List of important diesel power plants in the world in 2014 [4]

Country	No. of plants	Maximum design capacity (MWe)
Australia	8	414
Canada	10	2120
China	1	278
Denmark	1	646
Egypt	19	1360
France	5	2400
Germany	1	840
India	8	158
Iran	11	1890
Spain	4	892
Russia	6	1120
UK	12	1892

In India, according to the Central Electricity Authority, the total installed capacity of diesel power plants in the year 2010 was estimated to be about 1,199.75 MW [5]. Some of the currently operated diesel plants in India are listed in Table 1.2.

Table 1.2 List of diesel plants in India

Name of the diesel power plant	State	Capacity(MW)
GMR Vasavi	Tamil Nadu	200
Kozhikode	Kerala	128
Yelahanka	Karnataka	127.92
Brahmapuram	Kerala	106.6
Suryachakra	Andaman & Nicobar	20
Bemina	Jammu & Kashmir	5
Leh	J&K Govt	2.18
Ambala	Haryana	2.18
Upper Sindh	Jammu & Kashmir	1.70
Keylong	Himachal Pradesh	0.13
Kamah	Jammu & Kashmir	0.06
Gangtok	Sikkim	4
Ranipool	Sikkim	1
Total		598.77

1.1.2 Transportation

1.1.2.1 Land transportation

Transportation plays an important role in mobilizing human beings, materials, animals etc from one place to another. There are three modes of transportation, viz. (a) surface (b) water, and (c) air transportation. SI engines are primarily operated with gasoline as a fuel, followed by small percentages of ethanol, LPG, CNG. All the three modes of transportation utilize fossil fuels as main fuels. In the early days, coal was used as a primary fuel in road, rail and marine transport. During the industrial revolution in the late 1900s, and after the introduction of petroleum fuels, the use of coal was restricted to surface and sea transportation, while air transport uses only superior quality petroleum fuel. SI and CI engines are largely used in automotive vehicles. Light vehicles, such as two and three wheelers, and some of the passenger cars are operated by SI engines. And heavy duty on-road and off-road vehicles are operated by CI engines. In India, the largest consumer of oil is the transportation sector representing 50% of the total demand, followed by agriculture (18%) and the industry sector (11%), and diesel is the largest with 44% share in the year 2012. LPG and gasoline each has a share of 10% (IEA India). It is estimated that by the year 2020, the world's vehicle population is expected to reach 2 billion approximately, with cars representing at least 50% of the total vehicle population. China’s and India’s automobile vehicle populations are expected to grow at an annual rate of around 7 or 8%, while the slowest growth is expected in the United States, with less than 1% a year, and Western Europe, with 1 to 2% [5]. India has about 1.1

million natural gas vehicles as of December 2011 [6]. In 2012, a total of 84.1 million cars and commercial vehicles were built worldwide, led by China, with about 19.3 million motor vehicles manufactured, followed by the USA with 10.3 million, and Japan with 9.9 million [7].

1.1.2.2 Sea transportation

The IC engines, particularly diesel engines, are used in marine propulsion engines and marine auxiliary generators. Most modern ships use reciprocating diesel engines as their prime movers, due to their operating simplicity, robustness and fuel economy compared to most other prime movers. Different types of reciprocating diesel engines (2 and 4 stroke engines) are used in marine applications for both commercial and recreational purposes. Boats, cruises, ferries and ships are mainly used for marine applications. The low to high medium diesel engines of different constructions are used for driving. The slow speed (up to 300 rpm), medium (300-900 rpm) and high speed (above 900 rpm) engines are used in marine applications. In ships, dual fuel engines are used, which are run by either marine grade diesel, heavy fuel oil, or liquefied natural gas (LNG). Many war ships built since the 1960s have used gas turbines for propulsion. Gas turbines are commonly used in combination with other types of engines.

1.1.2.3 Air transportation

In aviation, shaft engines including reciprocating and turbine powered, jet and pulse jet, and rocket engines under the reaction type are mainly used. In addition to them, wankel, pre-cooled jet engines are also used. Aircraft reciprocating (piston) engines are typically designed to run on aviation gasoline. Turbine engines and aircraft diesel engines burn various grades of jet fuel. Jet fuel is a relatively heavy and less volatile petroleum derivative based on kerosene, but certified to strict aviation standards, with additional additives.

Figure 1.2 shows how the power is obtained for these three modes from different sources of energy and its various applications.

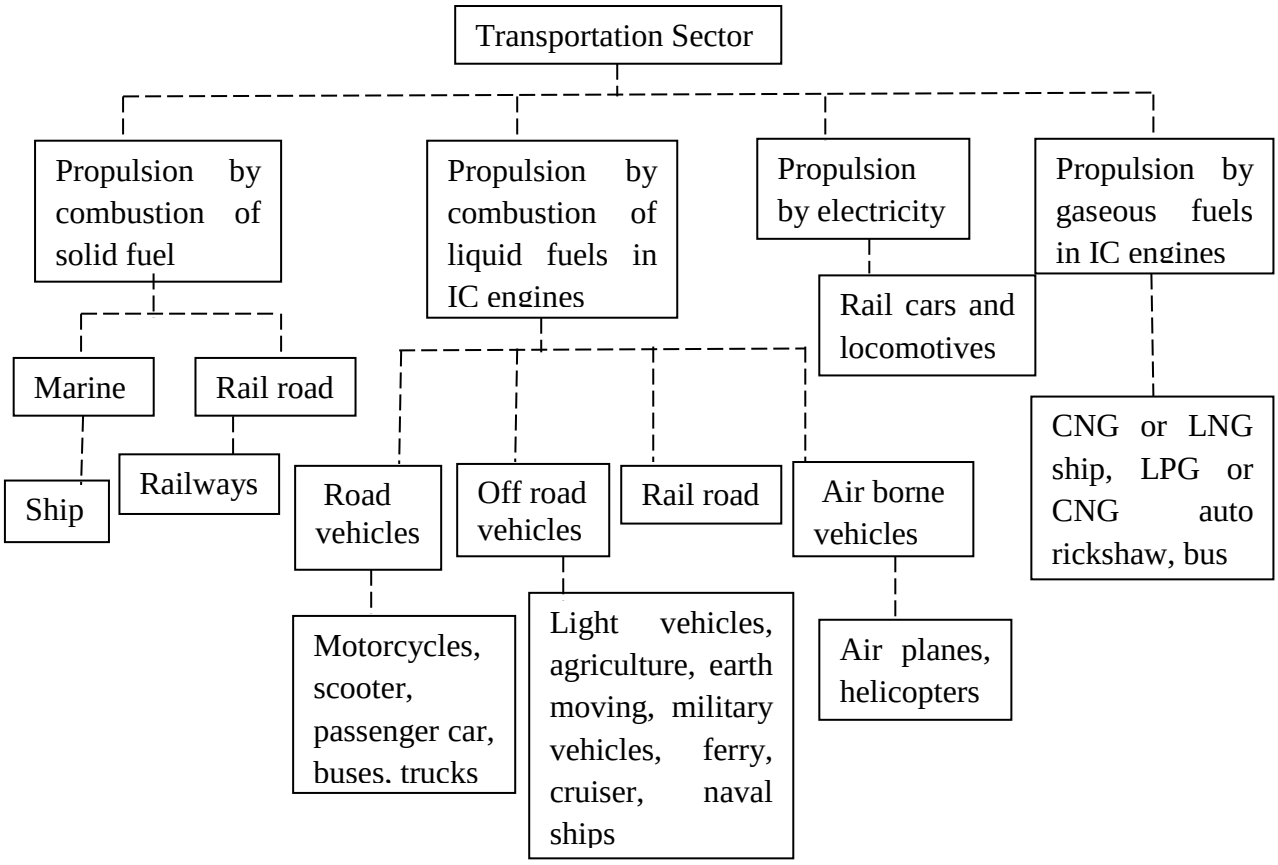

Fig. 1.2 Use of fuels and energy in the transportation applications

Table 1.3 gives the top 10 automobile manufacturing countries in the year 2012 and their corresponding annual production between the years 2010 and 2012.

Table 1.3 Annual motor vehicles production by top 10 countries

World rank	Country	2012	2011	2010
1	China	19.2	18.4	18.2
2	United States	10.3	8.6	7.7
3	Japan	9	8.3	9.6
4	Germany	5.6	6.3	5.9
5	South Korea	4.5	4.6	4.2
6	India	4.1	3.9	3.5
7	Brazil	3.3	3.4	3.3
8	Mexico	3	2.6	2.3
9	Canada	2.4	2.1	2
10	Thailand	2.42	1.4	1.6
	Total	63.82	59.6	58.3

A report indicated that cars share approximately 74% of the total annual motor vehicle production in the world [5]. The remaining 26% is shared by light commercial vehicles and

heavy trucks, buses, coaches and minibuses. It is also reported that the transportation share of the world liquid fuel's consumption would increase from 55% in the year 2010 to 57% in the year 2040.

1.1.3 Agricultural sector

Most of the countries in the world are agrarian countries. In the early days, irrigation was carried out by animal powered vehicles, water lifts (gravity-fed canal systems), and wind pumps. After the invention of the IC engines, irrigation, and transportation were carried out with the help of diesel engines. Off-road vehicles such as tractors, and power tillers are used largely for cultivation purposes in big lands, low lands, flooded rice fields, and hilly terrains, which in turn, increase the diesel consumption. The total number of tractors and power tillers sold in the year 2011-2012 was reported to be about 419270 and 39900 numbers respectively. At present, India is the largest manufacturer of tractors in the world. The agricultural sector also uses small powered vehicles for transporting agricultural wastes, grains, animal waste etc., in villages.

1.1.4 Industrial sector

Small and medium power generator sets are used in industries for standby power supply, when there is a shutdown or shortage of electrical supply. Many earth moving vehicles such as bulldozers, cable cars and hydraulic dozers are used for lifting and conveying goods. Other types of off-road vehicles, such as crawler tracks, excavators, ditchers, power revolving and stripper shovels, dumpers, and loaders are also widely used in the industrial sector. It is reported that the industrial sector accounts for about 57% of the projected growth of final energy demand in the year 2030.

1.1.5 Commerce

IC engines are used in many commercial applications such as entertainment applications, construction, and building services. The most widely used commercial diesel equipment are mobile cranes, road rollers, boring/trenching machines, etc. They are also used for small and medium electrical generator sets in commercial complexes, hospitals, cinema theatres, and educational institutions.

1.2 Consequences of air pollution

As a result of the combustion of fossil fuels and organic wastes, the other elements of the world like air, water and soil are also affected. The atmospheric air has been more affected than water and land, since the industrial revolution began in the 17^{th} century. Among all the five sectors discussed above, the transportation sector produces larger pollutants than the others. The main consequences of air pollution are discussed in the subsequent sections.

1.2.1 Greenhouse effect

The atmosphere of the Earth consists of a lot of gases such as water vapor, carbon dioxide (CO_2), methane, ozone and nitrous oxide (N_2O) which allow some solar radiation to reach the planet, but also absorb some of the heat radiating from the planet, trapping it and radiating it back to the surface. This cycle is called the greenhouse effect, and the gases are called as greenhouse gases (GHGs). The concentration of the GHGs increases day by day due to (i) combustion of fossil fuels or the decay of biomass, which produces more CO_2, (ii) anaerobic decay of organic material in landfills, wetlands, and rice fields; which produces methane, (iii) fertilizer use, animal waste management, fossil fuel combustion, automotive exhaust, and industrial activities which produce N_2O, and (iv) the use of chemicals like chlorofluorocarbons (CFCs), sulfur hexafluoride (SF_6) etc. As a result of this, the Earth's average surface temperature is gradually rising, which results in global warming. The weather patterns on the Earth are greatly affected by global warming and cause climate change.

1.2.2 Loss of flora and fauna

Air pollution due to inorganic pollutants like sulphur dioxide (SO_2), fluoride (F-), chlorine (Cl), and ozone (O_3), and organic pollutants like peroxyacetyl nitrate (PAN), ethylene (C_2H_4), and particulate matter (PM), affect the plant species, biological food web, wild life, and invertebrates. Plants are directly affected by the toxic effects of pollutants or indirectly by changing soil pH, followed by solubilisation of toxic salts of metals like aluminium. The effects of pollution on plants include mottled foliage, burning at leaf tips or margins, twig dieback, stunted growth, premature leaf drop, delayed maturity, early drop of blossoms, and reduced yield or quality. Also, the wildlife populations have suffered severe losses or even faced extinction due to effects of synthetic chemicals, oil spills, toxic metals, water contaminants and acid rain. Studies revealed that the water contaminants like mercury (Hg), lead (Pb), polychlorinated biphenyls (PCBs), hexachlorobenzene (HCB) and dichlorodiphenyltrichloroethane (DDT) are killing the marine whales.

1.2.3 Desertification

Desertification is the arid region of the world formed due to lack of water, vegetation and wildlife caused by climate change (global warming) and human activities (deforestation). It is reported that, the temperature in the dry lands will rise from 2°C to 5°C every time. The concentration of GHGs is expected to double in the next century. This may lead to severe drought, low rain fall and loss of agriculture. Desertification is cited as “potentially the most threatening ecosystem change impacting the livelihoods of the poor." In developing countries 90% of people are living in dry lands.

1.2.4 Melting of glaciers and sea level rise

The Earth’s largest fresh water reservoirs are glaciers, which are the ancient rivers of compressed snow that creep through the landscape, shaping the planet’s surface. These glaciers are melting down due to the increase in the average global temperature as a result of global warming, and heavy rain due to climate change. It is predicted that, the green land ice sheets could be triggered to lose their volume at a temperature increase of 2 to 3°C by the end of this century. The consequences of glacier changes increase the unsustainable water supplies from the major rivers, geohazards such as glacier-lake expansion, glacier-lake burst out and flooding, increase in the water levels in the rivers and also, sediments which could choke water supply, and affect agriculture, shortage of drinking water, loss of habitats, sea level rise etc.

The two main factors, viz., thermal expansion and melting of glaciers affect the sea level. The Inter-Governmental Panel on Climate Change (IPCC) reported that the increase in the sea level is a great danger, if the CO_2 level in the atmosphere reaches 550 ppm. The current sea level rise per year is 3mm worldwide. Studies revealed that, the world sea-level is expected to rise from 60cm to 70cm by the year 2100 due to thermal expansion, and 7m and 60m due to the melting of Greenland and Antarctica ice sheets respectively, by the year 2200, if the GHG emissions keep on rising. The consequences of sea level rise are high storms which hit lands, flooding of wet lands, loss of aquifers and agricultural soils, lost habitat for fish, birds, and plants, loss of coastal life, and a decrease in the economy of countries.

1.2.5 Acid rain

Acid rain is caused by the emissions of sulphur dioxide (SO_2) and oxides of nitrogen (NO_x) from the power plants and transportation sector, which react with the water vapour in the

atmosphere to produce acids. The adverse effect of acid rain includes (i) increased in the acid effect of the soil, (ii) killing of microbes due to acidic water and soil, (iii) minimization of the production of food crops, damage of buildings, historic monuments, and statues, especially those made of rocks, such as limestone and marble, that contain large amounts of calcium carbonate.

1.2.6 Human health

Pollutants like SO_2, NO_x, and PM, and volatile organic compounds may cause a lot of health problems to human beings, such as premature death due to heart or lung disease, aggravation of respiratory and cardiovascular illness, decrease in lung function and symptomatic effects, including acute bronchitis, aggravated coughing, and chest pain, chronic inflammation etc.

1.3 Alternative fuels

It is not possible to stop air pollution immediately. But, it is possible to control it by the following methods;

(i) Introducing low polluting and cleaner fuels
(ii) Adopting emission control devices
(iii) Increasing the consumption of renewable fuels

The alternative fuels proposed for IC engines from different sources are shown in Fig. 1.3.

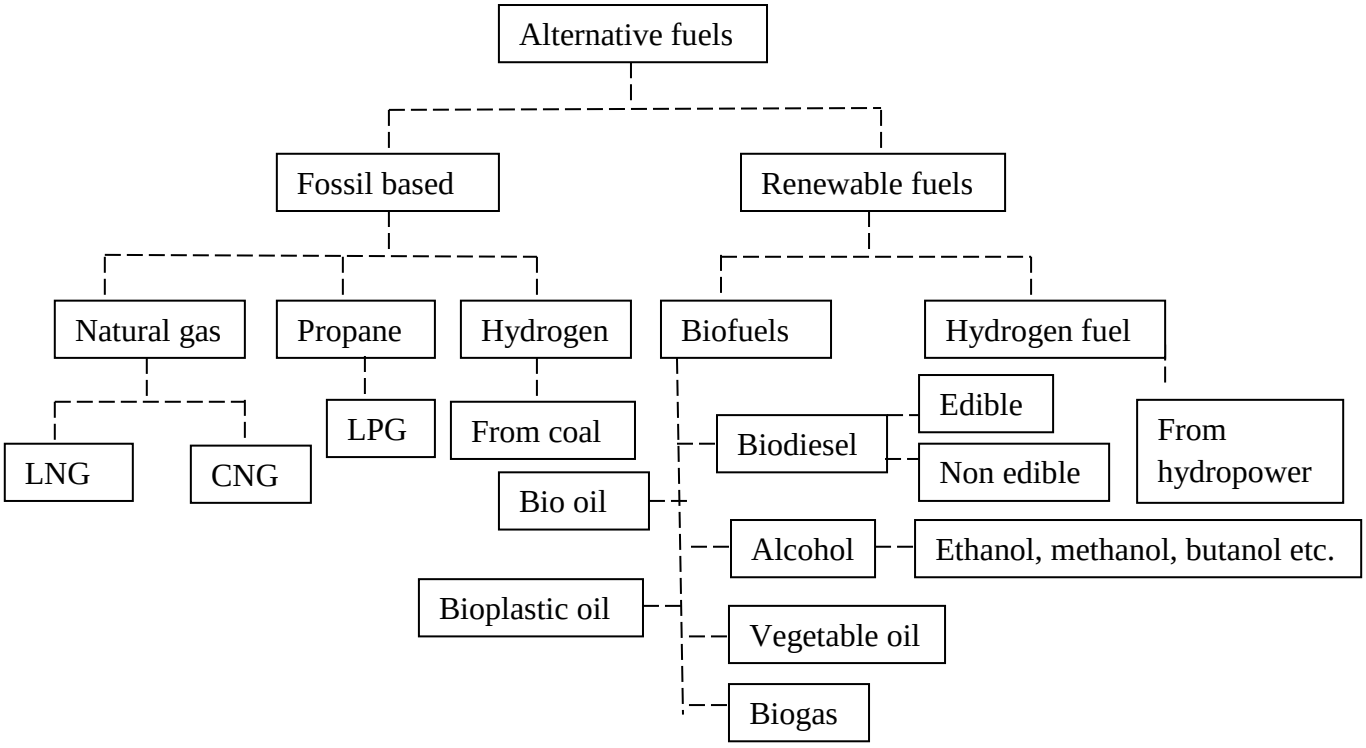

Fig. 1.3 Alternative fuels from different sources

1.3.1 Liquid biofuels for transportation

Liquid fuels such as biodiesel, and alcohols (methanol or ethanol/bioethanol), are now used as transportation fuels in some of the developed countries and they replace a certain quantity of petroleum fuels. Biodiesel and alcohols are renewable in nature and generate lesser pollutants in comparison with the petroleum based fuels. Other liquid fuels such as hydrogen, green diesel, bioethers etc., are being investigated as alternative fuels or additives for diesel engines. Examples of liquid fuels are described below;

1.3.1.1 Biodiesel

It is methyl or ethyl ester of a fatty acid produced from vegetable oil of edible or non edible types or animal fat or algae, by transesterification process using catalysts. Edible feedstocks such as Sunflower oil, Soy etc. or non edible feedstocks such as Jatropha, Karanja, Mahua etc. are commonly used for biodiesel production. Biodiesel has better lubricating properties and much higher cetane ratings than today's low sulfur diesel fuels [9]. Biodiesel addition reduces the fuel system wear. Biodiesel can be used in the pure form (B100), or may be blended with petroleum diesel in any concentration in most diesel engines for transportation purpose. But, the engine may face problems, such as low temperature operation, less durability and drop in power. New diesel fuel injection systems, such as common rail systems are equipped with materials that are compatible with biodiesel (B100). Biodiesel offers a substantial reduction in particulate matter (25%-50%), and a marginal increase of NO_x (1%-6%) when it is used as an alternative fuel in a CI engine. The major problems associated with biodiesel are (i) poor oxidation stability, (ii) higher viscosity and density, (iii) lower calorific value, and (iv) cold flow property. Blends of 20% and lower biodiesel can be used in diesel engines with no, or only minor modifications.

1.3.1.2 Alcohols

Alcohol fuels, such as methanol and ethanol/bioethanol, have been two promising fuels for SI and CI engines in the last few decades. Most developed countries have developed flexible fuel vehicles (FFV), which can easily switch over to either alcohol or petrol or diesel. The brief of methanol and ethanol are explained below;

1.3.1.2.1 Methanol

Methyl alcohol (methanol) is obtained from the steam reforming process of natural gas and CO_2, using a copper-based catalyst. It is a renewable fuel and can be made from wood, paper or waste by a microbial or photochemical conversion process. It is a toxic, colourless, tasteless liquid with a very faint odour. For transportation purpose, M85 (blend of 85% methanol and 15% unleaded petrol) and M100 are mostly used in some countries to substitute petrol and diesel respectively. Methanol is also used in a dual fuel operation of the diesel engines. The hydrocarbon emission (HC) can be reduced by 30-40% with M85 and up to 80% with M100 fuels [9]. But, formaldehyde emissions are increased in large amounts. Generally methanol has a high octane number of over 100; so it is a good fuel for SI engines. The disadvantages of methanol fuel are material corrosiveness due to its water content, lower energy density which is 24% less than that of ethanol, and the leak detection problem.

1.3.1.2.2 Ethanol/bioethanol

Ethyl alcohol (ethanol) is produced by two major techniques such as chemical synthesis and fermentation. The chemical synthesis process is the catalytic hydrolysis of ethylene. The fermentation process is the breakdown of the complex molecules of sugar, starch, carbohydrates, and cellulosic/lignocellulosic into ethanol/bioethanol, fermented by yeast, bacteria, enzymes, etc. The ethanol produced from biomass feedstock is known as bioethanol. The ethanol produced from food crops such as maize, wheat, sugar beet, and grain is known as the first generation bioethanol, and the ethanol derived from non-food crops or waste biomass such as waste of urban, agriculture, industries, institutions, and forest sources is known as the second generation bioethanol. Ethanol has already been used as a transportation fuel in many countries like Brazil and the US in the form of e-diesel (ethanol blending level as high as 15% or even 20% in conventional diesel), and gasohol (90% of gasoline and 10% ethanol blend). Generally, ethanol/bioethanol are used in gasoline engines in combination of E85 (85% ethanol blend) and gasohol. It can also be used in diesel engines by adopting different techniques, such as emulsion, addition of ignition improver, fumigation, surface ignition, spark ignition and dual fuel operation. Dual fuel operation can provide a maximum diesel replacement, i.e. 90% of diesel. The advantages of ethanol/bioethanol are its high oxygen content of 35% by weight, lesser gum formation, lower GHGs emissions, and high octane rating. It is reported that sugar-fermented and cellulosic ethanol/bioethanol can minimize the GHGs emissions by about 18%-29% and 85% over gasoline emissions [9]. The

demerits of ethanol/bioethanol are its lower energy density, engine durability issues, aldehyde emission, deposits and fouling in the fuel injection system. Ethanol is considered as the most attractive alternative fuel for developing countries, as many stationary diesel engines are used in the agricultural and commercial sectors, and for small scale power generation in the industrial sector.

1.4 Benefits of liquid biofuels over petroleum fuels

The advantages of biofuels are given below;

(i) Generate lower emissions
(ii) Renewability
(iii) Biodegradability
(iv) Low cost
(v) Energy security
(vi) Economic stimulation

1.5 Organisation of thesis

The thesis comprises of seven chapters which are given below;

Chapter 1 presents the introduction to the importance of energy, different sectors in which IC engines are used, consequences of air pollution, need for alternative fuels, liquid biofuels for transportation and their benefits.

Chapter 2 reviews the literature pertaining to production, characterisation and utilization of ethanol/bioethanol as an alternative fuel in the CI engines. The chapter also discusses the literature available, related to the assessment of the lubricating oil properties of ethanol/bioethanol used as fuel in a CI engine.

Chapter 3 details the production of bioethanol from the Madhuca Indica flowers by fermentation using *Saccharomyces cerevisiea*. The chapter also presents the characterisation of bioethanol using sophisticated instruments such as the Fourier transform infrared spectroscopy (FTIR), Gas chromatography and mass spectrometry (GC-MS) etc. The cost benefit analysis of bioethanol is also included. The cost of bioethanol production is also discussed.

Chapter 4 gives the information on the experimental test set up used in the study, various instruments used for measuring different parameters, and the uncertainties of the instruments. Also details the methodology adopted to carry out the investigation. This includes the

experimental techniques followed to use bioethanol, which has a lower viscosity and a lower cetane number than diesel fuel in a CI engine.

Chapter 5 describes the equations and co-relations used for the mathematical modeling of a DI diesel engine.

Chapter 6 presents the results and discussion of all the techniques adopted in the research work. The three major groups of parameters evaluated are (i) performance (ii) emission and (iii) combustion. The validation of the mathematical modeling is done with the best results obtained from the experimental results. The chapter also details the durability issues of the engine fueled with bioethanol used by a better technique.

Chapter 7 presents the conclusions of the experimental investigation carried out to evaluate the bioethanol obtained from the Madhuca Indica flowers as an alternative fuel for CI engines.

CHAPTER 2

LITERATURE SURVEY

2.1 General

In this chapter, the literatures collected by the researcher on methods of producing ethanol from biomass materials are discussed first. Then the literatures available for production of bioethanol from the Madhuca Indica flowers that are proposed by different researchers are discussed. Finally, the literatures available on utilization of ethanol/bioethanol in CI engines are discussed.

2.2 Over view of ethanol/bioethanol production

Ethanol production is a not a new technology. Over many years ethanol has been produced by fermentation. As the importance of alternative fuels was realized due to the increase in the cost of petroleum fuels and awareness on protecting the environment, research and development on the production of ethanol has increased extensively. Ethanol can be produced from the direct fermentation of simple sugars, or polysaccharides like starch or cellulose that can be converted into sugars. As ethanol can be produced in a larger quantity in comparison with the other liquid alternative fuels such as biodiesel, many researchers are trying to explore possible sources and methods to produce ethanol/bioethanol. Table 2.1 gives the world ethanol production in the year 2013 [10]. Many researchers documented their research works pertaining to the production of ethanol/bioethanol in the following categories; (i) biomass sources containing sugar, (ii) biomass sources containing starch, (iii) cellulosic and lignocellulosic materials [11-34].

Table 2.1 world ethanol production in the year 2013 [10]

Continent	Millions of gallons
United States	13,300
Brazil	6,267
Europe	1,371
China	696
India	545
Canada	523
Rest of World	727

2.2.1 Sugar feedstock

Biomass materials containing high levels of glucose or precursors can be fermented using microorganisms to produce ethanol. These microorganisms can typically use the 6-carbon sugars, one of the most common being glucose. One example of feedstock used in this method is sugar. Since sugar is an essential commodity for human life, these materials are usually too expensive to use for ethanol production. Badger reported [35] in his review that, fungi, bacteria, and yeast microorganisms can be used for fermentation; a particularly yeast *Saccharomyces cerevisiae* also known as Bakers' yeast, since it is commonly used in the baking industry) is frequently used to ferment glucose to produce ethanol. He reported that 100 grams of glucose would produce 51.4 g of ethanol and 48.8 g of CO_2. However, in practice, the actual yield is less than 100% because the microorganisms use some of the glucose for growth. Other biomass feedstocks rich in sugars (materials known as saccharides) include sugar beet, sweet sorghum, and various fruits.

Ethanol production is usually performed in three steps: (a) the collection of a solution of fermentable sugars, (b) fermentation of sugars into ethanol, and (c) ethanol separation and purification, usually by distillation–rectification–dehydration [36]. The step before fermentation, to obtain fermentable sugars, is the main difference between the ethanol production processes from simple sugar, starch or lignocellulosic materials. Sugar crops need only a milling process for the extraction of sugars to ferment (not requiring any step of hydrolysis), becoming a relatively simple process of sugar transformation into ethanol. In this process, ethanol can be fermented directly from cane juice or beet juice or from molasses, generally obtained as a byproduct after the extraction of sugar [13]. Currently ethanol fermentation is carried out mainly by batch processes with cell recycling, and a small part is produced through multi-stage continuous fermentation with cell recycling [37].

Cardona et al. [38] reviewed the process design and opportunities for ethanol production. They mentioned that sugar cane, either in the form of cane juice or cane molasses, are the most important feedstock utilized in tropical and sub-tropical countries for producing ethanol. In European countries, beet molasses are the most utilized sucrose-containing feedstock. Besides these energy crops, sweet sorghum has become a potential raw material, because the juice with a high content sucrose obtained from its stalks, can be extracted. Its grains contain a high amount of starch, and its bagasse is an important source of lignocellulosic biomass. The conversion of sucrose into ethanol is easier compared to the starchy materials and

lignocellulosic biomass, because the preliminary hydrolysis of the feedstock is not required, since this disaccharide can be broken down by the yeast cells; in addition, the conditioning of the cane juice or molasses favors the hydrolysis of sucrose. They pointed out that the availability and transportation cost of the feedstock play a crucial role, when new cost-effective production facilities are projected. Another source of simple sugars that can be used to produce ethanol is whey. Large quantities of whey are produced as a byproduct in the manufacturing of cheese. After whey protein has been extracted from whey by ultrafiltration, the remaining permeate is concentrated by reverse osmosis to attain higher lactose content for efficient fermentation. Lactose in whey permeate is fermented with some special strains of the yeast Kluyveromyces marxianus that are efficient in fermenting lactose [18, 39]. Alternatively, genetically engineered *Saccharomyces cerevisiae* strains may be used [21, 40].

2.2.2 Starchy feedstocks

Starch is another potential feedstock for ethanol production. The processes of ethanol production using starchy crops are well established and documented. Starch molecules consist of long chains of glucose molecules. So, starchy materials can also be fermented after breaking the starch molecules into simple glucose molecules. Cereal grains, potato, sweet potato, and cassava are some of the commonly available feedstocks available in this category. It is reported that maize and wheat are the two cereal grains used for ethanol production in the USA. They mentioned in their review that starchy materials required the reaction of starch with water (hydrolysis) to breakdown the starch into fermentable sugars (saccharification). Typically, hydrolysis is performed by mixing the starch with water to form a slurry, which is then stirred and heated to rupture the cell walls. Specific enzymes that will break the chemical bonds are added at various times during the heating cycle.

Pimentel et al., [41] have reported that the ethanol production using corn grain required 29% more fossil energy than the ethanol fuel produced, while grass required 50% more fossil energy. Ethanol production using wood biomass required 57% more fossil energy than the ethanol fuel produced. Demirbas [42] reported that grains like corn, require saccharification before fermentation. In this step, starch is gelatinized by cooking, and subjected to enzymatic hydrolysis to form glucose monomers, which can be fermented by microorganisms. In order to produce ethanol from starch, it is necessary to breakdown the chains of this carbohydrate for obtaining glucose syrup, which can be further converted into ethanol by yeast. This type

of feedstock is the most utilized for ethanol production in North America and Europe. Corn and wheat are mainly used for these purposes.

Yeast cannot be used with starch directly for ethanol production. Therefore, ethanol production from grains involves milling and hydrolysis of starch, that has to be wholly broken down to glucose, by the combination of two enzymes, α-amylase and amylo glucosidase, before it is fermented by yeast to produce ethanol. In tropical countries, other starchy crops such as tubers (e.g. cassava) can be used for the commercial production of fuel ethanol [16, 38]. Today, most fuel ethanol is produced from corn, by either the dry-grind (67%) or wet-mill (33%) process. The recent growth in the industry has been predominantly seen with dry-grind plants, because of less capital costs per gallon and incentives for farmer-owned cooperatives [43-44]. Figure 2.1 shows the block diagram of ethanol production from the starch materials.

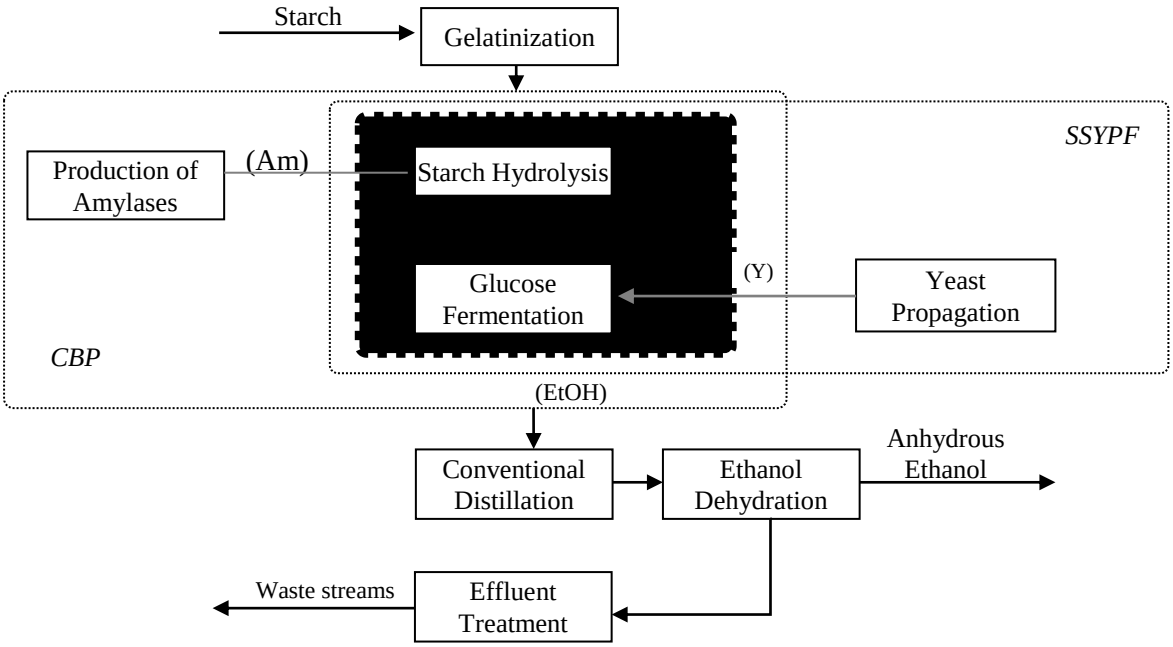

Fig. 2.1 Block diagram of fuel ethanol production from starchy materials [45]

2.2.3 Ethanol production from cellulosic materials

The production of ethanol from sugar and starchy materials also affects the food chain and fuel price. The food chain based feedstock-sugar molasses and starch materials can be replaced by alternative-cellulosic and lignocellulosic materials. Hence, ethanol produced from biomass materials is known as bioethanol [42]. Examples of cellulosic materials include paper, cardboard, wood, and other fibrous plant materials. Cellulosic resources are generally

available in different kinds. For example, forests comprise about 80% of the world's biomass which can be used from ethanol production. Cellulosic materials which are comprised of lignin, hemicellulose, and cellulose are called lignocellulosic materials. Lignin provides structural support to the plant. Thus, in general, trees have higher lignin content then grasses. Lignin which contains no sugars encloses the cellulosic and hemicellulosic molecules, making them difficult to reach. Cellulosic molecules consist of long chains of glucose molecules as do starch molecules, but have a different structural configuration. Because of these structural characteristics and their encapsulation by lignin, the cellulosic materials cannot be as easily hydrolyzed as starchy materials. Hemicellulose is comprised of long chains of sugar molecules; but it also contains, in addition to glucose (a 6-carbon or hexose sugar), pentoses (5-carbon sugars). It is reported by Badger [35] that since 5-carbon sugars comprise a high percentage of the available sugars, the ability to recover and ferment them into ethanol is important for effective production of ethanol. Special microorganisms have been genetically produced, which can ferment 5-carbon sugars into ethanol with a relatively high efficiency. Bacteria have drawn special attention from researchers, because of their speedy fermentation. In general, bacteria can ferment in minutes as compared to hours for yeast.

There are three basic types of ethanol production from cellulosic materials; they are (a) acid hydrolysis, (b) enzymatic hydrolysis, and (c) thermochemical conversion. The most common method is acid hydrolysis.

2.2.1.1 Acid hydrolysis

Any acid can be used for acidic hydrolysis; however, sulfuric acid is most commonly used since it is usually the cheapest. There are two basic types of acid processes: dilute acid and concentrated acid, each with variations. Dilute acid processes are conducted under high temperature and pressure, and have reaction times in the range of seconds or minutes, which facilitates continuous processing. As an example, using a dilute acid process with 1% sulfuric acid in a continuous flow reactor for a residence time of 0.22 minutes and at a temperature of 237°C (458°F) with pure cellulose, provided a yield of over 50% sugar. In this case, 0.9 t (1 ton) of dry wood would yield about 189 L (50 gallons) of pure ethanol. The combination of the acid and high temperature and pressure, require special reactor materials, which can make the reactor expensive. The most dilute acid processes are limited to a sugar recovery efficiency of around 50%. The reason for this is that, at least two reactions are part of this

process. The first reaction converts the cellulosic materials to sugar and the second reaction converts the sugars to other chemicals. Once the cellulosic molecules are broken apart, the reaction proceeds rapidly to break down the sugars into other products, most notably furfural, a chemical used in the plastics industry. Not only does sugar degradation reduce the sugar yield, but the furfural and other degradation products can be poisonous to the fermentating microorganisms. The biggest advantage of the dilute acid process is its fast rate of reaction, which facilitates continuous processing. One of the demerits is its low sugar yield. For a rapid continuous processing, in order to allow adequate acid penetration, feedstocks must also be reduced in size, so that the maximum particle dimension is in the range of a few millimeters. Since 5-carbon sugars degrade more rapidly than 6-carbon sugars, one way to decrease sugar degradation is to have a two-stage process. The first stage is conducted under mild process conditions to recover the 5-carbon sugars, while the second stage is conducted under harsher conditions to recover the 6-carbon sugars. Unfortunately, sugar degradation is still a problem, and the yields are limited to around 272 L/t (80 gallons of ethanol/ton) of dry wood. The concentrated acid process uses relatively mild temperatures and the only pressures involved are usually those created by pumping materials from vessel to vessel. One concentrated acid process was first developed by United States Department of Agriculture (USDA), and further refined by Purdue University and the Tennessee Valley Authority (TVA). In the TVA concentrated acid process, corn stover was mixed with dilute (10%) sulfuric acid, and heated up to 100ºC from 2 to 6 hours in the first (or hemicellulose) hydrolysis reactor. The low temperature and pressure minimize the degradation of sugars. To recover the sugars, the hydrolyzed material in the first reactor was soaked in water and drained several times. The solid residue from the first stage was then dewatered and soaked in a 30% to 40% concentration of sulfuric acid from 1 to 4 hours as a pre-cellulose hydrolysis step. This material was then dewatered and dried, so that the acid concentration in the material was increased to about 70%. After reacting in another vessel from 1 to 4 hours at 100ºC, the reactor contents were filtered to remove the solids and recover the sugar and acid. The sugar/acid solution from the second stage was recycled to the first stage to provide the acid for the first stage hydrolysis. The sugars from the second stage hydrolysis were thus recovered in the liquid from the first stage hydrolysis. The advantage of the concentrated process is the high sugar recovery efficiency, which can be in the order of over 90% of both hemicellulose and cellulose sugars. The low temperature and pressure employed also allow the use of relatively low cost materials, such as fiberglass tanks and piping. But, it is a relatively slow process and cost effective acid recovery systems have been difficult to

develop. Without acid recovery, large quantities of lime must be used to neutralize the acid in the sugar solution. This neutralization forms large quantities of calcium sulfate, which requires disposal and creates additional expense.

2.2.1.2 Enzymatic hydrolysis

Another basic method of hydrolysis is enzymatic hydrolysis. Enzymes are naturally occurring plant proteins that cause certain chemical reactions to occur. However, for enzymes to work effectively, they must obtain access to the molecules to be hydrolyzed. In order to have an effective enzymatic process, some kind of pretreatment process is thus required to break the crystalline structure of the lignocellulose and remove the lignin to expose the cellulosic and hemicellulosic molecules. Depending on the biomass materials, either physical or chemical pretreatment methods may be used. Physical methods may use high temperature and pressure, milling, radiation, or freezing, all of which require high energy consumption. The chemical method uses a solvent to break apart and dissolve the crystalline structure. After a dilute acid pretreatment, the slurry is detoxified to remove materials that would be poisonous to the microorganisms used in the process. A small part of this slurry is sent to a separate vessel that is used to grow microorganisms that produce the cellulase enzyme for the process. Another part of the slurry is sent to another vessel, to maintain and grow a yeast culture for fermentation. In a process developed by National Renewable Energy Laboratory (NREL), both enzymes and the fermentation microorganisms were added at the same time to the slurry, and sugar conversion and fermentation occurred simultaneously in a process called simultaneous saccharification and co-fermentation (SSCF).

Due to the tough crystalline structure, the enzymes currently available require several days to yield good results. The reactor vessels required for the process have to be either quite large or many of them must be used because they have to be used for a longer process time. It is reported that both the options are expensive. Currently, the cost of enzymes is also too high and research is continuing to bring down the cost of enzymes. However, if less expensive enzymes can be developed, enzymatic processes hold many advantages: (a) their efficiency is quite high and their byproduct production can be controlled; (b) their mild process conditions do not require expensive materials of construction; and (c) their process energy requirements are relatively low. The ethanol production process from biomass is shown in Fig. 2.2.

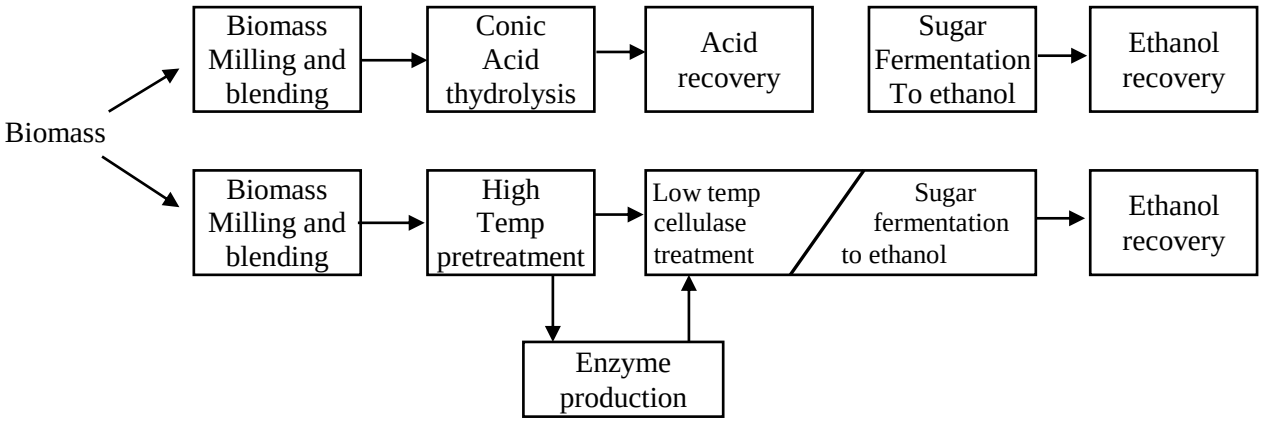

Fig. 2.2 Ethanol production process from biomass [44]

2.2.1.3 Thermochemical conversion

Thermochemical conversion is one of the methods that have been recently used to produce ethanol/bioethanol. There are two ethanol production processes that currently use thermochemical reactions in their processes. The first one is actually a hybrid thermochemical and biological system [46]. Biomass materials are first thermo chemically gasified and then synthesis gas (a mixture of hydrogen and carbon dioxides) bubbled through specially designed fermenters. A microorganism that is capable of converting the synthesis gas is introduced into the fermenters under specific process conditions to cause fermentation to ethanol. The second production process does not use any microorganisms. In this process, biomass materials are first thermo chemically gasified and the synthesis gas passed through a reactor containing catalysts, which cause the gas to be converted into ethanol. The yield of ethanol obtained in the synthetic gases-to-ethanol process is about 50%. Some processes that first produce methanol and then use catalytic shifts to produce ethanol, have obtained ethanol yields in the range of 80%. Consequently, the technologies used in the thermochemical conversion method, are more complex leading to higher ethanol production costs compared to those of cane, beet or corn.

2.2.4 Ethanol production from lignocellulosic materials

The use of polysaccharides present in the lignocellulosic materials (such as switch grass, wood chips, corn husks and other agricultural wastes) for ethanol production is of great interest today. In this case, the technologies involved in production are more complex, and the costs of production are higher in comparison with cane, beet or corn. However, most lignocellulosic materials are byproducts of agricultural activities and industrial residues, and show a great potential for the production of fuel ethanol on a large scale, and for worldwide

consumption as a renewable fuel. It is predicted that lignocellulosic biomass will become the main feedstock for ethanol production in the near future. The basic steps in producing ethanol from lignocellulosic biomass are: (i) pre-treatment to render cellulose and hemicellulose more accessible to the subsequent steps. Pretreatment generally involves a mechanical step to reduce the particle size and a chemical pre-treatment (diluted acid, alkaline, solvent extraction, steam explosion among others) to make the biomass more digestible; (ii) acid or enzymatic hydrolysis to break down polysaccharides to simple sugars; (iii) fermentation of the sugars (hexoses and pentoses) to ethanol using microorganisms; and (iv) separating and concentrating the ethanol produced by distillation–rectification–dehydration. Figure 2.3 illustrates the ethanol production from lignocellulosic biomass.

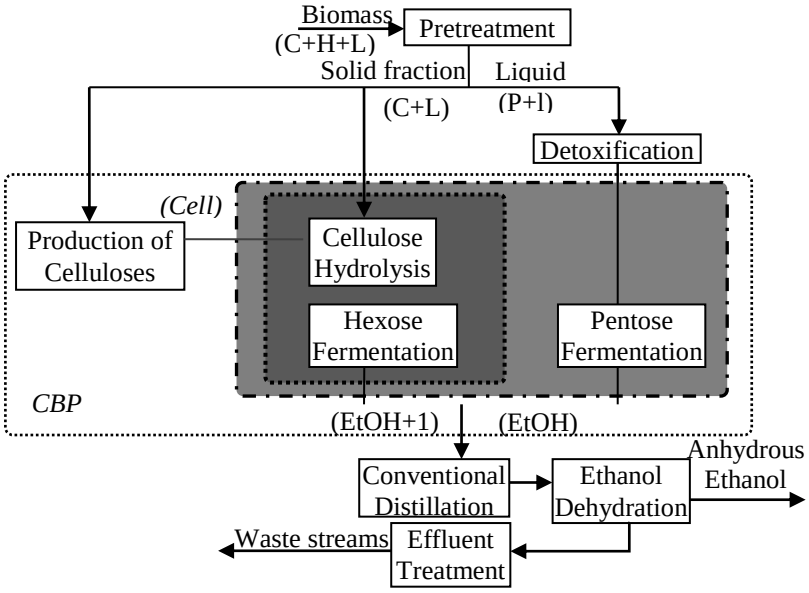

Fig. 2.3 Block diagram of fuel ethanol production from lignocellulosic biomass [38]

It is reported that some pre-treatments (step 1), such as diluted acid hydrolysis, result in the solubilization of sugars from hemicellulose, generally separating the biomass into a liquid fraction containing pentoses and a solid fraction composed of cellulose and lignin. The sugar yield is dependent on the kind of pretreatment and the conditions used. The main technologies proposed for the hydrolysis of cellulose (step 2) include concentrated acid hydrolysis and enzymatic hydrolysis. Acid hydrolysis is the most advanced technology, while enzymatic hydrolysis is considered as the technology which may reduce the cost of producing ethanol from biomass. Table 2.2 gives the different lignocellulosic materials and their composition [46].

Table 2.2 Different lignocellulosic materials and their composition

Lignocellulosic materials	Cellullose(%)	Hemicellulose(%)	Lignin(%)
Hardwoods stems	40 – 55	24 – 40	18 – 25
Softwood steam	45 – 50	25 – 35	25 – 35
Nut shells	25 – 30	25 – 30	30 – 40
Corn cobs	45	35	15
Grasses	25- 40	35 – 50	10 – 30
Paper	85 – 99	0	0 – 15
Wheat straw	30	50	15
Sorted refuse	60	20	20
Leaves	15 – 20	80 – 85	0
Cotton seed hairs	80 – 95	5 – 20	0
News paper	40 – 55	25 – 40	18 – 30
Waste papers from chemical	60 – 70	10 – 20	5 – 10
pulps	8 – 15	NA	24 – 29
Primary wastewater solids	6.0	28	NA
Swine waste	106 – 4.7	1.4 – 3.3	2.7 – 5.7
Solid cattle manure	25	35.7	6.4
Coastal Bermuda grass	45	31.4	12.0
Switch grass			

The recycling of the pentoses formed during the hydrolysis of hemicellulose was studied by Galbe et al. [47], resulting in the increase of ethanol yield and the decrease of energy consumption. However, these flow sheets had the drawback of the concentration of fermentation inhibitors being augmented. For this reason, further research for finding resistant microorganisms or the best way of detoxification should be carried out, including the utilization of cellulose producing fungi, like Trichodermareesei [48]. The researchers have also proposed the reutilization of cellulases through different strategies of recycling, using the substrates remaining during the batch hydrolysis of cellulose, although the content of lignin in the substrate negatively affected the cellulase activity. Mes-Hartree et al. [49] had proposed the recycling of both cellulases and substrate in order to save enzymes and to utilize the residual substrate for producing cellulases for the same process. Nguyen et al. [50] proposed the use of both microfiltration and ultrafiltration, in order to collect the cellulases from the enzymatic hydrolysis reactor during ethanol production from municipal solid waste (MSW). The configuration corresponds to the Separate hydrolysis and fermentation (SHF) process, and the hydrolysis reactor works in a fed-batch regime. They claimed that this technique for cellulase recycling combined with a fed-batch operation allowed significant reductions in the cost of cellulose hydrolysis. However, the difficulties related to the

recycling of adsorbed cellulases in the case of continuous processes, the increase in the expected effectiveness of cellulolytic enzymes, among other factors, have narrowed the application of this technique to batch and fed-batch SHF processes.

Bioethanol can be produced from raw materials containing fermentable sugars, such as sugar cane and beet that are rich in sucrose. In addition, bioethanol may also be produced from some polysaccharides that can be hydrolyzed for obtaining sugars convertible into ethyl alcohol. The starch contained in grains is the major polymer used for ethanol production. Lignocellulosic biomass (a complex comprised of several polysaccharides) is the most promising feedstock considering its great availability and low cost, but the large-scale commercial production of fuel ethanol from lignocellulosic materials has still not been implemented. Table 2.3 provides the different feedstocks for ethanol production and their yields, which are represented by the resources [34]. Table 2.4 gives the various pretreatment methods for lignocellulosic biomass for ethanol/bioethanol production [51].

Table 2.3 Ethanol yield from different sources [34]

Source	Ethanol yield (gal/acre)	Ethanol rield(Lha)
Corn stover	112 – 150	1050 – 1400
Wheat	277	2590
Cassave	354	3310
Sweet sorghum	326 – 435	3050 – 4070
Corn	370 – 430	3460 – 4020
Sugar beet	536 – 714	5010 – 6680
Sugarcane	662 – 802	6190 – 7500
Switch grass	1150	10,760
Microal gae	5000 – 15,000	46,760 – 140,290

Table 2.4 Various pretreatment methods for lignocellulosic biomass for ethanol/bioethanol production

Methods	Examples of pretreated materials
Physical methods:	
Mechanical comminution	Wood and forestry wastes (hardwood, straw), Corn stover, cane bagasse,Timothy, alfalfa
Pyrolysis	Wood, waste cotton, corn stover
Physical–chemical methods:	
Steam explosion	Poplar, aspen, eucalyptus, softwood (douglas fir) Bagasse, corn stalk, wheat straw, rice,straw, barley, straw, sweet sorghum,bagasse, Brassica carinata residue, timothy grass, alfalfa, reed canary grass
Liquid hot water (LHW)	Bagasse, corn stover, olive pulp, alfalfa fiber
Ammonia fiber explosion (AFEX)	Aspen wood chips, Bagasse, wheat straw, barley straw, rice hulls, corn stover, Switchgrass, coastal, Bermudagrass, alfalfa
CO_2 explosion	Bagasse, alfalfa, recycled paper
Chemical methods:	
Ozonolysis	Poplar sawdust, bagasse, wheat straw, cotton straw, green hay, peanut
Dilute-acid hydrolysis	Poplar wood, bagasse, corn stover, wheat straw, rye, straw, rice hulls, switchgrass, bermudagrass
Concentrated-acid hydrolysis	Poplar sawdust, bagasse
Alkaline hydrolysis	Hardwood, bagasse, corn stover, straws with low lignin content (10–18%), cane leaves
Oxidative delignification	Bagasse
Wet oxidation	Corn stover, wheat straw
Organosolv process	Mixed softwood (spruce, pine, Douglas fir)
Biological methods:	
Fungal pretreatment	Corn stover, wheat straw

2.3 Bioethanol from the Madhuca Indica flowers

Swain et al. [52] have studied the possible production of bioethanol from fresh and 12-month-stored Madhuca Indica flowers, using free and immobilized cells of *Saccharomyces cerevisiae* (strain CTCRI) in submerged shake-flask fermentation. The bioethanol yields with free and immobilized cells were found to be 193 and 205 g kg^{-1} respectively, for fresh flowers and 148 and 152 g kg^{-1} with 12-month-stored flowers. The maximum sugar conversion and bioethanol concentration were achieved by about 80-82% and 193-205 g kg^{-1} flowers respectively. They have also reported that bioethanol production from the Madhuca Indica flowers have considerable scope in India, due to their potential and availability.

Mohanty et al. [53] have produced bioethanol from the Madhuca Indica flowers by the solid-state fermentation process using *Saccharomyces cerevisiae*. They have studied different parameters which affect the production process, including the strain of *Saccharomyces cerevisiae* used, biochemical composition of the substrate, fermentation system and the condition under which the fermentation took place. They observed that the concentration of ethanol increased, with the increase in the fermentation time and yeast biomass. The maximum ethanol (195 ± 4 g/kg flowers) concentration (95%) was obtained after 72 h of incubation. The moisture level of 70%, pH value of up to 6.0 and temperatures ranging from 20-30 °C were favourable conditions to increase the ethanol yield/concentration. They have also concluded that the collection, storage and marketing of flowers should be more, to increase their commercial potential.

Benerji et al. [54] have investigated the physico-chemical and nutritional parameter of bioethanol from the Madhuca Indica flowers, using *Saccharomyces cerevisiae-3090* through submerged fermentation. They have proved that the flowers would be a suitable substrate, which consisted of high sugars of about 68% and metal ions such as Mg+, Cu+, phosphorus and protein. They concluded that the maximum ethanol productivity could be achieved for the substrate concentration of 28%, pH level at 5.0, inoculum level and age at 25 and 48 hours respectively.

Behera et al. [55] have studied the effect of using immobilized cells (in agar agar and calcium alginate) and free cells of *Saccharomyces cerevisiae* for bioethanol production from the Madhuca Indica flowers. They have carried out the statistical analysis using ANOVA for production. The bioethanol yield with immobilized cells (in agar agar and calcium alginate) and free cells were found to be 151.2, 154.5 and 149.1 g kg^{-1} flowers respectively. It was observed that the calcium alginate cells provide better results compared to the agar agar (2.2% more) and free cell (3.5% more). The immobilized cells were physiologically active compared to the free cells. They have concluded that bioethanol production from the Madhuca Indica flowers was highly economical in comparison with either starchy or lignocellulosic biomass.

Behera et al. [56] have also investigated the bioethanol production from the Madhuca Indica flowers using immobilized cells of *Saccharomyces cerevisiae* (CTCRI strain) and Zymomonas mobilis (MTCC 92) in calcium alginate as beads and in the submerged condition. They reported that the sugar utilization capacity by the immobilized cells of

Saccharomyces cerevisiae was faster than that of Zymomonas mobilis. The maximum bioethanol concentrations with *Saccharomyces cerevisiae* and Zymomonas mobilis were about 154.5 and 134.55 g kg^{-1} flowers respectively, in 96 hours of fermentation. The bioethanol yield was higher by about 14.8% with the immobilized cells of *Saccharomyces cerevisiae* in calcium alginate beads.

Behera et al. [57] have given a comparative study of two most widely used microorganisms for bioethanol production. The two strains of microorganisms *Saccharomyces cerevisiae* (yeast) and Zymomonas mobilis (bacteria) were used, and it was found that the *Saccharomyces cerevisiae* strain showed 21.2% more bioethanol production in comparison to Zymomonas mobilis. The ethanol yield (Yx/s), volumetric product productivity (Qp), sugar to ethanol conversion rate (%) and microbial biomass concentration (X) obtained by *Saccharomyces cerevisiae* were found to be 5.2%, 21.1%, 5.3% and 134% higher than those of Zymomonas mobilis, respectively, after 96 h of fermentation. The bioethanol yield was affected by Zymomonas mobilis, due to its low tolerance to temperature and utilization of limited substrate range.

Behera et al. [58] have used the dried spongy fruit of luffa (Luffa cylindrical L.) for immobilizing microbial cells for bioethanol production. They have stated that the submerged fermentation of the Madhuca Indica flowers using whole cells of *Saccharomyces cerevisiae* immobilized in luffa sponge discs, was physiologically active in three more cycles of fermentation without significant reduction (<5%) in ethanol production. The immobilized cell in luffa sponge was found to be superior compared to the immobilized cells in calcium alginate as beads. It was also an excellent cell carrier for bioethanol fermentation, by flocculating cells (*Saccharomyces cerevisiae*) and non-flocculating cells (Candida brassicae). The bioethanol productivity was observed to be 8.9% more with luffa immobilised yeast cell over free cells, due to the high value of biomass aggregated to it.

2.4 Use of ethanol/bioethanol in CI engines

As ethanol/bioethanol is a type of alcohol, this section presents the literature review pertaining to the use of ethanol in CI engines. The lower cetane number of ethanol compared to that of diesel is the main problem, in using ethanol in CI engines.

Six different techniques have been proposed and adopted by many investigators, particularly to use ethanol/bioethanol in CI engines; they are given below;

- diesel-alcohol solutions and emulsions
- cetane improving additives
- dual injection
- fumigation
- surface-ignition
- spark-assistance

2.4.1 Diesel-ethanol/bioethanol solutions and emulsions

Ethanol/bioethanol can be mixed with diesel fuel using a suitable surfactant or emulsifier. It can also be suspended in diesel fuel (diesel or biodiesel) in the form of minute droplets to make an emulsion. In a review [59], it was mentioned that the two fuels, however, do tend to separate, and an ethanol-diesel fuel emulsion is fairly unstable. These mixtures and emulsions could combust satisfactorily in CI engines. It was also mentioned that it would be possible to use up to 20% of ethanol/methanol by volume in the form of emulsion. Beyond 20% there would be a chance of severe loss of performance.

Strait et al. [60] studied the problems that were encountered with diesel and ethanol blends. They reported that though the diesel and anhydrous bioethanol were miscible at room temperature, only trace amounts of water in the diesel and bioethanol blends might cause a phase separation, and the fuel of low density may shift to the top of the container. A water concentration of only 0.05% might cause phase separation at 0 °C, and hence, the water tolerance of bioethanol and diesel blends was inadequate for practical use.

Wrage and Goering [61] studied the technical feasibility and performance parameters of diesel and ethanol blends. They considered a blend of 10% bioethanol and 90% diesel, and named it as diesohol. The efficiency and smoke emission of the engine with the blends were found to be decreased compared to that of diesel. They also stated that the most critical problem associated with the bioethanol blends was phase separation. Generally, the water tolerance of the blends increases with temperature.

Moses et al. [62] concluded that approximately 2% of a surfactant was required for each 5% aqueous ethanol to get the stable ethanol-diesel micro emulsions with a minor stirring. Micro emulsion was thermodynamically stable for several months and it was also noticed that the dispersion sizes were found to be lesser than a quarter of the wavelength of light. The effect

of the cetane number with emulsified ethanol was found to be less compared to that of ethanol solution/blends. This was due to the shielding effect of the emulsion structure which caused a delay in the evaporation of ethanol as compared to the solutions, where the ethanol molecules were free to evaporate immediately. They also observed a reduction in the BSEC and an improvement in the brake thermal efficiency.

Baker [63] investigated the use of stabilized and unstabilized emulsions of methanol-in-diesel fuel and ethanol-in-diesel fuel, in a two cylinder, two stroke engine. He reported that 9:10 and 3:2 parts by volume of alcohol to emulsifier were required for methanol and ethanol, respectively, to create stable emulsions. The maximum alcohol content was limited in emulsion or solution, to avoid the engine knocking due to a reduction in the cetane number. The thermal efficiency was improved at low load only compared to that of diesel.

Hardenberg and Schaefer [64] investigated the use of 95% ethanol with 1% castor oil in a fleet of trucks and buses in Brazil. They stated that the quality of ethanol had a strong influence on its corrosive effects. They also studied the viscosity and lubricity properties of the fuel. The evaporation time of the ethanol-diesel blends was found to be less due to the lower viscosities and increasing surface area of smaller Sauter mean droplet diameters.

Hardenberg and Ehnert [65] described the effect of ignition quality and cetane number of ethanol-diesel blends, when they were used as fuels in a diesel engine. They estimated that the cetane number of ethanol was between 5 and 15, and when it was blended with diesel, it lowered the cetane number. Generally, a lower cetane number may exhibit a longer ignition delay which can allow more accumulation and more time for vaporisation of fuel. The initial burning rates were reported to be faster, and sudden peak heat releases were obtained at a constant volume, which was a more efficient conversion process of heat into work. They reported that this might also lead to the noisy operation of the engine. Sometimes, more addition of ethanol might hinder the ignition quality due to a fall in the cetane number below 30. So, it was suggested to add an ignition improver to increase the cetane number of the ethanol–diesel blends, so that they would fall within the acceptable range equivalent to that expected of diesel.

Schaefer and Hardenberg [66] discussed a number of biomass derived nitrates as ignition improvers for the ethanol-diesel blends. They reported that triethylene glycol dinitrate

(TEGDN) was a satisfactory ignition improver for the ethanol-diesel blends, which is manufactured from ethanol itself.

Boruff et al. [67] used organic additives to form co-solvents and micro emulsions of aqueous ethanol and diesel blends, and also checked the suitability of these fuels in a naturally-aspirated, water cooled, DI diesel engine. The micro emulsion of 190-proof ethanol with diesel was done using a surfactant prepared from unsaturated (soybean) fatty acids, N, N dimethyl ethanolamine, 2·amino-2·methyl-l·propanol, and named as hybrid fuels. The detergentless micro emulsion was prepared by using 1-butanol, and was found to be superior in engine performance compared to ionic micro emulsion which was prepared from soybean fatty acids. The engine was able to achieve higher power and brake thermal efficiency compared to that of diesel with these hybrid fuels. Also, the exhaust gas temperature, exhaust smoke (about 64%) and CO emission were found to be lower with the hybrid fuel operation.

Letcher [68] evaluated the use of some co-solvents and ternary diagrams for the stability of the ethanol-diesel blends. The solubility of ethanol in diesel was affected mainly by two factors, the water content and temperature of the blend. This was avoided by the addition of a co-solvent and an emulsifier. Co-solvents allowed fuels to be ‘‘splash-blended’’ which simplifies the blending process, but emulsification usually required heating and blending steps to generate the final blend. He identified tetrahydrofuran and ethyl acetate as effective co-solvents, which were obtained from agricultural waste materials and ethanol respectively. He concluded that the ratio of ethyl acetate to ethanol to ensure complete miscibility down to 0 °C was 1:2.

Battelle [69] studied the flammability limits and storage of the ethanol–diesel blends. He considered 10%, 15% and 20% of the ethanol–diesel blends in his test. With the ethanol addition, the flash point of the blends decreased. More ethanol in the blends formed a vapour at the head of the storage tank, and was flammable in storage tanks at 12-42 °C, compared to diesel which was flammable at 64-150 °C. So, flame arrestors were installed in the filler necks. About 10-20% ethanol blends showed similar properties to those of diesel.

Gerdes and Suppes [70] have explained that the aromatic content and intermediate distillate temperature would have a significant impact on the miscibility limits of the ethanol-diesel blends. The miscibility of ethanol in diesel was improved with a reduction of the aromatic

content of diesel. It also had an effect on the amount of emulsifier required for stable emulsion.

Satge de Caro et al. [71] conducted experiments in DI and IDI engines by using 10-20% ethanol-diesel blends. They used two additives to get stability and to improve the ignition quality of the blends. They added 2% each of two additives such as 1-octylamino-3-octyloxy-2-propanol and dinitrated derivative *N*-(2-nitrato-3-octyloxy propyl), N-octyl nitramine for comparison purposes. They concluded that the additives kept the cetane number above 45, which ensured suitable ignition. The cetane number was increased by about 2% with 10% ethanol-diesel emulsions compared to that of diesel. When 20% of ethanol with an additive was used, the cetane number was found to be decreased by about 6.5% compared to that of diesel. The ignition delay was reported to be longer and cyclic irregularities were observed, when the ethanol content was increased in the emulsion. The performance and emission details are shown in Fig. 2.4 and Fig. 2.5 at full load.

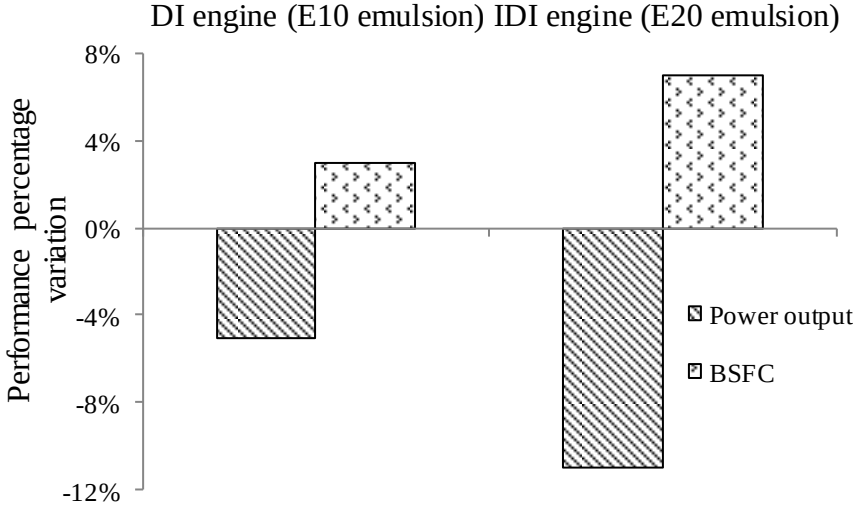

Fig. 2.4 Percentage variations of performance parameters

Hansen et al. [72] reviewed research works related to bioethanol-diesel fuel blends in diesel engines. They summarised that the ethanol percentages of 10% or less had no noticeable differences in the performance compared to diesel. They also mentioned that the addition of ethanol to diesel fuel would have a beneficial effect in reducing at least the particulate matter (PM) emissions. The NOx emission was reduced, while the CO and THC emissions were marginally higher than those of diesel. It was suggested that an advanced emission control system could minimise the CO and THC emissions. A small adjustment in the fuel injection system would be required for better results. Also, proper storage, handling and dispensing of bioethanol and diesel blends would be required.

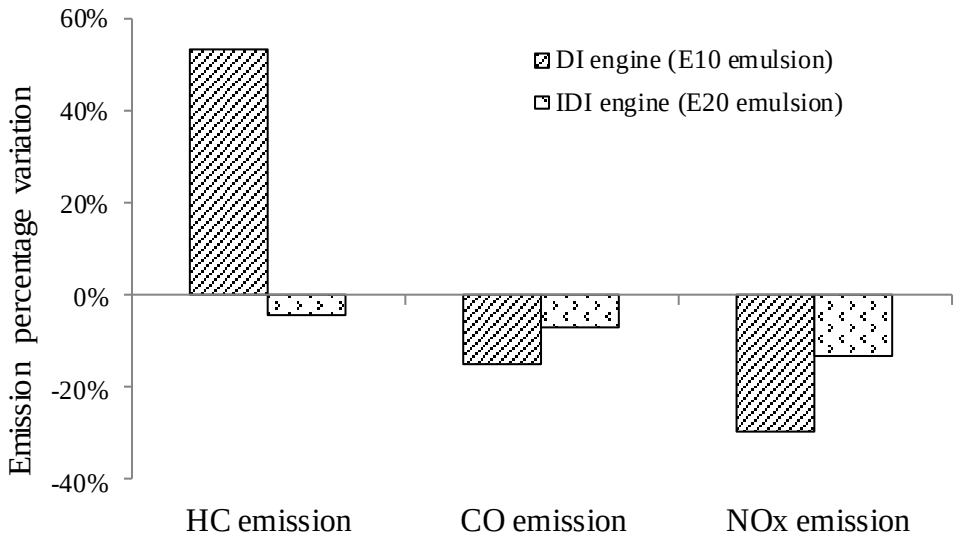

Fig. 2.5 Percentage variations of emission parameters

Lapuerta et al. [73] examined the stability range and effect of temperature, water content in the blends. They considered the test conditions of a sample as 5 °C and 2.5% water up to E-20 blend. The separation ratio was also discussed for better results of stability. They concluded that the blends with the bioethanol contents up to 10% v/v could be used in diesel engines, in countries where winter temperatures rarely fall to 5 °C. And blends with 7% bioethanol, such as those commercially used, could be used in even colder countries.

Rakopoulos et al. [74] investigated the performance and emission parameters of a six-cylinder, turbocharged and after-cooled, heavy duty, direct injection (DI), Mercedes-Benz engine, fueled with 5% and 10% (by vol.) of bioethanol in the bioethanol-diesel blends. The specific fuel consumption was observed to be higher with increasing percentage of bioethanol in the blends and the efficiency was marginally improved. The smoke density was significantly reduced with the bioethanol-diesel fuel blends, with respect to that of diesel with a corresponding increase in the percentage of bioethanol in the blend. A marginal increase in the HC emission was observed with the blends, and also the NO and CO emissions were marginally reduced in comparison with diesel at full load, with the increase in the percentage of the ethanol content. Figure 2.6 shows the percentage variation in the performance, and Fig. 2.7 shows the percentage variation in the emission parameters compared to those of diesel at full load.

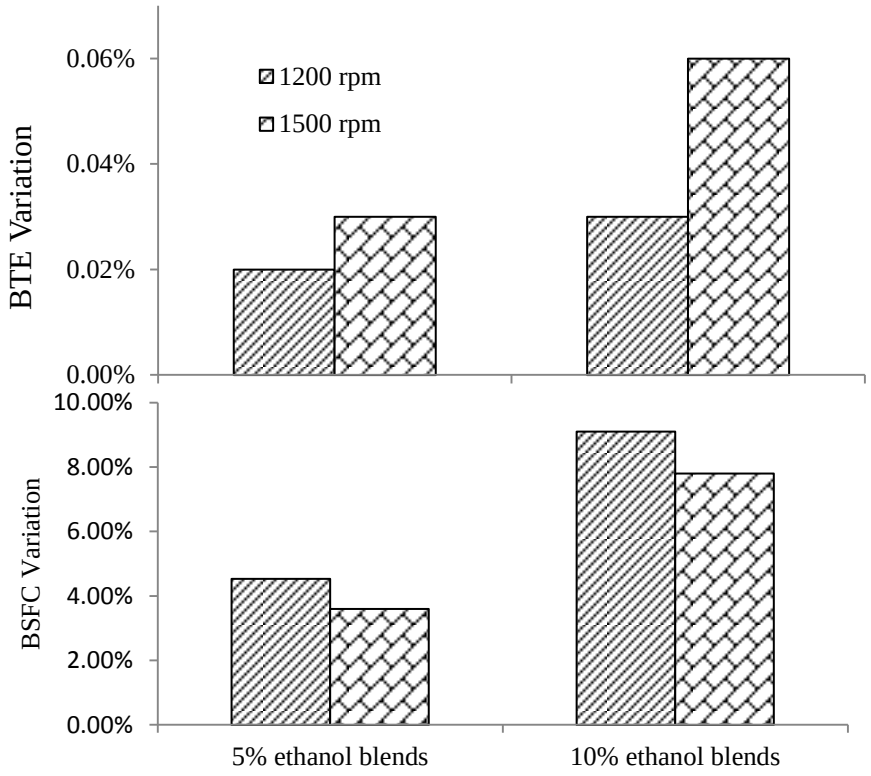

Fig. 2.6 Percentage variations of performance parameters

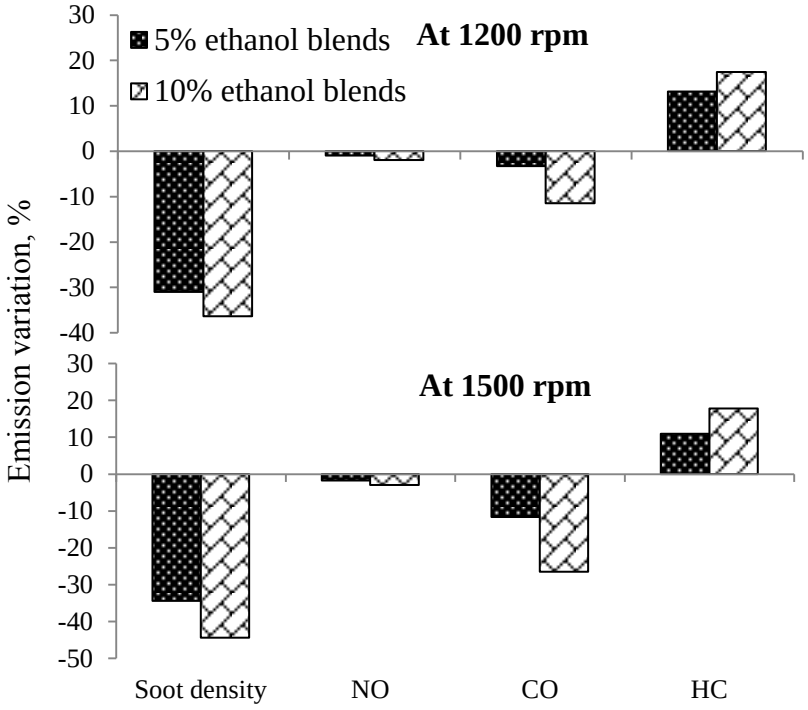

Fig. 2.7 Percentage variations of emissions parameters

Li et al. [75] studied the effects of ethanol-diesel blends in a single-cylinder DI diesel engine with ethanol of 5%, 10%, 15% and 20% blend on volume basis and found that BTE, BSFC, and THC were increased while the CO, NOx and smoke emissions were significantly reduced in comparison with neat diesel fuel.

Kumar et al. [76] studied the effect of addition of emulsifier at different percentage on the performance, combustion and emission characteristics of a DI diesel engine. They prepared the ethanol-diesel micro-emulsions with the addition of ethyl acetate (EA) emulsifier at the volume percentage of 7%, 13% and 17% and ethanol value of 13%, 17% and 23%. They reported that, the phase separation did not occur with ethanol-diesel micro-emulsions containing 13% of ethanol and 7% of EA, for which the BSEC and BTE were improved without any power reduction at a lower load. The NO and smoke emissions were found to be decreased, while the HC and CO emissions were increased at lower loads. The HC and CO emissions were improved at higher loads, but BSEC was increased.

Arapatsakos et al. [77] used ethanol amount of 20% to 30% on a volume basis in the diesel–ethanol blends, and studied the performance and emission characteristics of a 4-cylinder John Deer Tractor engine at full load. The concluded that, the addition of ethanol showed a positive effect on the CO and HC emissions, but a negative effect on engine power due to the small calorific value of ethanol.

Huang et al. [78] investigated the engine performance and exhaust emissions of a single cylinder, four stroke, and water cooled DI diesel engine fueled with 10%, 20%, 25% and 30% ethanol-blended diesel fuels with and without additive. The additive n-butanol about 5% was used to increase the blend stability and properties. The BTE found to be decreased as the amount of ethanol in the diesel–ethanol blends increased. The smoke emission was observed to be lower when the engine was fueled with the blend compared to that of neat diesel at full load. The CO emission was noticed to be lower at and above half loads compared to that of diesel, but were higher at low loads and low speeds. The HC emission was higher except at full loads and high speeds, while NO emissions varied at different speeds, loads and blends.

Ganesh et al. [79] emulsified ethanol at a percentage of 30%, 40% and 50% by volume with diesel using sorbitan monooleate as a surfactant and conducted the experiment in a single cylinder, four-stroke, water cooled, DI diesel engine to determine the effects of

emulsion/blend on the performance, combustion and emissions. They concluded that the 50% ethanol–diesel blend was best, compared to those of diesel and other blend ratios. Using the optimal blend, the delay period was reduced at a 24° injection angle. The BTE and NO emissions were found to be increased, but smoke density and PM were reduced, and the maximum heat release, peak pressure, cumulative heat release and cylinder pressure were noticed to be increased.

Song et al. [80] carried out the engine experiment in a 6-cylinder, heavy duty, non-catalyst turbocharged intercooler DI diesel engine with diesel and ethanol-diesel fuel blends at 1200, 1800 and 2600 rpm and studied the carbonyl emissions from the engine. They used the ethanol amount of 15% with a stability additive of 0.3% and 1.2% in diesel to prepare the blends/emulsion. The experimental results revealed that acetaldehyde was the foremost carbonyl produced by both fuels, followed by formaldehyde, acrolein, acetone, propionaldehyde and crotonaldehyde. The addition of ethanol to diesel fuel resulted in a decrease in acrolein emissions, while the other carbonyls increased at low engine speed. The brake specific emissions of each carbonyl compound decreased with the increase in engine load during the constant speed test. Carbonyl carbon (CBC) emissions from both diesel and the diesel–ethanol blends were found to be the highest at a high engine speed, while the total CBC emissions from the ethanol–diesel blends were higher than those from diesel under most engine operating conditions.

Banugopan et al. [81] investigated the performance and emission characteristics of a single cylinder, four stroke, water cooled, DI diesel engine using ethanol-diesel emulsion/ blends. They added 1% of isopropanol with 10%, 15%, 20%, 25% and 30% of ethanol-diesel blends, as an additive for enhancing homogeneity and preventing a phase separation. The inlet air was preheated to 40, 50 and 60 °C. The total fuel consumption (TFC) and specific fuel consumption (SFC) increased as ethanol concentration increased, while the BTE was found to be decreased without preheating. Simultaneously, they observed that preheating inlet air had negative effect on CO and HC emissions.

Lei et al. [82] studied the effects of ethanol-diesel blends on performance and emissions characteristics of a turbo-charged diesel engine under different atmospheric pressures (81, 90 and 100 kPa) conditions and compared the results with that of diesel. The amount of ethanol/bioethanol considered for the blend was 10%, 15%, 20% and 30% by volume basis.

They found that, the BSFC was significantly improved below 90 kPa, but a sharp increase in HC and CO emissions with increasing engine speed, load and the ethanol con-centration were observed at 81 kPa. On the other hand, atmospheric pressure and ethanol blending percentage did not affect NO emission at 90 and 100 kPa, while smoke was reduced below 90 kPa.

2.4.2 Use of cetane improvers

Low cetane number fuels generally have a tendency to exhibit longer ignition delay due to their ignition quality. The ignition quality can be improved by adding small quantities of ignition improvers or cetane number improvers. Examples of ignition improvers are organic peroxides, nitrates, nitrites and various sulphur compounds. Earlier, alkyl nitrates (isopropyl nitrate, primary amyl nitrates, primary hexyl nitrates, octyl nitrate) were commercially used. By adding these improvers, the ignition characteristics of poorer quality diesel fuel, particularly alcohols, will be improved when they are used in CI engines. The use of ignition improvers or cetane improvers offers two advantages when they are used with alcohols: firstly, alcohols can be used in CI engines without any major engine modification; and secondly, they offer total replacement of diesel fuel in diesel engines. An ignition improver of up to 15% by volume would normally be required to enable the ignition of alcohol fuels in CI engines. The cost of these additives is high, and hence, they are not largely used. In addition to these improvers, some cetane improvers produced from biomass can be used. Examples of these are Diethyl ether (DEE) and Dimethyl ether (DME).

Lyford-Pike et al. [83] operated a 14 litre, six cylinder, diesel engine with an ignition-improved ethanol. Hydrated ethanol (95% v/v) was used together with additives for ignition improvement, lubrication and protection against corrosion. The composition of the fuel was developed by Mercedes-Benz with the following additives:
(a) Alicolita (4.5% v/v)-this is a Tri Ethyl Glycol Di - Nitrate (TEGN) based additive; it promotes self - ignition in ethanol and mixes with hydrated ethanol
(b) Castor oil (1 % v/v) - used to improve the lubricating properties of ethanol
(c) Max lub 8027 (0.025% v/v) - used for protection against corrosion.

They modified the engine by operating it at different higher compression ratios, with the inclusion of a turbocharger, change of injectors, injection timing and duration and calibration of the fuel pump. They reported that by doing all this, the engine attained high in-cylinder temperatures and pressures necessary to promote self-ignition and to sustain combustion.

They changed the compression ratios to evaluate their effect on ignition delay for the ethanol operation. They concluded that, an overall decrease of 5 ^{o}CA in ignition delay was observed with an increase in compression ratio from 15.8:1 to 16.5:1. The engine attained a peak cycle pressure of 114 bar and achieved the same power output as that of diesel operation in the same engine. At rated load, the brake thermal efficiency of the alcohol engine was 38%, better than that of the corresponding diesel engine. The opposite was true at part load conditions.

Hodgson [84] evaluated the performance and emissions of a Perkins based naturally aspirated, 4 cylinder, DI diesel engine, running on ignition improved ethanol and methanol at a compression ratio of 16:1, which was the same as that for a diesel fueled engine. They changed the fuel pump and injectors to allow for expected larger fuel deliveries with the alcohol fuels. Higher brake thermal efficiency was reported when running on ignition improved ethanol than with gasoil on the corresponding standard engine.

Cai et al. [85] discussed the use of different percentages of a cetane enhancer (i.e. 0, 0.2, 0.4%) in 15% v/v ethanol-diesel blends, in a high speed diesel engine. Table 2.5 gives the percentage variation in performance and emission parameters with the addition of an ignition improver compared to that of diesel at full load.

Table 2.5 Percentage variation in parameters

Performance parameters	E15-D with 0.2% CN improver	E15-D with 0.4% CN improver
BSFC	+6.9%	+4.2%
BTE	+17.8%	+21.4%
Emission parameter		
Smoke	-44.8%	-45%
NO	-3.5%	-15.1%
HC	+20.7%	-42.1%
CO	-11.7%	-12.2%

They concluded that the brake specific fuel consumption (BSFC) increased, the diesel equivalent BSFC decreased, and the thermal efficiency improved remarkably. The NOx and smoke emissions decreased simultaneously. The ignition delay was found to be prolonged, and the total combustion duration shortened for the ethanol-diesel blends compared to that of diesel.

Ren et al. [86] studied the combustion and emission characteristics of a DI diesel engine, fueled with the diesel-ethanol blends (E5, E10, E15 and E20) and an ignition improver. They have added 0.2 vol% CN improver (isoamyl nitrite) with 5, 10, 15 and 20 vol% ethanol fraction in diesel. The ignition delay and premixed combustion duration of fuel blends with E10 and additives were found to be similar to those of diesel. They reported that the maximum rate of heat release increased with the increase in the ethanol mass fraction in the blends compared to that of diesel. The diesel equivalent BSFC was found to be lower, with an increase in the ethanol fraction at full load. Also, there was a simultaneous reduction of NOx and smoke compared to that of diesel. The percentage variations in the performance and emission parameters are given in Table 2.6.

Table 2.6 Percentage variations in parameters

Performance parameters	E5A	E10A	E15A	E20A
BSFC	+2.4%	+2.6%	+2.9%	+3.2%
BTE	-3.8%	+2.4%	+3.4%	+4.1%
Emission parameter				
Smoke	-7.8%	-22%	38%	56%
NO	-7.4%	-6.1%	-8.6%	-11.3%

Pidol et al. [87] discussed the use of ethanol-diesel blends in a low temperature combustion (LTC) engine. They have used fatty acid methyl ester (FAME) to increase the stability of the blends, and also to improve the cetane number. The flash point obtained was found to be decreased below -17 °C.

Can et al. [88] added an unsaturated fatty acid-based solvent as an additive and isooctyl nitrate as an ignition improver to the ethanol (10–30 vol%) -diesel blend in a single cylinder engine. The physicochemical properties and stability of the blend was observed to be improved. Also, they concluded engine emissions varied with changes in engine operating conditions, ethanol content, additives and ignition improver.

Ashok [89] added DME, DEE and H_2O_2 as additives with the diesel-ethanol emulsified fuel, and studied the performance, combustion and emissions of a diesel engine using these emulsified fuel. He showed that the higher cetane number of DME and DEE has led to a better performance, combustion and emission of a diesel engine. The oxygen enriched DME and DEE provided a lesser fuel consumption than H_2O_2 added ethanol diesel emulsion fuel.

The presence of oxygen in the fuel reduces self-ignition temperature and increases cetane number. As a result, the emulsified fuels with DME and DEE start burning early but release a lesser amount of heat with the improvement of premixed combustion phase. He stated that more the oxygen-enriched additive in fuel, higher is the value for cetane number of emulsified fuels and lower is the NO emission. Also, he concluded that the addition of DME and DEE with 50:50 ethanol-diesel emulsion have shown to improve BTE.

Ashok [90] extended the investigated to study effect of using emulsified ethanol-diesel fuel with 5% water and 6% H_2O_2 with the presence of hydrophilic surfactant TWEEN80. He concluded that the emulsified fuel without water showed a better performance than same with water. The presence of water reduces the quantity of free oxygen in the emulsion and hence the cetane number of the same.

2.4.3 Dual injection

The dual injection technique uses two separate injection systems, one for diesel fuel and the other for alcohol fuel. Combustion is started by injecting a small quantity (pilot) of diesel fuel before a larger quantity of alcohol is injected through the main nozzle. The pilot injection acts as an ignition source for the alcohol fuel. It is reported that up to 95% (vol) replacement of diesel fuel would be possible with the dual injection method [59]. The cost involved in this method for engine modification would be certainly high, because it would be necessary to include complex fuel control and metering systems. In addition to engine modification additives for lubrication would be required to ensure a satisfactory life.

Padala et al. [91] performed the experiment in a single-cylinder, common-rail, DI diesel engine based on dual fuel technology. They introduced the ethanol into the intake manifold using a port-fuel injector while diesel was injected directly into the cylinder and investigated the effect of ethanol energy fraction and the diesel injection timing on the engine efficiency and the tailpipe emissions. From the ethanol energy variation tests at fixed diesel injection timing, it was found that increased ethanol energy fraction increased the engine efficiency until the operation was limited by misfiring associated with an over-retarded combustion phasing. By energy fraction, up to 60% of diesel was replaced by ethanol, which achieved 10% efficiency gain compared with the diesel-only operation. The HC, CO and NO emissions were found to be increased with an increasing ethanol fraction.

Britto and Martins [92] conducted an experiment with a single cylinder, DI, diesel engine in a dual fuel mode where ethanol was injected with electronically controlled injector. They used two different combustion chamber for quiescent, and high swirl flow development, three different compression ratios of 14:1, 16:1 and 17:1, two injectors with a flow rate of 35 g/s and 45 g/s, and four diesel injection pressures namely 800, 1000, 1200 and 1400 bar. They concluded that, CR of 16:1 allowed the highest substitution rates, but it had some disadvantages in relation to 17:1 of CR, since the latter led to a greater efficiency. The indicated efficiency using ethanol was found to be higher with the lower injector flow rate (35 g/s) than using higher flow injectors (45 g/s). The maximum substitution of ethanol at loads greater than 5 bar IMEP was observed to be 51% with the higher flow injector at 800 bar injection pressure.

Britto and Martins [93] studied the emission results of diesel-ethanol, dual-fuel system of the engine. The NO emission was reduced up to 60% ethanol substitution with a higher injector flow, compression ratio of 17:1, and high swirl flow structure. The HC and CO emissions were found to be increased in the dual fuel mode.

2.4.4 Fumigation

Many researchers have proposed and used this technique to investigate CI engines run with methanol, ethanol and butanol. They introduced alcohols into the engine with the intake air. This method requires less engine modification than for dual fuel injection. A maximum of 50% (vol) replacement of diesel fuel would be possible, with the level of replacement limited by the onset of detonation of the air-fuel mixture. An accurate control of the fuel flow would be necessary in order to prevent misfire at light loads and knocking at high loads. The volumetric efficiency of the engine would reduce, and result in a power drop.

Ajav et al. [94] conducted the performance and emission test in a single cylinder, diesel engine using vaporised ethanol at the intake manifold with the help of a carburettor. They made a comparison between unheated and preheated vaporisation of ethanol at 50 °C. The BSFC with unheated and preheated vaporisation of ethanol was found to be lower by about 23% and 14% compared to that of diesel at full load. Up to 75% load, there was a decrease in the brake thermal efficiency, and after that there was a marginal increase with vaporised ethanol compared to diesel. At full load, the brake thermal efficiency was higher by about 8% and 6% with unheated and preheated vaporisation of ethanol compared to that of diesel. The

CO emission was higher by about 12.6% and 60.2% compared to that of diesel at full load. The NO emission was 0.4% higher with unheated vaporisation, while it was 0.7% lower with preheated vaporisation compared to that of diesel at full load. Surawski et al. [95] have performed the emission tests on a pre-Euro I, four-cylinder, Ford 2701C engine with the ethanol fumigation at two different speeds (2000 and 1700 rpm). The particle size was found to be half, with a higher substitution of ethanol fumigation compared to that of ethanol diesel blends, at full load. Heisey [96] also reported that by fumigating ethanol and methanol in amounts of up to 55% of the total fuel energy, the ignition delay and CO was found to be higher, and NO and thermal efficiency were found to drop at heavy loads.

Surawski et al. [97] have assessed the impact of the gaseous and particle emission concentrations in a 4-cylinder Ford 2701C engine by ethanol fumigation. The fumigation technique delivered the vaporised ethanol (10 to 40% by energy) into the intake manifold of the engine, using an injector, a pump and pressure regulator, a heat exchanger for vaporising ethanol and a separate fuel tank and lines. The NO and PM emissions were observed to be lower than those of diesel at full load. But, the BSCO and BSHC emissions increased considerably compared to those of diesel at full load. They have used a diesel oxidation catalyst to reduce the BSHC and BSCO emissions.

Chauhan et al. [98] conducted experiments in a small capacity diesel engine with a constant injection of ethanol at the intake manifold along with the air, to study the emission parameters. Ethanol was introduced in the intake manifold of the engine using a carburettor and its quantity was controlled by a butterfly valve according to the variation of loads. The conclusions made from the results were that, there was an improved performance and reduced NO and smoke emissions with the 15% of ethanol fumigation. The CO emission decreased with respect to an ethanol substitution at 20 and 45% load, but the HC emission was found to be increased during the entire engine operation.

Bodisco et al. [99] have conducted an experimental investigation on a modern turbo-charged inline 6-cylinder Cummins diesel engine (ISBe220 31) with a common rail injection system at 2000 rpm on neat automotive diesel and with the ethanol fumigation substitutions of 10%, 20%, 30%, and 40% at full load (760Nm), and at three quarters (570Nm) and half (380Nm) of full load. The combustion analysis indicated that on 40% substitution of ethanol, the ignition delay began to decrease, which may be due to the early ignition of the fumigated

ethanol. They have concluded that, there was an increase in the inter-cycle variability with the high substitutions of ethanol.

Lopez et al. [100] investigated the combustion characteristics, performance, emissions, particle number concentration and size distribution of an automotive diesel engine using hydrous ethanol and n-butanol fumigation at intake manifold. They observed that, both the alcohols exhibited higher premixed combustion peaks, faster combustion process, and higher coefficient of variation of indicated mean effective pressure (imep) and reduced maximum in-cylinder temperature, in comparison with the ultra low sulfur diesel (ULSD) irrespective of loads. Neither n-butanol nor hydrous ethanol presented better brake thermal efficiency (bte) and brake specific fuel consumption (bsfc) than ULSD. Both alcohols increased carbon monoxide (CO) and total hydrocarbons (THC) and reduced nitrogen oxides (NOx) and particulate matter (PM), in comparison with ULSD fuel. The n-butanol showed the best trade-off (PM vs NOx + THC) among all fuels. In comparison with ULSD, hydrous ethanol fumigation decreased the total number concentration of particles, while maintaining or increasing the geometric mean diameter, depending on the engine load. In comparison with ULSD, n-butanol maintained or reduced the total number concentration of particles and exhibited the opposite trend for the geometric mean diameter. The particle number concentration (PNC) and size distribution were not affected by engine load for n-butanol.

Sahin et al. [101] evaluated the combustion, smoke index (K) and oxides of nitrogen emission and performance parameters of a turbocharged IDI automotive diesel engine using ethanol fumigation at three diesel fuel delivery rates (FDRs), different engine speeds and various ethanol fumigation ratios (EFR). Ethanol was introduced into intake air by a carburetor, which main nozzle section is adjustable, given approximately 2%, 4%, 6%, 8%, 10% and 12% (by vol.) ethanol ratios. The experimental results showed that smoke index K reduced for up to 4–8% EFRs but then it began to increase. The ethanol fumigation tests results showed that the NOx emission values were lower than that of neat diesel fuel (NDF). The NOx emission decreased approximately 8.5%, 9.79% and 11.02% for 1/1, 3/4 and 1/2 FDRs respectively, at the selected engine speeds. For ethanol ratios higher than 8–10%, the engine performance parameters improved for 1/1 and 3/4 FDR, but they deteriorated for 1/2 FDR at selected engine speeds. In heat release rate diagram, two distinct peaks were observed for high ethanol additions. The first peak occurs before top dead center (TDC) and the second peak takes place after TDC.

2.4.5 Surface ignition

Alcohol fuels have a very low resistance to ignition on hot surfaces**.** Therefore, many researchers have used this technique [102]**.** The hot surface was used to ignite alcohol fuels in diesel engines. The technique offers possibilities for a complete substitution of diesel fuel with alcohol fuels. Many researchers have used a glow plug as a heating source for surface ignition. It was reported that the location of the fuel injector is an important factor, because the glow plug should not be affected by the direct impingement of the fuel spray on it.

Nagalingam et al. [103] developed a single-cylinder diesel engine with a rated power of 3.7 kW (5hp) to use alcohol fuels with an ignition assistance by a hot surface. They included a plug that incorporated a heated surface in the engine. With this arrangement they were able to run the engine at a compression ratio of 8.8:1 or 14.7:1. The original engine compression ratio was 16.5:1. They conducted the performance tests at engine speeds of 1000, 1500 and 2000 rpm. The injection timing was kept constant at 31 °CA bTDC (static setting). At the compression ratio of 8.8:1 and engine speed of 1500 rpm, the brake thermal efficiency curves for ethanol and methanol were found to be similar. The brake thermal efficiency curves for methanol, ethanol and petrol at a compression ratio of 14.7: 1 and engine speed of 1000 rpm were compared. The engine efficiency when running on petrol was found to be marginally better than that of methanol or ethanol. The engine was also run as a conventional CI engine on diesel at a compression ratio of 14.7: 1 (i.e.) without the use of the hot surface ignition. The brake thermal efficiency of the engine running in this mode was comparable to that of methanol at both 1000 and 1500 rpm. The maximum brake thermal efficiency recorded was 23%. They reported that it was possible to run the engine without the ignition assistance at high load and speed conditions, and especially, after a period of running with the ignition assistance. They also reported that there was a marginal increase in the ignition delay when operating without the ignition assistance with the heating plug.

Kapus et al. [104] conducted experiments in a glow plug assisted methanol engine. They reported that the emission levels from the methanol fueled engine complied with the Austrian legislative requirements, and also had high fuel economy. They also indicated that the nozzle configuration (symmetrical/asymmetrical) affected the engine performance in terms of the brake specific fuel consumption and emissions. The four hole asymmetrical nozzle showed a marginally better performance than the corresponding four hole symmetrical nozzle.

2.4.6 Spark ignition

The use of a spark plug to ignite the alcohol-air mixture would result in a minimal ignition delay and achieve smooth combustion [59]. A complete replacement of diesel fuel would be possible with a spark ignition. Johns et al. [105] reported that advancing the injection timing for alcohol fuel would be necessary. By doing this, the alcohol fuel will have sufficient time to vaporise and mix with air, to form an ignitable air-fuel mixture before it would be ignited by the spark plug. Newnham [106] used a conventional single spark automotive ignition system in his research work. He reported that this technique was a little complex, because it required a complete spark-ignition system in addition to the fuel injection system of diesel. He converted a standard single cylinder, naturally aspirated, DI diesel engine to run on alcohol fuels with a spark-assistance. He studied the effect of injection and ignition timings on the overall performance of the engine. He also evaluated the heat release rates of the fuel-air mixture over a range of injection and ignition timings. He reported that it was difficult to achieve smooth running of the engine on alcohol, at the original full power and speed specification. This was the case even when the original fuel pump was changed to one which was capable of delivering a larger volume.

2.5 Bioethanol-biodiesel-diesel blends

Biodiesel can be used with bioethanol-diesel blends to get the solubility and stability of the blends. It also improves the lubricity properties of the blends. When it is used in a diesel engine, it also reduces the diesel fuel consumption. Many research works have been documented, relating to the use of biodiesel in bioethanol-diesel blends in diesel engines.

Shi et al [107] used the blend ratio of 5:20:75 (ethanol: methyl soyate: diesel fuel) by volume in a heavy duty diesel engine. They observed that the NO and PM emissions were reduced significantly, whereas the CO emission was not conclusive; it depends upon the engine operating conditions. The THC from the blended fuel was lower than that of diesel fuel, under most of the controlled experimental conditions.

Kwanchareon et al [108] prepared diesohol blends (80% diesel, 15% biodiesel and 5% ethanol) and made an attempt to use them in a commercial single cylinder, vertical, four stroke, air cooled, DI diesel engine. They studied the emission characteristics of the engine. They have observed that the CO and HC emissions were reduced significantly at higher loads, whereas the NOx emission was increased, in comparison with diesel.

Chen et al [109] added vegetable methyl ester to the ethanol-diesel blends to study the solubility of the blends. They used the blends to study the emission characteristics of the Cummins 4B, four cylinder, diesel engine. They found that both the PM and smoke emissions were reduced. The CO emission was increased at lower loads and middle loads, whereas it was decreased at higher loads and full loads.

Chotwichien et al [110] used palm oil alkyl esters as additives in the ethanol-diesel and butanol-diesel blends. The addition of alcohol to diesel decreased the fuel properties such as fuel density, kinematic viscosity and cetane number, and these can be compensated by adding biodiesel to the bioethanol-diesel blend. They concluded that butanol has a higher solubility in diesel than ethanol, and it improved the fuel properties of the blends. They also concluded that the blend of 85% diesel, 10% palm oil ethyl ester, and 5% butanol provided a stable mixture and acceptable fuel properties for use as an alternative fuel in diesel engines.

Rahimi et al [111] studied the emission behaviour of a commercial RD270 Ruggerini, two cylinders, in-line, air cooled, naturally aspirated, DI diesel engine fueled with the ethanol-sunflower methyl ester-diesel blends (diesterol). They used bioethanol produced from potato waste. They observed that the fuel properties, such as flash point and viscosity of the blends, were reduced by increasing the amount of ethanol in the blends. The NO, CO and smoke emissions were reduced by increasing the biofuel composition of diesterol throughout the engine operating range.

Subramanian et al [112] used the diesel-ethanol-pungamia methyl ester blends in a multi cylinder, naturally aspirated, DI diesel engine. They compared the combustion, performance and emission parameters of the engine with diesel. They concluded that the brake thermal efficiency of the engine was marginally higher than that of diesel at full load. The smoke and NOx emissions were lower, but the HC emission was higher compared to that of diesel at full load.

Yilmaz [113] studied the performance and emission characteristics of the two-cylinder, liquid-cooled, DI, Kubota GL-7000 diesel engine fueled with biodiesel-methanol-diesel (BMD) and biodiesel-ethanol-diesel (BED) and results were compared with diesel fuel. He concluded that the biodiesel-alcohol-diesel blends resulted in a higher BSFC and CO and HC emission, whereas NO emission was found to be lower compared to those of diesel. The

methanol blends were more effective than ethanol blends for reducing CO and HC emissions, while NO reduction was achieved by ethanol blends.

Sukjit et al [114] have added rapeseed methyl ester (RME) to the alcohol-diesel blends to study the effect of carbon chain length and degree of unsaturation, on the combustion and emission behaviour of a diesel engine. They used both ethanol and methanol fuel for the alcohol-diesel blends. Also, they gave emphasis to the stability and lubricity properties of the alcohol-diesel blends. They concluded that the addition of 15% of all methyl esters was enough, to avoid the phase separation of the alcohol-diesel blends, and keep the wear scar diameter of the blends below the limitation required by the lubricity standard. The CO and soot emissions of the alcohol blends were found to be lower compared to those of biodiesel blends with the same oxygen content.

Di etal. [115] studied the emissions of a DI diesel engine fueled by ultra-low sulphur diesel with ethanol and biodiesel (2%, 4%, 6% and 8% in volume) used as oxygenated additives. The BTE improved slightly as the amount of ethanol and biodiesel in the fuel blends increased, while the HC and CO emissions found to be decreased, but NOx emission increased compared to those of neat diesel.

Tse et al. [116] investigated the influence on the combustion characteristics and particulate emissions of a 4 cylinder, naturally-aspirated, DI diesel engine fueled with DBE (diesel-biodiesel-ethanol) blended fuels at a steady state speed of 1800 rev/min under five engine loads. The diesel-biodiesel was blended with 0%, 5%, 10% and 20% of ethanol. They concluded that, the DBE blends effectively reduced brake specific particulate mass (BSPM), brake specific number concentrations (BSPN). With the increase of ethanol in the blended fuels, the ignition delay became longer for the DBE blend. The in-cylinder pressure and peak heat release became higher and retarded due to a more fuel burned in the premixed burning phase.

Oliveira et al. [117] tested the effects of fuel blends containing 5, 10 and 15 wt.% of anhydrous ethanol in diesel oil with 7% of biodiesel (B7) on the performance, emission and combustion characteristics of a diesel power generator were investigated at the different applied load varied from 5 to 37.5 kW. The results showed that the in-cylinder peak pressure, and the heat release rate were decreased at low loads and increased at high loads with the use

of ethanol in the blend. Also, it was observed that the increasing ethanol concentration in the blend caused the increased ignition delay, decreased the combustion duration and reduced the exhaust gas temperature. The CO, HC and NO emissions showed different behavior, depending on the load and ethanol concentration.

2.6 Conclusion

From the review of literature carried out, it is understood that there was no work on the utilisation of bioethanol obtained from the Madhuca Indica flowers as an alternative fuel for CI engines. The Madhuca Indica seed is always chosen as potential feedstocks for biodiesel production. The trees are largely available in coastal areas. It can grow any arid and non-arid regions. These flowers are used for local ethanol production. Most of the R&D, Ministry of New and Renewable Energy and Ministry of Rural Development are promoting such bioethanol production from biomass which will substitute even minor percentage of diesel. Generally, the Madhuca Indica flower is composed of a large amount of sugar than that of other feedstocks. Presently, research is mainly focused on exploration of large amount of biofuel from the biomass to mitigate the demand of energy security as well as reduction of engine tail pipe emissions which is the measure cause of climate change. The bioethanol derived from the biomass provide the significant reductions in GHG and smoke emissions compared to those of gasoline and diesel fuels. Though a lot of work has been carried out on utilization of bioethanol, the researcher tried to explored bioethanol from new biomass feedstocks and decided to first characterize bioethanol for its suitability to be used as an alternative fuel for a CI engine, by using various instruments, and then to adopt different techniques for its possible utilisation.

2.7 Objectives of the study

The objectives of the research work are as follows;

- To derive bioethanol from Madhuca Indica flower, a forest residue available in significance quantity in India.
- To characterize the bioethanol for its suitability for alternative fuel for an engine.
- To ensure the substitution of bioethanol to diesel by maximum percentage by evaluating combustion, performance and emission of a single cylinder, four stroke, air cooled, DI diesel engine adopting few fuel modification and engine modification.
- To validate the experimental results.

- To improve the lubricity properties by adding small quantity of biodiesel.
- Durability study for long term benefit.

The present work is in the early stage of research in utilizing bioethanol obtained from the Madhuca Indica flower as an alternative fuel for CI engines. The results of the research work are established for the first time.

CHAPTER 3

FUEL CHARACTERISATION

3.1 General

Whenever an alternative fuel is proposed, it is necessary to thoroughly study the availability of the raw material or feedstock for production. Once, the feedstock is chosen for production, the feedstock is subjected to one or more processes for producing the fuel. This may need mechanical processes such as classification, drying, grinding, and mixing, whichever is appropriately required before subjecting the feedstock to chemical processes that require converting the feedstock to fuel. The chemical processes may be of any kind, such as heating, distillation, esterification etc., according to the nature of the feedstock used for fuel production. Once the fuel is produced, it has to be characterized for its suitability as a fuel, according to the type of engine in which it will be used as an alternative fuel. This chapter discusses the method of bioethanol produced, and its characterization using the FTIR, GC-MS analysis. In addition to this, the chapter presents the physico-chemical properties of bioethanol used in this study.

3.2 Bioethanol from the Madhuca Indica flowers

3.2.1 Availability of feedstock

In the present investigation, bioethanol was produced from a flower from an Indian tropical tree-Maduca Indica. The tree is also known as Madhuca longifolia, Mahuwa or Mahua or Illuppai, and is found largely in the central and north Indian plains and forests in the Indian subcontinent. The botanical names of the tree are Bassia longifolia L., B. latifolia Roxb., Madhuca indica J. F. Gmel., M. latifolia (Roxb.) J.F.Macbr., Illipe latifolia (Roxb.) F.Muell., Illipe malabrorum (Engl.). In a technical report [118], it is mentioned that, it is a fast-growing tree that grows to approximately 20 meters in height, possesses evergreen or semi-evergreen foliage, and belongs to the family Sapotaceae. It is generally grown in an arid environment, being a prominent tree in tropical mixed deciduous forests in India in the states of Chhattisgarh, Jharkhand, Uttar Pradesh, Bihar, Maharashtra, Madhya Pradesh, Kerala, Gujarat and Orissa, in the Indian subcontinent. The Madhuca Indica tree and the flower are shown in Fig. 3.1 and Fig. 3.2 respectively.

Fig. 3.1 Madhuca Indica tree

Fig. 3.2 Madhuca Indica raw and dry flowers

It is considered as a holy and popular tree in the tribal belt of central India, where it is culturally most identified with Indian life in the plains. Its flowers are sweet, delicious and are consumed, besides its tasty fruits. But, the tree is popular due to the liquor produced from the flowers, which is used to make vinegar. The seeds yield fat known as Mahua butter is used in cooking, adulteration of Ghee, manufacturing chocolates and even soaps, besides the treatment of rheumatism and constipation. The seeds are also considered as one of the potential non edible feedstocks for biodiesel production in India. Mahua cake is insecticidal and is used for fishing. The Mahua flowers are edible and are a food item for tribals. The flowers are used to make syrup for medicinal purposes. The tribal people from the above mentioned states drink the country liquor (Mahua drink) obtained from the flower as a part of their cultural heritage. It is an essential drink for tribal men and women during celebrations. The main ingredients used for making it are granular molasses (chhowa gud) and dried Mahua flowers. The flowers are also used to manufacture jam. The flowering season extends from February to April in a year. It is rich in sugar (73%) and next to cane molasses. The yield of alcohol is 405 litres from one tonne of dried flowers. The kernel of the Mahua fruit contains about 50% oil. The oil yield by a small expeller is 34-37%. The annual production of Madhuca Indica flowers in India in the year 2006 was estimated to be approximately 48, 000 Metric tonnes [52-53].

3.2.2 Fermentation using *Saccharomyces cerevisiae*

Bioethanol was produced from the Madhuca Indica flowers by the fermentation process, using *Saccharomyces cerevisiae*. Figure 3.3 shows the production process of bioethanol from the Madhuca Indica flowers. The fresh flowers of Madhuca Indica were collected from a village in India, cleaned properly to remove the adhering soil particles, and dried in the

sunlight. The yeast (*Saccharomyces cerevisiae*) was cultured on Yeast extract nutrient broth (YENB) having 5% glucose and 1% of yeast extract for 48 h. The Madhuca Indica flowers were pretreated for the extraction of sugars. The flowers of Madhuca Indica and distilled water in a 2:1 ratio were autoclaved, at a pressure of 68.2 kPa for 15 min.

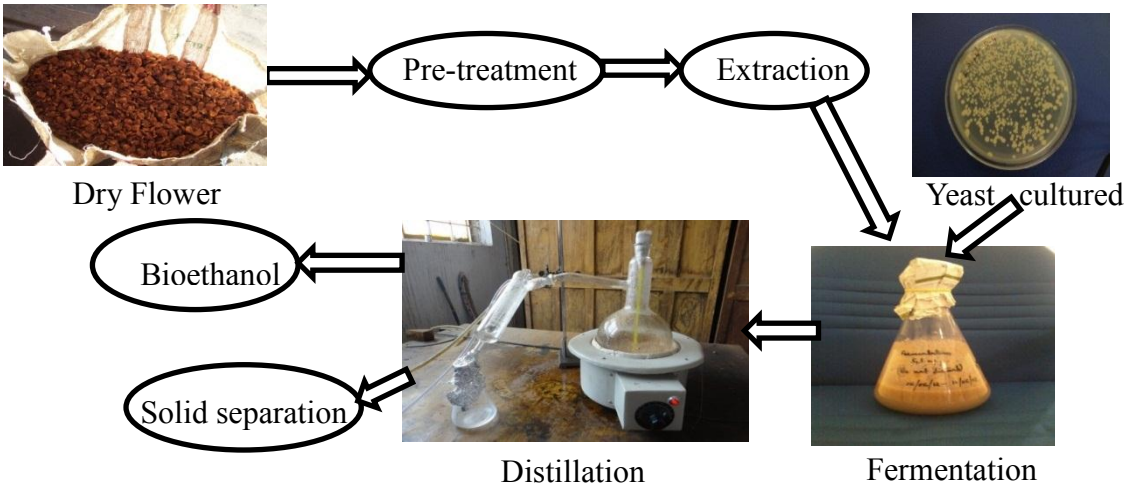

Fig. 3.3 Production process of bioethanol from the Madhuca Indica flowers

For the fermentation, a starter culture was added at the rate of 10% (v/v) to the Madhuca Indica extract taken in a 1000 ml Erlenmeyer flask, and fermentation was carried out in a batch on the laboratory bench at a temperature of 30 °C ± 2 °C for 96 h. After the fermentation process, first distillation was done to get the crude extract, and further, the fractional distillation was done for the removal of water. The steps involved for checking the purity of bioethanol by an alcoholmeter are shown in Fig. 3.4.

% of Alcohol = [1.05\(initial specific gravity–final specific gravity)\100]/final specific gravity.

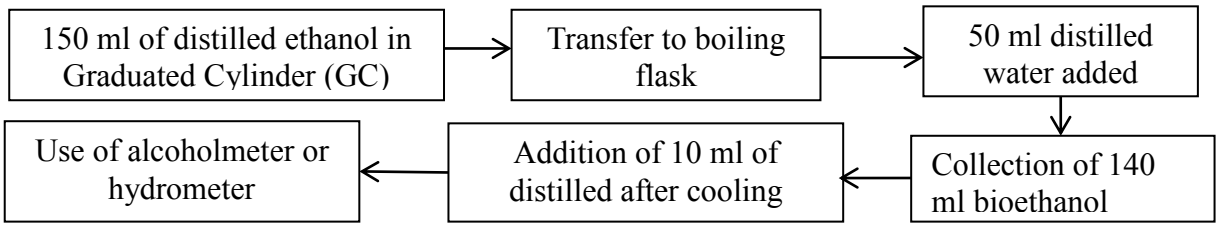

Fig. 3.4 Steps involved in checking the purity of bioethanol

The purity of bioethanol was checked by an alcoholmeter. Also, the conversion efficiency from sugar to bioethanol in the fermentation can be given as the overall ethanol yield (%).

Overall bioethanol yield= (concentration of bioethanol produced/ initial concentration of sugar added)*(1/0.51)*100= (5.067 g/10 g)*(1/0.51)*100=99.35%

where 0.51 indicates the theoretical ethanol yield (0.51 g-ethanol/g-sugar). The bioethanol yield is the ratio of the amount of bioethanol produced divided by the amount of sugar consumed during fermentation.

3.3 Characterisation of bioethanol

3.3.1 Identification of group compounds by FTIR

The FTIR offers a quantitative and qualitative analysis for organic and inorganic samples. It identifies the chemical bonds in a molecule by producing an infrared absorption spectrum [119]. The spectra produce a profile of the sample, a distinctive molecular fingerprint that can be used to screen and scan samples for many different components. The FTIR is an effective analytical instrument for detecting functional groups and characterizing covalent bonding formation. The FTIR test was carried out with a Perkin Elmer RX1 instrument which has a scan range of 450-4000 cm^{-1} with a resolution of 1.0 cm^{-1}. The photograph of the Perkin Elmer RX 1 is shown in Fig. 3.5. The results of the FTIR analysis are in the form of a graph, plotted between the wave length and the percentage transmittance, which will give the information about the position of various bond vibrations distinguished by several modes such as stretching, distortion, bending etc.

Fig. 3.5 Photograph of Perkin Elmer RX 1

Figure 3.6 shows the FTIR spectra present in bioethanol and diesel.

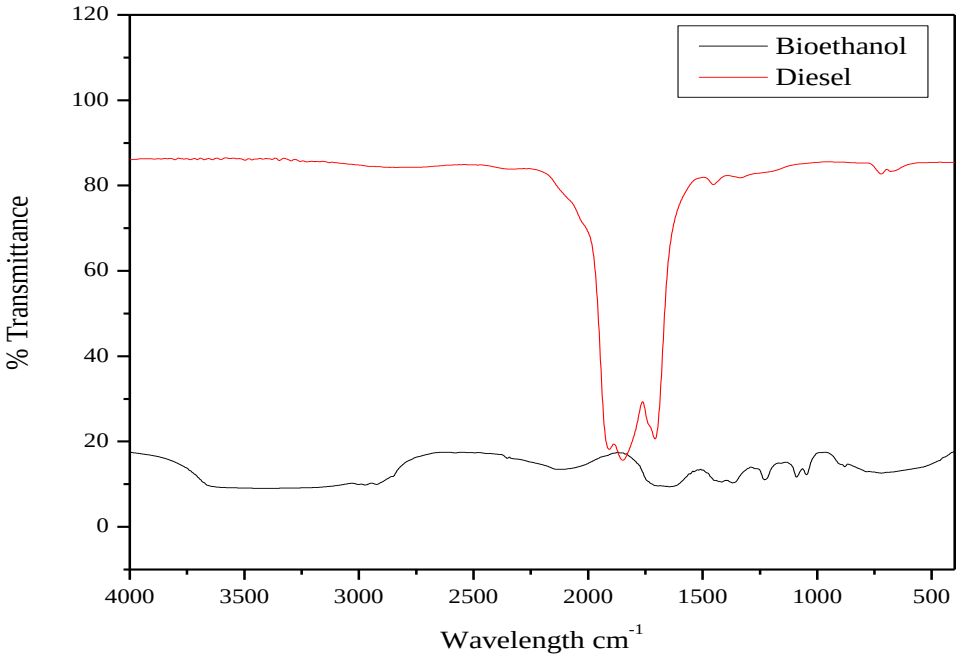

Fig. 3.6 FTIR spectra of bioethanol and diesel

From the FTIR analysis of bioethanol it was found that, the O-H stretching vibrations at 3401.8 cm^{-1} indicate the presence of alcohols and phenols. The C≡N stretching vibrations at 2122.1 cm^{-1} show the presence of nitriles. The presence of alkenes/aromatics was detected by the C=C stretching vibrations at 1644.1 cm^{-1}. The O-H bending vibrations at 1369.3 cm^{-1} show the presence of alcohols and phenols. The presence of amines is detected by the C-N stretching vibrations at 1230.2 cm^{-1} and also it represents the presence of acids, esters, ether and alcohols by C-O stretching. The species present in bioethanol and diesel are presented in Table 3.1 and Table 3.2 respectively.

Table 3.1 Various bonds present in bioethanol

Bond	Wave number(cm^{-1})	Wave length(μm)
O-H Stretch	3401.88	2.7 – 3.3
C≡C, C≡N Stretch	2122.08	4.2-4.8
C=C, Stretch	1644.12	5.9-6.3
O-H, Bending	1369.25	6.9-8.3
C-O,C-N Stretch	1230.16	7.7-11.1
Phosphate	1089.86	9.0-10.0
C-H	720.06	11.1-16.7

Table 3.2 Various functional bonds, peak and wavelength of diesel

Bond	Wave number(cm^{-1})	Wave length(µm)
C-H,Stretch	2921.33	3.0-3.7
C-H, Stretch	2812.72	3.0-3.7
C=C, C=N, Stretch	1605.47	5.9-6.3
O-H, Bending	1461.19	6.9-8.3
Nitrate	1376.55	7.2-7.4
C- Cl	722.05	13-14
C-Br	468.67	15-20

3.3.2 GC-MS analysis

The GC-MS is known as gas chromatography and mass spectrometry, and it identifies and quantifies the volatile and semi volatile organic compounds in complex mixtures. It also determines the molecular weights and elemental compositions of unknown organic compounds in complex mixtures [120]. The photograph of the Perkin Elmer GC-MS instrument is shown in Fig.3.7.

Fig. 3.7 Perkin Elmer GC-MS instrument

The GC-MS analysis of bioethanol extracts were done in the GC clarus 500 Perkin Elmer and the Gas chromatograph is interfaced to a Mass Spectrometer (GC-MS) equipped with an Elite-1 fused silica capillary column. An electron ionization system with ionizing energy of 70 eV was used for its detection. The carrier gas, Helium with a purity of 99.99% was sent at a constant flow rate of 1 ml/min and an injection volume of 2 µl was employed (Split ratio of 10:1); the injector temperature was 250°C; and ion-source temperature 280°C. The oven temperature was programmed from 110°C (isothermal for 2 min) with an increase of 10°C/min, to 200°C, then 5°C/min to 280°C, ending with a 9 min isothermal at 280°C. A mass spectrum was taken at 70 eV, a scan interval of 0.5 seconds and fragments from 45 to

450 Da. The total GC running time was 36 minutes. The relative percentage of each component was calculated by comparing its average peak area to the total areas, which were managed by the software present with the system. The main components present in the bioethanol from the GC-MS analysis are shown in Table 3.3.

Table 3.3 GC-MS results of bioethanol

Area %	Retention time(RT)	Compound name
28.74	8.402	Nonanoic acid, 9-bromo-, ethyl ester, 10-Bromodecanoic acid, ethyl ester, Octanoic acid, ethyl ester
8.37	11.060	Nonane, 1,1-diethoxy- Ethyl 3,3-diethoxypropionate, Decane, 1,1-diethoxy-
23.69	11.249	Ethyl tridecanoate , Decanoic acid, ethyl ester
11.63	13.718	Ethyl 13-methyl-tetradecanoate ,Heptadecanoic acid, ethyl ester
19.90	17.261	Hexadecanoic acid, methyl ester Hexadecanoic acid, methyl ester, Hexadecanoic acid, methyl ester
7.67	17.915	Hexadecanoic acid, ethyl ester Hexadecanoic acid, ethyl ester 1H-Indole, 5-methyl-2-phenyl-

3.3.3 Ultimate analysis and fuel properties

It is necessary to determine the elemental composition of a hydrocarbon substance which is proposed as an alternative fuel [121]. The ultimate analysis of a fuel helps to predict the reasons for pollutant formation in an engine. Table 3.4 gives the elemental analysis of bioethanol obtained from the Madhuca Indica flowers, in comparison with diesel.

Table 3.4 Elemental analysis of bioethanol and diesel

Component	Diesel	Bioethanol from the Madhuca Indica flowers
Chemical formula	$C_{10}H_{22}$	$C_{1.723}H_{4.348}O$
Molecular weight	144	41.024
C wt%	86	54
H wt%	13.60	14.489
N wt%	0.18	0.23
S wt%	0.40	0.717
O wt %	0	38.564
Molar ratio	6.32	3.72

It is also very important to know the fuel properties, such as density, heating value, flash and fire points, pour point, boiling point, sulphur content, carbon residue etc., when an alternative fuel is to be investigated for its use in an engine. These physical properties certainly affect the performance, emission and combustion parameters of the engine [122]. The important physical properties of bioethanol obtained from the Madhuca Indica flowers were determined in a standard fuel testing laboratory in India, compared with those of diesel fuel properties and listed in Table 3.5. The uncertainty of the instruments used for the measurements of fuel properties are given in Annexure I.

Table 3.5 Fuel properties of bioethanol obtained from the Madhuca Indica flowers and other feedstocks

Properties	ASTM Standard	Diesel	B1 [123]	B2 [74]	B3
Specific gravity @ 40 °C	D 4052	0.863	0.790	0.78	0.80
Lower heating value [MJ/kg]	D 4809	43.8	26.4	26.8	29.38
Flash point [°C]	D 2500	49	22	13	24
Cold filter plugging point [°C]	D 6371	-19	Nil	Nil	<-30
Pour point [°C]	D 97	-15	-116	-117	-103
Boiling point [°C]	D 7169-11	180–360	78	78	80
Sulphur content [wt%]	D 093	0.049	0	0	0
Bulk modulus of elasticity [bar]	D 6793	16000	Nil	13200	13800
Kinematic viscosity at 40 °C [cSt]	D 445	2.58	1.36	1.35	1.73
Moisture content [wt %, wet basis]	Nil	0.025	Nil	Nil	10
Ash [wt%, dry basis]	Nil	0.13	Nil	Nil	Nil
Carbon residue[%]	D 2500-05	0.1	Nil	Nil	Nil

Note B1- Bioethanol from sugar molasses, B2-Bioethanol from sugarcane, B3- Bioethanol from the madhuca indica flowers

3.4 Discussion of fuel properties

The discussion of different fuel properties are given as,

Density: The density is calculated from the specific gravity of the fuel. The engine performance characteristics and engine oil are affected by the density of fuel. It also affects the fuel atomisation efficiency and combustion characteristics. Other properties like cetane number, and heating value are also associated with density of fuel. The injection system used for diesel fuel, measures the fuel by volume thus the variation of the fuel density will affect the output power of the engine due to an altered mass of injected fuel. Generally, higher density causes a greater fuel flow resistance which results in a higher viscosity which may lead to inferior fuel injection. The density of ethanol is inferior to diesel fuel density.

Heating value: It is a property to determine its suitability as an alternative to diesel fuel. Calorific value is very important and lower heating value or the net calorific value of a fuel influences the power output of an engine directly. The calorific value of bioethanol is less than diesel fuel. The variation of the heating value of the bioethanol derived from the Madhuca Indica flowers is about ±3% of values of other feedstocks.

Flash point: It is a property of a fuel and referred for storage. It is the point at which fuels are flammable. The diesel fuel have a higher flash point than that of ethanol which means diesel is safer than ethanol to transport and storage.

Cold filter plugging point (CFPP): It is the temperature at which the test filter starts to plug due to fuel components that have started to gel or crystallize. CFPP mainly used to indicate the low temperature operation ability of any fuel and reflects their cold weather performance. CFPP required for the fuel which is a climate-dependant.

Pour point: It is the lowest temperature at which a liquid can flow. As the temperature of a fuel approaches to its pour point it becomes cloudy due to the formation of crystals and finally the crystals solidify. This causes major operability problems. Generally, ethanol has an extremely low pour point compared to that of conventional diesel.

Kinematic viscosity: It affects the fuel drop size, the jet penetration, quality of atomization, spray characteristics and the combustion quality. Very high or low viscosity of fuel affects

the engine. For example, if the viscosity is very low, then it will not provide enough lubrication which will increase wear and leakage. A higher viscous fuel will form a larger droplet during injection, which affects combustion quality thus lead to a higher exhaust emission. The viscosity of ethanol is lower than diesel fuel.

Sulfur levels: It is added to the diesel fuel to improve the anti-wear performance to match that of conventional winter grade diesel fuels with sulfur levels mainly in the range of 0.1-0.2% m/m. If sulfur value is more than that of desirable amount, it produces more sulfur dioxide emission in the engine exhaust which is the cause of acid rain.

3.5 Production cost of one litre of bioethanol

The cost of one litre of bioethanol production in laboratory level process is given below;
For one litre bioethanol, the amount of dry flowers required is 5 kg (approximately).
After the fermentation process, the bioethanol extraction requires three units of energy consumption. Again, in the fractional distillation process five unit of energy is consumed.
Then the cost of one litre bioethanol production in rupees (Indian currency) is= (cost of 5 kg flower) + (cost of 8 unit) + tax=25+18.4+4=Rs 47.4 (or $ 0.77)
The comparison of the production cost of bioethanol from the Madhuca Indica flowers and other feedstocks is given in Table 3.6.

Table 3.6 Comparison of production cost of bioethanol

Feedstocks	Average price (Rs./L)
Sugar cane	25.04
Wheat	45.9
Corn	54.25
Sugar beets	45.9
Lignocellulosic materials	62.60
Madhuca indica flower	50

CHAPTER 4

EXPERIMENTATION AND METHODOLOGY OF PRESENT WORK

4.1 General

In order to have a perfect measurement in an experimental investigation, to study the combustion, performance, and emission parameters of a CI engine run on any alternative fuel, it is essential to chalk out the plan of work and select the engine to be used for investigation, and the necessary instrumentation. Also, it is important to know the principles of operation and use, and the procedure to be followed in conducting the experiments for each and every module of the investigation. Whatever the brand and type of engine, the acquired one must be first converted according to the requirement of the present investigation. In this chapter, the preliminary work carried out before the start of the investigation, the experimental set up, the experimental procedure and the method of calculating the parameters are described.

4.2 Elementary work for investigation

The following elementary steps were carried out before starting the investigation:

1. The required test fuel-bioethanol of about 50 litres was produced for the study. The fuel sample was characterized by its physico-chemical properties for its suitability as an alternative fuel. The fuel was also characterized for its group compounds by FTIR and GC-MS as described in Chapter 3.

2. The fuel consumption would be higher if a multi cylinder engine is used for the investigation. Also, as this is an early stage in the investigation to establish the bioethanol obtained from the Madhuca Indica flowers as an alternative fuel for CI engines, a single cylinder, four stroke, air cooled, DI diesel engine with a developing power of 4.4 kW at a rated speed of 1500 rpm was selected for the investigation.

3. An experimental setup was developed to conduct experiments with fuel or engine modifications to evaluate the combustion, performance and emission parameters at different loads of the engine. The necessary fuel and air measuring instruments were selected and incorporated in the experimental setup, and they are discussed in the subsequent sections.

4. A piezo-electric pressure transducer was flush mounted on the cylinder head to obtain the pressure data of the engine. A top dead center (TDC) marker was mounted on the flywheel for obtaining every crank angle of the piston. The descriptions of the pressure sensor and TDC marker are given in the subsequent section 4.3.3.

4.3 Experimental setup

Figure 4.1 shows the overall schematic diagram of the experimental set up used for all the experiments conducted in the investigation.

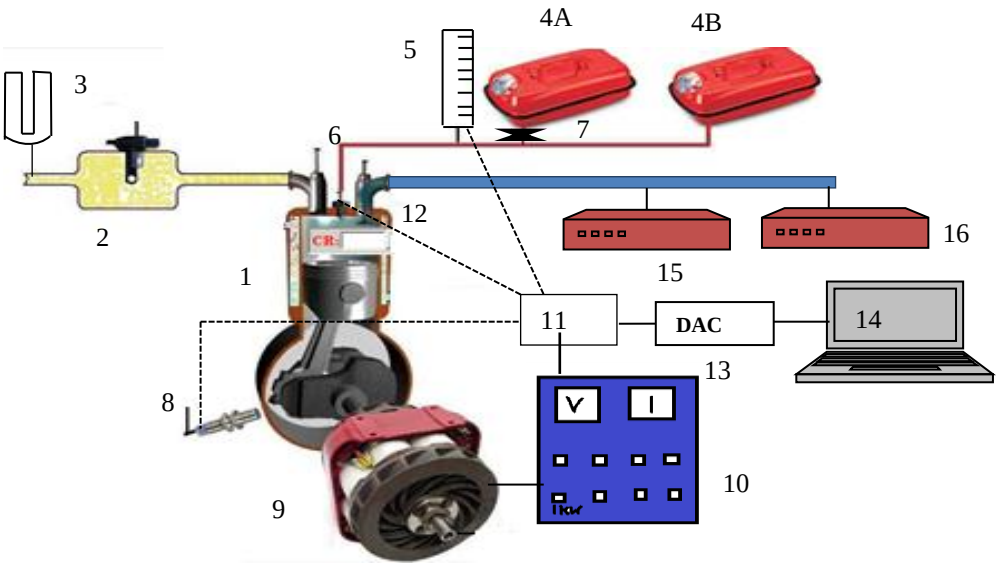

1. Engine	5. Burette	11. Control panel
	6. Fuel injector	12. Pressure transducer
2. Air box	7. Valve	13. Data acquisition card
3. U-tube manometer	8. Crank angle encod	14. Personal computer
4A.Fuel tank for diesel	9. Alternator	15. AVL437C smoke meter
4B.Fuel tank for emulsion	10. Load cell	16. AVL Digas 444 analyser

Fig. 4.1 Schematic diagram of the experimental setup

A photographic view of the experimental setup is shown in Fig. 4.2.

Fig. 4.2 Photographic view of the experimental setup

4.3.1 Test engine

The test engine used in this investigation was a Kirolaskar TAF-1, single cylinder, four-stroke, air cooled, constant speed, DI diesel engine (1). The technical specifications of the engine are given in Appendix A1. The general experimental setup provided in the study is discussed below;

An air box (2) is fixed with the intake manifold of the engine to maintain a constant suction pressure, to facilitate a constant air flow through the orifice meter. An orifice meter is attached with the anti-pulsating drum, to measure the volume of air drawn into the cylinder with the help of a U-tube manometer (3). It gives the reading of the difference in the water level in two columns, which is used to calculate the water head in terms of the pressure difference. Fuel tanks (4A) and (4B) are used to store diesel and an alternative fuel (bioethanol-diesel emulsion/blends/bioethanol) respectively. A burette (5) is fitted with two optical sensors one each at the high and low levels of both the ends. Fuel is drawn from a six litre capacity fuel tank to the burette under gravity. When fuel passes through the optical sensor, it sends a signal to the computer for automatic start/stop of time required for the fixed amount of fuel supply, i.e. 20 cc, to measure the fuel consumption and again the burette is refilled automatically for the next measurement. A fuel injector (6) injects fuel when it receives fuel from fuel pump. A two way valve (7) is fitted after fuel tank (4A). A crank angle encoder is fitted to the output shaft to measure the crank angle (8). The engine is

coupled with an alternator (9) which is connected to a load cell (10) bank for loading purpose. As the armature of the alternator is rotated by the engine, the field current/field strength will be induced, which tends to pull the field coils and the casing along with it. This rotation can be opposed in the same way as with the hydraulic dynamometer. This induced field strength is usually dissipated as heat through the banks of the electrical resistances. The load and speed can be increased or decreased on the alternator and thereby on the engine, by switching on or off the load resistances in the load cell bank, and by varying the field strength. A non-contact type PNP sensor gives the pulse output for each revolution of the crank shaft for the measurement of the engine speed in revolution per minute (RPM). A control panel (11) is used to regulate the resistance that offers load to the engine. A pressure transducer (12) is flush mounted into the combustion chamber to receive pressure pulses. All the data received from the engine are collected by a data acquisition system (13), processed and displayed in a personal computer (14). An AVL 437C smoke meter (15) measures the smoke density of the exhaust gas. The unburnt hydrocarbon (HC), carbon monoxide (CO), and nitric oxide (NO) emissions are measured with the help of an AVL 444 Digas analyser (16). The acquired pressure data for every crank angle are given as inputs to software to calculate the remaining parameters like ignition delay, heat release rate, and combustion duration. A K-type (Cr Al) thermocouple with a sensor is used for the measurement of the exhaust gas temperature with a temperature range of 0-900^{o}C.

4.3.2 Exhaust gas measurements

4.3.2.1 CO and CO_2 measurements

The CO and CO_2 species in the exhaust of the engine are measured with the help of the gas analyser that works on the non-dispersive infrared (NDIR) principle [124]. Figure 4.3 gives the pictorial information of the gas analyser which uses the NDIR principle. The instrument has two remote sampling heads controlled by a main control unit, and is capable of sampling CO and CO_2 simultaneously in two locations. Each constituent gas in a sample will absorb some infra-red rays at a particular frequency. By shining an infra-red beam through a sample cell (containing CO or CO_2), and measuring the amount of infra-red absorbed by the sample at the necessary wavelength, the NDIR detector is able to measure the volumetric concentration of the CO or CO_2 in the sample.

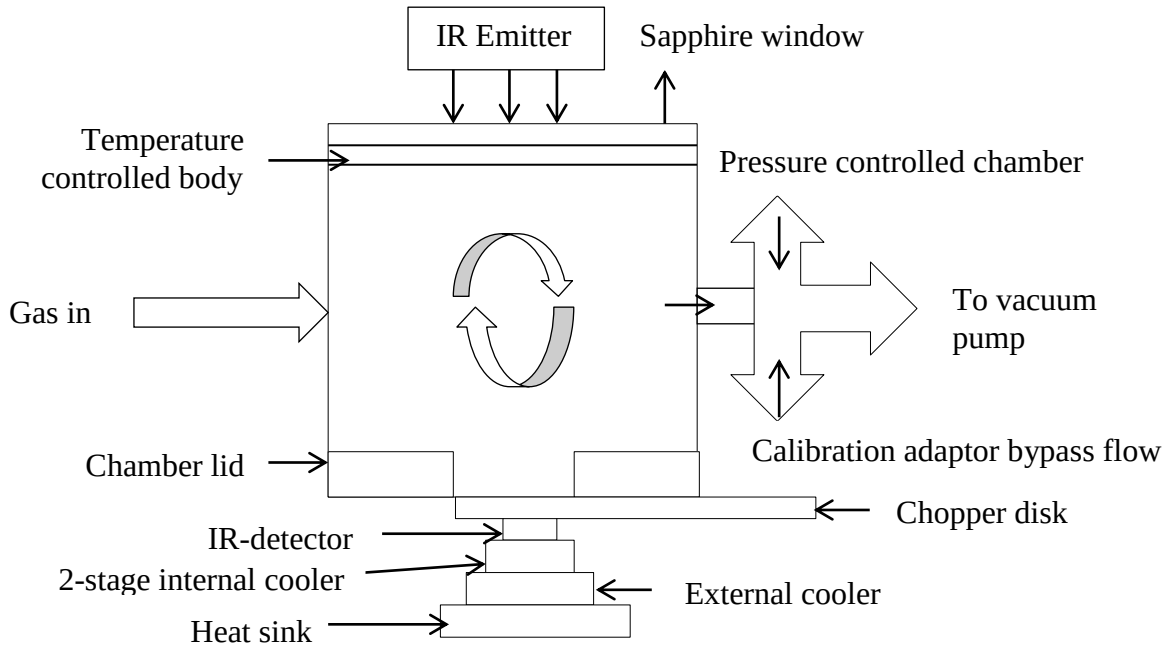

Fig. 4.3 NDIR principle for measuring the CO/CO_2 species in the exhaust [124]

A chopper wheel mounted in front of the detector continually corrects the offset and gain of the analyser, and allows a single sampling head to measure the concentrations of two different gases.

4.3.2.2 FID for HC measurement

The flame ionisation detector (FID) is the industry standard method of measuring HC concentration [125].

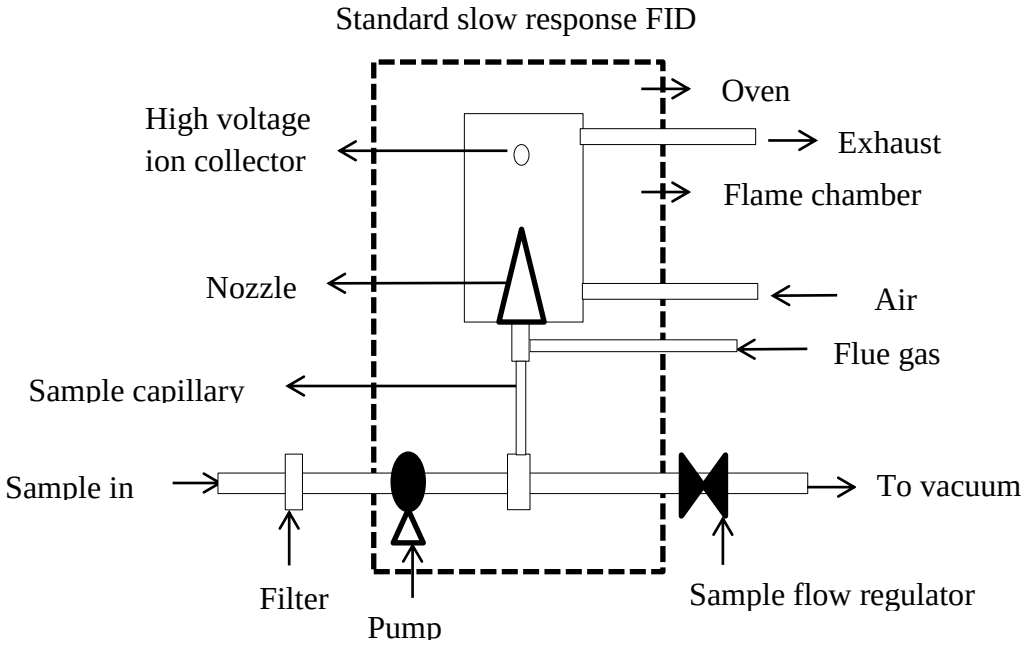

Fig. 4.4 FID principles for HC measurement [125]

Figure 4.4 illustrates the working principle of the FID technique that is used to measure the HC component in the engine exhaust. The sample gas is introduced into a hydrogen flame inside the FID. Any hydrocarbons in the sample will produce ions when they are burnt. The ions are detected using a metal collector which is biased with a high DC voltage. The current across this collector is thus proportional to the rate of ionisation, which in turn, depends upon the concentration of HC in the sample gas. The ionisation process is very rapid, and hence, the slow time response of the conventional FIDs is mainly due to sample handling. A typical slow analyser might have a response time of 1-2 seconds.

4.3.2.3 Electrochemical principle for NO measurement

The electrochemical principle for the NO measurement is used to find out the controlled and uncontrolled emissions from the combustion sources, such as boilers, heaters, engines and turbines. Generally, it measures the emissions of NO, nitrogen dioxide (NO_2), and the sum of their concentrations (NO_x). The electrochemical principle is based upon the use of the electrochemical sensors, in which the reacting gases are used to generate electrical signals proportional to the gas concentrations. It consists of the sensing electrode (or working electrode) and a counter electrode separated by a thin layer of electrolyte. The working principle is shown in Fig.4.5.

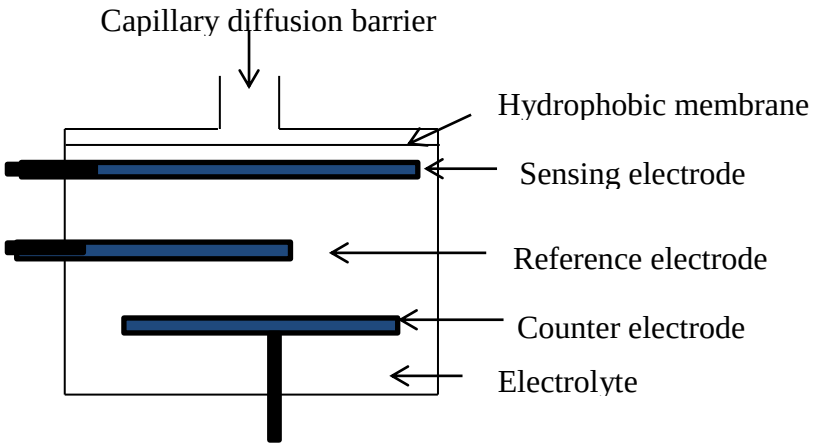

Fig. 4.5 Electrochemical principle for NO measurement

The exhaust gas first passes through a small capillary type opening, diffuses through a hydrophobic barrier, and then it reaches the electrode surface. These approaches can prevent the leaking of the electrolyte from the sensor. Then, the gas that diffuses through the barrier can react at the surface of the sensing electrode involving either an oxidation or reduction mechanism. According to the desired gas of interest, the reactions are catalyzed by the

electrode materials. With a resistor connected across the electrodes, a current proportional to the gas concentration flows between the anode and the cathode. The current is measured to determine the gas concentration. Because the current is generated in the process, the electrochemical sensor is often described as an amperometric gas sensor or a micro fuel cell [126].

The reactions at the sensing electrode (anode) for some gases are as follows:

$$NO + 2H_2O \rightarrow HNO_3 + 3H^+ + 3e^- \quad (4.1)$$

Some sensors are used for the reduction reaction of the target gas, such as the reduction of nitrogen dioxide, chlorine, and ozone at the cathode, produce water as a by-product.

$$NO_2 + 2H^+ + 2e- \longrightarrow NO + H_2O \quad (4.2)$$

All the above mentioned principles are incorporated in a gas analyser provided by AVL Ltd. Therefore, the researcher used AVL Digas 444 analyser in this investigation. At the exhaust of the engine, the probe of the gas analyser is inserted and kept for a few minutes for the measurement of unburnt HC in ppm, CO in vol%, and NO in ppm. The NO emission is measured by a photochemical sensor. A photographic view of the exhaust gas analyzer is shown in Fig. 4.6. The detailed specifications of the AVL DiGas 444 analyzer are presented in Appendix A2. The recommended periodic calibration of the gas analyzer was carriedout, in order to ensure the accuracy of measurement. The gas analyzer's electronics, optics and its response to environmental factors were checked through calibration. The general calibration procedure involves the injection of calibration gases of known concentration, and validating the response. The compositions of CO, CO_2 and HC gases are; 3.5% volume of CO, 14% volume of CO_2, 2000 ppm volume of propane and the remainder nitrogen, whereas the calibration gas for the NO component is 2200 to 3000 ppm volume of the NO and the remainder N_2.

Fig. 4.6 Photographic view of the exhaust gas analyzer

The instrument outputs are then adjusted to the known inputs to correct the variations in the electronic response due to temperature effects, drift, or other interferences. Thus, the accuracy of the analyser is assured, and an accurate response to the sampled gas is achieved after calibration.

4.3.2.4 Diesel smoke measurement

In the early days, smoke from the diesel engine exhaust was measured with the help of filter papers. Later on, due to the advancement in instrumentation, smoke from a diesel engine exhaust was measured with the help of the Hatridge smoke meter principle. The principle of the working of the diesel smoke meter is described below;

It is based on the light extinction type testing method in which the intensity of a light beam is reduced by smoke, which is the measure of the smoke intensity. A standard length of tube is considered, through which the exhaust gas sample of the engine is passed. One end of the tube is connected to the light source, which can be transmitted through this tube, and the other end is used for the measurement of the transmitted light with a suitable device. The fraction of the light transmitted through the smoke (T) and the length of the light path (L_l) are related by the Beer-Lambert law [127] which is given by,

$$T = e^{-K_{ac}L_l} \tag{4.3}$$

where K_{ac}=nA ψ

K_{ac}=Optical absorption co-efficient of the obscuring matter per unit length
n= Number of soot particles per unit volume
A=Average projected area of each particle
ψ= Specific absorption per particle

The working principle of smoke emission measurement is shown in Fig. 4.7.

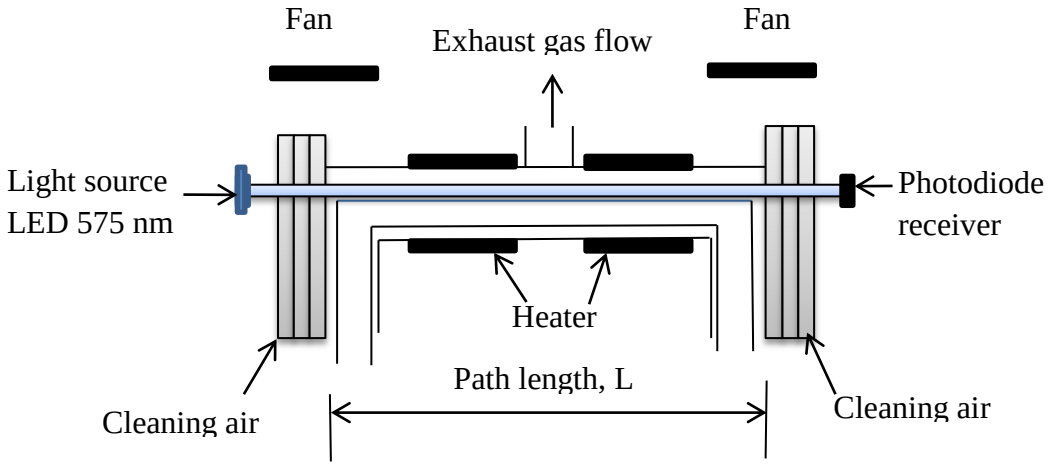

Fig. 4.7 Principle of diesel smoke measurement

The same principle is adopted in an AVL437C, which is used to measure the smoke in percentage opacity. The results obtained from the measurements are fully compatible with Hatridge Smoke Units (HSU), which are given in percentage of opacity. This measuring instrument consists of a sampling probe that sucks a specific quantity of the exhaust sample through a white filter paper fitted in the smoke meter. The reflectivity of the filter paper is measured by the smoke meter. Before testing or measuring the every sample, it is ensured that the exhaust from the previous measurement is completely driven off from the tube and pump. A photographic view of the diesel smoke meter is shown in Fig.4.8. The detailed specifications of the diesel smoke meter are presented in Appendix A3.

Fig. 4.8 Photograph of the diesel smoke meter

Calibration of the smoke meter was done periodically. It was done by warming the heating elements up to 70^{o}C. The pre-heating was carried out to prevent the temperature falling below dew point, and thus, to avoid measurement error or condensation of smoke. Fresh air was allowed to enter the measurement chamber which was drawn through the fitter paper,

underwent measurement and set the zero point for calibration. The halogen bulb current irradiated the column of the fresh air volume, and the signals from the detector were measured by the microprocessor and set as the reference value for 0% opacity. The linearity was checked by gently pushing the linearity check knob down, up to its dead position. The calibration plate was thus measured in front of the detector, and the measured opacity value was indicated and printed on the protocol print out. The probe of the exhaust gas analyzer was inserted at the end of the exhaust pipe during the measurement of emissions. Once the engine reached stable operation, the probe was inserted into the exhaust pipe and the measurements were taken.

4.3.3 Combustion parameters

It is necessary to study the combustion parameters, such as ignition delay, heat release rate, combustion duration, rate of pressure rise etc., for the efficiency of the engine and suitability of the fuel used. In order to evaluate such parameters, it is essential to collect the pressure values corresponding to each crank angle diagram. The cylinder pressure measurement at a particular crank angle is achieved with the help of a Kistler made quartz piezoelectric pressure transducer (Model Type 5395A), mounted on the cylinder head in the standard position. The piezoelectric pressure sensor is in line with the charge amplifier, which converts the electric charge generated in a piezoelectric pressure sensor to voltages that can be input into conventional measurement and data recording equipment. The charge amplifier can operate with a power supply of 7-32 V DC and range of 0-100 bar, and works with a time constant of 5s. Fins are attached to the pressure transducer body to provide the cooling medium. A photographic view of the Kistler pressure transducer is shown in Fig.4.9. The specifications of the pressure transducer and the charge amplifier are given in Appendix A4.

Fig. 4.9 Photographic view of Kistler pressure transducer

Figure 4.10 shows the photographic view of the pressure transducer mounted on the cylinder head.

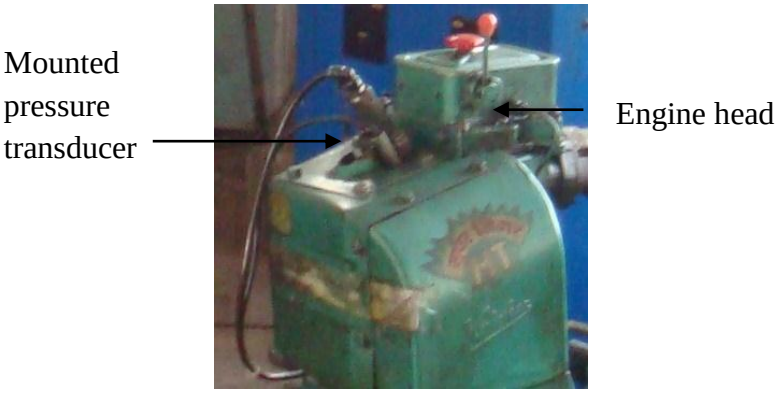

Fig. 4.10 Pressure transducer mounted on the engine head

A crank angle encoder 365C is fitted to the end of the engine shaft to measure the angular position of the crankshaft. It is a high precision optical pickup instrument with a pulse count of 360 ppr (pulse per revolution) used for torsional analysis for IC engines. All the data measured by sensors are processed, analysed and displayed with the help of a data acquisition system (DAS). The single cable input to the DAS from different output cables of sensors is achieved by the control panel board. The DAS has a data card for filtration and linearization of data, and also converters which convert analog input to digital output. The data like cylinder pressure, ignition delay, heat release rate, mass fraction burnt, and estimated end of combustion are analysed, with the help of software developed in house, and displayed on the personal computer, supporting the digital to analog (DA).

A continuous circulation of air is maintained to cool the transducer using fins to maintain the required temperature. The cylinder pressure data are acquired for 20 consecutive cycles and then averaged in order to eliminate the effect of cycle-to-cycle variations. The personal computer (PC), through an analog to digital converter (ADC) reads the output of the charge amplifier. There is a small drift in the voltage measured (-2 mV/s) due to charge leakage in the pressure transducer. Since the signal from a piezoelectric transducer indicated only relative pressures, it is necessary to have a means of determining the absolute pressure at some point in the cycle. Hence, the differential pressure has to be compared to a reference. This is done by assuming that the cylinder pressure at the bottom dead center (BDC) is equal to the mean intake manifold pressure. The TDC on the flywheel of the engine is connected to

the output shaft, to record the crank angle. Figure 4.11 shows the photographic view of TDC position sensor located on the fly wheel of the test engine and the corresponding sensor.

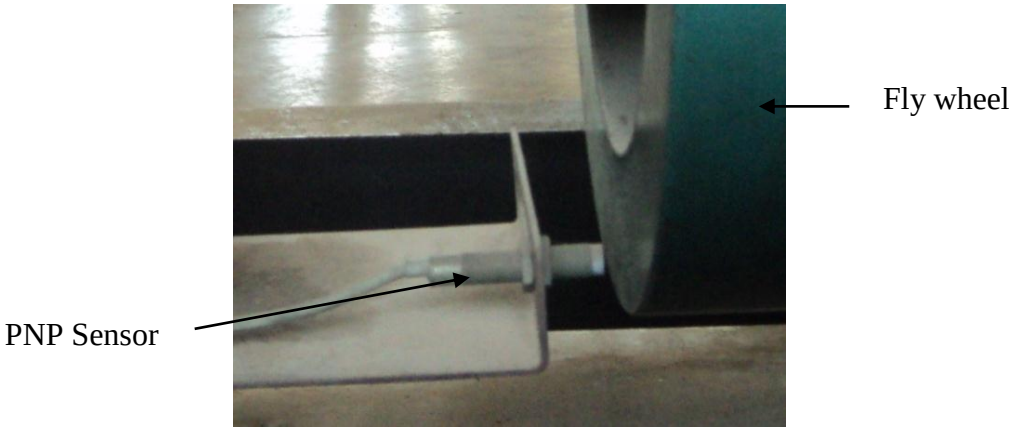

Fig. 4.11 TDC position sensor

For installation, a hole is made at the TDC and used to indicate the position of the TDC by providing a voltage pulse exactly when the TDC position is reached. This sensor consists of a matched pair of infrared diode and phototransistor, so that the infrared rays emitted from the diode would fall on the phototransistor when it is not interrupted. A continuous disc with a small cut at the TDC position with respect to the sensor point is made, to get the signal when the piston reaches the TDC exactly. At this point, the output voltage from the photo-transistor rises to 5 volts, and at all other points it is approximately zero. Voltage signals from the optical sensor are fed to the ADC and then to the DAS along with the pressure signals for recording. The engine cylinder pressure and the TDC signal are acquired using a digital DAS and stored in a computer. A 12 bit ADC is used to convert analog signals to digital signals. The analog to digital card has both an external and internal trigger facility. The pressure and crank angle data are collected in an excel spreadsheet installed in the DAS.

The instantaneous experimental data are acquired over several cycles. For averaging, the pressure data of approximately 50 thermodynamic cycles are chosen. The first in the voltage signal due to the TDC indicator is taken as a TDC position. The clock frequency of the data acquisition card is 100 kHz; approximately 370-380 pressure-voltage readings are acquired by the PC for each rotation of the crank shaft. By interpolation, the pressure-voltage readings are arranged at a spacing of 1 ^{o}CA. The interpolation is more accurate if done through spline fitting. Since the engine is the four stroke type, 720 such interpolated data points correspond to one complete thermodynamic cycle (intake, compression, combustion and exhaust) of the

engine. The interpolated data are corrected for the transducer drift by subtracting from them, a linearly increasing voltage (≈2 mV/s). Subsequently, these data are multiplied by the constant "B" to obtain it in relative pressure values at each instant. These pressure data are required to be referenced using a particular known pressure; hence, the pressure at the inlet BDC is taken as equal to the inlet manifold pressure. This is because at this instant, the inlet valve is completely open and the cylinder pressure is considered in equilibrium with the inlet manifold pressure, which was atmospheric pressure in the naturally aspirated engine case. After the pressure and crank angle were obtained at every load, other combustion parameters such as ignition delay, heat release rate and combustion duration are calculated, using the necessary formulae or empirical relations. The methods of calculation are described in the subsequent paragraphs. The value of the calibration constant for the pressure transducer is found to be 9.9 bar/V and the linear curve fit equation between pressure and voltage yields:

Pressure (bar) = 9.9831 (charge amplifier voltage in volts) – 0.0263 (4.4)

Ignition delay is the time lag between the start of injection and the start of combustion. From the heat release curve, the ignition delay is measured.

Along with the pressure signal, the TDC position signal is also acquired by the ADC installed in the DAS. These voltage signals are stored in two columns in a file at uniform time intervals. Since a piezo-electric pressure transducer provides only relative pressures, it is necessary to know the absolute pressure at some point in the cycle, so that the pressure at all other points could be determined. For this, the cylinder pressure at suction BDC is assumed to be equal to mean manifold pressure [128].

The rate at which combustion occurs, i.e., the rate of heat release, affects the efficiency, power output and emissions of an engine. The heat release rate curve provides an idea about the combustion process that takes place in the engine. A set of empirical relations and equations is used to compute the heat release rate, based on the first law of thermodynamics. This is done with the help of an excel spreadsheet. The heat release rate analysis is given in Appendix A5. The combustion duration in a particular power output is calculated as the crank angle duration, at which 90% of the heat release rate curve is covered. The crank angle at which there is a sudden rise in the heat release rate is taken as the start of combustion. The end of combustion is determined from the cumulative heat release curve. It is taken as the point where 90% of the heat release had occurred.

4.4 Different methods of using bioethanol in diesel engine

4.4.1 Investigation on the bioethanol-diesel emulsions

As bioethanol has poor miscibility with diesel and a lower cetane number, emulsification with a higher cetane is the appropriate method to use it as an alternative fuel in a CI engine [86]. For the experimental investigation, bioethanol was emulsified in three different proportions from 5% to 15% at regular steps of 5% on a volume basis with diesel accordingly with the help of a suitable surfactant. The important physical properties of the surfactant used in this study are listed in Table 4.1.

Table 4.1 Properties of the Surfactant Span-80

Properties	Value
Chemical name	Sorbitan Monooleate
Molecular Formula	$C_{24}H_{44}O_6$
Molecular Weight	428.6
Density (kg/m^3)	0.995 ~ 1.0 5
Saponification value (mgKOH/g)	140 ~ 160
HLB no.	4.3
Hydroxyl value (mgKOH/g)	190 ~ 220
Acid no. (mgKOH/g)	8
Iodine value (mg iodine/g)	60 ~ 75

The emulsion was denoted as BMDE, followed by the numerical value, which represents the percentage of bioethanol in the emulsion. For example, the numerical value in the emulsion BMDE5 indicates 5% of bioethanol. Similarly, other blends were denoted as BMDE10 and BMDE15. The emulsion was stirred well with the help of a mechanical agitator, to get a homogeneous stable mixture.

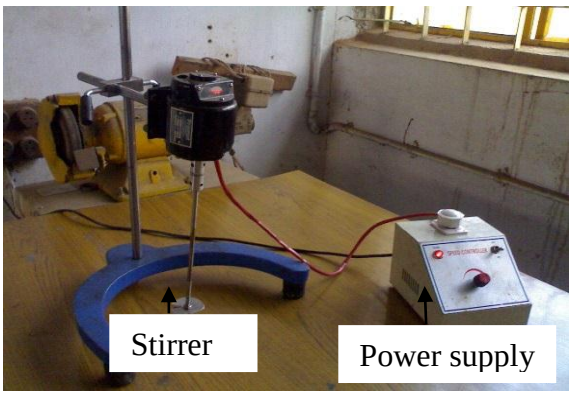

Fig. 4.12 Photographic view of the mechanical agitator

Figure 4.12 shows the photographic view of the mechanical agitator used for stirring in this investigation. Samples of different bioethanol diesel emulsions were kept in the open atmosphere, and observed for their miscibility, deposits or surface reactions after several weeks of monitoring. The samples of the bioethanol-diesel emulsions are shown in Fig. 4.13.

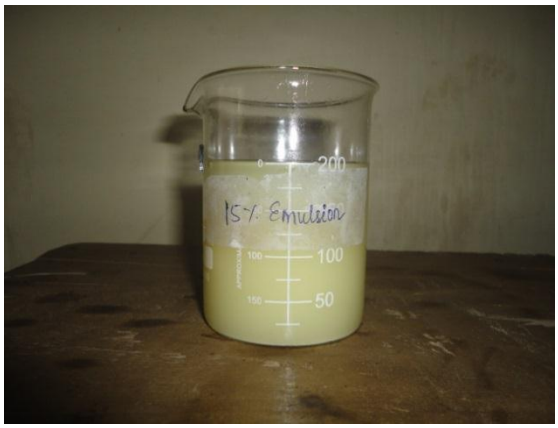

Fig. 4.13 Photographic view of the bioethanol-diesel emulsion samples

The comparison of the density, viscosity and gross calorific value of the blends with diesel are given in Table 4.2.

Table 4.2 Properties of test fuels

Properties	ASTM Standard	BMDE5	BMDE10	BMDE15
Specific gravity @ 40 °C	D 4052	0.823	0.811	0.809
Lower heating value [MJ/kg]	D 4809	38.21	37.02	35.34
Kinematic viscosity at 40 °C[cSt]	D 445	2.31	2.01	1.95
Flash point [°C]	D 2500	30	29	26
Cold filter plugging point [°C]	D 6371	-15	-20	-23
Pour point [°C]	D 97	-9	-12	-36
Sulphur content [wt%]	D 093	0.012	0.007	0.002
Boiling point [°C]	D 7169-11	165-342	142-326	114-298
Surface tension at 40°C [N/m]	D 3825	0.016	0.019	0.02

4.4.2 Experimental test procedure

All the tests were conducted by starting the engine with diesel only. After the engine was warmed up, it was switched to the bioethanol operation. At the end of the test, the fuel was switched back to diesel, and the engine was kept running for a while, before shut-down, to remove the traces of bioethanol diesel emulsion from the fuel line and the injection system. All the tests were conducted at a constant speed of 1500 rpm. All readings were taken only after the engine reached stable operation. The gas analyzers were switched on before starting the experiments, to stabilize them before starting the measurements. The injector opening pressure of 200 bar and injection timing of 23^{o}bTDC set by the manufacturer were kept constant at the rated value, during this phase of the study. The engine output was varied from no load to full load in steps of 25%, 50%, 75% and 100% in the normal operation of the engine. At each load the fuel flow rate, air flow rate, exhaust gas temperature, emissions of CO, HC and NO, and smoke readings were recorded. The pressure crank angle history of 50 cycles was also recorded, by using the data acquisition system and stored in the personal computer. The data was processed to get the average pressure crank angle variation and used for further calculations.

4.4.3 Investigations with the bioethanol diethyl-ether blends

As bioethanol obtained from the Madhuca Indica flowers has a lower cetane number, it might produce a longer ignition delay, when it was operated with diesel in the form of emulsions. Therefore, in the second phase of study, it was proposed to investigate the engine run with the bioethanol-diesel-emulsion with the addition of small quantities of the ignition improver. The different ignition improvers used at present to improve the ignition quality of a lower cetane fuel are, dimethyl ether, diglyme, and diethyl ether. As diethyl ether (DEE) has a high cetane number and is cheaper compared to other ignition improvers, it was decided to use DEE in this study. The physical properties of DEE are listed in Table 4.3. DEE in small quantities, viz. 1%, 1.5%, 2% and 2.5%, was blended with the BMDE15 emulsion. The blends were stirred thoroughly and checked for their stability. The maximum percentage of DEE was ensured by the operational behavior of the engine. When the percentage of DEE was increased beyond 3%, the engine suffered the vapour lock problem, and hence, it was stopped with the maximum percentage of 3%.

Table 4.3 Properties of DEE

Properties	DEE
Density at 40 °C (kg/m^3)	713
Lower heating value (MJ/kg)	33.89
cetane number	>125
Kinematic viscosity at 40 °C (cSt)	0.224
Auto-ignition temperature (^{o}C)	160
Boiling point (^{o}C)	34.4
Latent heat of vaporisation (kJ/kg)	465

Each blend was denoted as DE followed by the percentage of DEE in the blend. For example, DED1% indicates BMDE15 emulsion and 1% DEE in the blend. Similarly other blends were designated. Table 4.4 gives the tested fuels and their corresponding viscosity and calorific value.

Table 4.4 Properties of test fuels

Fuel	% of bioethanol (% vol)	% of DEE	Density, kg/m^3	Viscosity, cSt@40^{o}C	Lower calorific value, MJ/kg
Diesel	0	0	860	2.4	44.8
Blend 1	15	0	809	1.95	35.34
Blend 2	15	1	802	1.52	36.23
Blend 3	15	1.5	799	1.32	37.02
Blend 4	15	2	794	1.29	37.48
Blend 5	15	2.5	780	1.12	37.67

The experimental set up and test procedure described in subsection 4.3.1 and 4.4.2 respectively, for testing bioethanol-diesel emulsions was adopted in this study also. There was no engine modification adopted. The injection timing and nozzle opening pressure were not changed.

4.4.4 Investigations with the bioethanol-DEE on dual fuel mode

DEE was blended with a maximum of 2.5% with bioethanol because beyond 3% the engine gave the vapor lock problem. Hence, it was decided to run the engine in the dual fuel mode.

In the dual fuel mode, bioethanol was injected into the cylinder, while the DEE was admitted into the engine along with the air. For this, DEE was introduced in small quantities, near the intake port. A hole was made in the suction pipe near the intake manifold (100 mm away from the intake manifold). A small syringe was inserted into the hole. The other end of the syringe was connected to a storage bottle in which DEE was stored for use. The quantity of DEE admitted through the syringe was controlled by a regulator, which was located in between the storage bottle and the syringe. The experimental setup used in this study is shown in Fig. 4.14.

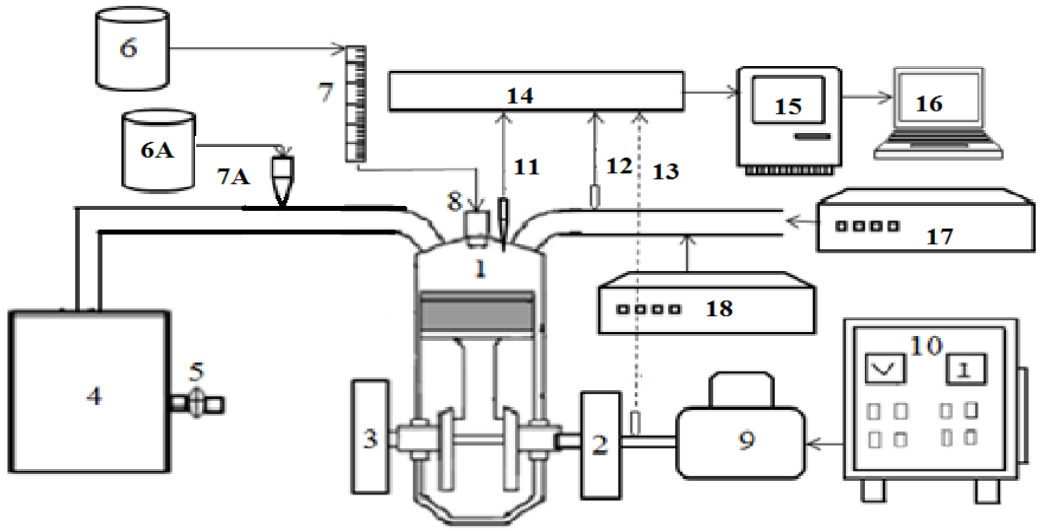

1. Engine
2. Flywheel
3. Crankshaft
4. Air box
5. Manometer
6. Fuel tank for Diesel
7. Burette

6A. DEE fuel tank

7A. Fuel injection valve
8. Injector
9. AC generator
10.Load bank
11.Pressure transducer

12.Exhaust gas temperature sensor
13.Speed sensor

14.Control panel board
15.Data acquisition system
16.Computer
17.AVL Digas 444 analyser
18.AVL 437 C smoke meter

Fig. 4.14 Experimental setup for bioethanol dual fuel mode

The engine was allowed to run with the maximum quantity of DEE based on the combustion behavior of the engine. Until there was no problem noticed with abrupt pressure, the engine was run with DEE, by varying its quantity.

4.4.5 Investigations with the use of bioethanol on fumigation

In this study, the maximum quantity of bioethanol utilisation was investigated by running the engine with bioethanol fumigation. Generally, the dual fuel mode offers a reduction in smoke emission [129]. Therefore, it was also decided to find out how much reduction in smoke would be possible with bioethanol. Hence, the fumigation technique was chosen in this study. In the fumigation technique, the liquid fuel with a low cetane fuel is vaporised with the help of a vaporiser or heater, and the vapour is introduced in the intake of the engine. Small quantities of a high cetane fuel are injected as a pilot fuel to create a hotter environment in the engine which will help to ignite the low cetane fuel. The fumigation was done with the help of a fuel tank, an electronically controlled injector, a fuel pump, and a vaporizer. The arrangement used in this study for the fumigation of bioethanol is shown in Fig. 4.15.

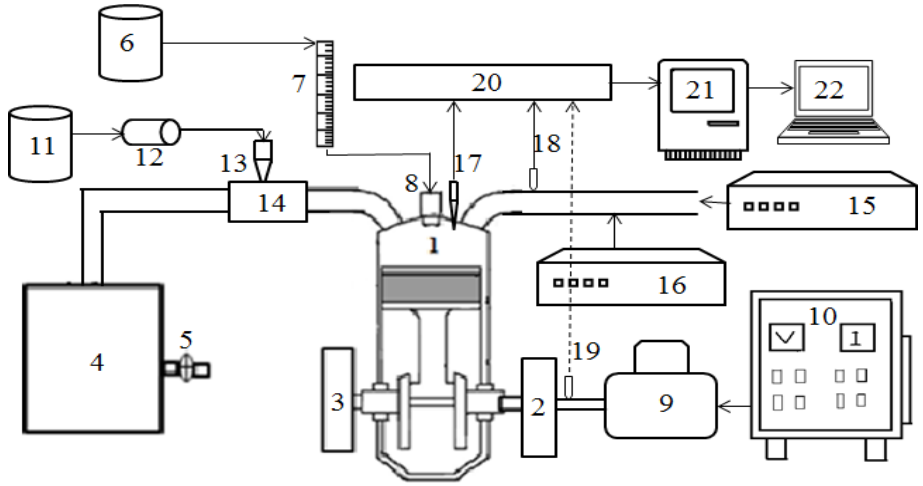

1. Engine
2. Flywheel
3. Crankshaft
4. Air box
5. Manometer
6. Fuel tank for Diesel
7. Burette
8. Injector
9. AC generator
10. Load bank
11. Fuel tank for Bioethanol
12. Fuel pump
13. Electronically controlled injector
14. Vaporiser
15. AVL 437 C smoke meter
16. AVL Digas 444 analyser
17. Pressure transducer
18. Exhaust gas sensor
19. Speed sensor
20. Control panel board
21. Data acquisition system
22. Computer

Fig. 4.15 Arrangement used in this study for the fumigation of bioethanol

The block diagram representing the arrangement for the fumigation technique is shown in Fig. 4.16. The flow chart of the fuel injection system is given in Fig. 4.17. A 12 V, 5 nozzles, solenoid based electronic fuel injector of 300 kPa injection pressure was connected to the intake manifold of the diesel engine. Bioethanol stored in a tank was pumped using a 12 V

fuel supply pump and supplied to the fuel injector. One of the output pins of a microcontroller (Atmega-328) was connected to the injector through a motor driver (L293D).

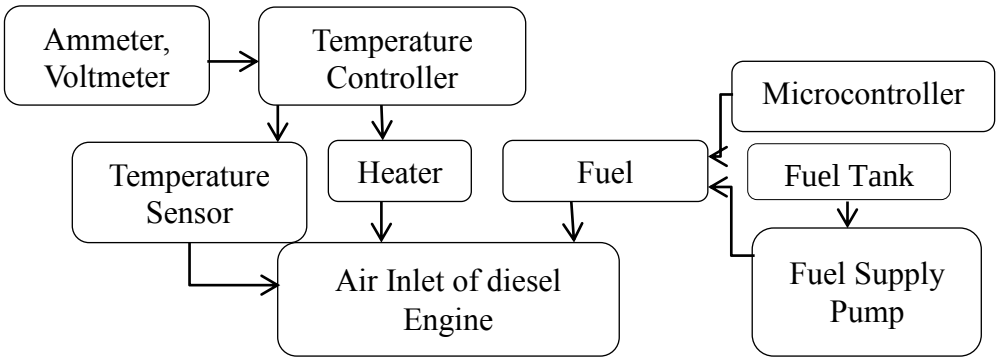

Fig. 4.16 Block diagram representing the arrangement for the fumigation technique

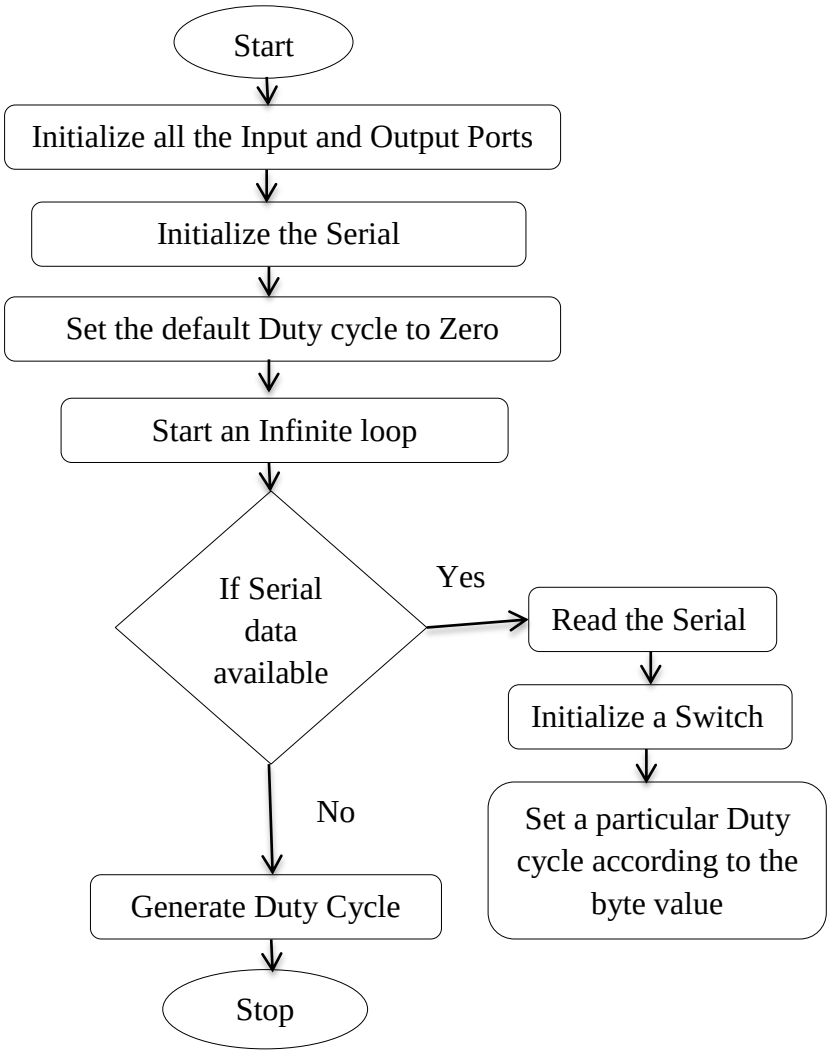

Fig. 4.17 Flow chart of the fuel injection system

The microcontroller worked at 5 V and the injector works at 12 V with high current; L293D was used to provide the proper current and voltage to the injector. The microcontroller was programmed to generate a pulse width modulation (PWM), to control the quantity of bioethanol to be injected. The PWM was basically a duty cycle, which delivered bioethanol in different quantities. Bioethanol was injected continuously at regular intervals. Four different flow rates, viz., 0.24, 0.48, 096 and 1.22 kg/h were used in this investigation. An algorithm for the function of the electronically controlled injector is given in Annexure A1. The multi-point fuel injector was attached to an electric heater whose temperature was maintained at 70^{o}C.

As bioethanol was supplied at four different flow rates, the total energy supplied to the engine was not fixed, and also the global equivalence ratio would change for different flow rates. The method of calculating the global equivalence ratio (Φ) is discussed in the forthcoming subsection 4.5.1.6.

Similarly in the diesel operation, the engine always operated in a lean combustion mode, as diesel was injected into the cylinder; the special distribution of the fuel–air ratio in the combustion chamber varied widely from rich to lean [122]. In bioethanol fumigation, when bioethanol was injected at 0.24, 0.48, 0.96 and 1.22 kg/h flow rates, the bioethanol energy ratio changed, and air was also displaced by the fumigated bioethanol, as it was inducted along with the air; so the global equivalence ratio varied according to the actual fuel–air ratio, though the stoichiometric fuel–air ratio was constant. Therefore, the bioethanol energy share (r) was calculated. The method of calculating the bioethanol energy share is discussed in the forthcoming subsection 4.5.1.7.

Initially, the engine was operated with diesel to obtain the reference data at different loads, ranging from 0% to 100% for 1 h to complete one set of measurement. Further, the experiments were conducted with bioethanol fumigation at different loads. The engine parameters in terms of performance, emission and combustion were drawn in variation with the global equivalence ratio.

Figure 4.18 illustrates the experimental techniques that are used to establish bioethanol with diesel/DEE for CI engines.

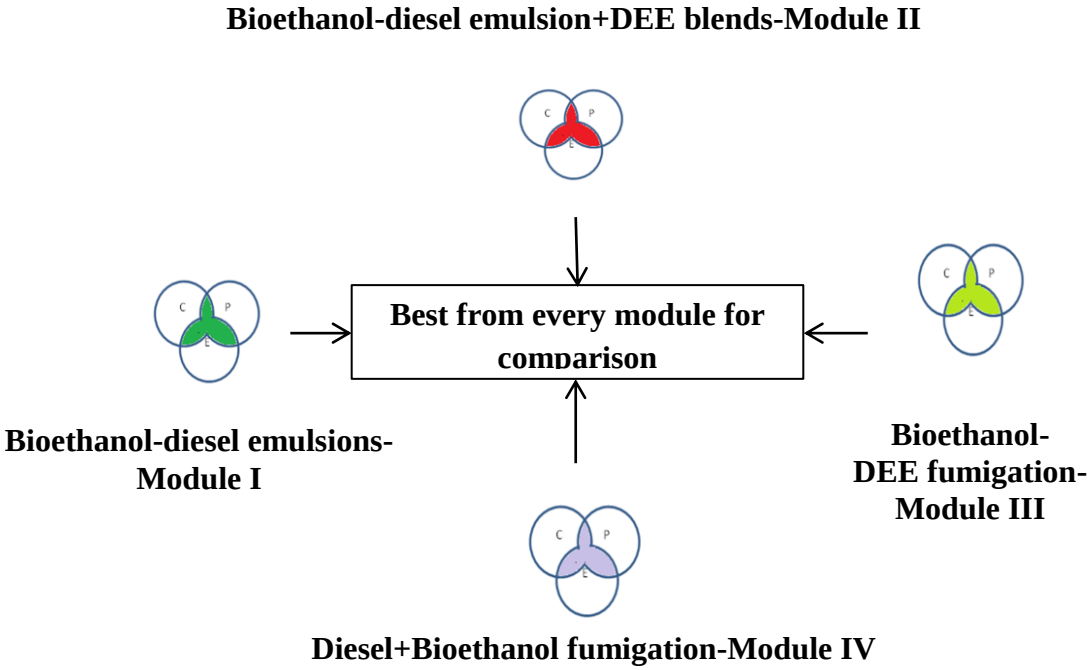

Fig. 4.18 Experimental techniques used for bioethanol application in the diesel engine

4.4.6 Mathematical modeling for validation

To validate the experimental results of the best technique, a mathematical analysis was done using a MATLAB program.

4.4.7 Investigation with the bioethanol-biodiesel-diesel blends

It was observed that with the bioethanol-diesel emulsion, the engine could experience lower lubricity and this would increase the frictional power of the engine. So for long term use, it is not feasible. In order to improve the properties of the bioethanol-diesel emulsion, different percentage of biodiesel were added. The blending of fuel was prepared with the help of ternary diagram which is shown in Fig. 4.19. The biodiesel was added to BMDE15 in the volume percentages of 5, 10 and 15%, and designated as BEBDD5, BEBDD10 and BEBDD15. The comparison of properties of the blends with BMDE15 and diesel is given in Table 4.5.

Table 4.5 Properties of test fuels

Properties	diesel	BMDE15	BEBDD5	BEBDD10	BEBDD15
Density at 40 °C [kg/m^3]	860	809	843.3	851.25	852.2
Lower heating value [MJ/kg]	43.8	35.34	42.25	41.9	41.7
Kinematic viscosity at 40 °C [cSt]	2.58	1.95	2.91	2.76	2.63
Cetane number	51	36	45	46.09	46.61

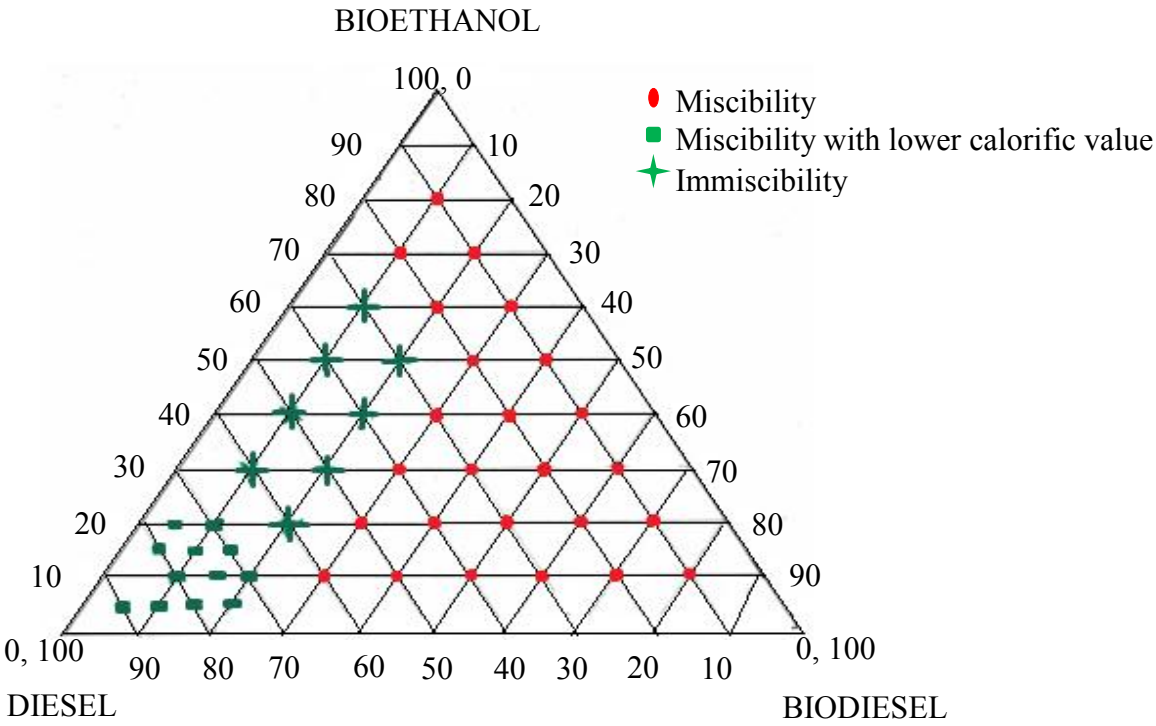

Fig. 4.19 Ternary diagram for the checking of stability

4.4.8 Comparative study of the endurance test

Bioethanol has a low viscosity compared to diesel fuel, and hence, it acts as a poor lubricant which will affect the long durability of the engine. Therefore, it was decided to determine the changes in the lubricating oil properties when the engine was run with the best possible technique by which bioethanol could be used. Since the bioethanol diesel emulsion gave better results in terms of performance and emissions in comparison with other techniques, it was decided to use bioethanol diesel emulsion for studying the change in the lubricating oil properties, before and after the run.

4.5 Analyses and procedure

During the investigation the humidity of the atmospheric air was measured with the help of the hygrometer, and it was 41%.

4.5.1 Performance parameters

4.5.1.1 Fuel consumption measurement

When fuel passes through the optical sensors that are fixed in the fuel, the burette senses the upper and lower levels of the fuel in the burette and sends signals to the computer for automatic start/stop of time required for the fixed amount of fuel supply, i.e. 20 cc, to measure the fuel consumption, and the burette is refilled automatically for the next measurement.

4.5.1.2 Air consumption measurement

The U-tube manometer fitted in the air plenum shows the reading of the water head in terms of pressure difference, which is used to calculate the air consumption of the engine.

4.5.1.3 Speed and EGT measurements

A non-contact type PNP sensor gives the pulse output for each revolution of the crank shaft for the measurement of the engine speed in RPM. The pulse frequency is converted into the voltage output, which displays the speed in the computer.

A K-type (Cr Al) thermocouple with sensor, is used for the measurement of the EGT, with a temperature range of 0-900 ^{0}C.

4.5.1.4 BSEC calculation

Three performance parameters, viz, BSFC and EGT were determined for diesel operation. The BSFC is not a reliable parameter if fuels of different viscosity and density are used. The BSEC is a product of the BSFC, and the calorific value of the fuel at a particular load. Therefore, the BSEC rather than the BSFC is discussed in the chapter results and discussion. The calculations used for determining the BSEC from the BSFC are given in Appendix A6.

4.5.1.5 Thermal energy balance calculation

The thermal energy balance can be calculated using the following equation-

The heat supplied by the fuel is given as;

$Q = CV * M_f$ (kJ/h) (4.5)

where, CV=Calorific value (kJ/kg)

M_f=Mass of fuel consumption (kg/h)

Heat converted to useful work (or) brake work is given as;

Useful work (q_1) = Brake power * 3600 (kJ/h) (4.6)

Percentage of useful work= (useful work/Q)*100

Heat loss through the exhaust (q_2) is given as;

$q_2 = (Ma + M_f) * C_{pg} * (T_g - T_a)$ (kJ/h) (4.7)

where, Ma= Mass of air consumption (kg/h)

C_{pg}= Specific heat of gas at different exhaust temperatures (kJ/kg °C)

T_g= Exhaust gas temperature (°C)

T_a= Atmospheric temperature (30 °C)

Heat carried away by the lubricating oil (q_3) is calculated as;

$q_3 = M_{oil} * C_{oil} * (T_f - T_i)$ (kJ/h) (4.8)

where, M_{oil}= Mass flow rate of lubricating oil (kg/h)

= (Volume of oil * density of oil)/3600

C_{oil}= Specific heat of oil at mean average temperature (kJ/kg °C)

$(T_f - T_i)$= Temperature rise in oil (°C)

Unaccounted heat loss is given as;

$q_4 = Q - (q_1 + q_2 + q_3)$ (kJ/h) (4.9)

4.5.1.6 Global equivalence ratio

The global equivalence ratio (Φ) is given by the following equation,

$$\Phi = (M_d * \left(\frac{A}{F}\right)_{s,d} + M_{bt} * \left(\frac{A}{F}\right)_{s,bt}) / M_a \quad (4.10)$$

where M_d, M_{bt} and M_a are the mass flow rates of diesel, bioethanol and air in kg/h. $(A/F)_{s,d}$ and $(A/F)_{s,bt}$ are the stoichiometric fuel–air ratios for diesel and bioethanol. If $\Phi < 1$, the fuel–air mixture is called lean, if $\Phi > 1$, the mixture is rich, and if $\Phi = 1$, the mixture is stoichiometric.

4.5.1.7 Bioethanol energy share

The bioethanol energy share (r) was calculated by the following equation;

$$r = \frac{M_{bt} * H_{ubt}}{M_{bt} * H_{ubt} + M_d * H_{ud}} * 100 \quad (4.11)$$

where H_{ubt} and H_{ud} were lower heating values of bioethanol and diesel respectively. When r = 0%, the engine was run with conventional diesel only. The boiling point of bioethanol is low; therefore when it was supplied with a high pressure injection into the vaporiser, it mixed properly with the air to form a homogeneous mixture, as in a premixed combustion engine.

4.5.2 Emission measurements

The emission parameters such as HC, CO and NO, were directly obtained with the help of the exhaust gas analyzer. The units of these emissions were measured in ppm, %vol and ppm respectively. These values were converted into g/kWh. The conversion formulae are given in Appendix A6. Smoke values are directly obtained with the help of the smoke meter.

4.5.3 Combustion parameter measurements

4.5.3.1 Ignition delay

The ignition delay is calculated by using following equation,

Ignition delay in degree crank angle=degree crank angle at 5% heat is liberated-degree crank angle at which fuel is injected (4.12)

4.5.3.2 Heat release rate analysis

The heat release analysis can provide information about the effects of the engine design changes, fuel injection system, fuel type, and engine operating conditions, on the combustion process and engine performance. The heat release rate was calculated by making an analysis of the first law of thermodynamics. Sorenson et al. presented the following equation for heat release:

$$\frac{\partial E}{\partial \theta} = \vartheta \frac{\partial P}{\partial \theta}(1/\gamma\text{-}1) + P \frac{\partial \vartheta}{\partial \theta}(\gamma/\gamma\text{-}1) \quad (4.13)$$

where,

$\frac{\partial E}{\partial \theta}$ = rate of heat release (J/°CA)

ϑ = gas volume (m^3)

P=cylinder pressure (bar)

θ = crank angle (°)

γ = ratio of specific heats, C_p and C_v

In this equation, the heat release rate corresponding to crank angle was calculated with the help of cylinder pressure data at crank angle. The cylinder gas pressure was measured using a Kistler piezo-electric transducer (model 5395A) in conjunction with a Kistler charge amplifier. The cylinder gas pressure data was recorded as the average of 20 cycles of data, with a resolution of 0.5°CA using a data acquisition system. From the average values of the cylinder pressure data, the heat release rate was calculated and recorded in an excel file with an in-house data acquisition system software. The instantaneous cylinder volume can be obtained from the engine geometry and crank angle values and is constant at every cycle. The value of γ given in the equation was considered for air.

4.5.3.3 Smoothing of P-θ curve

The heat release rate is calculated by considering 20 cycles. A particular cycle, a total of 1200 data points for both cylinder pressure and volume are recorded at each load. The smoothing of the instantaneous pressure data was done by using the following equation:

$$P_n = \frac{[P_{n-1}+2P_n+P_{n+1}]}{4} \tag{4.14}$$

The change of pressure for unit crank angle was determined by using the equation,

$$\frac{dP}{d\theta} = \frac{[(P_{n-2})-8(P_{n-1})+8(P_{n+1})-(P_{n+2})]}{[12(\Delta\theta)]} \tag{4.15}$$

4.5.3.4 Rate of pressure rise

The rate of pressure rise provides information of the design of the engine to operate smoothly. The rate of pressure rise is the derivative of pressure (dP/dθ) with respect to the crank angle.

4.5.3.5 Combustion duration

Combustion duration is measured from the 5% heat release rate to 90% heat release rate.

4.5.3.6 Mass fraction burned (MFB)

The energy conversion during a combustion cycle can be described by the Mass Fraction Burned (MFB) at a specific crank angle degree (CAD). In an IC engine, the MFB depends on the engine geometry, engine speed, A/F, ignition angle, residual mass etc. The MFB in each individual engine cycle is a normalized quantity with a scale of 0 to 1, describing the process of chemical energy release as a function of the crank angle. The MFB includes the determination of the start and end of combustion. One well-established method was developed by Rassweiler and Withrow [130] for estimating the mass fraction burned profile from the cylinder pressure and volume data. In this method, the mass fraction burned is given by;

$$MFB = \frac{m_b(i)}{m_b(total)} = \frac{\sum_{0}^{i} \Delta P_c}{\sum_{0}^{N} \Delta P_c} \tag{4.16}$$

where,

0-denotes the start of combustion,

N – end of combustion (N is the total number of crank intervals)

ΔP_c – pressure rise due to combustion

i- integer crank angle location

4.6 Uncertainty analysis

Any measurement, irrespective of the type of instrument used, possesses a certain amount of uncertainty or error. Some of these errors are of a random nature and need a device to specify consistently the uncertainty in an analytical form. Hence, a brief attempt was made to estimate the uncertainty of various measurements by theoretical methods. An uncertainty analysis was performed using the method described by Holman [127]. The range, accuracy and percentage of the uncertainty of each instrument are given in Appendix A7. The procedure used for the uncertainty analysis is given in Appendix A8.

CHAPTER 5

MATHEMATICAL MODELLING

5.1 General

In recent years, the validation of the experimental results by mathematical modelling or simulation through an advance software is essential, so that the randomness of the results is minimised. In this chapter, a mathematical modelling was developed to validate the experimental results obtained from a single cylinder, four stroke, air cooled, DI diesel engine, that was run on the BMDE15 emulsion. A MATLAB program was developed for a two zone model for the validation. One zone consisted of pure air called the non-burning zone, and the other consisted of fuel and combustion products, called the burning zone. In order to obtain the cylinder pressure and temperature by mathematical modelling, the first law of thermodynamics and the equation of state were used for both the zones. The combustion parameters, such as ignition delay and heat release rate and the chemical equilibrium composition were calculated theoretically, using the two zone model. As the NO and soot emissions are important in a CI engine, they were calculated using a semi-empirical model. A comparison of the theoretical and experimental results of the BMDE15 emulsion is presented in this chapter. A spray profile of diesel and the BMDE15 emulsion is also obtained using a MATLAB program and presented.

5.2 Spray formation model

In a CI engine, the fuel air mixture is obtained inside the combustion chamber of the engine. The injected fuel absorbs the heat from the surrounding air and vaporises. Further, the fuel vapor mixes with the available air in the cylinder. The fuel injector plays an important role in the injection process, because it atomises the liquid fuel into finer droplets in the form of a spray. Depending on the spray, the fuel air mixture is obtained in the cylinder. The better the fuel spray, the better the mixture formation. The combustion, performance and emission of the engine are analysed with the help of a spray pattern of the fuel. In this section, the two-dimensional, multi-zone model of fuel sprays is developed, where the issuing jet is divided into discrete volumes, called zones. The descriptions of the model are discussed in the following subsections.

5.2.1 Fuel injection process

During the compression of fluid in the fuel injection process, a pressure wave is propagated down the connecting pipe at a sonic speed, to open the needle of the injector. The speed of sound is given by;

$$a_s = \sqrt{\frac{K_{bm}}{\rho_1}} \tag{5.1}$$

Then, the time for the pressure wave to travel down the connecting pipe length (L_p) i.e. injection delay was expressed by,

$$\Delta\varphi_{injdel} = \left(\frac{L_p}{a_s}\right) 6N \tag{5.2}$$

The pressure wave in the injector nozzle holes has a magnitude of,

$$\Delta p_w = a_s \rho_1 c_{pump} \left({F_{pump}}/{F_{nozzle}} \right) \tag{5.3}$$

where F_{pump} and F_{nozzle} are the cross sectional areas of the pump barrel and of the total of the nozzle holes.

5.2.2 Fuel jet break up point and initial angle

To obtain the location of the spray tip as a function of time, based on the relevant experimental data and turbulent jet theory, a correlation developed by Arai et al. [131] is incorporated in the modelling. Other correlations [132-134] are also used to obtain the fuel break up point, swirling motion of the air and spray penetration containing the swirl ratio.
The mean jet velocity from each nozzle hole is given by,

$$\bar{u}_{inj} = C_d \sqrt{{2\overline{\Delta p}_{inj}}/{\rho_1}} \tag{5.4}$$

$The\ C_d$ value was taken as 0.39.

The mean fuel injection rate per jet (kg/°CA) is given as,

$$\acute{\bar{m}}_{finj} = \left({\pi {D_n}^2}/{4} \right) {\rho \bar{u}_{inj}}/{6N} \tag{5.5}$$

For the given global air to fuel ratio, the total fuel mass to be injected in the cycle m_{ftot} is fixed, if the total air mass trapped in the cylinder m_{atot} is known. Then, the value of the total duration of the fuel injection is given in degrees of the crank angle,

$$\Delta\varphi_{inj} = \left(m_{ftot}/Z\right)/\dot{\bar{m}}_{finj} \tag{5.6}$$

The spray development will continue until the penetration of each spray reaches a value of (D/2+πD/z), or until it entrains the maximum quantity of air equal to m_{atot}/z.

The break up time t_{br} was obtained by equating the two spray penetration correlations before and after t_{br}, corresponding to the break up length $S = S_{br}$

$$S = 0.39\sqrt{2\overline{\Delta p}_{inj}/\rho_1}\,.t \qquad \text{for } 0 < t \le t_{br} \tag{5.7}$$

$$S = 2.95\left(\overline{\Delta p}_{inj}/\rho_a\right)^{0.25}\sqrt{D_n.t} \qquad \text{for } t \ge t_{br} \tag{5.8}$$

Then t_{br} is given by,

$$t_{br} = 28.61\rho_1.\,D_n/\sqrt{\rho_a.\overline{\Delta p}_{inj}} \tag{5.9}$$

where ρ_a is the density of air inside the cylinder just before the beginning of the combustion of fuel.

The break up length is given as,

$$S_{br} = \bar{u}_{inj}.t_{br} \tag{5.10}$$

The break up length with the swirl ratio can be written as,

$$S_{brs} = S_{br}\left(1 + \pi.R_s.N.S_{br}/30.\bar{u}_{inj}\right)^{-1} \tag{5.11}$$

The corresponding break up time is given by,

$$t_{brs} = {S_{brs}}/{\bar{u}_{inj}} = \left({S_{brs}}/{S_{br}}\right).t_{br} \quad (5.12)$$

The initial spray angle (rad) is [135],

$$\theta = 2\arctan\left(\frac{1}{\acute{A}}4\pi\sqrt{\frac{\rho_a}{\rho_1}}\frac{\sqrt{3}}{6}\right) \quad (5.13)$$

where $\acute{A}$ is constant and given by the empirical relations,

$$\acute{A} = 3 + 0.28\left({L_n}/{D_n}\right) \quad (5.14)$$

5.2.3 Fuel spray development

The following steps are used for the spray development of each zone,

(a) For axial zones, the zones are taken as $i_{max} = {\Delta\varphi_{inj}}/{\Delta\varphi}$, and for radial zones, they are divided into $j_{max} = {i_{max}}/{2}$ to i_{max}. The instantaneous fuel injection velocity and injection rate in each spray, using instantaneous values of $\Delta p_{inj} = \Delta p_w$ are given as,

$$u_{inj}(i) = C_d\sqrt{{2\overline{\Delta p}_{inj}(i)}/{\rho_1}} \quad (5.15)$$

And $\acute{m}_{finj}(i) = \left({\pi {D_n}^2}/{4}\right){\rho u_{inj}(i)}/{6N}$ (5.16)

Then the cumulative fuel injected in each spray is,

$$m_{finj}(i) = \int_0^{\varphi}\acute{m}_{inj}(i)d\varphi \quad (5.17)$$

(b) The fuel is distributed equally in to the radial zones j_{max} at each crank angle in steps of "i", which is given by the following equation,

$$m_{finj}(i) = {\acute{m}_{inj}(i)d\varphi}/{j_{max}} \quad (5.18)$$

(c) The Sauter mean diameter (D_{SM}) [136] is calculated for each step.

(d) The mid zone is selected as $j_{mid} = {j_{max}}/{2 + 1}$ (5.19)

(e) The mid-zone penetration in the radial distance from the cylinder axis is calculated as,

$$r_{mid}(i) = \sqrt{x^2(i, j_{mid}) + y^2(i, j_{mid})} \quad (5.20)$$

(f) The mid-zone velocity in each crank angle step (i) is calculated as,

$$u_{mid}(i) = 2.95\beta\left(\Delta p_{inj}(i)/\rho_a\right)^{0.25}\sqrt{D_n}\,\frac{1}{t^{1-\beta}} \quad (5.21)$$

(g) The center line angle for each zone is given as,

$$\theta_z(i, j) = -\frac{\theta}{2} + \frac{j-1}{j_{max}}\theta + \frac{\theta}{2j_{max}} \quad (5.22)$$

(h) The velocity distribution for a lower axis penetration located at the jet periphery for each zone is calculated as,

$$u_z(i, j) = u_{mid}(i)exp\left[-\alpha {\theta_z}^2(i, j)\right] \quad (5.23)$$

where $\alpha = 4.5^2$

(i) The swirl coefficient before the wall impingement is calculated by the following equation,

$$C_{swz}(i, j) = 1 + \frac{\pi R_n N\sqrt{x^2(i, j_{mid}) + y^2(i, j_{mid})}}{30u_z(i, j)} \quad (5.24)$$

while $C_{swz}(i, j)$ is 1 after the wall impingement. The coordinates of x and y are calculated from the previous step.

(j) Also the drop of the Sauter mean diameter from the center line of the spray with increasing distance is considered as,

$$D_{SM}(i, j) = \left(1 - \frac{1}{w}\right)D_{SMM}(i) + \left(\frac{2}{w}\right)D_{SMM}(i)(j - 1)/(j_{mid} - 1) \quad (5.25)$$

where w is in the range of 5-10.

(k) The number of droplets in each zone is also calculated with the following mathematical relation,

$$N_{drop}(i, j) = m_{fz}(i)/\left[\left({\pi}/{6}\right)\right]D_{SM}(i, j)^3\rho_1] \quad (5.26)$$

(l) The zone velocity with swirl is calculated,

$$u_{zs}(i, j) = {u_z(i, j)}\Big/{C_{swz}(i, j)} \quad (5.27)$$

(m) The mass of air in each zone is calculated as,

$$\mathrm{m_{az}(i,j)} = \mathrm{m_{fz}(i)}\frac{\mathrm{u_{inj}(i)} - \mathrm{u_{zs}(i,j)\cos\theta_z(i,j)}}{\mathrm{u_{zs}(i,j)\cos\theta_z(i,j)}} \quad (5.28)$$

(n) The fuel air equivalence ratio of the zone is,

$$\emptyset_{\mathrm{z}}(\mathrm{i,j}) = \frac{\mathrm{m_{fz}(i)/m_{az}(i,j)}}{\left(\frac{1}{\mathrm{AF_{st}}}\right)} \quad (5.29)$$

(o) The effect of swirl for each zone on the angle is considered as,

(i) For $j < j_{mid}$,

$$\theta_{zs}(i,j) = \theta_z(i,j)C_{swz}(i,j)^2 \quad (5.30)$$

(ii) For $j = j_{mid}$,

$$\theta_{zs}(i,j_{mid}) = \frac{1}{2}\theta_{zs}(i,j_{mid}) + \frac{1}{2}\theta_{zs}(i,j_{mid}-1) \quad (5.31)$$

(iii) For $j > j_{mid}$,

$$\theta_{zs}(i,j) = \theta_z(i,j) + \theta_{zs}(i,j_{mid}) \quad (5.32)$$

(p) The location of the co-ordinates for each zone is calculated with the following equation,

(i) Before the wall impingement,

$$x(i,j) = x_0(i,j) + u_{zs}(i,j)cos\ \theta_{zs}(i,j)\frac{\Delta\varphi}{6N} \quad (5.33)$$

$$y(i,j) = y_0(i,j) + u_{zs}(i,j)sin\ \theta_{zs}(i,j)\frac{\Delta\varphi}{6N} \quad (5.34)$$

(ii) After the wall impingement,

$$x(i,j) = r_{zimp}(i,j)cos\ \theta_{zs}(i,j) \quad (5.35)$$

$$y(i,j) = r_{zimp}(i,j)sin\ \theta_{zs}(i,j) \quad (5.36)$$

5.2.4 Fuel droplet evaporation

The fuel evaporation in each zone is considered with the calculation of the Sauter mean diameter, which is given by the following relations,

$$D_{SM,1} = 0.38{Re_{inj}}^{0.25}{We_{inj}}^{-0.32}\left({v_1}/{v_a}\right)^{0.37}\left(\frac{\rho_1}{\rho_a}\right)^{-0.47}D_n \quad (5.37)$$

$$D_{SM,2} = 4.12{Re_{inj}}^{0.12}{We_{inj}}^{-0.75}\left({v_1}/{v_a}\right)^{0.45}\left(\frac{\rho_1}{\rho_a}\right)^{0.18}D_n \quad (5.38)$$

Also, the equivalence ratio for each zone is calculated using the evaporation model,

$$\emptyset_{\mathrm{zvap}}(\mathrm{i,j}) = \frac{\mathrm{m_{fzvap}(i)/m_{az}(i,j)}}{(\frac{1}{\mathrm{AF_{st}}})} \quad (5.39)$$

5.2.5 Calculation of Whitehouse-Way fuel preparation rate constant

After the fuel is injected into the cylinder chamber, it will undergo physical and chemical processes for burning inside the chamber. In the physical process, the fuel gets atomised, heated, evaporated and mixed with sufficient air to form the charge mixture. Then, the chemical kinetic reactions occur, to burn the mixture in the chemical process. The Whitehouse and Way model [137] was used for the comparison of the results obtained from the fuel evaporation model.

So, the penetration rate proposed by the Whitehouse-Way model was given as,

$$\frac{dm_{pr}}{d\varphi} = K_{pr}{m_{inj}}^{1-x}{m_{fup}}^{x}{p_{ox}}^{m} \quad (5.40)$$

where

$$m_{finj} = \int_0^{\varphi}\frac{dm_{finj}}{d\varphi}d\varphi \quad (5.41)$$

$$m_{fup} = m_{finj} - \int_0^{\varphi}\frac{dm_{finj}}{d\varphi}d\varphi \quad (5.42)$$

5.3 General description of the model for combustion

In this investigation, a single cylinder, four stroke, air cooled, direct injection (DI) diesel engine is used. The combustion chamber is a bowl in piston type and the fuel injector has a three hole nozzle. The model used in this study is a two zone thermodynamic model. It is assumed that the cylinder contents a non burning zone of air, and another burning zone in which the fuel is continuously injected during injection and burnt with the available air from the air zone. The model considers only those processes which occur during the possession of compression and expansion stroke. It is assumed that the inlet and exhaust valve are fully closed during the stroke. The compression process in practically all engines is a polytropic one, which begins from the moment the inlet valve, closes and ends when the injection

process starts. The fuels considered for the analysis and their chemical formulae and important properties are given in Table 5.1.

Table 5.1 Properties of diesel and BMDE15

Description	diesel	BMDE15
Chemical formula	$C_{16}H_{34}$	$C_{5.471}H_{6.039}O$
Molecular weight	170	48
Density at 40 °C	2.4	1.73
Carbon	86	65.65
Hydrogen	13.60	10.21
Nitrogen	0.18	0.14
Sulfur	0.22	0.01
Oxygen by difference	0	24

The main calculation is based on the integration of the first law of thermodynamics and the ideal gas equation. The following assumptions are made for the analysis;

(a) The cylinder contains the non-burning zone and burning zone.

(b) The pressure and temperature in each zone are uniform and vary with the crank angle. The content of each zone follows the perfect gas laws.

5.3.1 Energy equations

During the compression stroke, only one zone (of pure air) exists. Then, the first law of thermodynamics for a closed system is applied, together with the perfect gas state equation [128]. The change in internal energy is expressed [138] as follows:

$$\frac{d(mu)}{d\theta} = \frac{dQ_r}{d\theta} - \frac{dQ_h}{d\theta} - \frac{dW}{d\theta} \tag{5.43}$$

By replacing the work transfer term dW/dθ with PdV/dθ or by the ideal gas law PV = mRT, the above equation (5.43) can be rearranged as,

$$m\frac{du}{d\theta} = \frac{dQ_r}{d\theta} - hA\frac{dT}{d\theta} - RT\frac{dV}{d\theta} \tag{5.44}$$

where, V is the instantaneous cylinder volume with respect to the crank angle, which is given by,

$$V = V_{cl} + (\pi D^2/4)r\left[1 + \lambda^{-1} - \cos\varphi - (\lambda^{-2} - sin^2\varphi)^{1/2}\right] \quad (5.45)$$

In the above equations, the term dQ is given as the fourth order polynomial expression of the absolute temperature T, including the enthalpy of formation at absolute zero.

The internal energy calculation as a function of temperature is :

$$\frac{hi}{R_{mol}T} = ai1 + ai2/2\,T + ai3/3T^2 + ai4/4T^3 + ai5/5T^4 + ai6/3T^5 \quad (5.46)$$

$$ui = hi - RT \quad (5.47)$$

For the surrounding air zone, which only loses the mass (air) to the burning zone, the first law of thermodynamics for the unburned zone is written as,

$$dE = dQ - pdV - h_a dm_a \quad (5.48)$$

The burning zone not only receives the mass from the air zone, but also there is an enthalpy flow from the fuel, which is ready to be burned in the time step. So, the first law of thermodynamics for the burning zone becomes

$$dE = dQ - pdV + h_a dm_a + h_f dm_f \quad (5.49)$$

The first law of thermodynamics for the combustion in time step dt is

$$f(E)=E(T_2) - E(T_1) - dQ + dW + dm_f\, Q_{vs} = 0 \quad (5.50)$$

If f(E) is greater than the accuracy, the required new value of T_2 is calculated using the Newton-Raphson numerical method. The unburned zone temperature is calculated using the equation,

$$T_u = T_{soc}\left(\frac{P}{P_{soc}}\right)^{\gamma-1/\gamma} \quad (5.51)$$

5.3.2 Heat transfer model

The heat transfer between the cylinder trapped mass and the surrounding walls is calculated, using the formula of Annand [139]. The Annand formula to calculate the heat loss from the cylinder, is

$$dQ/dt = a\frac{\lambda_g}{D}(Re)^b\left(T_w - T_g\right) + c.\left({T_w}^4 - {T_g}^4\right) \quad (5.52)$$

In this equation 'T_w' is the cylinder wall temperature which is assumed as 450 K, and a, b, c are constants. The constant values are taken as, a=0.2626, b=0.6, c=5.67*10^{-8} W/m^2/K.

5.3.3 Ignition delay

The time delay between the start of injection and the start of combustion is defined as the ignition delay period. The determination of the start of combustion (SOC) by selecting the proper method is a key issue in ignition delay studies. In the combustion model, the ignition delay is also taken into account. The ignition delay period is calculated by integrating Wolfer's relation, using the trapezoidal rule [133].

$$\int_{t_{inj}}^{t_{ign}} \frac{dt}{t(p,T)} = \frac{1}{K_{t_{inj}}} \int_{t_{inj}}^{t_{ign}} \frac{dt}{(p(t))^{-q} \exp(\frac{E}{RT(t)})} = 1 \quad (5.53)$$

The values of various constants corresponding to a DI diesel engine are K =2272; q = -1.19; E/R = 4650.

where K=thermal conductivity

q=heat losses

E/R=activation energy/universal gas constant

A MATLAB programme was written to determine the values of ignition delay with respect to load. The MATLAB programme is given in Annexure III.

5.3.4 Wiebe's combustion model

The Wiebe function is used to predict the mass fraction burnt and the burn rate in IC engines, operating with different combustion systems and fuels. Wiebe linked the chain chemical reactions with the fuel reaction rate in IC engines and his approach is based on the premise that a simple one-step rate equation would not be adequate to describe the complex reacting systems, such as those occurring in an IC engine. The Wiebe functions [140] for the non-dimensional burn fraction x as a function of the degrees of crank angle can be written as

$$x = 1 - exp\left[-6.908\left(\frac{\theta-\theta o}{\Delta\theta}\right)^{m+1}\right] \quad (5.54)$$

The heat release rate calculated with the help of the Wiebe function is,

$$\frac{dQ_c}{d\theta} = 6.908(m+1)\left(\frac{Q_{av}}{\Delta\theta}\right)\left(\frac{\theta-\theta_o}{\Delta\theta}\right)^m exp\left[-6.908\left(\frac{\theta-\theta o}{\Delta\theta}\right)^{m+1}\right] \quad (5.55)$$

where x is the mass fraction burned, θo is the start of combustion and $\Delta\theta$ is the combustion duration. The parameter m represents the rate of combustion. Q_{av} is the heat released per cycle. The value of m for both the fuels is taken as 3.0

When calculating the heat release, prior knowledge of the actual overall equivalence ratio is necessary. The term equivalence ratio is defined as the ratio of the actual air-fuel ratio to the stoichiometric air-fuel ratio. This helps in fixing the mass of fuel to be admitted.

5.3.5 Chemistry of combustion

In a combustion process, the fuel and the oxidizer react to produce products of different compositions. The theory of combustion is a complex one, and has been the topic of intensive research for many years. Let us represent the chemical formula of a fuel as $C\alpha H\beta O\gamma N\delta$. In the present case, it was considered that 10 species were present in the combustion product, and the combustion equation is given by:

$$\epsilon\varphi C\alpha H\beta O\gamma N\delta + 0.21O_2 + 0.79N_2 \rightarrow \nu 1CO_2 + \nu 2H_2O + \nu 3\ N_2 + \nu 4O_2 + \nu 5CO + \nu 6H_2 + \nu 7H + \nu 8O + \nu 9OH + \nu 10NO \quad (5.56)$$

From the atomic balance of each species C- H- O- N the following 4 equations, are obtained.

$$C \quad \epsilon\varphi\alpha = (y1+y5)\ N1 \quad (5.57)$$

$$H \quad \epsilon\varphi\beta = (2y1+2y6+y7+y9)\ N1 \quad (5.58)$$

$$O \quad \epsilon\varphi\gamma+0.42 = (2y1+y2+2y4+y5+y8+y9+y10)\ N1 \quad (5.59)$$

$$N \quad \epsilon\varphi\delta +1.58 = (2y3+y10)\ N1 \quad (5.60)$$

The chemical reactions considered in equilibrium, are as follows:

$$0.5H_2 \longrightarrow H \quad (5.61)$$

$$0.5O_2 \longrightarrow O \quad (5.62)$$

$$0.5H_2+0.5O_2 \longrightarrow OH \quad (5.63)$$

$$0.5O_2+0.5N_2 \longrightarrow NO \quad (5.64)$$

$$H_2+0.5O_2 \longrightarrow H_2O \quad (5.65)$$

$$CO+0.5O_2 \longrightarrow CO_2 \quad (5.66)$$

The use of the equilibrium constant is identical to maximizing the entropy of the gas. This method is similar, when considering a restricted species list such as the present case [141].

Once the composition is known, the thermodynamic properties of interest like enthalpy, entropy, specific volume and internal energy, can be computed.

5.3.6 Nitric oxide (NO) formation model

The current approach to model the NOx emissions from diesel engines is, to use the extended Zeldovich thermal NO mechanism, by neglecting other sources of NOx formation. The extended Zeldovich mechanism consists of the following reactions,

$$O + N_2 \longrightarrow NO + N \tag{5.67}$$

$$N + O_2 \bullet \longrightarrow NO + O \tag{5.68}$$

$$N + OH \longrightarrow NO + H \tag{5.69}$$

This mechanism can be written as an explicit expression for the rate of change of the concentration of NO [142]:

The change of NO concentration is expressed as follows:

$$(d(NO))/dt = 2(1-\alpha^2) R_1/(1+ \alpha R_1/(R_2+R_3)) \tag{5.70}$$

where Ri is the one-way equilibrium rate for the reaction i, defined as,

$$R_1 = k_{1f}(N)e(NO)e, \quad R_2 = k_{2f}(N)e(O_2)e, \tag{5.71}$$

$$R_3 = k_{3f}(N)e(OH)e, \quad \alpha = (NO)/(NO)e \tag{5.72}$$

5.3.7 The net soot formation model

The exhaust of the CI engine contains solid carbon soot particles that are generated in the fuel rich regions inside the cylinder during combustion. Soot particles are clusters of solid carbon spheres, with the HC and traces of other components absorbed on the surface. They are generated in the combustion chamber in the fuel rich zones, where there is not enough oxygen to convert all the carbon to CO_2. Subsequently, as the turbulence motion continues to mix the components, most of these carbon particles find sufficient oxygen to react and form CO_2. Thus, soot particles are formed and consumed simultaneously in the combustion chamber.

The net soot formation rate was calculated by using the semi-empirical model proposed by Hiroyasu et al. [143]. According to this model, the soot formation rate (index sf) and soot oxidation rate (index sc) were given by,

$$\frac{dm_{sf}}{dt} = A_{sf}\left(m_{f.ev} - m_{f.bu}\right)^{0.8} p^{0.5} \exp\left(-E_{sf}/R_{mol}T\right) \tag{5.73}$$

$$\frac{dm_{sf}}{dt} = A_{sc} m_{sn} (p_{o2}/p) p^{1.8} \exp(-E_{sc}/R_{mol}T) \tag{5.74}$$

where, the pressures are expressed in bar and d_{mf} is the unburned fuel mass in kg to be burned in time step dt. Therefore, the net soot formation rate is expressed as

$$\frac{dm_{sn}}{dt} = \frac{dm_{sf}}{dt} - \frac{dm_{sc}}{dt} \tag{5.75}$$

A computer program using MATLAB was generated, with all the above mentioned equations and considering all the values of the constants, in order to predict the combustion attributes, like the in- cylinder pressure, crank angle, heat release rate, heat losses and the NO emissions. The MATLAB program used for this analysis is given in Annexure IV.

CHAPTER 6

RESULTS AND DISCUSSION

6.1 General

The present study establishes the experimental results obtained from operating a CI engine with bioethanol obtained from the Madhuca Indica flowers, which is an early stage of research in its kind. As mentioned in Chapter 5-Metholdology of the present work, bioethanol was used in the test engine adopting the following techniques: (i) emulsifying it with diesel in different percentages (ii) adding small quantities of an ignition improver (DEE) with an optimum percentage of bioethanol diesel emulsion (iii) inducting DEE in suction at different percentages while bioethanol was injected in small quantities, and (iv) fumigating bioethanol in suction while diesel was injected as a pilot fuel. The results of the combustion, performance and emission characteristics of the engine run on each technique were collected, analysed and compared with those of diesel operation of the same engine. The best technique was chosen based on the analysis of the results. The results of the best technique were also validated with the theoretical analysis using a MATLAB program. Furthermore, the engine was run for about 100 hours as per IS: 10000 (Part IX)-1980 ‘Methods of tests for internal combustion (IC) engines Part IX Endurance tests’ for constant speed engines, to study the durability issues associated with the best technique chosen in this investigation and the results were analysed. In addition to these, the results pertaining to the combustion, performance and emissions of the engine run on the bioethanol-diesel-biodiesel emulsions were also analysed. All the analysis of the results of this investigation is presented in the subsequent sections.

6.2 Results obtained from the engine fueled with bioethanol-diesel emulsions

In this section, the results obtained from the engine fueled with different bioethanol diesel emulsions are analysed, compared and presented.

6.2.1 Combustion parameters

Combustion parameters such as pressure, ignition delay, heat release rate, combustion duration and rate of pressure rise were collected for every brake mean effective pressure (BMEP) of the engine. The values of BMEP 0, 1.4, 2.8, 4.5 and 5.6 bar are obtained at 0, 25%, 50%, 75% and 100% load respectively. Using the collected data, different graphs were

plotted by taking the measured parameters in variation with the crank angle or BMEP for the analysis. The analysis of the measured combustion parameters are discussed in this subsection.

6.2.1.1 Pressure (P)-crank angle (θ) diagram

Figure 6.1 depicts the variation of cylinder pressure with crank angle for diesel and the three different emulsions,

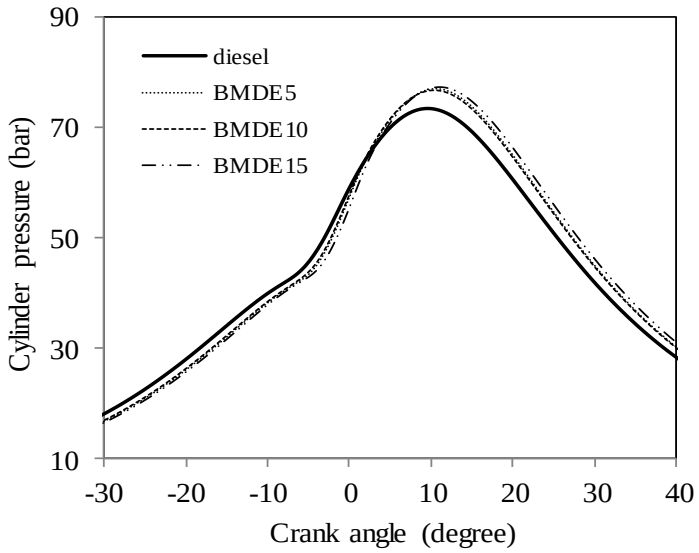

Fig. 6.1 Variation of cylinder pressure with crank angle

It can be observed from the figure that, the commencement of ignition is the earliest for diesel, followed by BMDE5, BMDE10 and BMDE15. This is because of the higher cetane number of diesel. With the increase in the percentage of bioethanol the cetane number of the emulsion decreases, and hence, the commencement of ignition is delayed at full load or full load. The cylinder peak pressures for the BMDE5, BMDE10 and BMDE15 emulsions are found to be about 77.0 bar, 76.8 bar and 77.4 bar respectively, which are attained approximately at 370.4 ^{o}CA, 370.2 ^{o}CA and 371.3 ^{o}CA respectively at full load, whereas for diesel, it is 73.5 bar at 369.6 ^{o}CA at full load. For the BMDE15 emulsion, the combustion pressure occurs approximately about 2^{o}CA after the diesel ignition. Generally, the peak pressure of the CI engine is attributed to the ignition delay, and the mixture preparation in the delay period [127]. As a result of the lower cetane number of the emulsion, the peak pressures in the bioethanol operation are found to be higher than that of diesel operation, at full load. The results are similar to the results reported by Rakopoulus DC et al. [144].

6.2.1.2 Ignition delay

The variation of ignition delay for diesel and the bioethanol-diesel emulsions for different BMEP is illustrated in Fig. 6.2. The ignition delay decreases with an increase in the engine load or BMEP. When the engine load increases, the heat prevailing inside the combustion chamber increases, and hence, decreases the ignition delay.

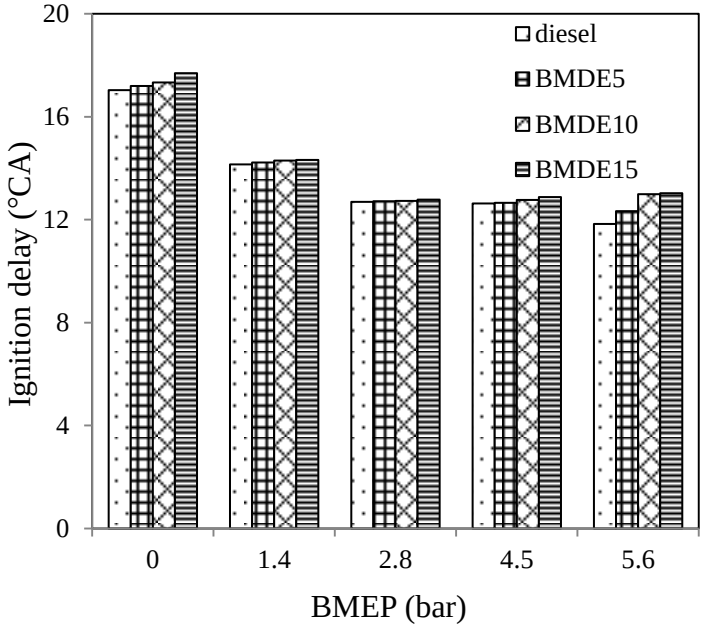

Fig. 6.2 Ignition delay for diesel and the bioethanol-diesel emulsions for different BMEP

It is apparent from the figure that the ignition delay increases with the increase in the bioethanol content throughout the load spectrum or increasing load, as a result of the decrease in the cetane number. Also, the ignition delays of all the emulsions tested in this study are found to be longer than that of diesel in the entire engine operation. The maximum difference in the ignition delay between diesel and the bioethanol-diesel emulsions at full load is about 2 °CA. At full load, the BMDE15 emulsion shows the longest ignition delay compared to that of diesel.

6.2.1.3 Heat release rate (HRR)

Figure 6.3 illustrates the variation of the heat release rate with crank angle for diesel and the bioethanol-diesel emulsions at full load. The maximum heat release rate in the premixed combustion stage depends upon the quantity of fuel accumulated in the delay period, the burning rates and duration of the delay period. As a result of the longer ignition delay and lower viscosity of the bioethanol diesel emulsions, the maximum HRR is found to be the

highest with the BMDE15 emulsion followed by the BMDE5, BMDE10 emulsions and diesel.

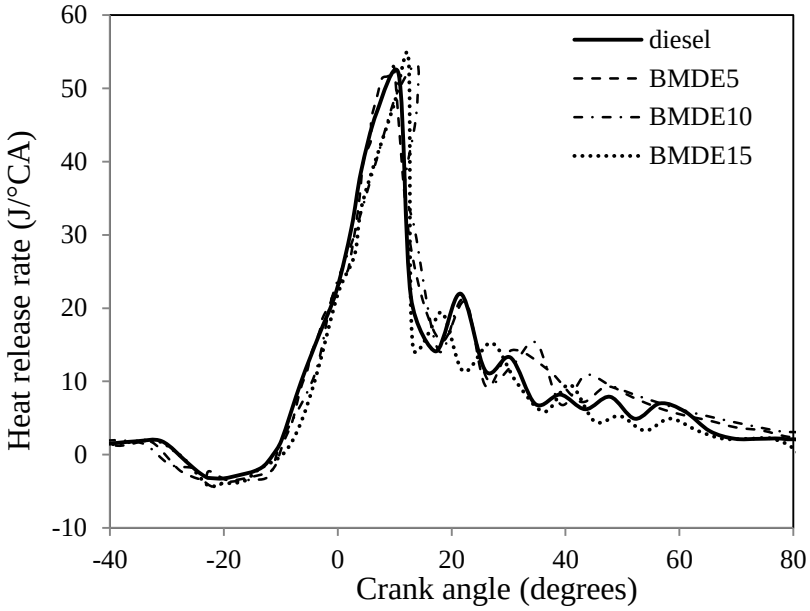

Fig. 6.3 Variation of the heat release rate for diesel and bioethanol-diesel emulsions at full load

Another reason may be due to better mixing, and more complete combustion of the fuel-air mixture. In the case of the BMDE10, the latent heat of vaporisation of the emulsion may dominate the other fuel properties, and hence, a lower heat release rate is noticed. The approximate values of the maximum heat release rate for diesel, BMDE5, BMDE10 and BMDE15 are 51.8, 52.9, 53.3 and 54.0 J/°CA respectively at full load.

6.2.1.4 Maximum cylinder pressure

Figure 6.4 portrays the cylinder pressure for different percentages of bioethanol in the emulsions for different BMEP. The cylinder peak pressure of a compression ignition (CI) engine is mainly due to the amount of fuel accumulated in the delay period, and the combustion rate in the initial stages of premixed combustion [128]. It is evident from the figure that the maximum cylinder pressures for the bioethanol-diesel emulsions are found to be higher than that of diesel operation, as a result of higher heat release rates. The maximum cylinder pressure for diesel ranges approximately from 53.4 bar to 73.5 bar, from no load to full load respectively. For the BMDE5 emulsion, the values of the maximum cylinder pressure ranging from no load to full load are approximately 54.3 to 77.0 bar respectively. In

the case of the BMDE10 and BMDE15 emulsions, the maximum pressures are found to be in the range of 52.5 to 76.8 bar and 54.3 to 77.4 bar at no load to full load respectively.

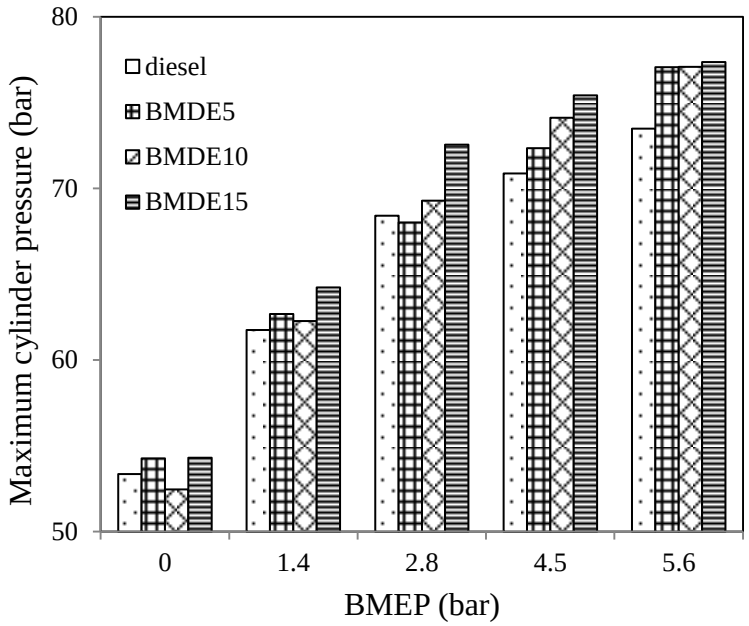

Fig. 6.4 Variation of the maximum pressure for diesel and the bioethanol-diesel emulsions for different BMEP

The percentage increase of the maximum cylinder pressure for the BMDE5, BMDE10 and BMDE15 emulsions are about 3.3, 2.7 and 3.8 % respectively, compared to that of diesel at full load.

6.2.1.5 Maximum rate of pressure rise

One of the important factors affecting the life of the CI engine is the mechanical load that is imposed on the engine components [128]. The greater the engine load or BMEP imposed, the lesser the expectancy of the life of the engine. The mechanical load or BMEP is mainly influenced by the rate of pressure rise. As per the standards, the value for the maximum rate of pressure rise prescribed for a single cylinder, four stroke, DI diesel engine is 8 bar/°CA. If the maximum rate of pressure rise exceeds this value, then the life of the engine will certainly decrease. The variation of the maximum rate of pressure rise with the engine BMEP for the fuels tested in this study is portrayed in Fig. 6.5. From the figure, it is noticed that the maximum rate of pressure rise is the highest at full load, in this study. With a higher proportion of bioethanol addition, the ignition delay is increased and more fuel gets accumulated, and reacts for more time with oxygen. So, there is a rapid pressure rise, which

may impact on the piston suddenly. At minimum BMEP conditions, the lower proportion of bioethanol in the emulsion may have better miscibility and good mixture formation quality.

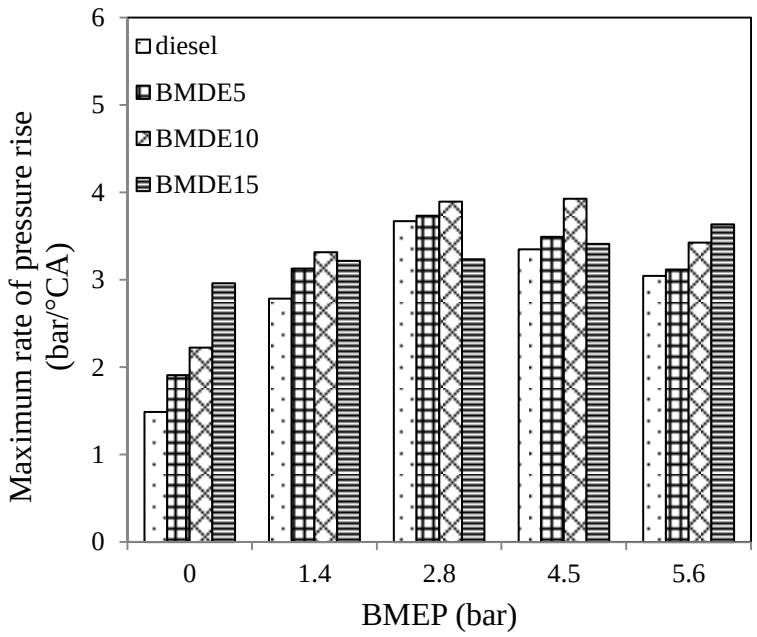

Fig. 6.5 Variation of the maximum rate of pressure rise of bioethanol diesel emulsions and diesel with BMEP

Hence, the maximum rate of pressure rise is more compared to diesel at minimum load conditions.

6.2.1.6 Combustion duration

Figure 6.6 shows the combustion duration with respect to the percentage of bioethanol in the emulsions at different BMEP. The combustion duration decreases with an increase in the bioethanol. The addition of bioethanol with diesel decreases the heating value of the emulsion. On the other hand, the oxygenated fuel can promote the combustion rate, especially the diffusive combustion rate. It can be observed from the figure, that at maximum load, all the bioethanol-diesel emulsions exhibit shorter combustion durations compared to that of diesel. The reason may be the faster combustion rate as a result of longer ignition delay and oxygen enhanced combustion.

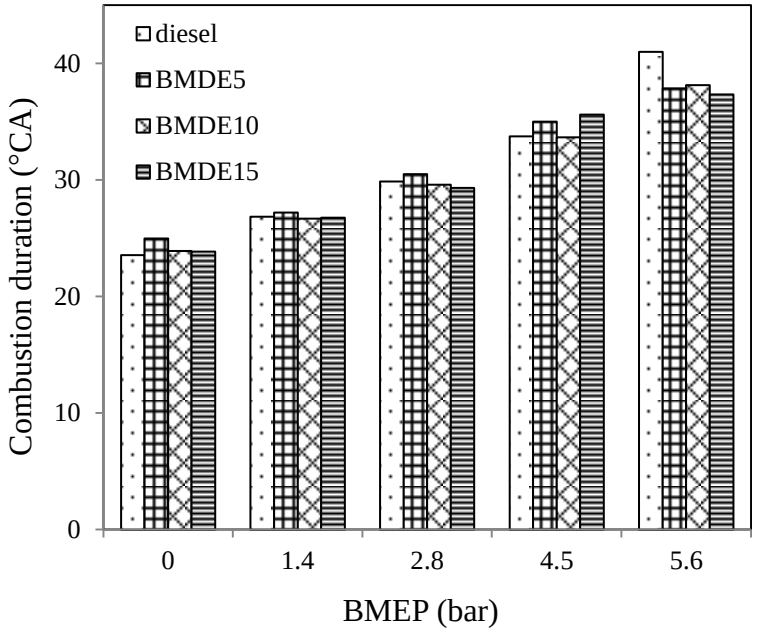

Fig. 6.6 Variation of combustion duration for diesel and the bioethanol-diesel emulsions with BMEP

Similar results are reported by Rakopolous DC et al. [145] in their study of the HSDI engine.

6.2.2 Engine performance analysis

The brake specific energy consumption, exhaust gas temperature and thermal energy balance are important parameters, which describe the performance of the diesel engine, when it is run with an alternative fuel blend or emulsion. Therefore, the results of the above mentioned factors obtained for the bioethanol diesel emulsions are analysed in comparison with those of diesel operation of the same engine and discussed in the following subsections.

6.2.2.1 Brake specific energy consumption (BSEC)

Figure 6.7 illustrates the variation of the BSEC of diesel and the bioethanol-diesel emulsions for different BMEP. If two different fuels of different densities and calorific values are blended, then the BSEC is considered instead of the BSFC, and the unit is expressed in MJ/kWh. It can be observed from the graph that the BSEC decreases with an increase in the engine load as a result of the increase in the cylinder temperature. The BSEC for the BMDE5, BMDE10 and BMDE15 emulsions is found to be higher by about 17.3, 17.5 and 30.1 % respectively, than that of diesel at full load. Bioethanol has a lower heating value than diesel.

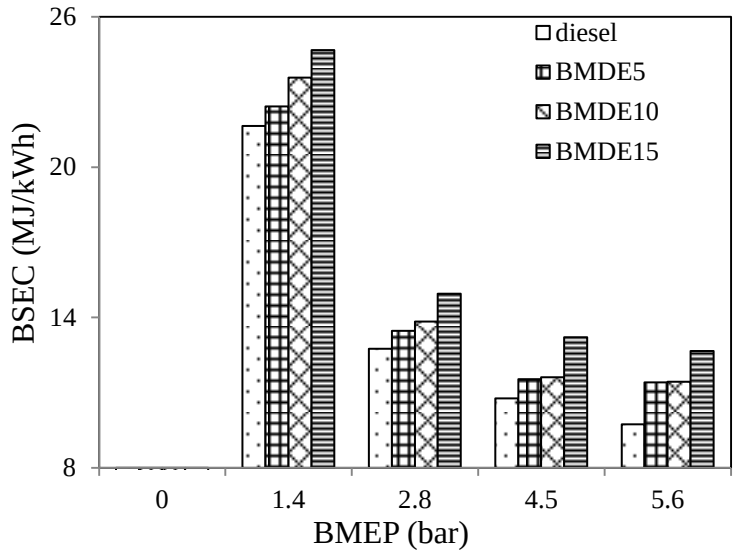

Fig. 6.7 Variation of BSEC for diesel and the bioethanol-diesel emulsions with BMEP

When small percentages of it are emulsified with diesel, the heating value of the resultant emulsion is also lower than that of diesel. Hence, the BSEC of the engine fueled with the bioethanol diesel emulsions is higher than that of diesel operation at any given output.

6.2.2.2 Exhaust gas temperature (EGT)

One indication of good energy conversion of the engine is defined by the measurement of its EGT [122]. The variation of the EGT with respect to different percentages of bioethanol in bioethanol-diesel emulsions for different loads, is shown in Fig 6.8.

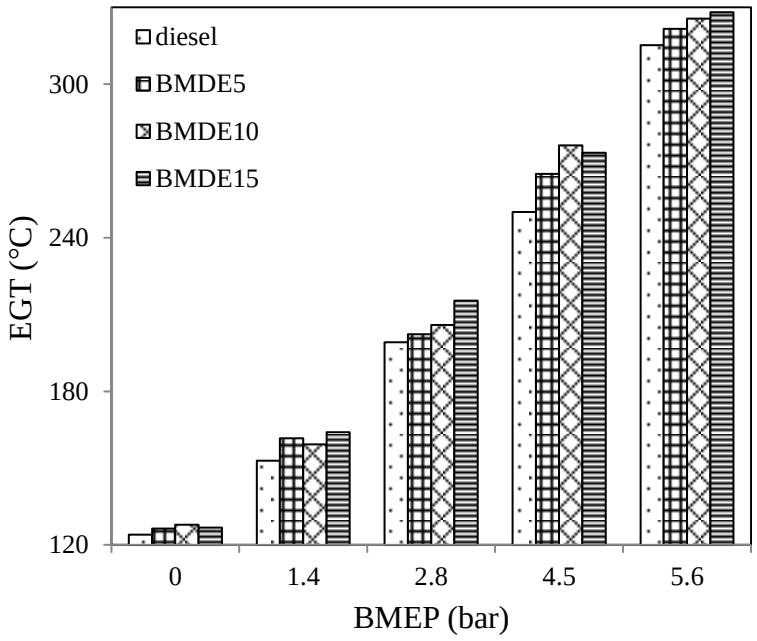

Fig. 6.8 Variation of EGT for diesel and the bioethanol-diesel emulsions with BMEP

The EGT increases with the increase in load for all the tested fuels. The EGT for diesel, BMDE5, BMDE10 and BMDE15 is found to be about 315.3, 321.6, 325.6 and 328.2 °C respectively, at full load. BMDE5 has a lower EGT compared to that of BMDE10 and BMDE15 throughout the entire engine operation. This may be due to the effective combustion which takes place in the early stages of the exhaust stroke, and hence, there is a saving with respect to the exhaust gas energy loss. The BMDE15 possesses a higher EGT compared to that of diesel, BMDE5 and BMDE10 at full load. The reason may be due to more energy consumption and shorter combustion duration of the BMDE15 emulsion.

6.2.2.3. Thermal energy balance

Thermal energy balance is defined as the heat input given by fuel in respect of useful work, heat loss through the exhaust, heat carried away by the lubricating oil and unaccounted losses (radiation, vapour in the exhaust, heat transfer through fins etc.) [145]. The method of calculating the thermal energy balance has already been discussed in Chapter 4.

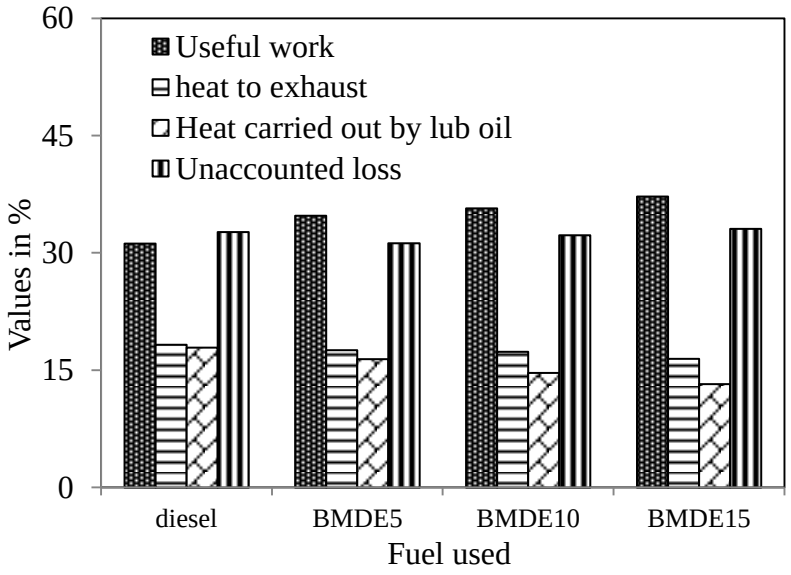

Fig. 6.9 Variation of thermal energy balance for diesel and the bioethanol-diesel emulsions at full loads

The variation of the thermal energy balance for diesel and the bioethanol-diesel emulsions at full load is shown in Fig. 6.9. It is evident that the useful work increases for all the tested fuels, but other losses are decreased. The useful work for the BMDE5, BMDE10 and BMDE15 emulsions is found to be higher by about 3, 4 and 6% compared to that of diesel at full load. This may be due to an efficient combustion of emulsion, and the cooling effect of bioethanol. A similar result has been reported by Ajav et al. At full load, the heat loss through

the exhaust is found to be higher for all the emulsions compared to that of diesel. Though an efficient work is achieved by the emulsions, some amount of heat is lost, which may be due to the burning of fuels at the end of the expansion stroke. Other losses are minimised with a higher percentage of bioethanol operation.

6.2.3 Emission analysis

In this subsection, the emission parameters for a given power output, viz., hydrocarbon (HC), carbon monoxide (CO), nitric oxide (NO), and smoke of the engine fueled with the different bioethanol diesel emulsions are analysed, compared with those of diesel operation, and presented.

6.2.3.1 Brake specific hydrocarbon (BSHC) emission

The HC emission of the diesel engine is primarily influenced by fuel quality, and the oxygen available for complete combustion. It is also influenced by the ignition delay and rate of reaction and engine design [128]. The HC emission is relatively lower for CI engines compared to SI engines. Figure 6.10 shows the variation of the BSHC emissions with respect to different percentages of bioethanol in bioethanol-diesel emulsions for different loads.

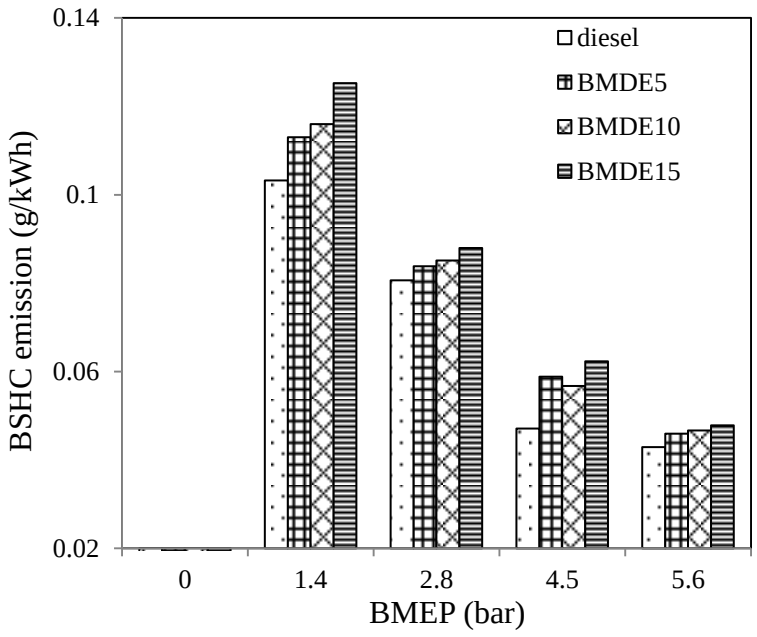

Fig. 6.10 Variation of BSHC for diesel and the bioethanol-diesel emulsions at different loads

The BSHC emissions of the three bioethanol diesel emulsions tested in this study are found to be higher than that of diesel at full load. The BSHC emissions of BMDE5, BMDE10 and

BMDE15 are found to be higher by about 4.3%, 8.3% and 22.2 %, compared to that of diesel at full load. The increase in the volume of bioethanol increases the heat of evaporation and formation of a quench layer. This may slow down the vaporization and mixing of fuel with air, and hence, the BSHC emissions for a given power output increased with an increase in the percentage of bioethanol in the emulsions. The BSHC values of diesel, BMDE5, BMDE10 and BMDE15 at full load are recorded as 0.042, 0.045, 0.046 and 0.047 g/kWh respectively at full load.

6.2.3.2 Brake specific carbon monoxide (BSCO) emission

The variation of BSCO emissions with respect to different percentages of bioethanol in bioethanol-diesel emulsions for different loads is shown in Fig. 6.11. The BSCO emission is a product of incomplete combustion, due to insufficient amount of oxygen available in the air-fuel mixture, or insufficient time in the cycle for completion of combustion at every load.

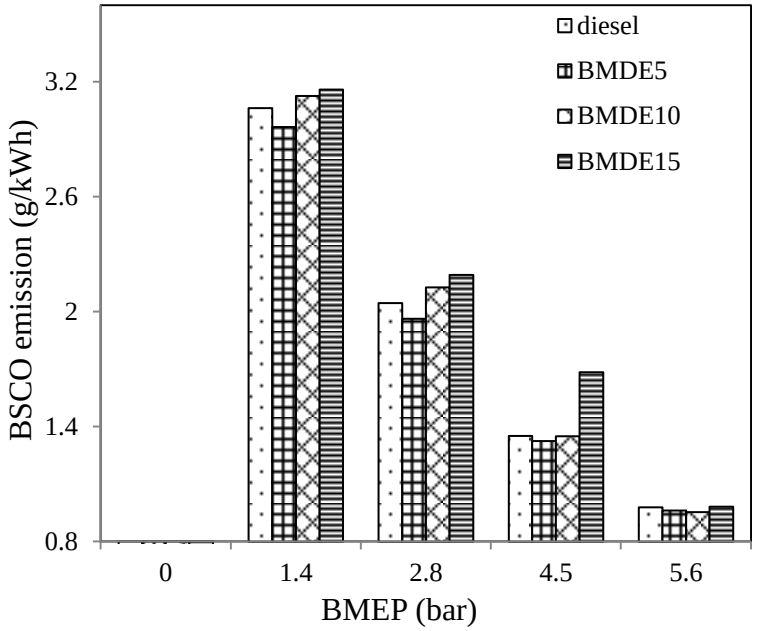

Fig. 6.11 Variation of BSCO for diesel and the bioethanol-diesel emulsions at different BMEP

At full load, the BSCO emission is marginally lower for BMDE5 and BMDE10 compared to that of diesel. This may be due to the proper mixture formation achieved at a lower percentage of bioethanol in the emulsion. But at a lower load, the BSCO emission is found to be more for BMDE10 and BMDE15 compared to both BMDE5 and diesel. At lower loads, less fuel is injected and there is less time for mixture formation; hence, the combustion temperature is low, which may lead to more BSCO emission.

6.2.3.3 Brake specific nitric oxide (BSNO) emission

The two principal factors that affect the formation of NO emission in a CI engine are the cylinder gas temperature and oxygen availability for combustion [122]**.** The variation in the BSNO emission given in g/kWh with respect to different percentages of bioethanol for different loads is depicted in Fig. 6.12. The BSNO emission for the bioethanol-diesel emulsions is found to be lower than that of diesel throughout the engine operation [145]. This is due to the higher latent heat of vaporisation of bioethanol, that results in a lower cylinder temperature. Similar results have been reported by researchers who have investigated with the ethanol/bioethanol emulsions obtained from sugarcane and sugar molasses [123, 146-147]. The reductions of BSNO in percentage for the BMDE5, BMDE10 and BMDE15 emulsions with respect to diesel at full load are 8%, 14% and 24% respectively. The BSNO emission for BMDE15 decreases with the increase in the percentage of bioethanol in the emulsion at full load, as a result of the high latent heat of vaporisation.

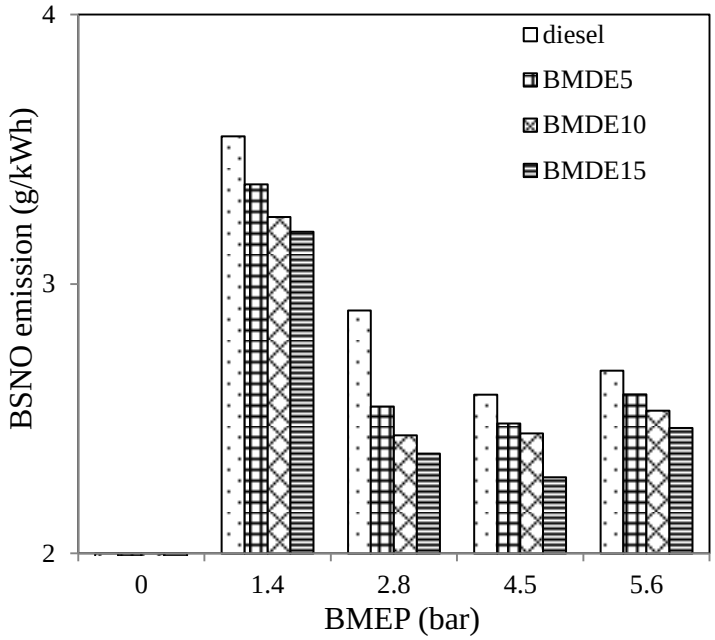

Fig. 6.12 Variation of BSNO for the diesel and the bioethanol-diesel emulsions at different BMEP

However, the BMDE5 and BMDE10 emulsions exhibit lower BSNO emissions compared to those of diesel, and the BMDE15 emulsion at part loads.

6.2.3.4 Smoke emission

Figure 6.13 shows the variation of the smoke emission for different percentages of bioethanol in the bioethanol-diesel emulsions for different loads.

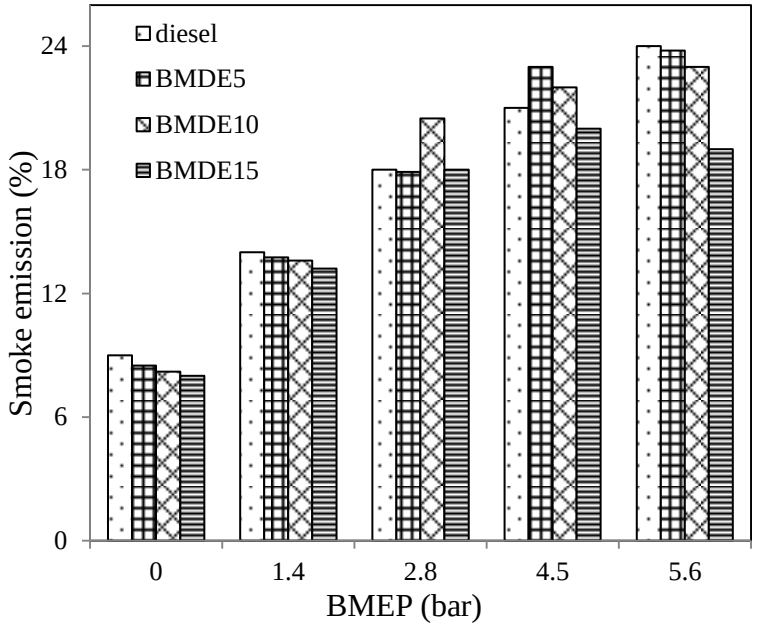

Fig. 6.13 Variation of smoke emission for diesel and the bioethanol-diesel emulsions at different BMEP

The bioethanol has less number of carbon atoms in it, and hence, the ratio of carbon to hydrogen is two. As a result, lower smoke emissions are recorded for the bioethanol-diesel emulsions. Bioethanol is an oxygenated fuel, which may increase more complete combustion. This may be another possible reason for the reduced smoke levels of the bioethanol-diesel operation in comparison with the diesel operation, at full load [148]. The smoke emission of the BMDE5, BMDE10 and BMDE15 emulsions are found to be lesser by about 2.31, 4.8 and 20.8% respectively, compared to that of diesel at full load.

6.2.4 Summary

After conducting an experimental study on a diesel engine run with the three different bioethanol-diesel emulsions, varying the bioethanol fraction from 5 to 15% at a regular interval of 5% on a volume basis, the following are summarised;

The ignition delay of the bioethanol-diesel emulsions increased by about 1-3^{o}CA in comparison with diesel, which is due to a decrease in the cetane number of the emulsions. The maximum cylinder pressures of the emulsions are higher by about 1-4% respectively, compared to that of diesel at full load. The NO emissions for the bioethanol-diesel emulsions are found to be lower, with a maximum reduction of about 24% in comparison with diesel at full load, which is due to the higher latent heat of vaporization of bioethanol. In comparison with diesel, the smoke emissions of bioethanol diesel operation exhibited lower smoke

emissions with a maximum reduction of 21% with BMDE15, at full load, as a result of the lower carbon-to-hydrogen ratio and more complete combustion. However, the HC emission with the bioethanol diesel emulsions is found to be higher as a result of the quench layer, in comparison with the diesel operation, though the CO emissions are found to be lower. The BMDE15 is found to be better than BMDE5 and BMDE10, based on the performance and emission parameters. There is a noisy and rough operation noticed with BMDE15, due to its cetane number. If there is any possibility of increasing the cetane number of the emulsion, it may improve the engine operation, by reducing the delay period.

6.3 Investigation of bioethanol-diesel-DEE blends

When the engine was run with different bioethanol and diesel emulsions, the engine produced low NO and smoke emission. The performance of the engine was also comparable with that of diesel operation. But, it was able to run with a maximum of 15% bioethanol in the emulsion, and 15% bioethanol in the emulsion gave shrugging due to its lower cetane number.

Cai et al. [85, 149] explained that the cetane number will gradually decrease when ethanol is added in higher percentage to a diesel engine. For the smooth operation of the engine, the cetane number should not be less than 30. Due to this, an ignition improver (DEE) was added in small quantities to the BMDE15 emulsion (diesel+bioethanol 15% emulsion) to reduce the ignition delay and engine knocking. The different types of fuel used in this study were DED1%, DED1.5%, DED2% and DED2.5% where DED refers to bioethanol-diesel emulsion of 15%, and the numeric values were percentages of DEE added to the emulsion. This chapter discusses the results obtained from the experimentation done in a DI diesel engine fueled with the optimum bioethanol-diesel emulsion blended with different percentages of DEE, up to a maximum of 2.5%.

6.3.1 Combustion parameters

The results of the combustion parameters of the engine fueled with the optimum bioethanol diesel emulsion blended with different percentages of DEE are analysed, compared with the diesel data and presented in the following subsections.

6.3.1.1 P-θ diagram

The variation of cylinder pressure with crank angle for the BMDE15 emulsion, with and without an ignition improver, and diesel is illustrated in Fig. 6.14. The start of the combustion of diesel air mixture is noticed as the earliest, and the peak cylinder pressure is the lowest among the fuels tested in this study. This is attributed to the higher cetane number of diesel. The start of combustion of BMDE15 is the farthest, due to the reduced cetane number, and the higher latent heat of vaporisation, which requires more time for the mixture formation. Adding DEE in small quantities up to 2.5% with BMDE15 advances the start of combustion, and lowers the cylinder peak pressure. The peak cylinder pressure occurs by about 9.6°CA away from the TDC, for diesel at full load. But, in the case of BMDE15, it occurs at 11.3°CA

away from the TDC. The peak cylinder pressure curve is slightly shifted towards the TDC, than that of BMDE15 with the ignition improver, but still away from the diesel curve.

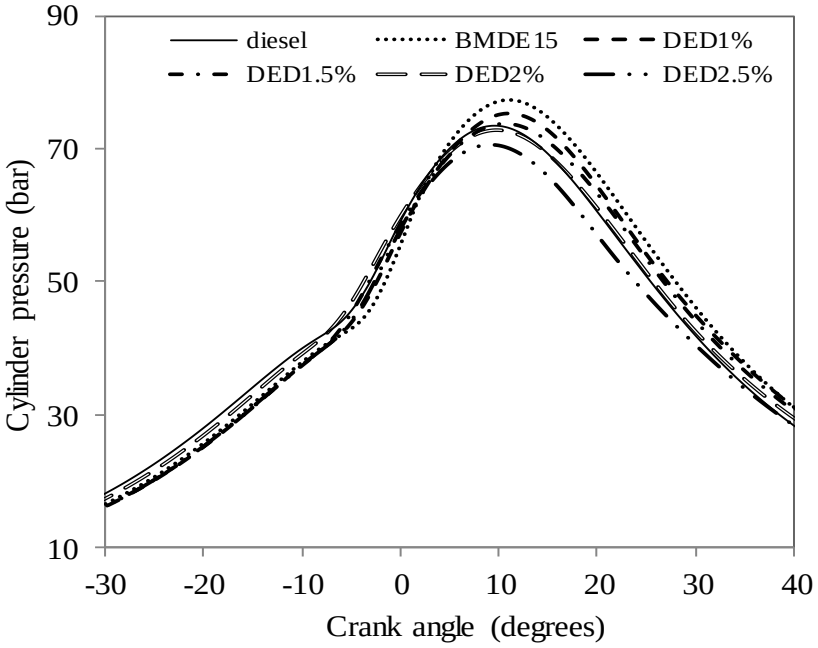

Fig. 6.14 Variation of cylinder pressure with crank angle

The cylinder peak pressures for BMDE15, DED1%, DED1.5%, DED2% and DED2.5% are 77.4 bar, 75.3 bar, 73.8 bar, 72.8 bar and 70.6 respectively, and are attained approximately at 371.3 ^{o}CA, 370.8 ^{o}CA, 370.7 ^{o}CA,369.9 ^{o}CA and 369.2 ^{o}CA respectively at full load, whereas for diesel, it is 73.5 bar at 369.6^{o}CA.

6.3.1.2 Ignition delay

The variation of the ignition delay for diesel, BMDE15, DED1%, DED1.5%, DED2% and DED2.5% at different BMEP is shown in Fig. 6.15. The ignition delay of all the tested fuels in this study decreases with an increase in the load, as a result of increased cylinder gas temperature. It is apparent from the figure that, the ignition delay is found to be reduced with the higher addition of DEE. The black zone which represents the band width of 10-12 °CA for the delay period indicates that at high loads, the ignition delay is significantly lower, and the deviation of the ignition delay between lower and higher loads is about 6 °CA. The 10-12 °CA band width for the ignition delay is more in the case of DED2% and DED2.5% from no load to full load. The higher band width of ignition delay about 16-18 °CA is achieved in the case of BMDE15 at no load, compared to that of diesel and BMDE15 with the ignition improver.

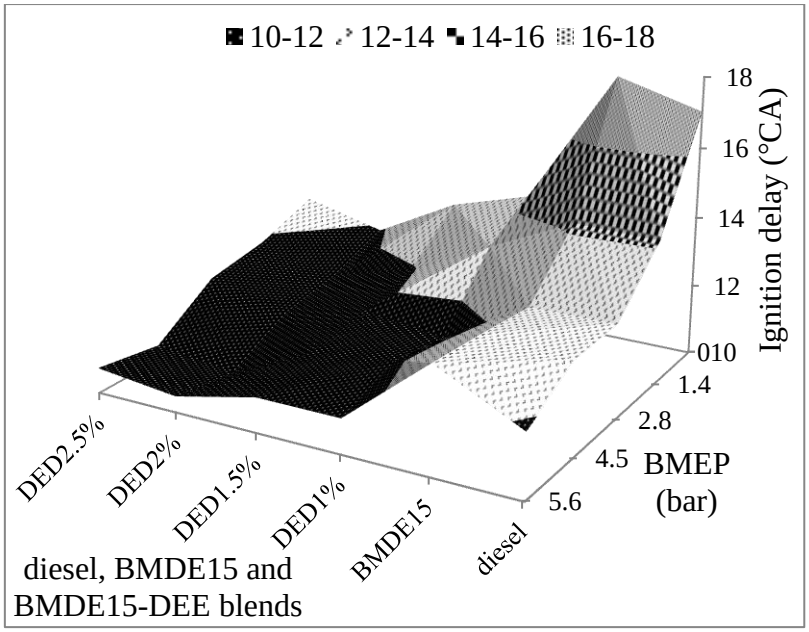

Fig. 6.15 Variation of ignition delay with BMEP

The higher latent heat of vaporisation of bioethanol increases the physical delay period of ignition delay. The ignition delay for BMDE15, DED1%, DED1.5%, DED2% and DED2.5% varies from 1 to 2 °CA at full load, compared to that of diesel.

6.3.1.3 Heat release rate (HRR)

Figure 6.16 illustrates the variation of the heat release rate with the crank angle for diesel, 15% bioethanol diesel emulsion, with and without the ignition improver at full load. The heat release rate was calculated using the method described in Chapter 5. The premixed combustion duration is the time interval from the start of combustion to the time of the first peak on the heat release curve. It is seen from the figure, that the HRR is the highest for BMDE15 followed by DED1%, DED1.5%, diesel, DED2% and DED2.5%. The higher HRR exhibited by BMDE15 is mainly due to more accumulation of the fuel air mixture in the delay period, as a result of the longer ignition delay. It may also be due to the better mixing and complete combustion of the fuel air mixture. The addition of DEE with the emulsion up to 1.5% reduces the heat release rate a little, because of the influence of the ignition improver.

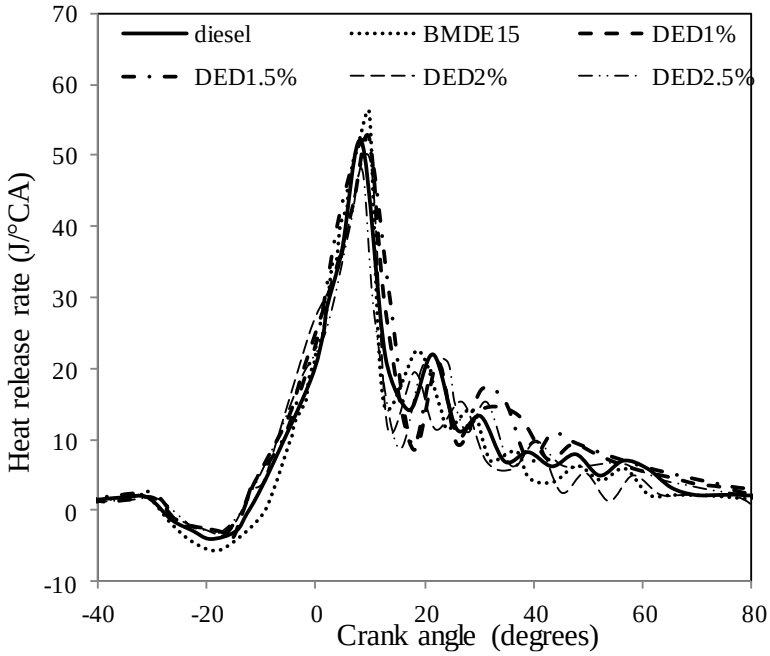

Fig. 6.16 Variation of heat release rate with crank angle at full load

However, the ignition improver dominated more, over combustion, and hence, results in lower heat release rates than that of diesel at full load.

6.3.1.4 Maximum cylinder pressure

Figure 6.17 portrays the variation of the maximum cylinder pressure with BMEP, for diesel, BMDE15, DED1%, DED1.5%, DED2% and DED2.5%.

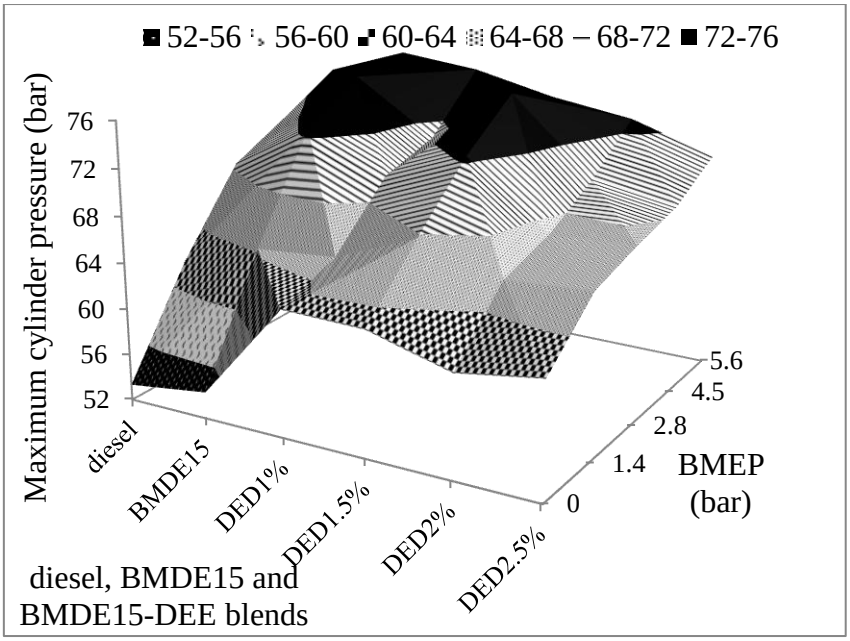

Fig. 6.17 Variation of maximum cylinder pressure with BMEP

The peak cylinder pressure for the BMDE15 emulsion is found to be higher than that of diesel operation, which is due to a longer ignition delay at full load. Due to the accumulation of more fuel and better combustion, the cylinder pressure increases. The cylinder peak pressure for diesel varies from 53.4 bar to 73.5 bar, from no load to full load respectively. For the BMDE15 the values of the maximum cylinder pressure from no load to full load are 54.3 to 77.4 bar respectively. In the case of DED1%, DED1.5%, DED2% and DED2.5%, the peak pressures are found to be in the range of 63.0 to 75.3 bar, 62.8 to 73.8 bar, 60.9 to 72.8 bar and 62.1 to 70.6, from no load to full load respectively. It is also noticed that the maximum cylinder pressure, 72-76 band width is achieved up to DED1.5% blend, but after that, it shows a declining trend. This may be due to the shorter ignition delay, which allows a lesser accumulation of fuel, and also to the lower calorific value of bioethanol and DEE; hence, a lower peak pressure is noticed.

6.3.1.5 Maximum rate of pressure rise

It can be observed from Fig. 6.18, that the peak of rate of pressure rise for the DED2% and DED2.5% is found to be less than that of diesel. But, the peak of DED1.5% is found to be closer to that of diesel at full load.

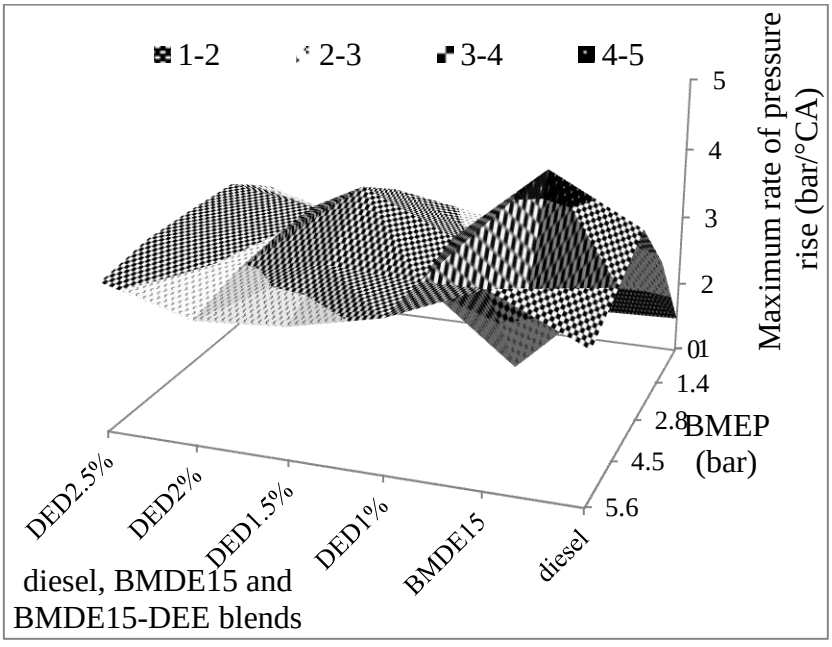

Fig. 6.18 Variation of maximum rate of pressure rise with BMEP

The maximum rate of pressure rise of 4-5 bar/°CA band width is observed for the BMDE15 compared to that of diesel and BMDE15 with ignition improvers, due to the longer ignition

delay. The addition of DEE to the emulsions reduces the delay period, and hence, results in a smoother operation than that of BMDE15. The figure also shows that, the engine experiences a lower rate of pressure rise for all the fuels throughout the load spectrum, except at no load with BMDE15.

6.3.1.6 Combustion duration

Figure 6.19 depicts the variation of combustion duration for the BMDE15 emulsion, with and without an ignition improver, and diesel at different load. The combustion duration has a shorter band width of 20-30 °CA at low loads. The band width of 60-70 °CA at high loads is the result of more fuel being injected, irrespective of the fuels tested in this study. The combustion duration for BMDE15 is found to be lesser than that of diesel at full load. As bioethanol is an oxygenated fuel, the lower viscosity of the BMDE15 emulsion reduces the diffusion combustion phase, and hence, results in a shorter combustion duration. This is also reflected in the heat release rate curve.

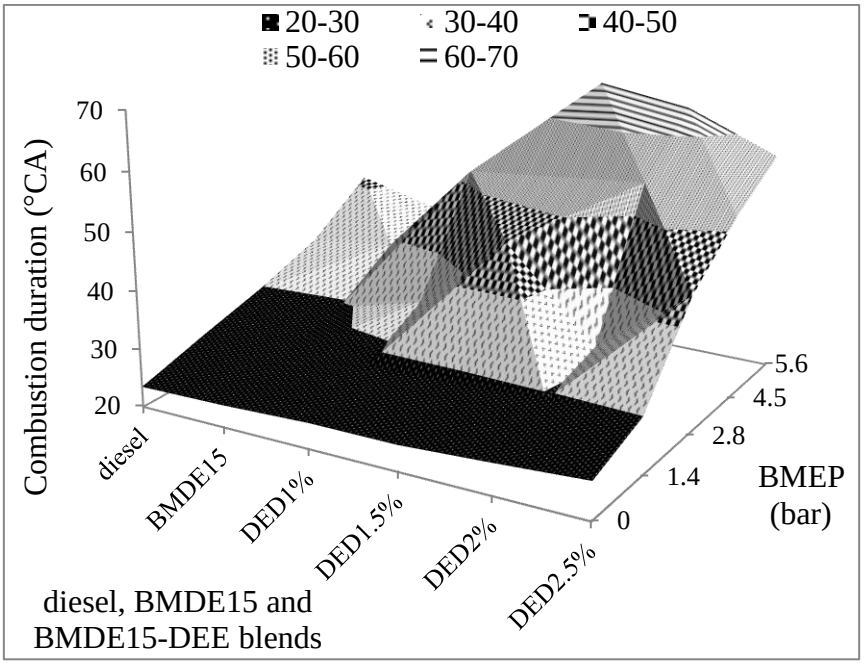

Fig. 6.19 Variation of combustion duration with BMEP

The combustion duration increases with the increase in the percentage of DEE addition. It is observed that at full load, the combustion duration is more for DED1.5% and DED2% in the band width of 60-70 °CA. This is due to increased diffusion combustion, as a result of the cooling effect of the DEE.

6.3.2 Engine performance analysis

The engine performance parameters, such as brake specific fuel consumption, and exhaust gas temperature of the engine operated with different BMDE15-DEE blends, are analysed and compared with the diesel data of the engine and presented in the subsequent subsections.

6.3.2.1 BSEC

Figure 6.20 depicts the variation of the BSEC of diesel, BMDE15, DED1%, DED1.5%, DED2% and DED2.5% with BMEP. It is apparent from the graph, that at full load, the BSEC for the DEE blends increases with the increase in the percentage of DEE.

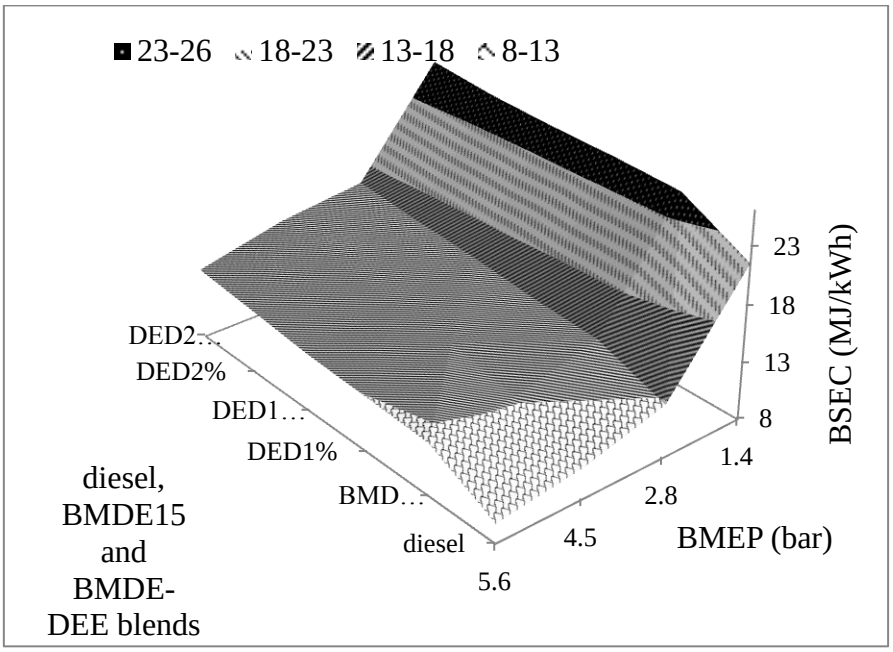

Fig. 6.20 Variation of BSEC with BMEP

At full load, the BSEC for diesel, BMDE15, DED1%, DED1.5%, DED2% and DED2.5% is found to be 9.7, 12.7, 12.9, 13.2, 13.7 and 14.3 MJ/kWh, respectively. The band width of 8-13 MJ/kWh is noticed for diesel and BMDE15 at full load. But, for BMDE15 with the ignition improver, the band width of 13-18 MJ/kWh is found to be increased at full load. At no load, a higher band of 23-26 MJ/kWh is noticed for the BMDE15, DED2%, DED2.5%. This is due to the low heating value of DEE.

6.3.2.2 EGT

Figure 6.21 depicts the variation of the EGT for diesel, BMDE15, DED1%, DED1.5%, DED2% and DED2.5% with BMEP. The EGT increases with the load for all the tested fuels in this study, which is due to the increase in the fuel consumption to meet the power

requirement at every load. At full load, the EGT for diesel, BMDE15, DED1%, DED1.5%, DED2% and DED2.5% is found to be 315.3 °C, 328.7 °C, 361.8 °C, 406.6 °C, 383.2 °C and 386.1 °C respectively. The EGT is the lowest for diesel as a result of the higher conversion of heat into work.

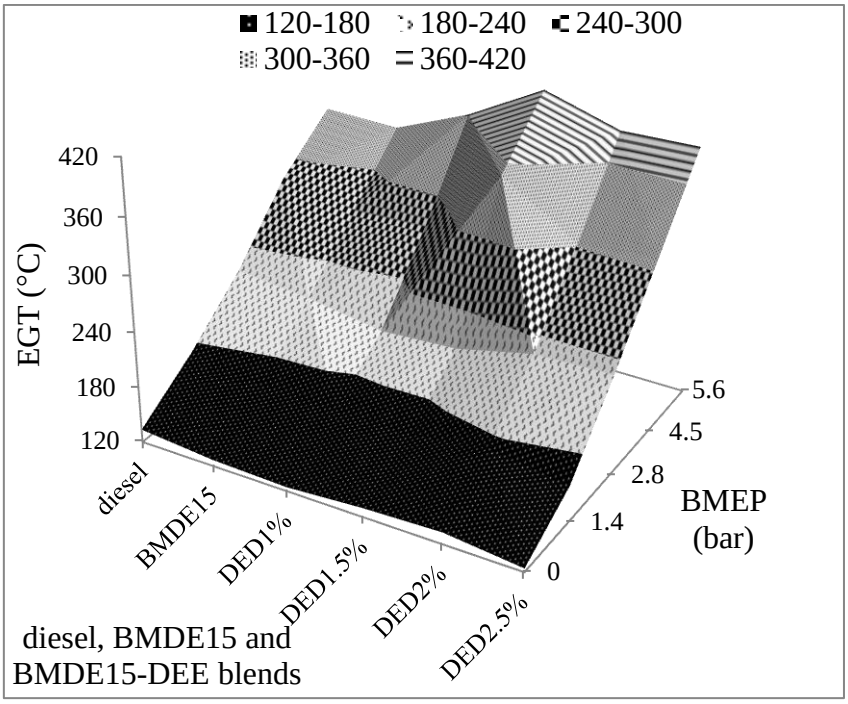

Fig. 6.21 Variation of the EGT with BMEP

It is seen that, with the increase in the percentage of DEE in the BMDE15-DEE blend, the EGT is increased throughout the load spectrum. A higher band width of 360-420 °C is observed for the DED1%, DED1.5%, DED2% and DED2.5% at full load. When the DEE percentage in the blend is increased, the diffusion combustion phase increases, due to the cooling effect of DEE. More fuel gets accumulate, as a result of which more heat is liberated and found as waste.

6.3.2.3 Thermal energy balance

Figure 6.22 shows the variation of thermal energy balance for diesel, BMDE15 and BMDE15-DEE blend at full load. It is evident from the figure that the BMDE15-DEE blend operation provides lower useful work compared to that of diesel and BMDE15. This due to a lower heat supplied by the BMDE15-DEE blends when these are used an alternative fuel for diesel engine. The unaccounted heat loss is observed to be high with the BMDE15-DEE blend operation compared to those of diesel and BMDE15.

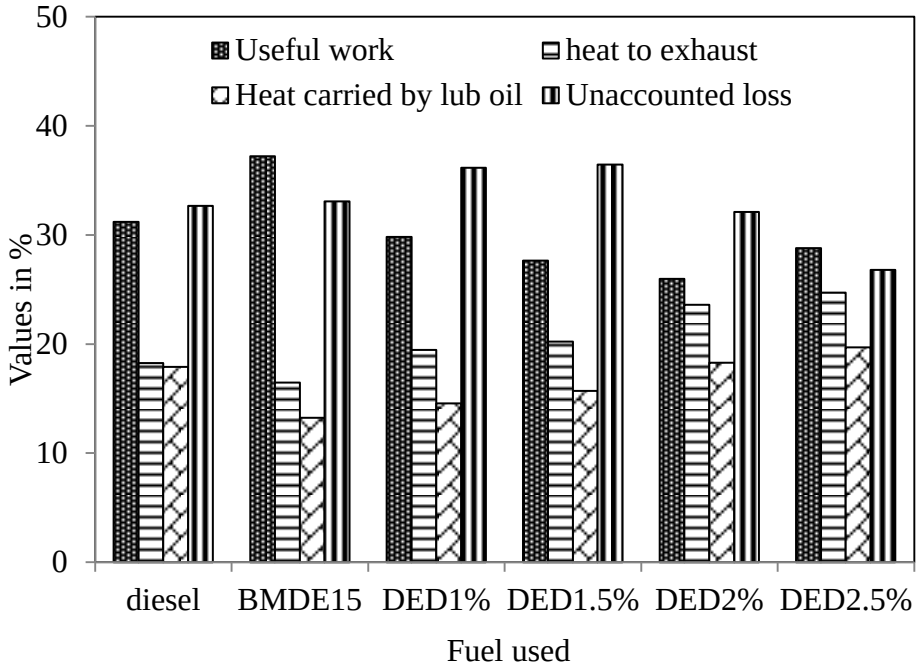

Fig. 6.22 Variation of thermal energy balance for diesel, BMDE15 and BMDE15-DEE blends at full load

As both bioethanol and DEE have a low lubricity property, the frictional losses are more. Hence heat losses are noticed to be high with the BMDE15-DEE blend operation.

6.3.3 Emission analysis

This subsection discusses the exhaust emissions from the engine fueled with the BMDE15 emulsion, with DEE in different percentages, in comparison with diesel.

6.3.3.1 BSHC emission

The unburned hydrocarbon emission in a diesel engine is due to over-mixing, under-mixing, and nozzle dribbling [122]. The variation of the BSHC of diesel, BMDE15, DED1%, DED1.5%, DED2% and DED2.5% with BMEP is shown in Fig. 6.23. It is depicted that, at low load, the BSHC emission for the DED2% and DED2.5% is found to be increased by about 4% and 6%, compared to that of diesel, showing a higher band width. The reason may be the suppression of the flame due to the cooling effect of the DEE. At full load, the BSHC emission for BMDE15, DED1% and DED1.5% is found to be lesser by about 14%, 21% and 23% respectively, in comparison with diesel.

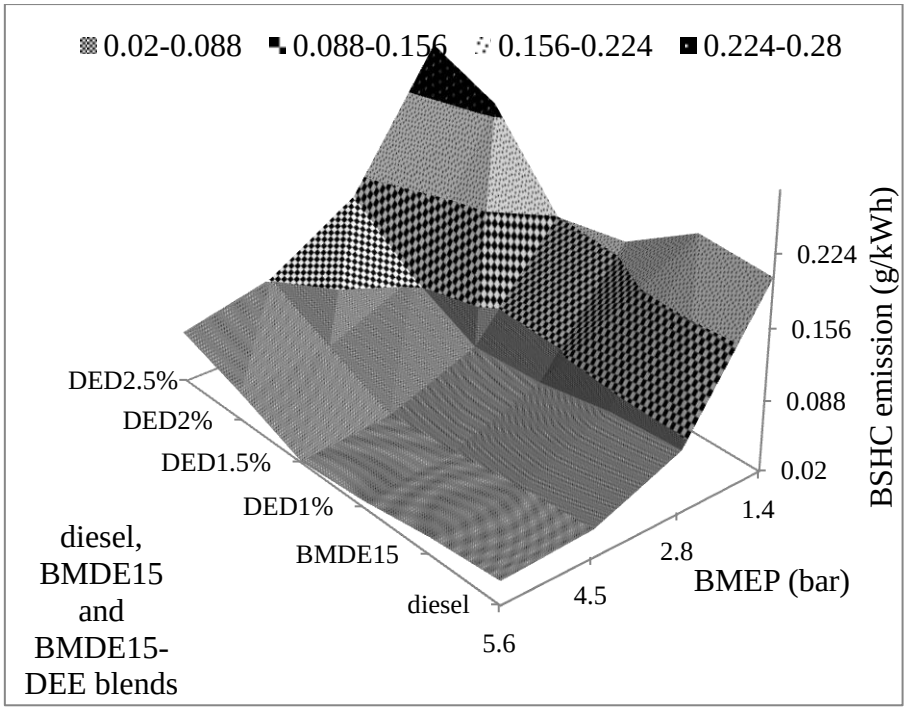

Fig. 6.23 Variation of BSHC emission with BMEP

But, for DED2% and DED2.5%, the BSHC emission is found to be higher by about 22% and 27% compared to that of diesel, at full load. The reason may be the over-mixing; i.e., some fuel particles mix with the burned gases, so that the BSHC emissions are higher.

6.3.3.2 BSCO emission

Figure 6.24 depicts the variation of the BSCO emission with BMEP. The BSCO emission is the result of incomplete combustion. At low load, the BSCO emission is seen to be higher for DED2% and DED2.5%, compared to those of DED1.5%, DED1% and BMDE15. This may be due to the higher induction of DEE, which increases the cooling effect of the engine. At full load, the BSCO emission for diesel, BMDE15, DED1%, DED1.5%, DED2% and DED2.5% is found to be 0.98, 0.48, 0.39, 0.29, 0.71 and 1.21 g/kWh. The maximum BSCO emission band width is noticed with DED2% and DED2.5% compared to all other fuels tested in the study. A better emission band is found with DED1% and DED1.5%.

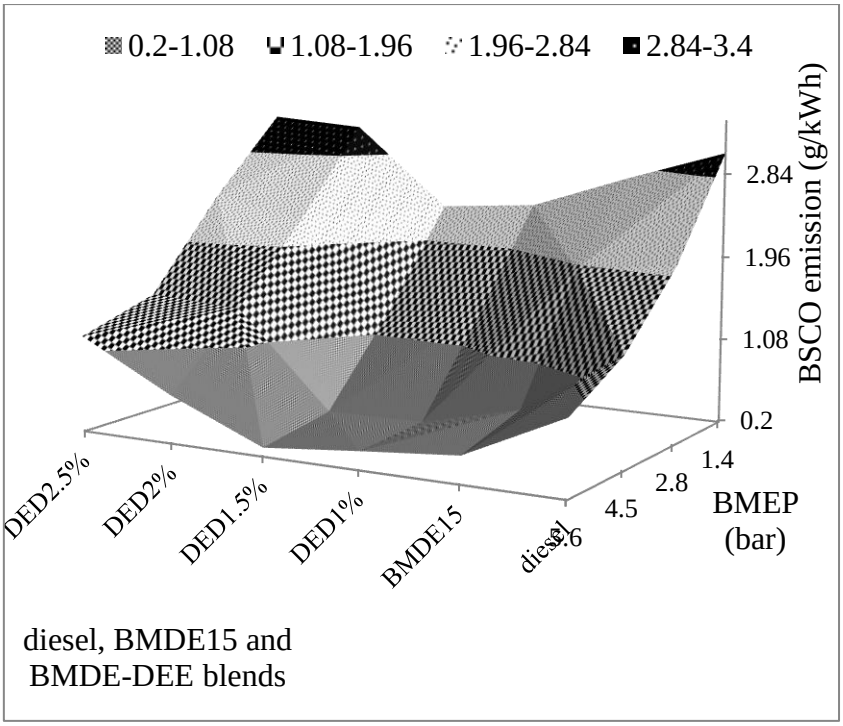

Fig. 6.24 Variation of BSCO emission with BMEP

This is attributed to the more complete combustion of DED1% and DED1.5%. But, with DED2% and DED2.5%, the emission is found to be more due to combustion deterioration.

6.3.3.3 BSNO emission

Figure 6.25 shows the variation of the BSNO emission for diesel, BMDE15, DED1%, DED1.5%, DED2% and DED2.5% with BMEP. At low load, the BSNO emission for diesel, BMDE15 and DED1% is found to be higher, compared to those of the other blends, due to the complete combustion, resulting in higher cylinder gas temperature, which is reflected in the heat release curve. It is also indicated that a 3.2-3.8 g/kWh band width is noticeable for diesel, BMDE15 and DED1% at low load. But, for DED1.5%, DED2% and DED2.5%, the BSNO emission is less with a band width of 2-2.6 g/kWh, due to the reduction in the cylinder temperature, by the higher addition of DEE. At full load, the BSNO emission for DED1%, DED1.5%, DED2% and DED2.5% is found to be reduced by about 4%, 6.7%, 11.3% and 17% respectively, compared to that of diesel. With the DEE operation, the ignition delay is shortened, and hence, the accumulation of fuel is reduced. As a consequence of this, the peak of the heat release rate is reduced, resulting in lower BSNO emission.

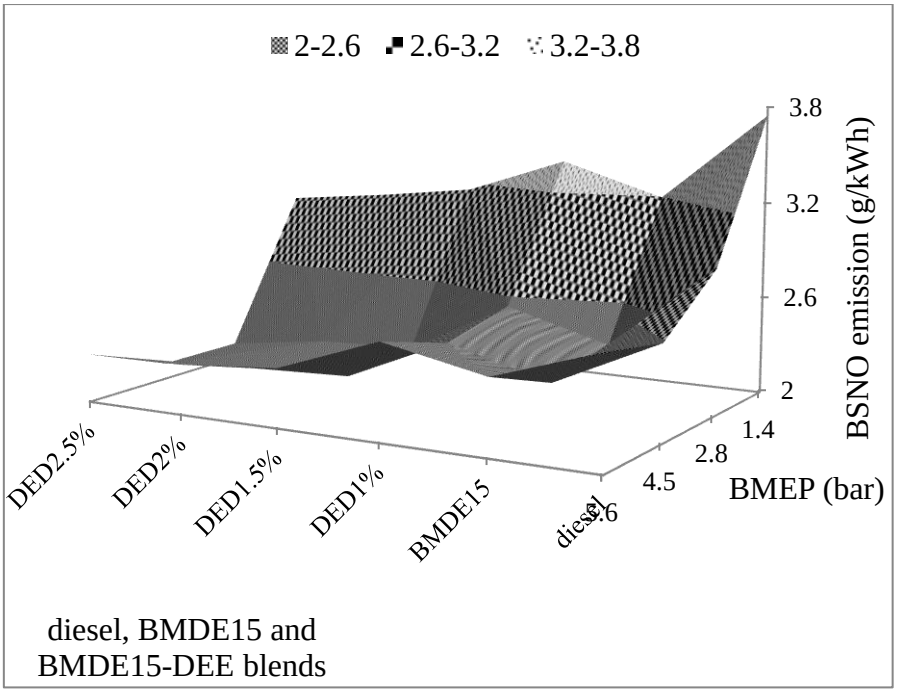

Fig. 6.25 Variation of BSNO emission with BMEP

Another reason may be the high latent heat vaporisation of DEE, which lowers the in cylinder temperature. The BSNO emission for the DED1% is found to be higher by about 3%, compared to that of BMDE15. More heat is released in the case of DED1% due to the availability of more oxygen, and therefore, the emission is more compared to that of BMDE15.

6.3.3.4 Smoke emission

Figure 6.26 depicts the variation of smoke with BMEP. Bioethanol has a low soot tendency, because of its less carbon-to-hydrogen ratio, and also, because it has no aromatic content. At no load and full load, the smoke emission for the BMDE15 emulsion without the ignition improver is found to be lesser, compared to that of diesel, and the BMDE15 emulsion with the ignition improver, due to better combustion, as bioethanol is an oxygenated fuel. DEE has a higher cetane number, and is added in small quantities to BMDE15. From the figure, it is observed that the smoke emission for DED2% and DED2.5% is found to be more compared to that of BMDE15, but less than that of diesel operation, at low load. At full load, the smoke emission for BMDE15, DED1%, DED1.5%, DED2% and DED2.5% is found to be lesser by about 21%, 10.3%, 13.8%, 7.6% and 3.2% respectively, compared to that of diesel. The reduction of smoke with the DEE operation is due to the proper mixing of fuel and air, and the oxygen available in the diffusion combustion phase.

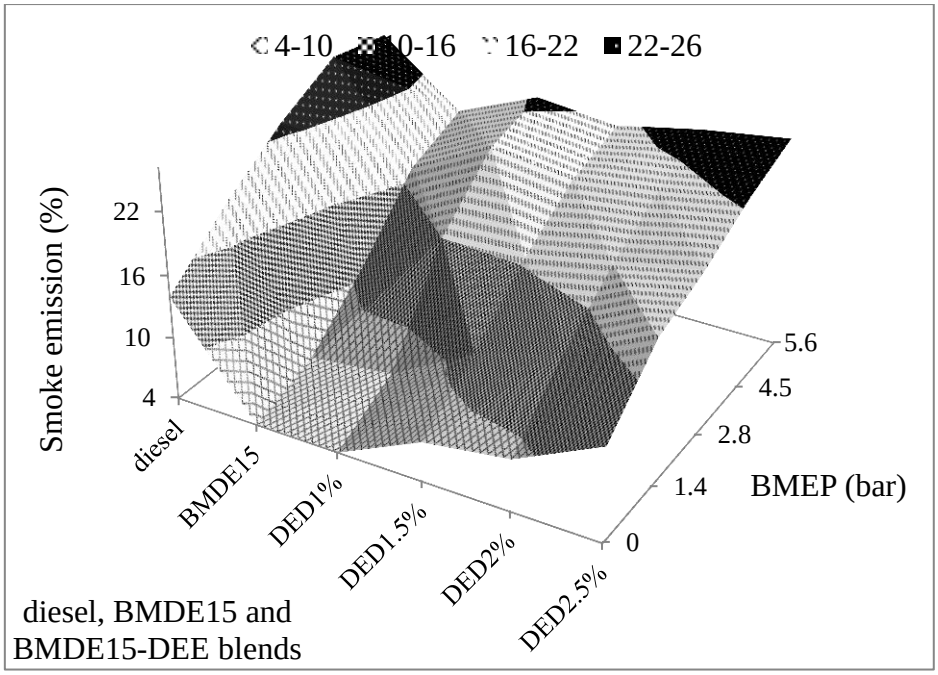

Fig. 6.26 Variation of smoke emission with BMEP

The DEE fuel is oxygenated, and it has a low carbon-to-hydrogen ratio. It has a positive effect on the elimination of soot formation [150].

6.3.4 Summary

The summary of the results analysis of the engine operated with different bioethanol diesel DEE emulsions is given below;

The ignition delay and maximum cylinder pressure are closer to those of diesel for DED1.5%, at full load. The maximum cylinder pressure for diesel is 73.5 bar, and for DED1.5%, 73.8 bar. DED1.5% shows better performance and lower emissions compared to DED1%, DED2% and DED2.5% at full load. The BSEC and EGT are found to be increased by about 35% and 67 °C for DED1.5% compared to that of diesel at full load. The BSCO, BSHC, BSNO, and the smoke emission for DED1.5% are found to be reduced by about, 18%, 23%, 11.3% and 13.76% respectively, compared to that of diesel at full load. It is possible to reduce the NO and smoke emission from the engine when it is run with 15% bioethanol in the bioethanol-diesel emulsion, by adding small quantities of DEE. There is a scope for replacing a maximum of 15% diesel by bioethanol in fuel modification. Further investigation is necessary to use neat ethanol with suitable engine modifications.

6.4 Bioethanol operation with DEE fumigation

Bioethanol has a cetane number of less than 20. It is reported that it can be used directly in the diesel engine, with the fumigation of a high cetane fuel [151]. In this chapter, DEE which has a cetane value of greater than 125, is fumigated at four different flow rates of 60 g/h, 120 g/h, 180 g/h and 240 g/h, while neat bioethanol is injected directly into the combustion chamber with the help of an injector. The results are compared with the diesel data and presented in this chapter.

6.4.1 Combustion parameters

The combustion data such as ignition delay, heat release rate, combustion duration, rate of pressure rise were collected with respect to the crank angle or load. The results are analysed and discussed in this chapter by plotting a graph of the combustion parameters of neat bioethanol with DEE fumigation and diesel.

6.4.1.1 P-θ diagram

Figure 6.27 depicts the variation of cylinder pressure with crank angle of diesel and neat bioethanol operation with the help of an ignition enhancer.

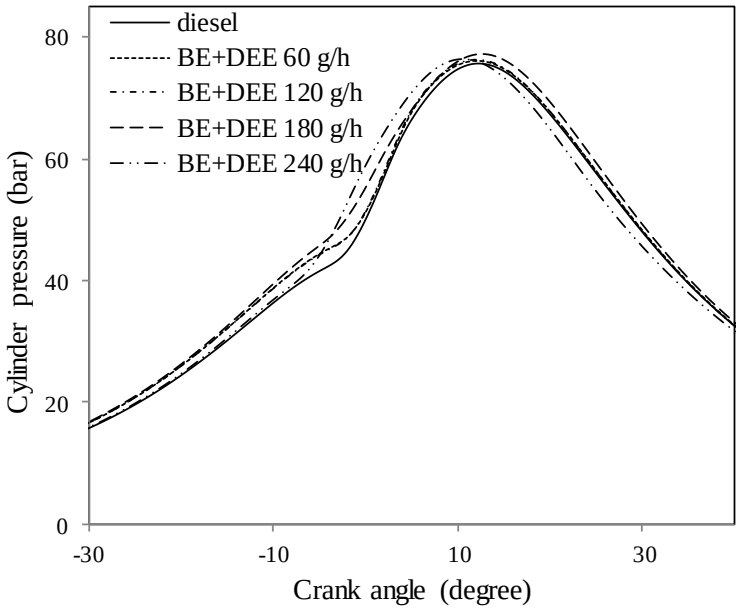

Fig. 6.27 Variation of cylinder pressure with crank angle

DEE fumigation enhances the combustion process of a neat bioethanol fueled diesel engine. As the DEE evaporates easily, it mixes with air properly and creates a rapid flame front

propagation, which may ignite the bioethanol easily. With a lower proportion of DEE, the cylinder pressure is more, but with higher induction of DEE, it is found to be lower due to its cooling effect. The peak cylinder pressure of 180 g/h is found to be more, followed by 120 g/h, 60 g/h, 240 g/h and diesel, which is achieved at the crank angles of 0.2-0.8 °CA variations.

6.4.1.2 Ignition delay

The variation of ignition delay with respect to load for diesel and bioethanol, with DEE fumigation at four different flow rates of 60 g/h, 120 g/h, 180 g/h and 240 g/h, is shown in Fig. 6.28.

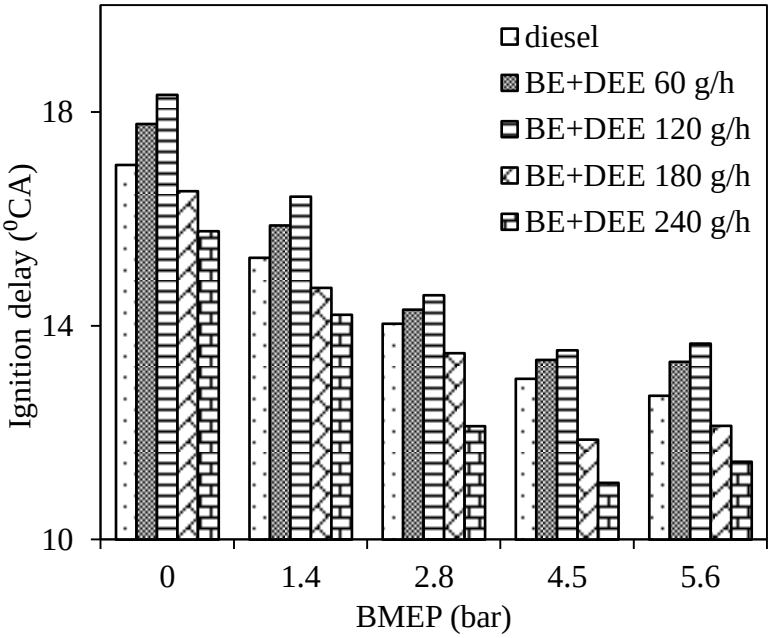

Fig. 6.28 Variation of ignition delay with BMEP for diesel and bioethanol operation with DEE fumigation

It is inferred from the figure that the bioethanol operation with 60 g/h and 120 g/h of the DEE fumigation at the intake manifold, exhibited a longer ignition delay compared to that of diesel at every load. The values of ignition delays vary from 0.5-1 °CA, from the diesel data. The DEE fumigation at the intake manifold generally lowers the intake charge temperature due to its cooling effect and hence, a longer ignition delay is achieved. But, the ignition delay is found to be shorter by about 1-2 °CA with bioethanol and DEE fumigation at 180 g/h and 240 g/h flow rates, in comparison with diesel at every load. When high cetane fuel is introduced at a higher percentage, the cetane number of bioethanol also increases and the fuel may ignite better. The delay period is also shortened due to the mixture homogeneity. The

DEE mixes properly with the air when it is inducted at the intake manifold, and the time required for the physical and chemical delay is reduced. The ignition delay for all the tested fuels in this study shows a declining trend from no load to full load, due to a higher cylinder gas temperature.

6.4.1.3 Heat release rate (HRR)

Figure 6.29 illustrates the variation of the heat release rate with respect to the crank angle for diesel and bioethanol operation at full load.

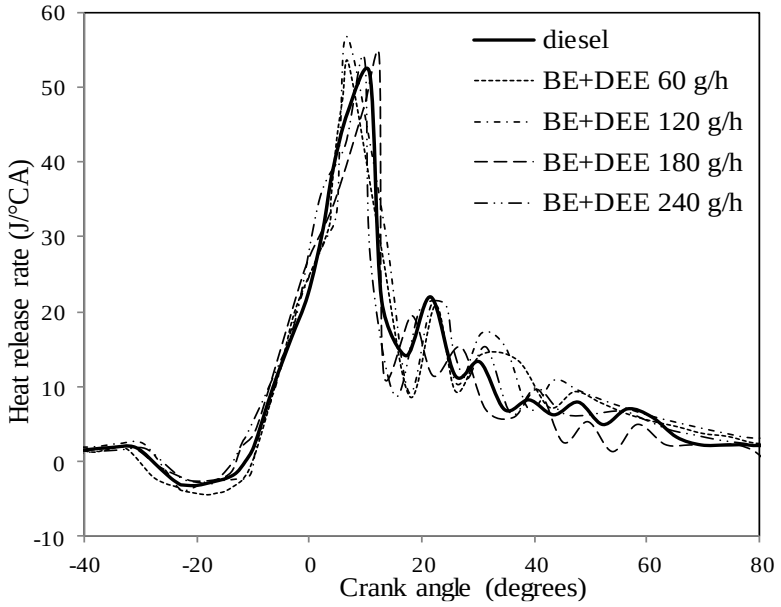

Fig. 6.29 Variation of heat release rate with crank angle for diesel and bioethanol operation with DEE fumigation

The bioethanol operation with the DEE fumigation at the flow rates of 60 g/h, 120 g/h, 180 g/h and 240 g/h shows a higher heat release rates compared to that of diesel at full load. It varies by about 2-3 J/°CA from diesel data at 9-14 °CA aTDC. The maximum heat release rate for diesel is 51.8 J/°CA which occurs at 10.7 °CA aTDC at full load. With 60 g/h and 120 g/h, the ignition delay is longer compared to that of diesel; hence, more accumulation of fuel in the delay period is achieved. The boiling temperature of DEE is 34.4 °C. So, it can vaporise and mix with air easily. DEE burns faster compared to bioethanol, and it helps the bioethanol to ignite as it has a higher auto ignition temperature. Both DEE and bioethanol are oxygenated fuels; the fuel in the local region can get oxygen to burn easily. With the higher induction of DEE, the heat release rate is also found to be higher with a little shift of the crank angle towards the TDC compared to that of diesel. Due to the lower auto ignition temperature and higher cetane number of DEE compared to those of bioethanol, more heat

release is achieved in the premixed phase by the DEE, which will burn the bioethanol, and this results in higher maximum heat release rates and peak cylinder pressure. There is an abrupt combustion with an audible knock with at higher induction of DEE, beyond 240 g/h. Hence, the engine was not operated with the flow rate of DEE higher than 240 g/h.

6.4.1.4 Maximum cylinder pressure

Figure 6.30 portrays the variation of the maximum cylinder pressure of diesel and neat bioethanol with DEE fumigation, at the flow rates of 60 g/h, 120 g/h, 180 g/h and 240 g/h with respect to the crank angle at different loads. Generally, the performance and knocking characteristics of the engine with a specific fuel can be better clarified with the help of cylinder pressure and crank angle history. The occurrence of the maximum cylinder pressure with diesel and neat bioethanol operation is observed to vary from 10-12 °CA aTDC, at full load. From the figure, it is noticed that all the flow rates of DEE with neat bioethanol have higher cylinder pressure compared to that of diesel at full load.

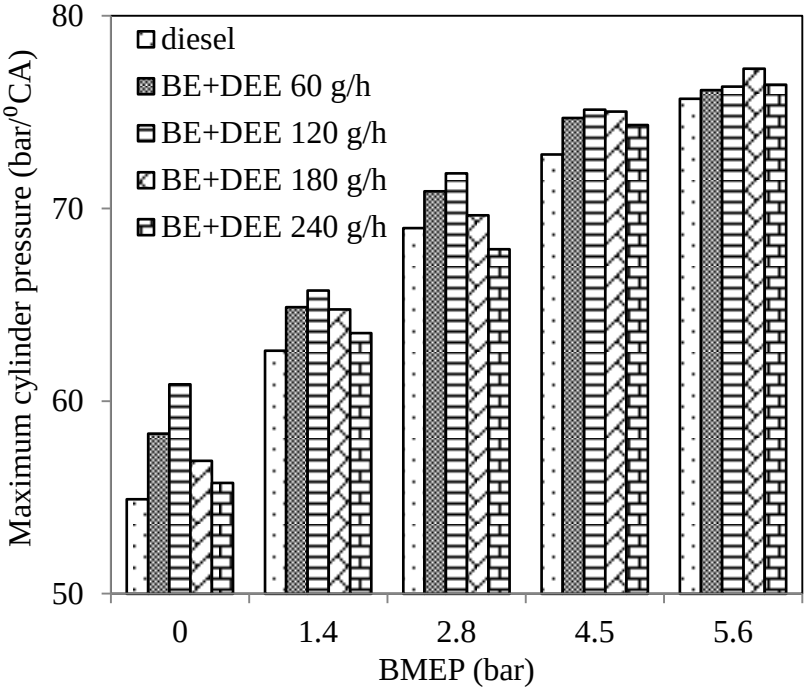

Fig. 6.30 Variation of the maximum cylinder pressure with BMEP for diesel and bioethanol operation with DEE fumigation

The values of the maximum cylinder pressure for bioethanol and DEE fumigation varies from 1-3 bar compared to that of diesel at full load. The reason may be the high cetane number and oxygen content of DEE, which ignites bioethanol easily. With the higher induction of DEE, the premixed combustion is accelerated with the higher burning velocity of DEE in neat

bioethanol operation. The lower viscosity and higher volatility of bioethanol results in more accumulation of bioethanol in the delay period, which may also be the reason for the higher cylinder pressures.

6.4.1.5 Maximum rate of pressure rise

Figure 6.31 depicts the variation of the maximum rate of pressure rise for diesel and bioethanol, and DEE operation with respect to load.

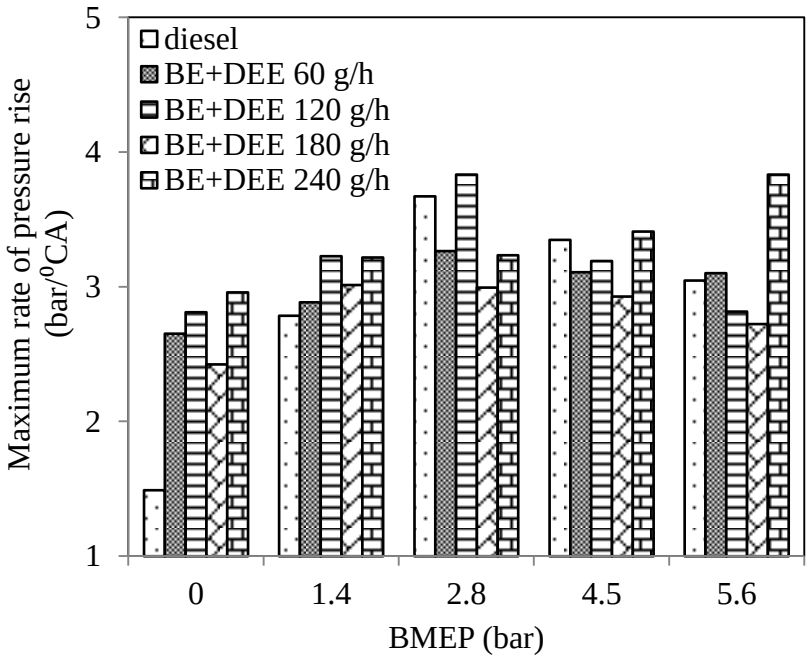

Fig. 6.31 Variation of the maximum rate of pressure rise with BMEP for diesel and bioethanol operation with DEE fumigation

It can be observed from Fig. 6.30, that the maximum rate of pressure rise for the flow rates of 60 g/h and 240 g/h is found to be higher compared to that of diesel at full load. For all the flow rates of DEE in the bioethanol operation, the maximum rate of pressure rise ranges from 0.5-2 bar/°CA in comparison to diesel, at full load. At 240 g/h flow rate of DEE, the delay period gets shortened, and rapid combustion is achieved with audible knock.

6.4.1.6 Combustion duration

Figure 6.32 depicts the variation of the combustion duration of diesel and bioethanol operation with the DEE fumigation with respect to load. The combustion duration for all the tested fuels in this study, shows an increasing trend with respect to load. When the load is increased, the fuel consumption is also increased to overcome the friction and generate the required power. And the fuel undergoes the oxidation process with the help of the entrapped

residual gases in the previous cycle in the early stage of combustion. The combustion is very rapid, which minimises the premixed combustion phase; all the fuel may not burn in this phase, and hence, takes part in the post oxidation process. So, the combustion period gets prolonged. The combustion duration data are observed to be shorter by about 2-4 °CA and longer by about 1-3 °CA according to the lower and higher values of DEE compared to that of diesel respectively.

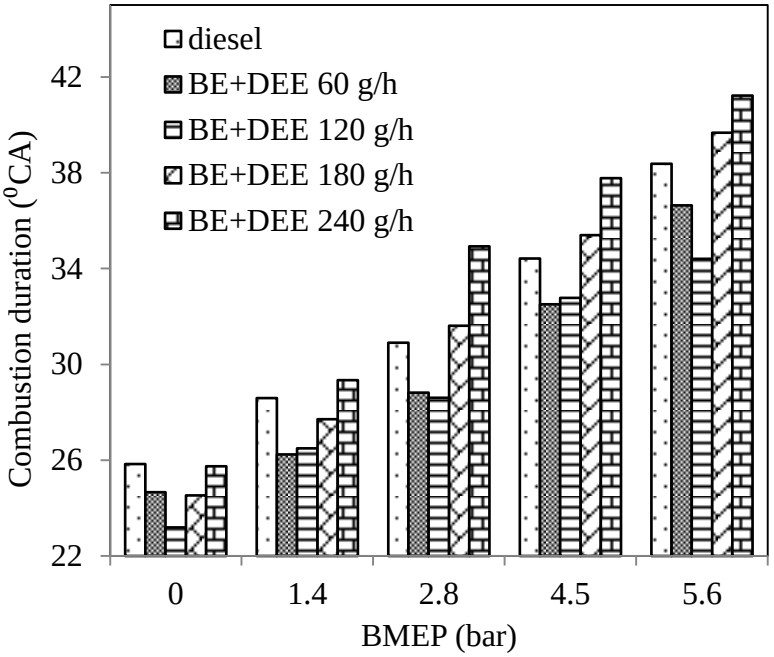

Fig. 6.32 Variation of combustion duration with BMEP for diesel and bioethanol operation with DEE fumigation

As discussed earlier, DEE fumigation at the flow rates of 60 g/h and 120 g/h allows more fumigation of bioethanol due to the longer delay period. All the injected fuel gets a sufficient time for ignition, and the combustion is also faster, due to the faster burning velocity of the DEE. So, the combustion duration is reduced with these two flow rates. But, the higher flow rates of DEE reduce the premixed combustion phase, and some fuel gets combusted with the help of the local oxygen in the diffusion combustion phase.

6.4.2 Engine performance analysis

In this section, the energy share of DEE is provided for the performance analysis purpose. The thermal energy balance is also given to represent the other performance parameters, such as fuel consumption, exhaust gas temperature etc. The data of neat bioethanol operation with DEE fumigation is compared with that of diesel, by plotting the graph against the load.

6.4.2.1 Energy share

The energy share of DEE in the bioethanol operation is shown in Table 6.1. The energy share is found to be increased with the higher flow rates of DEE. The reason is that a large amount of air is displaced by the DEE due to more flow rates of DEE. From no load to full load, the DEE energy share shows a decreasing trend, due to the higher gas temperature of the cylinder.

Table 6.1 Energy share of DEE in bioethanol operation

Flow rates	No load	25% load	50% load	75% load	Full load
BE+DEE 60 g/h	13.9	12.2	8.3	6.7	5.6
BE+DEE 120 g/h	26.7	20.9	16.5	13.8	10.7
BE+DEE 180 g/h	34.4	26.7	18.7	14.8	11.3
BE+DEE 240 g/h	45	39.2	29.4	23.7	19.5

When the energy share of DEE increases, the performance of the engine is also found to be increased, due to the combustion of fuel achieved closer to TDC. As it is an oxygenated fuel, the fuel gets combusted easily, due to good mixture formation.

6.4.2.2 Brake specific fuel consumption (BSFC)

The variation of BSFC for diesel and bioethanol with DEE fumigation at four different flow rates with respect to load is shown in Fig. 6. 33.

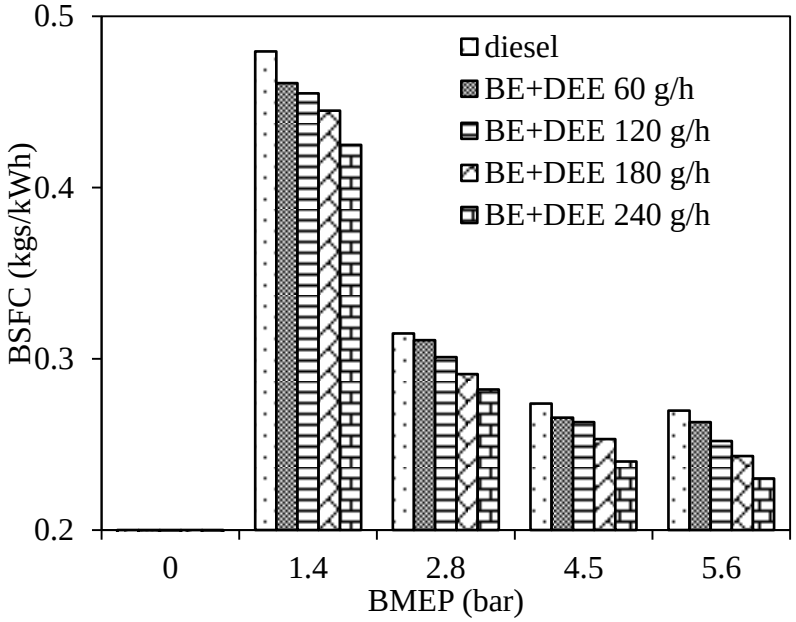

Fig. 6.33 Variation of BSFC with BMEP for diesel and bioethanol operation with DEE fumigation

It is observed from the figure, that the BSFC is found to be low for the bioethanol operation with DEE fumigation in comparison with diesel at full load. This is due to high oxygen content of the fuel. The energy share of DEE is found to be increased with load and it enhances the combustion, due to which BSFC reduces.

6.4.2.3 EGT

The variation of EGT for diesel and bioethanol operation with DEE fumigation at four different flow rates is shown in Fig. 6.34.

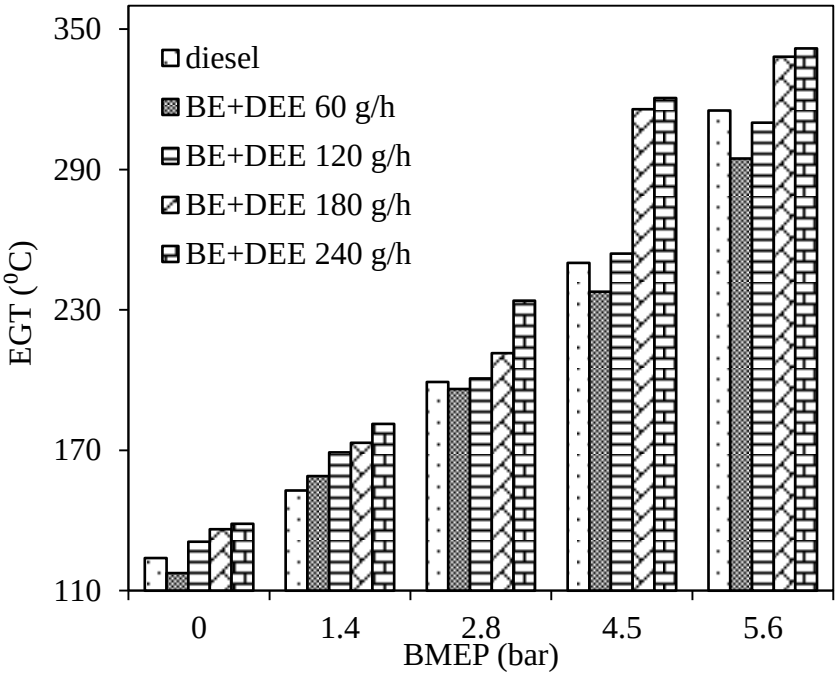

Fig. 6.34 Variation of EGT with BMEP for diesel and bioethanol operation with DEE fumigation

It is apparent from the figure that, the EGT is found to be more with a higher flow rate of DEE at full load. At higher flow rates of DEE, the combustion is closer to TDC, hence some amount of heat is available as a waste at the exhaust. Also the combustion is faster due to oxygen availability in the delay period. At a lower flow rate of DEE, the heat is converted to useful work.

6.4.2.4 Volumetric efficiency

Figure 6.35 depicts the variation of the volumetric efficiency of diesel and bioethanol operation with the DEE fumigation with respect to load. The volumetric efficiency of a CI engine pertains to the breathing ability of a four stroke engine [122]. Generally, a gaseous

fuel displaces air and, therefore, the breathing capacity of the engine is reduced. Usually, the volumetric efficiency of diesel is between 85 and 90%. With the induction of DEE at the intake manifold of the engine, the molar mass of the fuel-air mixture reduces, lowering the density of the intake mixture. This may be due to the supply of more DEE at higher load, which reduces the air consumption. The equation used to calculate the volumetric efficiency of the engine is given in Chapter 5.

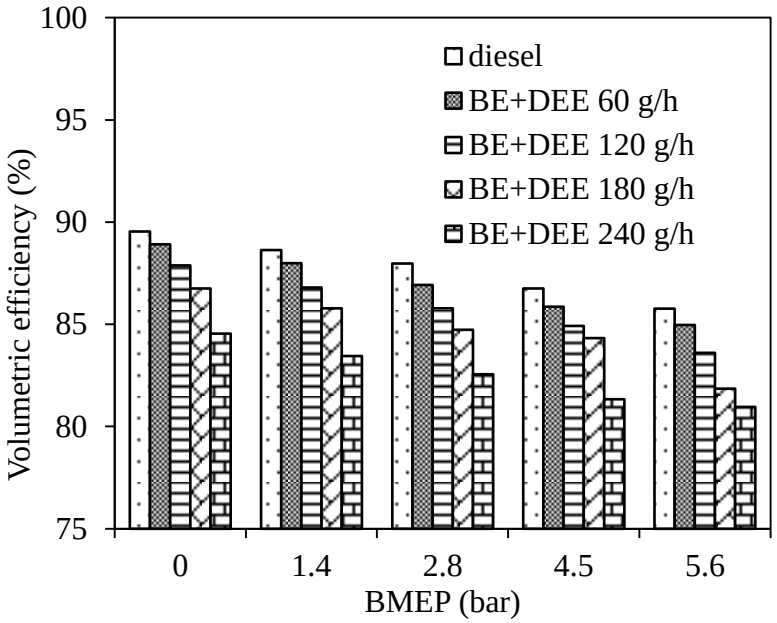

Fig. 6.35 Variation of volumetric efficiency with BMEP for diesel and bioethanol operation with DEE fumigation

The bioethanol operation with DEE fumigation at four different flow rates at the intake manifold reduces the air consumption and volumetric efficiency of the engine is found to be reduced. The volumetric efficiency of the engine fueled with diesel and the bioethanol operation at 60 g/h, 120 g/h, 180 g/h and 240 g/h is found to be 85.7%, 84.9%, 83.6%, 81.8% and 80.9% respectively, at full load.

6.4.2.5 Thermal energy balance

At full load, the useful work for bioethanol with DEE fumigation is found to be higher compared to that of diesel. This may be due to better combustion and lesser heat loss compared to that of diesel. The unaccounted losses are minimised, and hence, more useful work is obtained. It is also observed that the heat carried by the lubricating oil is increased with the bioethanol and DEE operation compared to that of diesel. Generally, bioethanol and DEE have less lubricity properties in comparison with diesel. The temperature of the

lubricating oil is increased in overcoming the friction. Figure 6.36 shows the variation of the thermal energy balance for diesel and bioethanol operation with DEE fumigation.

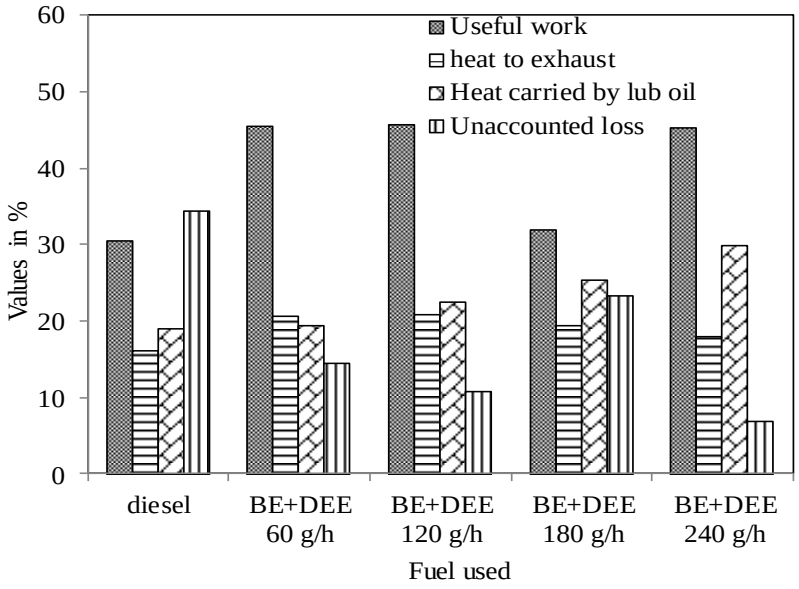

Fig. 6.36 Variation of thermal energy balance for diesel and bioethanol with DEE fumigation at full load

6.4.3 Emission analysis

This subsection discusses the emission available in the engine exhaust when neat bioethanol is supplied in the engine and DEE is used as an ignition improver. The emissions data are compared with those of diesel, and presented in the subsections.

6.4.3.1 BSHC emission

The variation of BSHC emission for bioethanol operation with DEE fumigation at flow rates of 60 g/h, 120 g/h, 180 g/h and 240 g/h from diesel is given in Fig. 6.37. There is a reduction of BSHC emission for the bioethanol operation with the DEE fumigation at the flow rate of 60 g/h at every load, and at full load it is found to be lower by about 9.6% compared to that of diesel. At this flow rate, the fuel gets combusted by the faster burning velocity of the DEE and mixture homogeneity without flame quenching. The percentage increase with the DEE fumigation at the flow rates of 120 g/h, 180 g/h and 240 g/h is found to be about 3.2%, 5.6% and 11.3% respectively, compared to that of diesel at full load. With these flow rates, though the heat release is more, the BSHC emission is also found to be more compared to that of diesel. Due to the increased admittance of DEE, some fuel would not have burnt because of the quenching effect. The burning velocity may be rapid, which will not combust the fuels close to the cylinder wall, which is also a fuel rich zone surrounded by the cooled DEE.

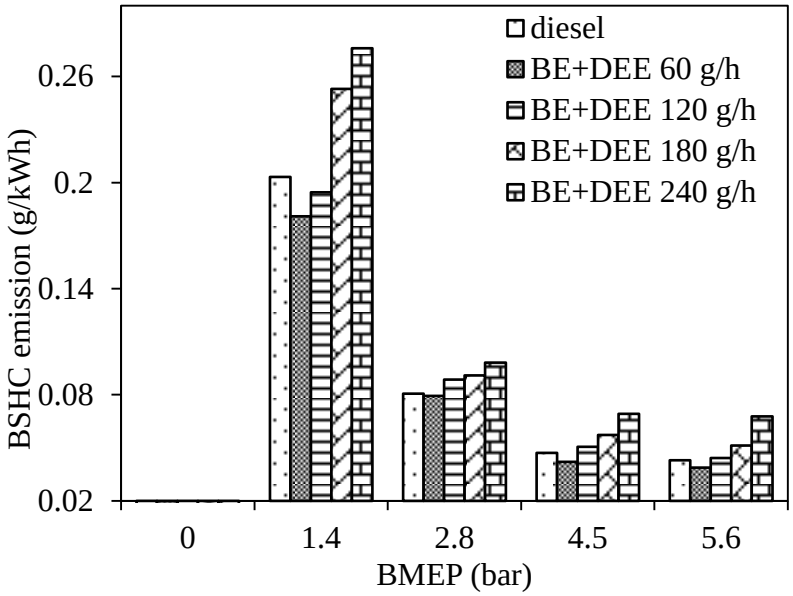

Fig. 6.37 Variation of BSHC emission for sole bioethanol operation with DEE and diesel at different BMEP

6.4.3.2 BSCO emission

Figure 6.38 shows the variation of BSCO emission for the bioethanol operation with the DEE fumigation at flow rates of 60 g/h, 120 g/h, 180 g/h and 240 g/h, from the diesel data.

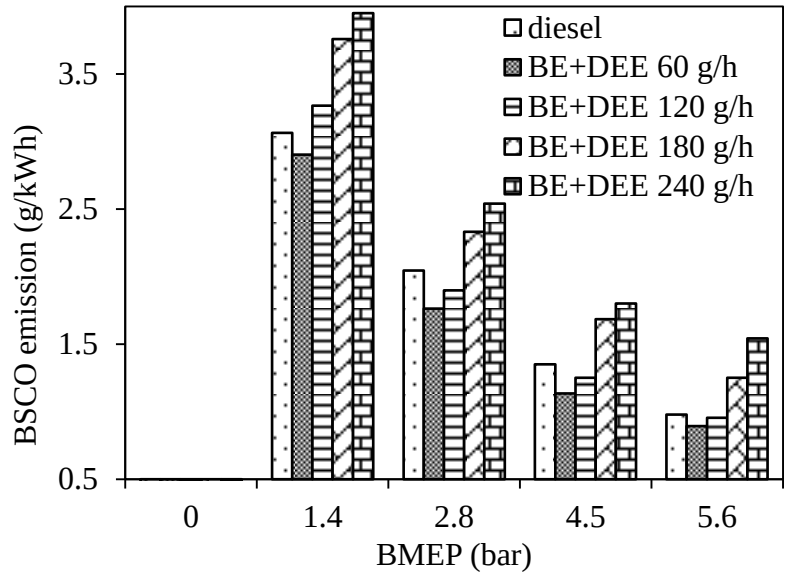

Fig. 6.38 Variation of BSCO emission for sole bioethanol operation with DEE and diesel at different BMEP

The BSCO emission for the bioethanol operation with 60 g/h and 120 g/h flow rates of DEE is found to be lower by about 8.8% and 2.6% respectively, compared to that of diesel at full load. This is due to the more complete combustion achieved by the homogeneous mixture.

The figure portrays that the BSCO emission percentage for bioethanol is increased with the flow rates of 180 g/h and 240 g/h by about 17.5% and 25.4% respectively at full load. With a higher induction of DEE, the mixture of air and DEE may be rich and some of the mixture is nearer to the wall and the crevice volume, where the flame cannot propagate properly. When this mixture gets in contact with the hot combustion gases during the latter part of the power stroke, and also in the exhaust manifold, oxidation reactions occur, but do not have time to undergo combustion.

6.4.3.3 BSNO emission

The variation of BSNO emission for the bioethanol operation with the DEE fumigation at the flow rates of 60 g/h, 120 g/h, 180 g/h and 240 g/h, from diesel with respect to load is given in Fig. 6.39.

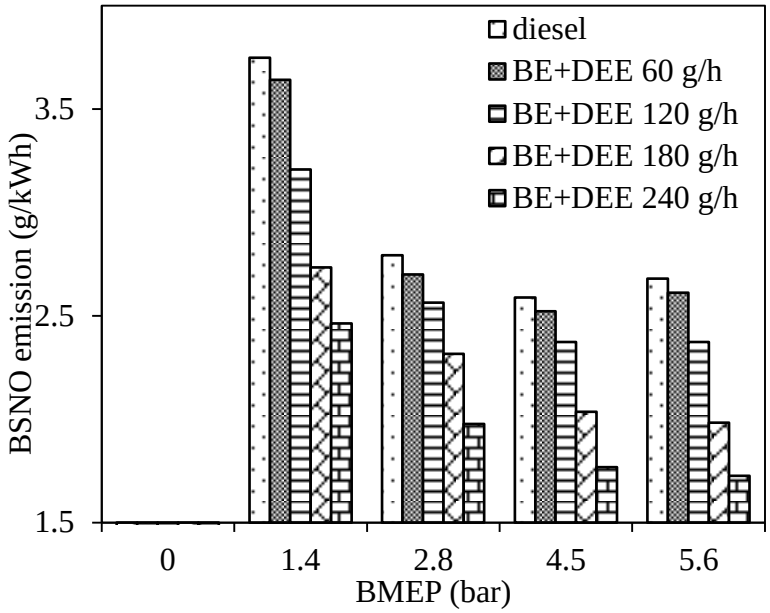

Fig. 6.39 Variation of BSNO emission for sole bioethanol operation with DEE and diesel at different BMEP

It can be observed from the graph, that the percentage of the BSNO emission with the bioethanol operation, is found to be lower compared to that of diesel with respect to load. At full load, the BSNO emission is found to be lower by about 2.6%, 11.5%, 26.2% and 35.6% with DEE fumigation of 60 g/h, 120 g/h, 180 g/h and 240 g/h respectively, compared to that of diesel. The BSNO emission is due to the premixed combustion phase. High cetane fuels have the advantage of reducing the BSNO emission. Also, the latent heat of vaporisation of bioethanol is higher compared to that of diesel. It requires more energy to ignite; so, the heat liberated due to the DEE is utilized to ignite the bioethanol and hence a lower BSNO

emission is achieved. The nitrogen available in the air gets less time to react with oxygen in the shorter ignition delay with higher flow rates of DEE.

6.4.3.4 Smoke emission

Smoke is predominantly affected by the type and quantity of fuel used its carbon content, C/H ratio, and aromatic content. Figure 6.40 depicts the variation of smoke emission for bioethanol and diesel operation with respect to load.

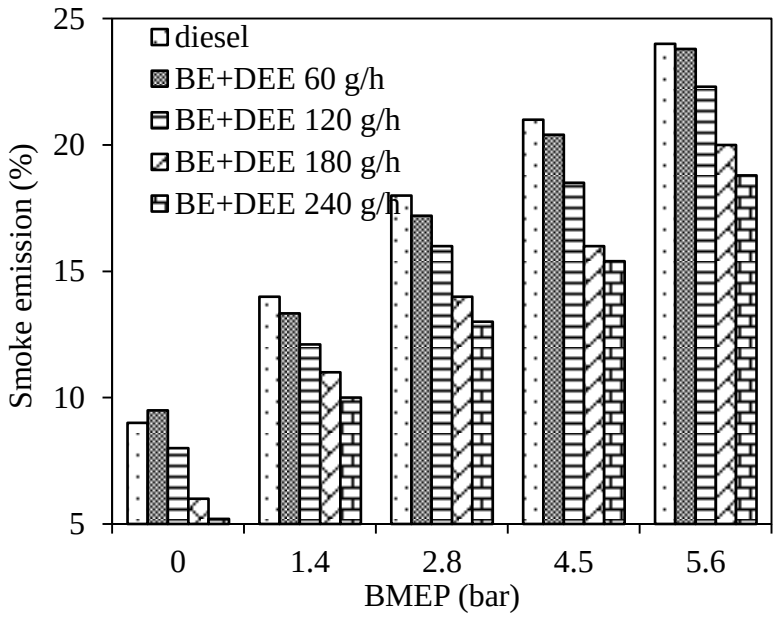

Fig. 6.40 Variation of smoke emission for sole bioethanol operation with DEE and diesel at different BMEP

At full load, the percentage reduction in smoke opacity for bioethanol with the DEE fumigation at flow rates of 60 g/h, 120 g/h, 180 g/h and 240 g/h is found to be about 1%, 7.1%, 16.6% and 21.6% respectively, compared to that of diesel. The molecular weight of bioethanol and DEE is 42 and 74.2. But for diesel, the molecular weight is 170. Generally, a fuel with a high molecular weight is a complex compound; it is difficult to break, and requires more oxygen in the combustion period. This results in more smoke emission. Both the bioethanol and DEE have low molecular weights and are oxygenated fuels. With the higher induction of DEE, the diffusion combustion phase is prolonged and more oxygen reacts with hydrogen. As a result, less smoke is observed at the exhaust in the bioethanol operation in comparison with diesel operation at any load.

6.4.4 Summary

The summary of the results obtained in the investigation are as follows,

The ignition delay for lower flow rates of DEE is found to be shorter, but it is longer with the higher flow rates. The useful work is increased with an increase in the flow rates of DEE. The BSCO and BSHC emissions are found to be higher with the flow rates of DEE. But, there is a simultaneous reduction in the BSNO and smoke emissions with neat bioethanol and the DEE operation. The flow rate of 180 g/h, of DEE provides better combustion, useful work, less heat loss, and lower emissions, compared to that of diesel and other flow rates of DEE.

6.5 Diesel-bioethanol dual fuel mode

Bioethanol fumigation is one of the techniques of bioethanol application in diesel engine [59]. Generally, in the fumigation operation, a low cetane fuel is vaporised and admitted into the engine with the help of a necessary arrangement. It is reported that up to 50% of the energy at full load can be provided through ethanol fumigation, which lies between the energy substitutions achievable by blends (~25%) and dual injection (~90%) [152]. This chapter discusses the results of the combustion, performance and emission of a single cylinder DI diesel engine, run on bioethanol fumigation with diesel as a pilot fuel. As mentioned in Chapter 4 'Experimentation and methodology', bioethanol was injected at the intake manifold with the help of a programmed electronic injector and vaporised with the help of a heater connected with an automatic temperature controller. The experiments were conducted with four different flow rates of bioethanol such as 0.24, 0.48, 0.96 and 1.22 kg/h, and the results compared with those of diesel.

6.5.1 Combustion parameters

The combustion data in bioethanol fumigation, in the diesel engine are analysed and compared with the diesel data and presented in the subsequent subsections.

6.5.1.1 P-θ diagram

The pressure crank angle history for diesel and the bioethanol fumigation at 0.24, 0.48, 0.96 and 1.22 kg/h, at full load of the engine, are depicted in Fig. 6.41. The pressure crank angle history gives a gross indication of the performance and knocking condition of the engine. It is depicted from the figure that, the peak cylinder pressure of 1.22 kg/h bioethanol fumigation is found to be the highest followed by diesel, 0.48 kg/h, 0.96 kg/h and 0.24 kg/h, at full load in this study. The occurrence of the maximum cylinder pressure for diesel is approximately at 12.4 °CA aTDC, which is the earliest among the tested fuels in this study. For bioethanol fumigation, the occurrences of the maximum cylinder pressure at 0.24, 0.48, 0.96 and 1.22 kg/h are found to be approximately at 10.2, 11.6, 11.3, 10.4 °CA aTDC, respectively at full load. Bioethanol is an oxygenated fuel, which has an oxygen content of 35%. As more oxygenated fuel is accumulated during the delay period, the diesel will get more oxygen to burn. This may result in a rapid pressure rise and peak cylinder pressure.

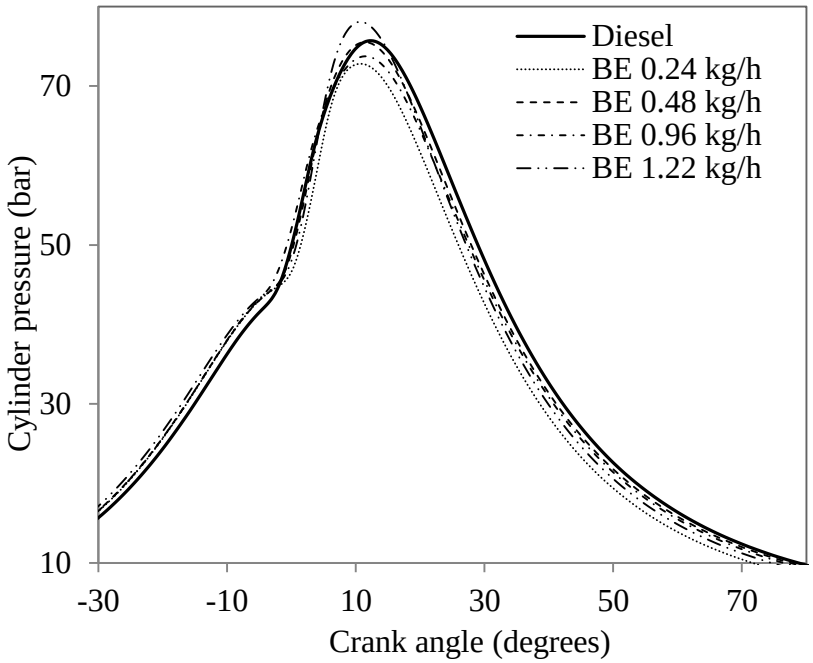

Fig. 6.41 Pressure crank angle diagram at full load

Also, the reason for the rapid pressure rise may be due to unpredictable flame front development, because of potential homogeneous charge compression ignition combustion and non-uniform combustion from the presence of hot-spots created by isolated bioethanol-only combustion [99].

6.5.1.2 Ignition delay

The ignition delay (τid) in a dual fuel operation is a function of the mixture temperature, pressure, equivalence ratio, kinetics of the fuel oxidation at lower temperatures, mixture homogeneity and fuel properties [128]. The variation in the ignition delay with the global equivalence ratio is given in Fig. 6.42. The definition of the global equivalence ratio and method of calculation have already been discussed in Chapter 5 "Methodology of the present work". The ignition delay in terms of the crank angle for bioethanol fumigation at 1.22 kg/h flow rate, is followed by 0.96, 0.48, 0.24 kg/h, and diesel with the least ignition delay. For diesel, the global equivalence ratio (Φ) value ranges from 0.31 to 0.7. The ignition delay for diesel at Φ=0.31 is 17.01 °CA and for Φ=0.7, it is 12.69 °CA. For bioethanol fumigation at 0.24, 0.48, 0.96 and 1.22 kg/h flow rates, the values of ignition delay are found to be about approximately 14.6, 13.9, 14.9 and 15.8 °CA at higher values of Φ=0.85, Φ=0.88, Φ=0.90 and Φ=0.74.

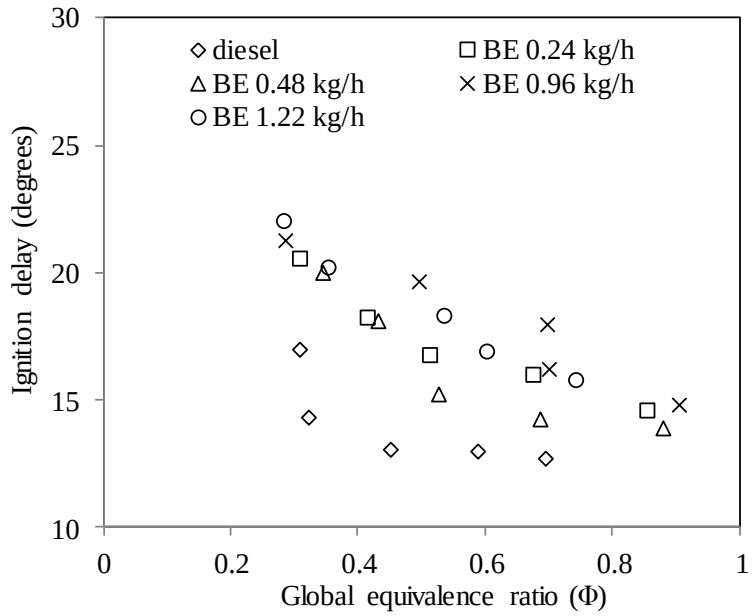

Fig. 6.42 Variation in the ignition delay with the global equivalence ratio

The longer ignition delay is due to the low cetane number and the large latent heat of vaporisation of bioethanol.

6.5.1.3 Heat release rate (HRR)

Figure 6.43 shows the variation in the heat release rate with the crank angle at full load for diesel and bioethanol fumigation at different flow rates.

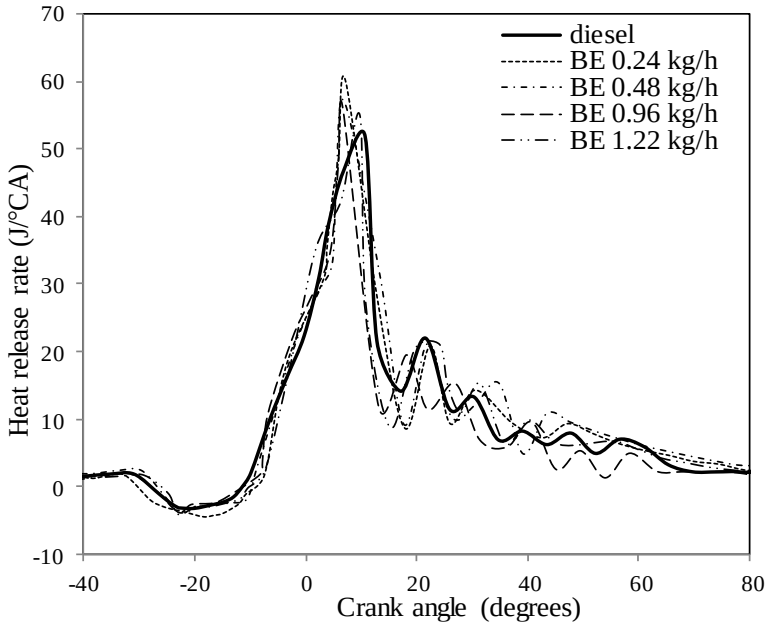

Fig. 6.43 Variation in the heat release rate with crank angle at full load

The maximum heat release rate for diesel, at 0.24, 0.48, 0.96 and 1.22 kg/h flow rate of bioethanol is found to be about 51.8, 60.2, 57.0, 50.1 and 66.1 J/°CA, respectively, which is achieved at about 10.7, 7.1, 7.0, 6.7 and 7.5 °CA aTDC at full load. For bioethanol fumigation at 1.22 kg/h, the heat release rate is found to be higher than that of other flow rates, due to the availability of more oxygen and shorter combustion duration which provide enhanced combustion.

6.5.1.4 Maximum rate of pressure rise

Figure 6.44 presents the variation in the maximum rate of pressure rise with global equivalence ratio for diesel and fumigated bioethanol at 0.24, 0.48, 0.96 and 1.22 kg/h, respectively at full load. The maximum rate of pressure rise for diesel and bioethanol fumigation at 0.24, 0.48, 0.96 and 1.22 kg/h is found to be about 3.7, 4.1, 4.0, 4.2 and 4.5 bar/°CA respectively, which is achieved approximately at 2.3, 4.2, 3.5, 2.0 and 3.9 °CA aTDC respectively, at full load.

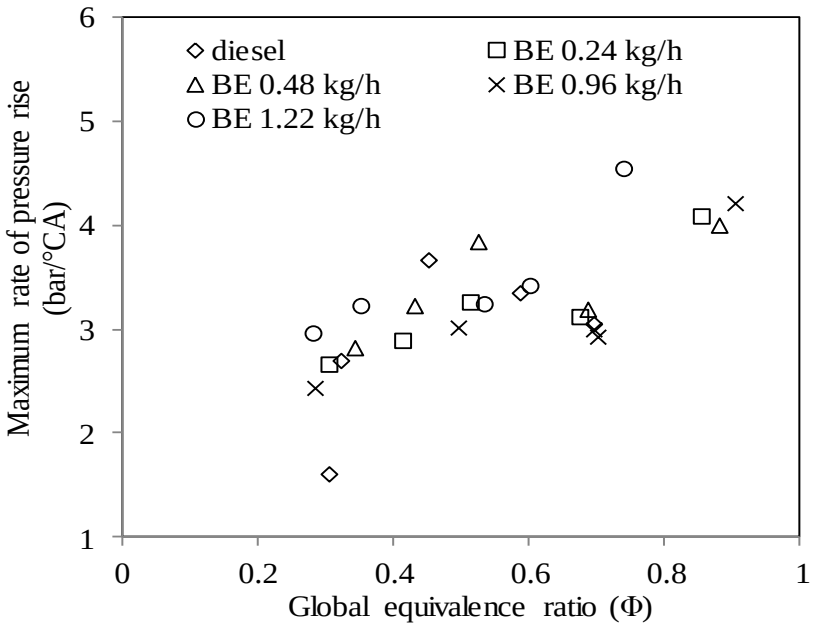

Fig. 6.44 Variation in the maximum rate of pressure rise with the global equivalence ratio

From the figure, it is also inferred that the bioethanol fumigation at a flow rate of 1.22 kg/h gives the highest maximum rate of pressure rise compared to diesel and other flow rates of bioethanol, which in turn, provide the noisy operation during the engine's run. It may be due to the longer ignition delay and shorter combustion duration.

6.5.1.5 Combustion duration

Figure 6.45 depicts the variation in the combustion duration with the global equivalence ratio for diesel, and the fumigation of four different bioethanol flow rates viz. 0.24, 0.48, 0.96 and 1.22 kg/h, respectively. The combustion duration increases with the increase in the equivalence ratio for all the tested fuels. It is because of more time of mixing of fuel and air with the increase in load. At higher values of the equivalence ratio of all the fuels, the combustion duration shows a decreasing trend. As bioethanol is atomised with an injector of high pressure and vaporised with a heater at a temperature of 70 °C, it mixes with the air properly and provides a homogeneous mixture for burning.

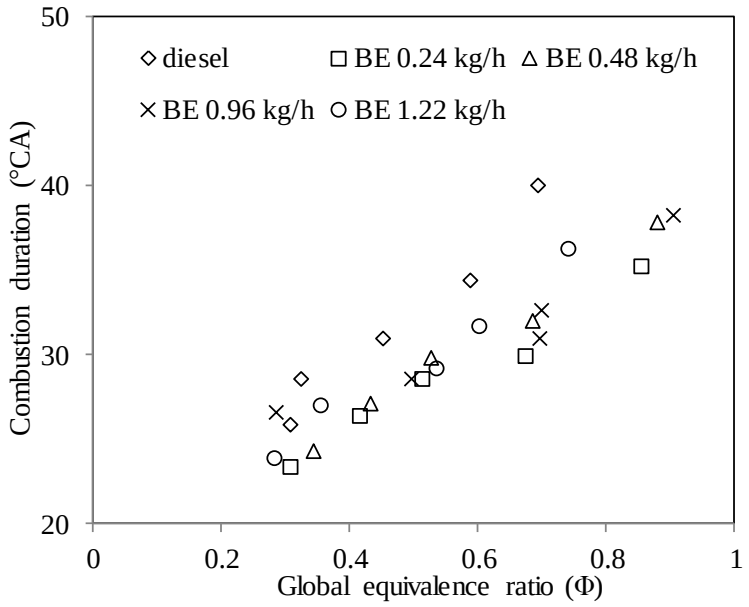

Fig. 6.45 Variation in the combustion duration with the global equivalence ratio

At higher values of Φ=0.7, Φ=0.85, Φ=0.88, Φ=0.90 and Φ=0.74 for diesel, and four flow rates of fumigated bioethanol, the combustion duration is found to be about 38.4, 30.9, 37.8, 38.3 and 34.0 °CA respectively.

6.5.2 Engine performance analysis

The engine performance parameters, such as volumetric efficiency, brake specific fuel consumption, and brake thermal efficiency, are analysed and presented for the diesel bioethanol dual fuel operation, in comparison with the diesel operation of the same engine.

6.5.2.1 BSFC

Figure 6.46 shows the variation in the BSFC with the global equivalence ratio of diesel and bioethanol fumigation at different flow rates. The BSFC is found to be lower with the global equivalence ratio for bioethanol fumigation. As bioethanol is an oxygenated fuel, it reduces the diesel quantity. At Φ=0.85 and 0.24 kg/h, the BSFC is found to be higher by about 1.2% compared to that of diesel. This is due to the low calorific value of fuel, and less amount of oxygen supplied.

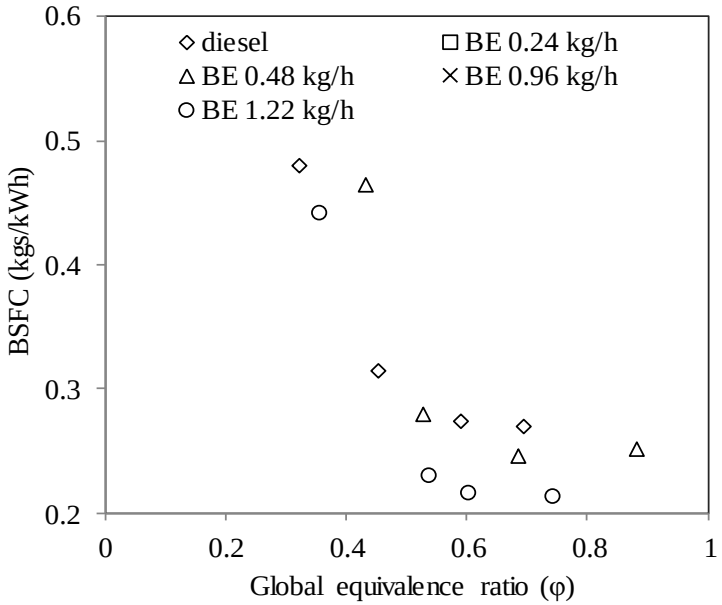

Fig. 6.46 Variation in the BSFC with the global equivalence ratio

At Φ=0.88, Φ=0.90 and Φ=0.74, the bioethanol fumigation of 0.48, 0.96 and 1.22 kg/h has a BSFC, which is lower by about 2.2, 4.5 and 20% respectively, than that of diesel. It is obvious that the bioethanol fumigation replaced a certain amount of diesel.

6.5.2.2 EGT

Figure 6.47 portrays the variation in the EGT of diesel and bioethanol fumigation at different flow rates with the global equivalence ratio. At Φ=0.7, Φ=0.85, Φ=0.88, Φ=0.90 and Φ=0.74 for diesel, and four flow rates of fumigated bioethanol, the EGT is found to be about 315.3 °C, 331 °C, 337.2 °C, 342.5 °C and 344.2 °C respectively, at full load. The EGT for the bioethanol fumigation operation is observed to be high in comparison with diesel. This may be due to the higher oxygen content present in bioethanol that provides the enhancement of combustion with increase in the flow rates of bioethanol. Due to longer ignition delay, more

accumulation of fuel is achieved with increasing global equivalence ratio, which enhances the premixed combustion phase.

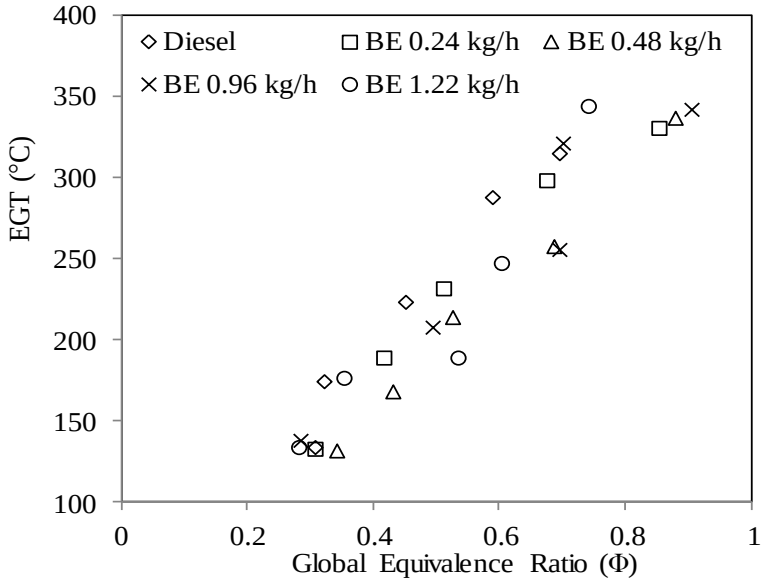

Fig. 6.47 Variation in the EGT with the global equivalence ratio

Hence, more heat is available in the exhaust. Also, it may be due to the better atomisation of the diesel droplets, because of the preheated air achieved by the vaporiser.

6.5.2.3 Volumetric efficiency

The variation in the volumetric efficiency of diesel and bioethanol fumigation at different flow rates with the global equivalence ratio is shown in Fig. 6.48.

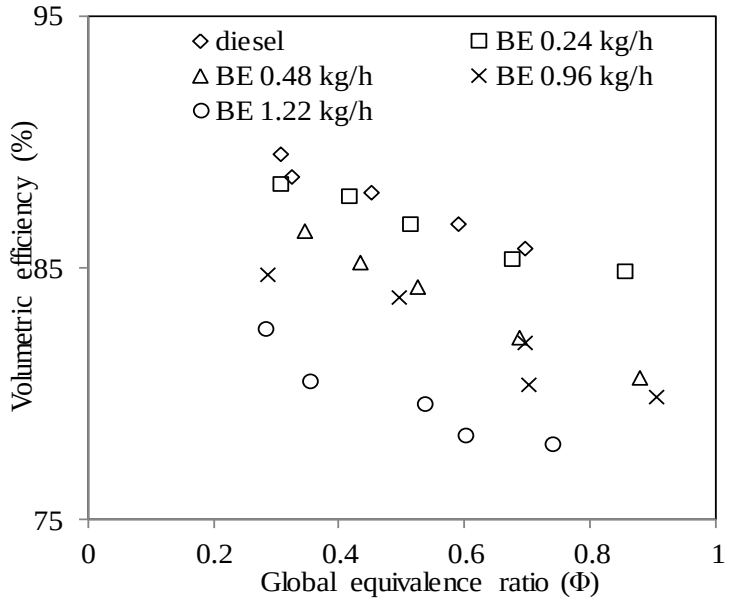

Fig. 6.48 Variation in the volumetric efficiency with the global equivalence ratio

With bioethanol fumigation at different flow rates, the volumetric efficiency is found to be lower with the global equivalence ratio, compared to that of diesel. As bioethanol is fumigated, it displaces some amount of air. At Φ=0.7, Φ=0.85, Φ=0.88, Φ=0.90 and Φ=0.74 for diesel, and four flow rates of fumigated bioethanol, the volumetric efficiency is found to be about 85%, 84.87%, 80.6%, 79.8% and 77.9% respectively.

6.5.2.4 Thermal energy balance

Figure 6.49 shows the variation of the thermal energy balance for diesel and bioethanol fumigation operations at four different flow rates. At full load, the useful work of fumigated bioethanol at 0.24, 0.48, 0.96 and 1.22 kg/h flow rates is found to be about 32%, 34.2%, 36.5% and 37.8%, whereas for diesel, it is by about 30.47%.

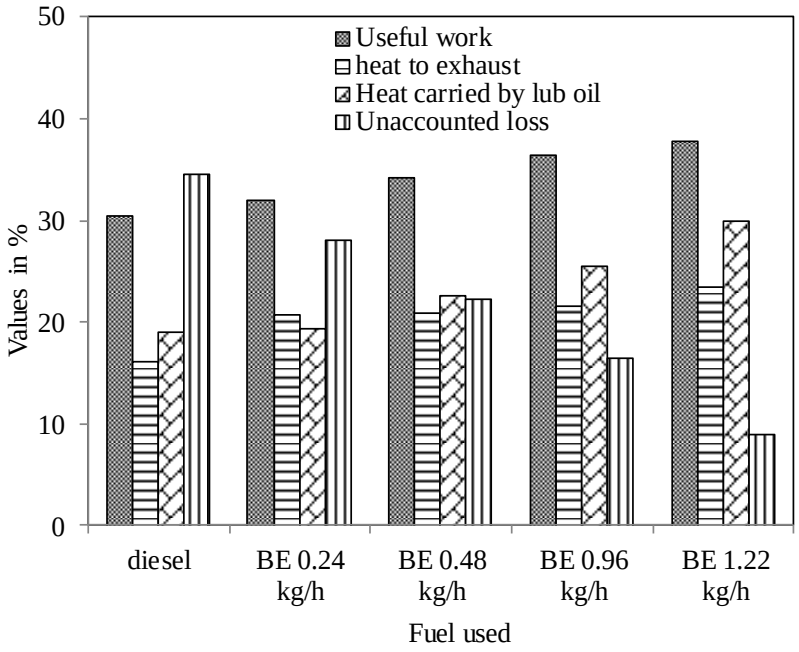

Fig. 6.49 Variation of thermal energy balance for diesel and bioethanol fumigation at full load

The proper atomization and vaporization of fuel is achieved due to the electronically controlled injector and heater, which can provide the homogeneous charge mixture to burn. Hence more useful work is obtained with bioethanol fumigation at four different flow rates, at full load. The heat carried by lubricating oil is also found to be increased with bioethanol fumigation, due to lower lubricity property of bioethanol. But unaccounted heat losses are observed to be low for bioethanol fumigation in comparison with diesel at full load.

6.5.3 Emission analysis

This subsection analysis and presents the results of the exhaust gas emissions recorded with the diesel-bioethanol operation in comparison with the diesel operation.

6.5.3.1 BSHC emission

Figure 6.50 portrays the variation in the BSHC emission for diesel and bioethanol fumigation at different flow rates with the global equivalence ratio.

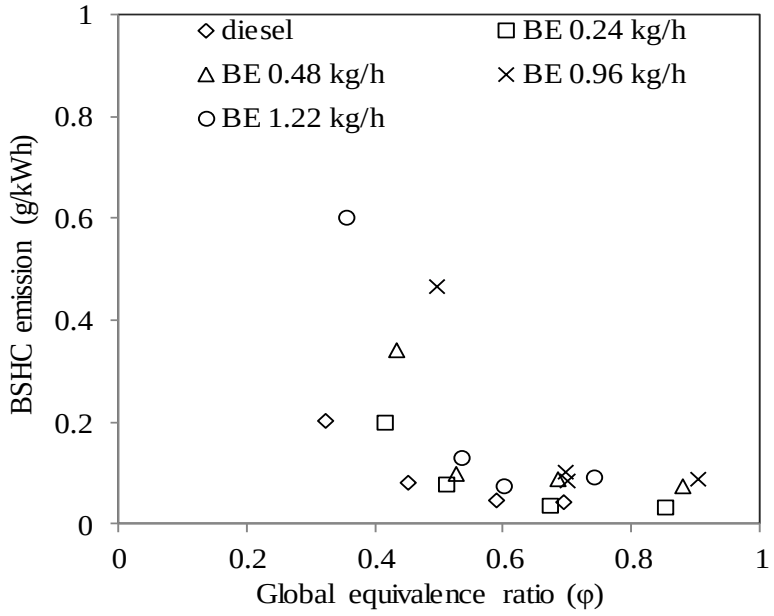

Fig. 6.50 Variation in the BSHC with the global equivalence ratio

At a lower limit of the global equivalence ratio, the BSHC emission for diesel, 0.24, 0.48, 0.96 and 1.22 kg/hr is found to be approximately 0.04, 0.03, 0.07, 0.08 and 0.09 g/kWh respectively. As the flow rate of bioethanol in fumigation is increased at low load, more air and bioethanol will be inducted due to the ram effect, which also increased the ignition delay leading to an over-mixing of the fuel-air mixture for combustion. With over-mixing, some fuel particles will be mixed with the already burned gas and will, therefore, not combust totally. But, at part loads, the BSHC emission for all the flow rates is found to be lower, due to a proper air mixture. At Φ=0.88, Φ=0.90 and Φ=0.74, the BSHC emission for 0.48, 0.96 and 1.22 kg/h is found to be higher, by about 1.8, 2.4 and 3.5% respectively, compared to that of diesel. This may be due to the under-mixing of the fuel air mixture, and the formation of a quench layer developed by the fumigated bioethanol [152].

6.5.3.2 BSCO emission

Figure 6.51 shows the variation in the brake specific carbon monoxide (BSCO) emission of diesel and fumigated bioethanol at different flow rates, with respect to the global equivalence ratio. On the lean mixture side, the BSCO emission for 0.24 and 0.48 kg/h is found to be lower by about 6.2 and 6.1% respectively compared to that of diesel, but for 0.96 and 1.22 kg/h, it is found to be higher by about 12.8 and 9% respectively, compared to that of diesel. At lower flow rates and low load, a better air utilization is achieved due to the presence of a homogeneous bioethanol charge [152], and hence, the BSCO emission is found to be less. But, at higher flow rates, more bioethanol is admitted and less fuel is supplied. A proper fuel-air mixture for combustion will not be achieved, due to the lean mixture at low loads. From the graph, it is also observed that with an increase in the load, the equivalence ratio also increases and the BSCO emission is found to be lower, because of more turbulence in the cylinder (effective mixing), and relatively high combustion temperatures in comparison with the low loads [152].

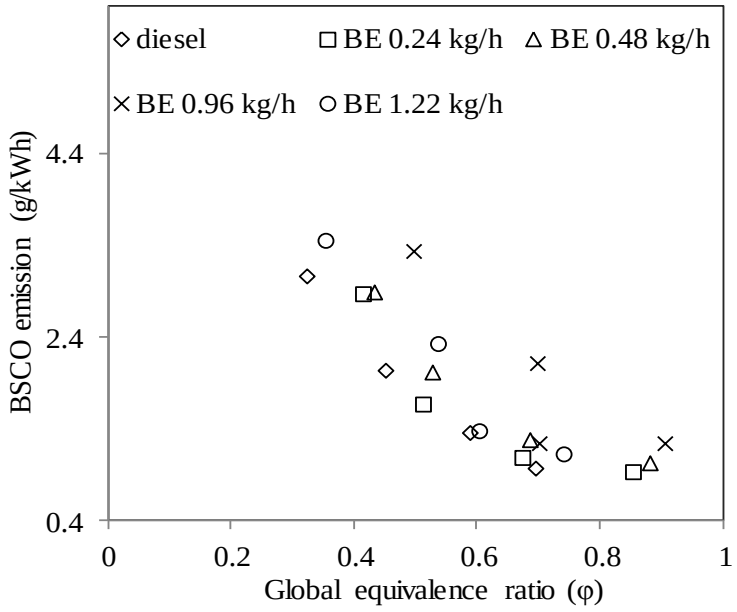

Fig. 6.51 Variation in the BSCO with the global equivalence ratio

At higher values of the equivalence ratio, the BSCO emission for the bioethanol flow rates is more, compared to that of diesel. With bioethanol operation, the global equivalence ratio is found to be closer to the stoichiometric region, where the BSCO emission is found to be high. When $\Phi>0.8$, the BSCO emission will increase, due to the decrease of the dissociation of CO_2 into CO [122].

6.5.3.3 BSNO emission

Figure 6.52 depicts the variation in the BSNO of diesel and bioethanol fumigation at different flow rates with the global equivalence ratio.

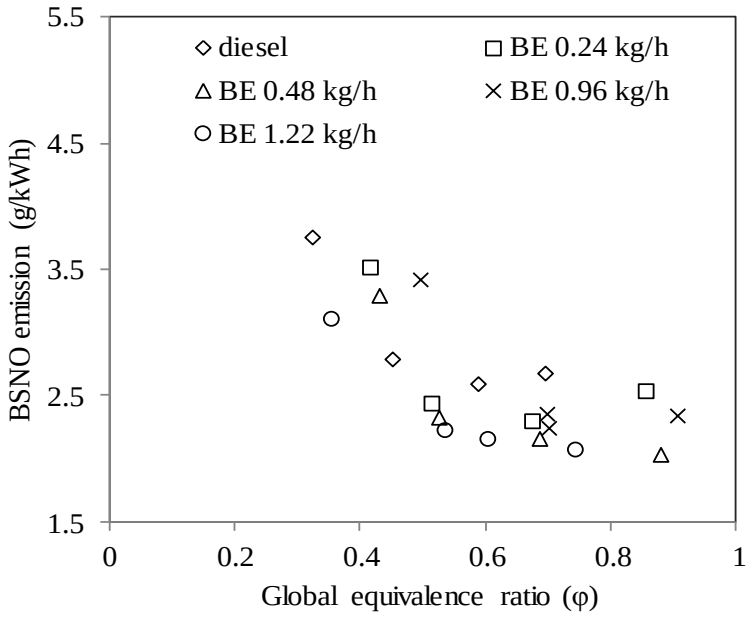

Fig. 6.52 Variation in the BSNO with the global equivalence ratio

The BSNO emission can be formed through a number of mechanisms, during both the premixed and diffusion burning. It also depends upon the in cylinder temperature and oxygen present. The BSNO emission for 0.24, 0.48, 0.96 and 1.22 kg/h at Φ=0.85, Φ=0.88, Φ=0.90 and Φ=0.74 is found to be approximately 2.5, 2.03, 2.3 and 2.1 g/kWh. With the bioethanol fumigation, the BSNO emission is found to be lower than that of diesel at all equivalence ratios, due to the high latent heat of vaporisation of bioethanol. Also, it may be due to the reduction of air induction, which has higher N_2, which signifies that the Zeldovich mechanism is less likely to proceed for NO production. In the premixed combustion phase, the rate of heat release starts slowly, and hence, the BSNO emission is found to be lower compared to that of diesel.

6.5.3.4 Smoke emission

The variation in the smoke opacity for diesel and bioethanol fumigation at different flow rates with the global equivalence ratio is shown in Fig. 6.53. In the bioethanol operation, there is an increase in the hydrogen content in the mixture, which reduces the engine smoke [59]. At Φ=0.85, Φ=0.88, Φ=0.90 and Φ=0.74, the smoke opacity for 0.24, 0.48, 0.96 and 1.22 kg/h

flow rates, is found to be lower by about 4.2, 5.5, 12.5 and 25% respectively, compared to that of diesel operation. Smoke is produced more in the fuel rich region within the cylinder during combustion. But, bioethanol fumigation has a global equivalence ratio of less than unity. A higher molecular weight fuel produces higher smoke, but bioethanol has a low molecular weight compared to that of diesel, and hence, lower smoke emission is noticed. The smoke emission also depends upon the period after the burning phase, which starts from the point of the maximum cycle temperature, and continues over part of the expansion stroke, i.e., 70-80 °CA from TDC.

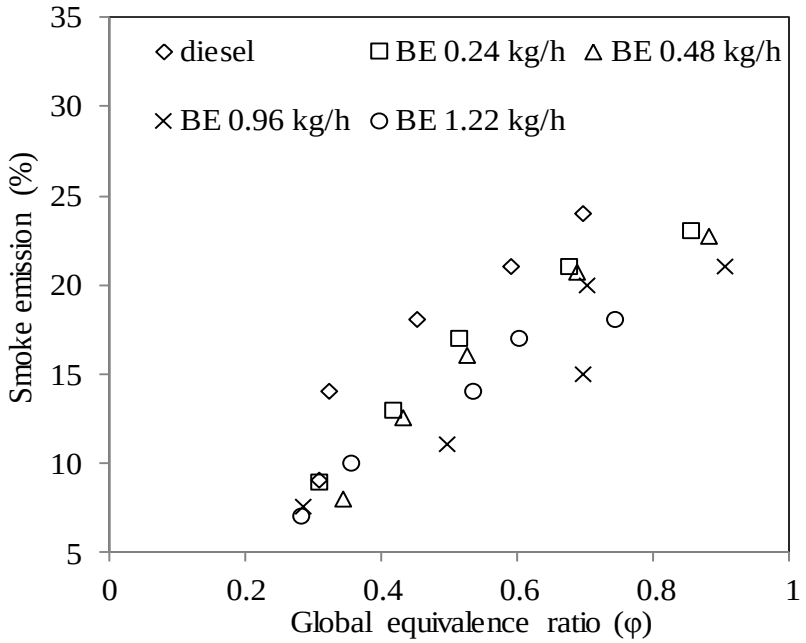

Fig. 6.53 Variation in the smoke emission with the global equivalence ratio

In this phase, the unburnt and partially burnt fuel is left in the combustion chamber, due to the unavailability of oxygen. As bioethanol is an oxygenated fuel, the velocity of diffusion and turbulent mixing of unburned and partially burnt fuel with oxygen will increase, and less smoke will be generated. Similar results have been reported by many investigators when they investigated bioethanol fumigation and use of an oxidation catalyst, in a small capacity diesel engine [94, 98, 153].

6.5.4 Summary

The bioethanol fumigation at four different flow rates, viz., 0.24, 0.48, 0.96 and 1.22 kg/h is run successfully in a diesel engine. The results obtained are summarised as follows,

The ignition delay of bioethanol fumigation at all the flow rates in this study exhibited an overall longer ignition delay of 2-4^{o}CA at full load. The fumigation operation with bioethanol gave lower BSNO and smoke emissions compared to that of diesel operation at full load. However, the BSCO and BSHC emissions were found to be higher with bioethanol fumigation at full load.

6.5.5 Comparison of the results obtained from four different techniques

The results obtained in terms of combustion, performance and emission from the engine run on bioethanol using four different techniques are compared with diesel data for choosing a better technique. The optimum emulsion/blend/flow rate from the better technique is chosen for validation. Table 6.2 gives the comparison of all the results of four different techniques, which is provided in the next page.

From the results of the four techniques adopted for the utilisation of bioethanol in the diesel engine, it is understood that bioethanol can be used in the form of emulsion up to 15%, with or without an ignition improver, without any engine modification. The maximum utilisation of bioethanol is possible with diesel bioethanol dual fuel operation. It is also understood that BMDE10 (bioethanol diesel) can be chosen, based on the technical feasibility, cost involved in engine hardware, and simple operation.

Ethanol has a low viscosity which affects the lubricity [59, 64]. Therefore, further analysis is required, to assess the durability issues when the engine is run with bioethanol diesel emulsion.

Table 6.2 Comparison of all the results of four different techniques

Title	diesel	Emulsion			DEE blending				DEE fumigation				Bioethanol fumigation			
		BMDE5	BMDE10	BMDE15	DED 1%	DED 1.5%	DED 2%	DED 2.5%	60 g/h	120 g/h	180 g/h	240 g/h	0.24 kg/h	0.48 kg/h	0.96 kg/h	1.22 kg/h
Combustion parameters																
ID	11.8	12.3	12.9	13.02	11	11	10.4	10.7	13.32	13.6	12.1	11.4	14.5	13.9	14.7	15.7
HRR	51.84	52.92	53.29	53.96	52.5	51.9	49.6	47.8	53.17	53.1	54.15	53.9	60.2	56.9	56.2	54.9
Max. pressure	73.5	77.07	77.09	77.4	75.33	73.79	72.83	70.63	76.14	76.3	77.2	76.4	72.7	75.	69.4	78.06
Maxm ROPR	3.046	3.11	3.42	3.63	3.10	2.81	2.72	3.07	3.101	2.8	2.7	3.8	4.08	3.9	4.2	4.5
CD	41	37.8	38.12	37.34	52.3	65.5	63.3	57.17	36.6	34.4	39.6	41.2	35.2	37.8	38.3	36.3
Performance parameters																
BSEC/BSFC	9.7/0.26	11.4	11.4	12.67	12.9	13.2	13.7	14.23	0.263	0.25	0.24	0.23	0.27	0.25	0.23	0.21
EGT	315.3	321.6	325.6	328.2	361.8	406.6	383.2	386.1	294	310.1	338.24	341.2	335	317.1	346.5	289.4
BTE	30.47	27	27.5	28	23.38	21.1	19.59	23.5	30.13	30.32	32.53	33.67	31.2	31.3	30.8	32.5
Volumetric efficiency	85.7	-	-	-	-	-	-	-	84.9	83.6	81.8	80.9	84.8	80.6	79.8	77.9
Emission parameters																
BSHC	0.042	0.045	0.0466	0.0478	0.026	0.02	0.047	0.06	0.038	0.041	0.04	0.047	0.03	0.07	0.086	0.092
BSCO	0.97	0.96	0.95	0.982	0.39	0.29	0.702	1.208	0.8	0.95	1.15	1.22	0.93	1.02	1.24	1.12
BSNO	2.67	2.59	2.52	2.46	2.59	2.36	2.31	2.3	2.61	2.37	1.98	1.72	2.53	2.03	2.34	2.07
Smoke	24	23.78	23.001	19	22.42	21.56	23.1	24.2	23.8	22.3	20	18.8	23	22.6	21	18

6.6 Validation of experimental results of BMDE15 through mathematical modelling

6.6.1 Spray profile of diesel and BMDE15

In a CI engine, once the fuel is injected into the compressed air stream in the cylinder, the fuel jet disintegrates into a core of fuel surrounded by the spray envelope of air and fuel particles. The spray envelope is created both by the atomisation and vaporisation of the fuel. The turbulence of air in the combustion chamber passing across the jet tears the fuel particles from the core. A mixture of air and fuel is found at some location in the spray envelope and the oxidation starts [122]. Thus, the study of formation of spray is important for any diesel fuel, when it is used in a diesel engine. In this study, the fuel spray patterns for diesel and the BMDE15 emulsion are obtained using the MATLAB program which is given in Annexure III. Figures 6.54 and 6.55 show the spray profile of diesel and BMDE15 respectively at full load.

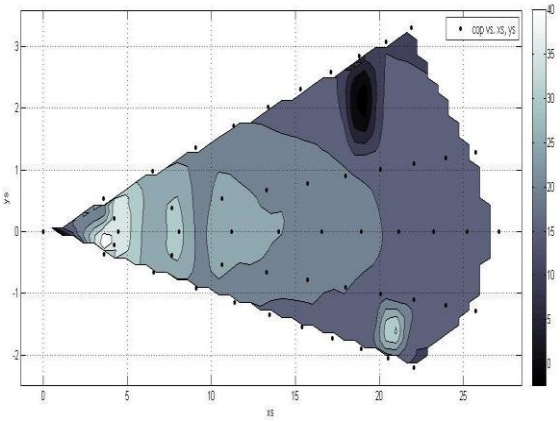

Fig. 6.54 Diesel spray

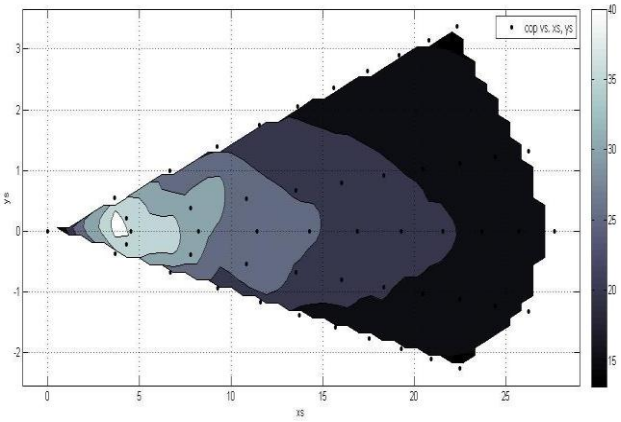

Fig. 6.55 Emulsion spray

This is due to the better mixture formation. With the BMDE15 emulsion, the flame propagation is uniform from the point of impingement compared to that of diesel. The density of bioethanol is lower and when it is emulsified with diesel, it lowers the density of the emulsion. Hence, a better atomisation and vaporisation will be achieved with the BMDE15 emulsion. Also, due to the availability of oxygen in the fuel, more complete combustion will be obtained compared to that of diesel.

6.6.2 Results and discussion

6.6.2.1 Cylinder pressure

Figure 6.56 depicts the experimental and simulated results of the diesel engines fueled with diesel and BMDE15, at full load. The simulated results of both the test fuels gave higher

values compared to the experimental results. The lower cylinder pressure for the experimental results may be due to the instruments' error, and physical condition during the experiments and the uncertainty of the data. It is apparent from the figure that the ignition of diesel is the earliest for the simulated results followed by its experimental results, the BMDE15 simulated results, and finally, the BMDE15 experimental results. The peak cylinder pressure of a CI is predominantly influenced by the ignition delay, the amount of fuel burnt in the initial stage of fuel combustion and the mixture formation in the delay period. The peak cylinder pressure for the BMDE15 is found to be the highest, followed by the BMDE15 experimental results, diesel simulated and experimental results. The difference in the peak cylinder pressure of BMDE15 between the simulated and experimental results is about 3%. The peak pressure is shifted away from the top dead centre by about 5 to 7 °CA. In the case of diesel, the peak cylinder pressure for the simulated and experimental results is about 75 to 70.6 bar which is attained close to the TDC. The peak cylinder pressures of BMDE15 operation, both in the simulated and experimental results, are higher than those of diesel operation, due to longer ignition delay and better fuel mixture formation, that results in more complete combustion.

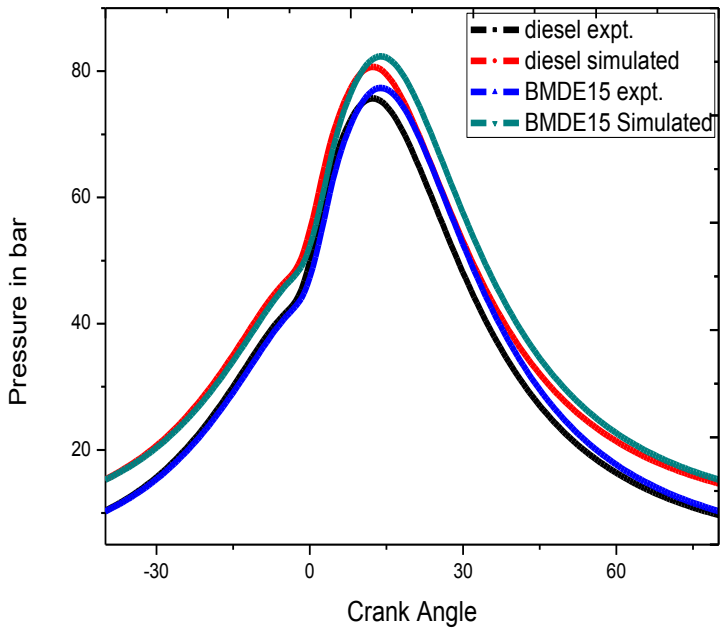

Fig. 6.56 Cylinder pressure with crank angle for diesel and BMDE15

From the spray pattern of BMDE15, it is also observed that after the impingement of fuel, the spray development is faster due to the proper atomisation, vaporisation and mixture

formation, due to its low density compared to that of diesel. The deviation between the simulated and the experimental results for diesel and BMDE15 is about 2 to 4 °CA respectively.

6.6.2.2 Ignition delay

Figure 6.57 illustrates the variation of ignition delay at different loads for diesel and BMDE15 operations. It is evident from the figure, that the simulated and the experimental results for the ignition delay in the diesel and BMDE15 operations follow a similar trend. The ignition delay increases with the increase in the load as a result of the increase in the cylinder gas temperature. The deviation between the simulated and experimental results for the diesel operation is about 1-6 °CA from no load to full load respectively, whereas for the BMDE15 operation, it is 3-5 °CA from no load to full load. The ignition delay is found to be longer for the simulated and experimental results in the BMDE15 operation than those of diesel operation.

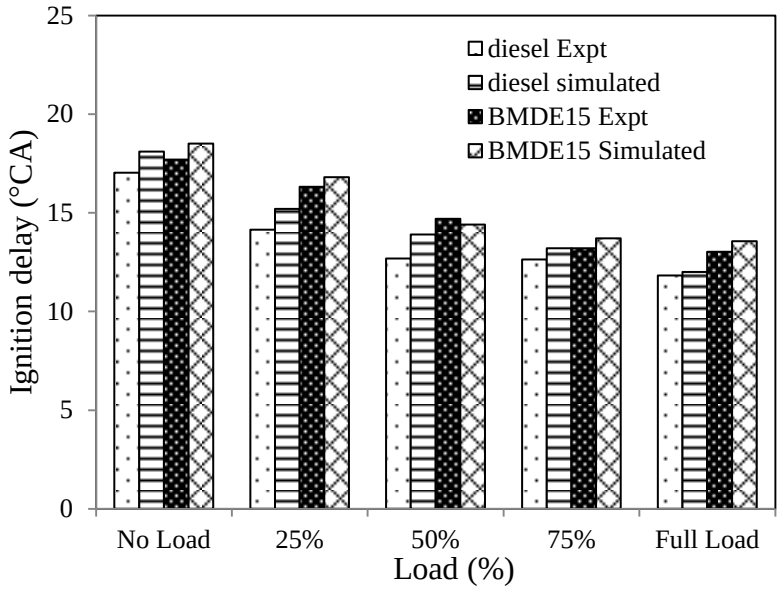

Fig. 6.57 Variation of ignition delay with load

The calculated values for ignition delay in the BMDE15 operation are higher than those of diesel values, which is due to the influence of the temperature, pressure and the time of injection. The longer ignition delay of the BMDE15 operation than that of diesel operation throughout the load spectrum, is due to the lower cetane number of BMDE15.

6.6.2.3 NO emission

In a CI engine, the NO_x emission is one of the major pollutants and is predominantly influenced by the amount of oxygen available, and the in-cylinder temperature. The NO_x emission is composed of NO, NO_2, N_2O, N_2O_5, NO_3. Nitric oxide is the major constituent and NO_2 is a minor constituent, while the others are negligible. At elevated temperatures (i.e.) above 1500°C, N_2 can react with O_2 faster and may result in more NO_x emission. As CI engines have a higher compression ratio and are lean burn engines, the peak temperature is well above 1500°C; hence, there is a higher NO_x formation. The comparison between the simulated and experimental results for NO emission from diesel and BMDE15 operations is shown in Fig. 6.58. The brake specific NO emissions are obtained from the simulation and experiments for both diesel and BMDE15, show a declining trend as the load increases.

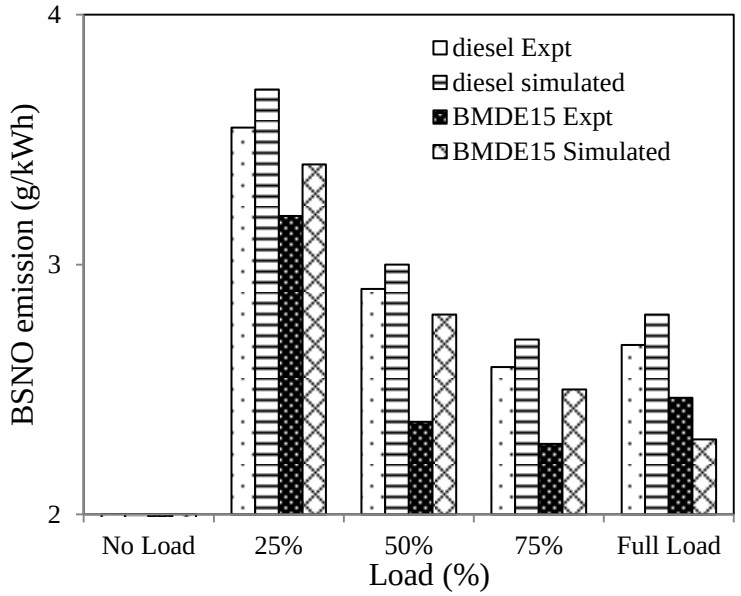

Fig. 6.58 Variation of BSNO emission with load

This is because of the increase in the load which is a denominator for the calculation of NO. The NO emission values obtained from the simulation and experiments are found to be lower than those of diesel operation, because of the higher latent heat of the vaporisation of BMDE15. An overall marginal deviation of 2 to 1% is noticed between the simulation and experimental results of the NO emission values in diesel operation from no load to full load, while the deviation is 2 to 1% from no load to full load in the BMDE15 operation.

6.6.2.4 Smoke

The variation of the simulated and experimental results of smoke emission for diesel and BMDE15 is shown in Fig. 6.59. The simulated results of diesel for smoke emission are found to be high compared to the experimental results of diesel and the simulated and experimental results of BMDE15. The smoke emission is a result of the oxygen unavailability in the diffusion combustion phase, use of high molecular weight fuel and the aromatic content of fuel. Diesel has a high carbon to hydrogen ratio, high molecular weight, less oxygen and high aromatic content. Hence, higher smoke emission is observed with the diesel operation compared to that of BMDE15 operation. The deviation between the simulated and experimental values of diesel and BMDE15 is about 3% and 4% respectively, at full load.

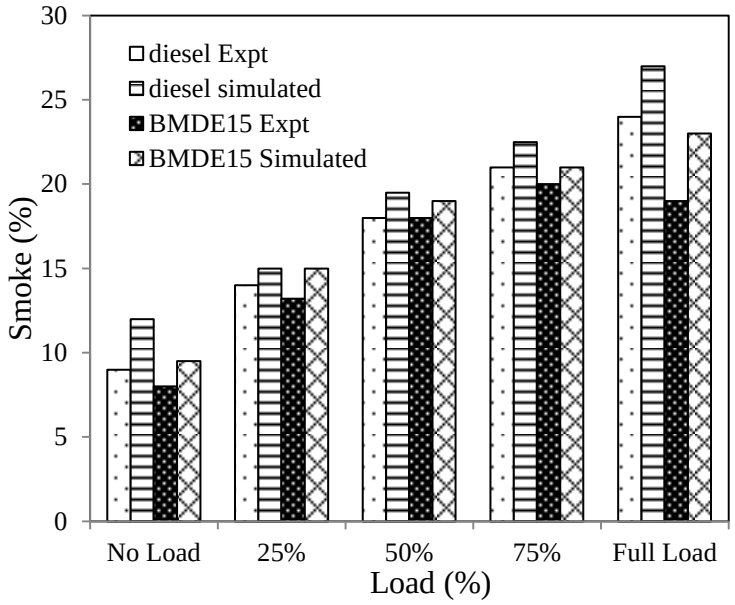

Fig. 6.59 Variation of smoke with load

6.6.3 Summary

A comprehensive two zone model was developed to validate the experimental results obtained from a single cylinder, four stroke, air cooled, DI diesel engine run on two different fuels, viz., diesel and BMDE15. It is concluded that the experimental results are in good agreement with the simulated results. The following is the summary of the results;

(i) The experimental and simulated results show that the peak cylinder pressure of the BMDE15 is found to be marginally higher than that of diesel. The deviation between the simulated and the experimental results in the diesel operation at full load is about 5%. In the case of the BMDE15 operation, the deviation is about 3% at full load.

(ii) The ignition delay of BMDE15 is found to be longer than that of diesel throughout the entire engine operation. The values of ignition delay obtained in the experimentation for both the fuels are close to the values obtained by simulation.

(iii) The NO emission of the engine run on BMDE15 is found to be lower than that of diesel which is due to the high latent heat of vaporisation. This is validated with the NO emission model. The deviation between the simulated and experimental results in the diesel and BMDE15 operations are about 7.1% and 5% respectively, at full load.

(iv) The smoke opacity is found to be lower for the BMDE15 operation compared to that of diesel. The smoke opacity of BMDE15 in the simulation condition is higher by about 4% than that of the experiment.

6.7 Running on engine with bioethanol-biodiesel-diesel blends

6.7.1 Combustion parameters

6.7.1.1 P-θ diagram

The variation of cylinder pressure with crank angle for diesel and the bioethanol-biodiesel-diesel blends is shown in Fig 6.60.

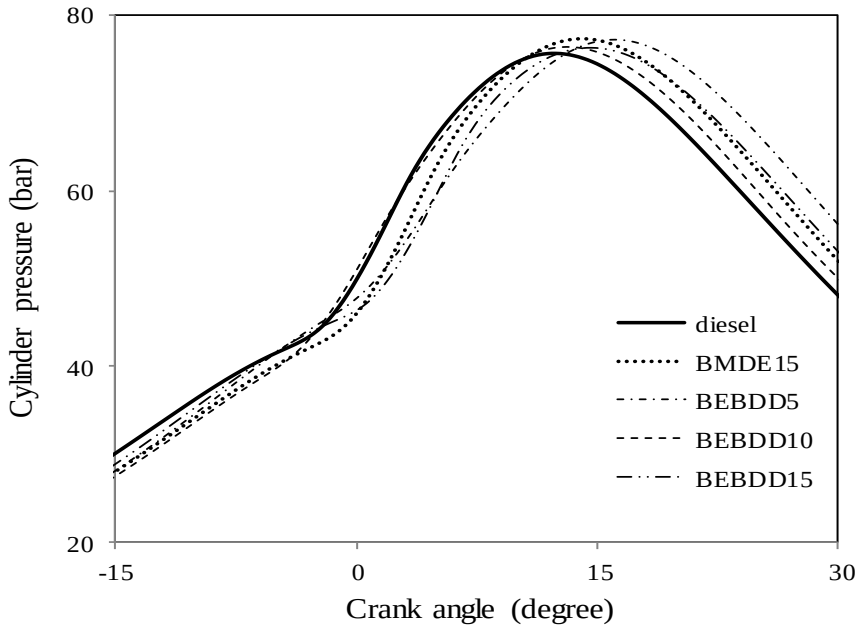

Fig. 6.60 Variation of cylinder pressure with crank angle

It can be observed from the figure, that, at full load, the commencement of ignition for diesel is the earliest, followed by the three bioethanol-biodiesel-diesel blends and the BMDE15, in this investigation. The earliest commencement of ignition of diesel is due to its higher cetane number than those of bioethanol-diesel emulsion (BMDE15), and the bioethanol-biodiesel-diesel blends. The start of ignition for diesel occurs approximately at 9.8 ^{o}CA bTDC, and the maximum cylinder pressure is attained at about 6 ^{o}CA aTDC at full load. For the BMDE15 emulsion, the start of ignition is attained at about 8.3 ^{o}CA bTDC, while the maximum pressure occurs at about 12.4 ^{o}CA aTDC at full load. The bioethanol-biodiesel-diesel blends ignite later than diesel and, but earlier than the BMDE15 emulsion. The delayed ignition of both the fuel types is influenced by their lower cetane number. Another reason may be their higher latent heat of vaporisation, which makes the fuel to evaporate slower as they require more amount of heat to evaporate. As the start of ignition is delayed, the attainment of maximum pressure is shifted by about 2-3 ^{o}CA farther away from the TDC. As the

percentage of biodiesel increases in the bioethanol-biodiesel-diesel blend, the start of ignition is advanced.

6.7.1.2 Ignition delay

The variation of ignition delay for diesel, BMDE15 and bioethanol-biodiesel-diesel blends is depicted in Fig. 6.61.

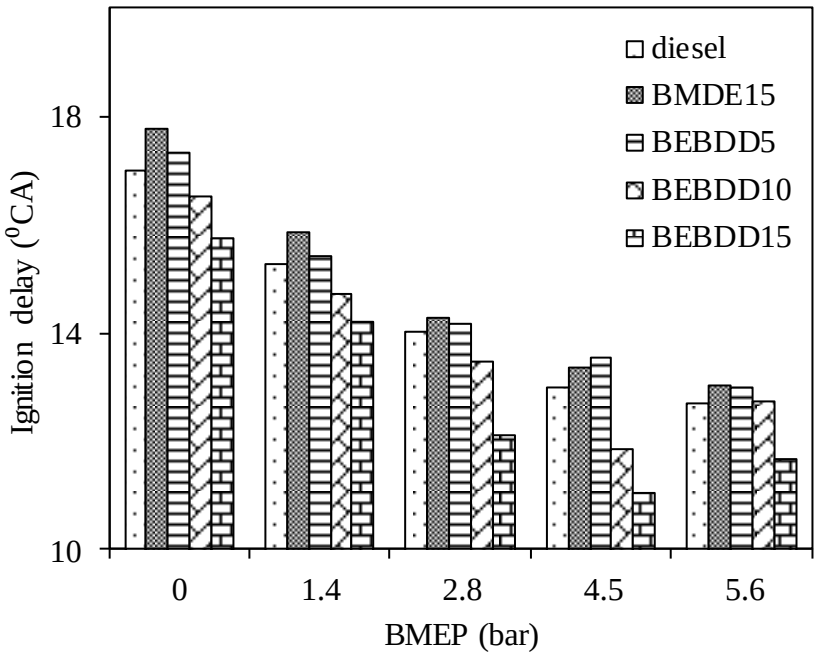

Fig. 6.61 Variation of ignition delay with BMEP

The ignition delay decreases with an increase in the load as expected, for all the fuels tested in this study. The ignition delay of the BMDE15 emulsion is longer than that of diesel, and bioethanol-biodiesel-diesel blends throughout the load spectrum. The longer ignition delay of the emulsion is due to its lower cetane number. In the case of the bioethanol-biodiesel-blends, when biodiesel is added to bioethanol, and the diesel quantity is reduced, the ignition delay decreases gradually. This is because of the marginal increase in the cetane number of the blends. However, the ignition delays of the bioethanol-biodiesel-diesel blends are marginally longer than that of diesel in the entire engine operation. This is because of the lower cetane number of the blends. This is evidenced from Table 5.5. A maximum reduction in the delay of 4 to 2 °CA is noticed from no load to full load, between the BMDE15 operation and bioethanol-biodiesel-diesel operation. Similar results are reported by Sukjit et al. when they conducted experiments with methyl esters on the combustion and emissions of ethanol and butanol, to determine the combustion and emission parameters of the diesel engine [154].

6.7.1.3 Heat release rate (HRR)

The heat release rate (HRR) pattern for diesel, BMDE15 and the bioethanol-biodiesel-diesel blends at full load is shown Fig. 6.62.

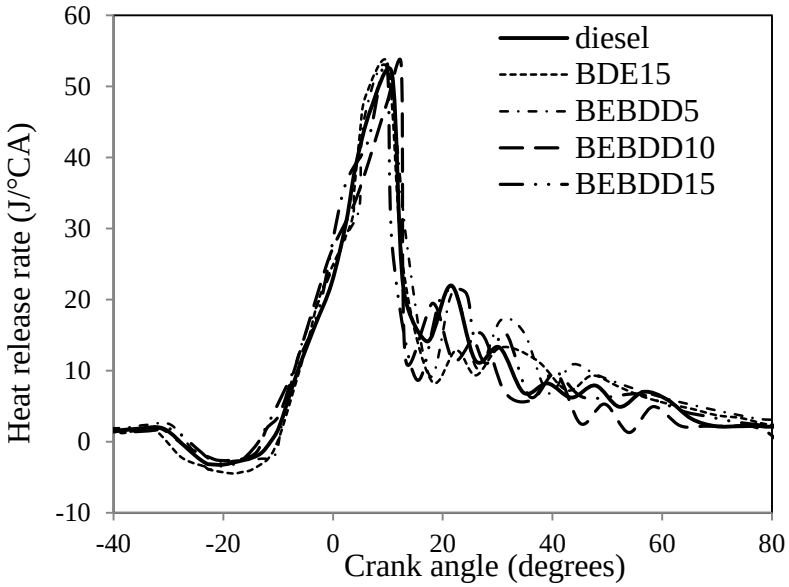

Fig. 6.62 Variation of Heat release rate with crank angle

At full load, the peak heat release rate is found to be the highest for the BMDE15 emulsion, which occurs approximately at 10.8 ^{o}CA aTDC, in this study. This is attributed to the accumulation of more fuel in the delay period due to longer ignition delay. The maximum heat release rates for the bioethanol-biodiesel-diesel blends (BEBDD5, BEBDD10 and BEBDD15) are lower than that of BMDE15 emulsion, but higher than that of diesel at full load. The lowest heat release rate of diesel is due to its lower cetane number than those of the bioethanol-biodiesel-diesel blends. The occurrences of the peak heat release rates for BEBDD5, BEBDD10 and BEBDD15 are approximately at 9.8, 8.9 and 7.8 ^{o}CA respectively, aTDC at full load. The peak heat release for all the fuels tested in this study occurs approximately at 1-2 ^{o}CA aTDC.

6.7.1.4 Maximum cylinder pressure

Figure 6.63 depicts the variation of the maximum cylinder pressure with BMEP for diesel, BMDE15 and the bioethanol-biodiesel-diesel blends. It is apparent from the figure that the maximum cylinder pressure is found to be the highest for the BMDE15 emulsion followed by BEBDD5, BEBDD10, BEBDD15 and diesel, at full load. This is also evidenced from the heat release rate curve in Fig. 6.51. Due to the accumulation of more fuel in the delay period,

the maximum cylinder pressure was higher for the BMDE15 emulsion (BMDE15). For the bioethanol-biodiesel-diesel blends also, the ignition delay is longer than that of diesel at full load. Due to this, their maximum cylinder pressures are found to be higher than that of diesel throughout the load spectrum, but marginally lower than that of BMDE15.

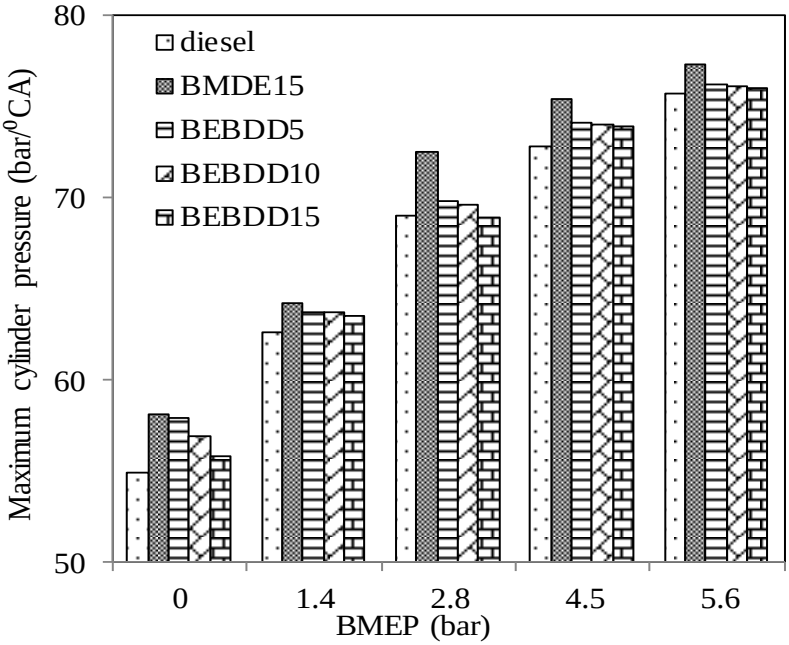

Fig. 6.63 Variation of the maximum cylinder pressure with BMEP

The oxygen present in biodiesel may promote more complete combustion in the case of the bioethanol-biodiesel-diesel blends (BEBDD5, BEBDD10, and BEBDD15). At full load, the maximum cylinder pressure is found to be higher by about 1-2 bar for the bioethanol-biodiesel-diesel blends than that of diesel, while they are lower in the range of 1-2.2 bar than that of BMDE15 at full load.

6.7.1.5 Combustion duration

Figure 6.64 portrays the variation of combustion duration with BMEP for diesel, BMDE15 emulsion, and the three bioethanol-biodiesel-diesel blends (BEBDD5, BEBDD10, and BEBDD15). The combustion duration increases with the increase in the engine load for the fuels tested in this study. This is because of more fuel injected with the increase in the load. The combustion duration is found to be the lowest for the BEBDD5 followed by BEBDD10, BEBDD15, BMDE15 and diesel at full load. By adding biodiesel to the bioethanol-diesel mixture, the cetane number marginally increases. Also, due to the oxygen present in both the fuels, there is a better mixture formation which provides more complete combustion in the diffusion combustion phase.

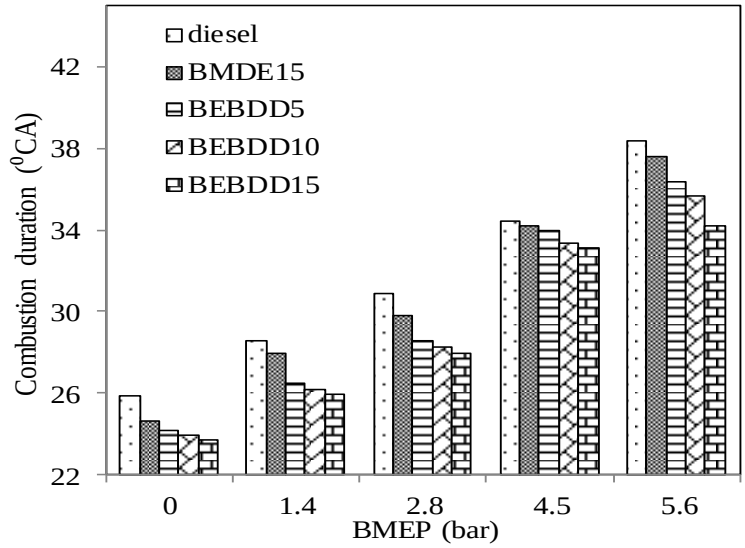

Fig. 6.64 Variation of combustion duration with BMEP

Hence, the combustion duration of the bioethanol-biodiesel-diesel blends is shorter than those of BMDE15 and diesel. The longer combustion duration for the BMDE15 emulsion is due to the poor mixture formation than those of the bioethanol-biodiesel-diesel blends.

6.7.1.6 Maximum rate of pressure rise

The variation of the maximum rate of pressure rise for diesel, BMDE15 and the bioethanol-biodiesel-diesel operation is depicted in Fig. 6.65.

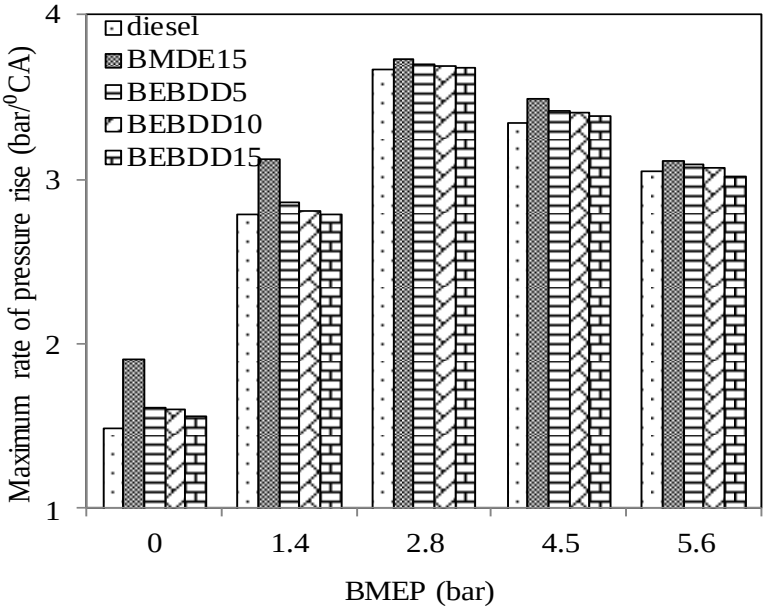

Fig. 6.65 Variation of maximum rate of pressure rise with BMEP

The maximum rate of pressure rise is the highest for the BMDE15 emulsion followed by the BEBDD5, BEBDD10, BEBDD15 blends and diesel at full load. There is abrupt pressure

variation due to the large accumulation of the oxygenated fuel in the longer delay period. The maximum rate of pressure rise for the bioethanol-biodiesel-diesel blends varies from 0.02-0.05 and 0.01-0.08 bar/°CA compared to those of diesel and BMDE15 respectively, at full load.

6.7.2 Performance analysis

6.7.2.1 BSEC

Figure 6.66 shows the variation of BSEC for diesel, BMDE15 emulsion and bioethanol-biodiesel operation with BMEP.

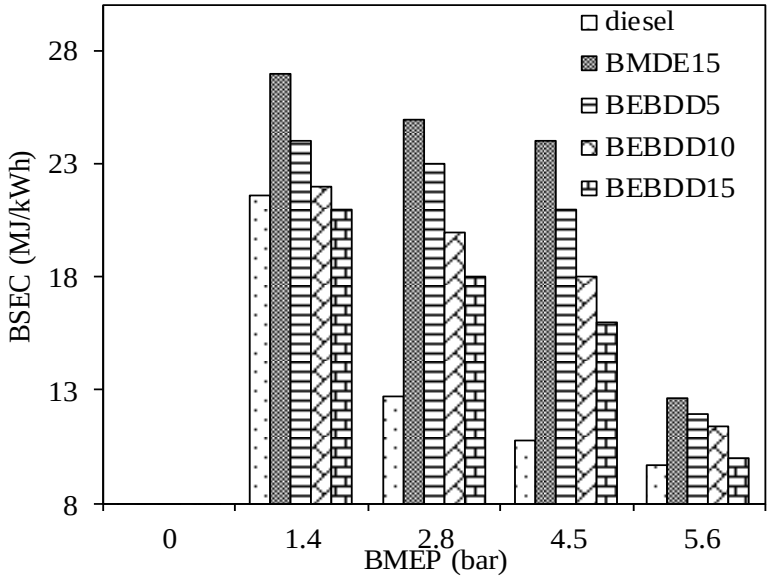

Fig. 6.66 Variation of BSEC with BMEP

The BSEC is found to be low with increase in the load, due to the residual gases present inside the chamber. The BSEC is found to be higher for the BMDE15 emulsion compared to those of diesel and the bioethanol-biodiesel-diesel blends. The BMDE15 emulsion has less heating values; hence, more fuel is consumed in the delay period to meet the required power output of the engine. But, with the bioethanol-biodiesel-diesel operation, the BSEC is found to be lower in comparison with BMDE15, due to increase in the fuel property. The BSEC for the bioethanol-biodiesel-diesel blends is found to be in the range of 3 to 6 MJ/kWh compared to that of BMDE15 at low load and 1 to 2 MJ/kWh compared to that of BMDE15 at full load.

6.7.2.2 EGT

Figure 6.67 portrays the trend of EGT with BMEP for diesel, BMDE15 and the bioethanol-biodiesel-diesel operation. The EGT is found to be lower for the bioethanol-biodiesel-diesel

blends than that of BMDE15, but marginally higher than that of diesel. This may be due to the increased ignition delay of the blends. The oxygen bound combustion yields more complete combustion for the bioethanol-biodiesel-diesel blends than for the BMDE15 emulsion. The values of EGT for diesel, BMDE15, BEBDD5, BEBDD10 and BEBDD15 are found to be 315.31 °C, 328.74 °C, 326.85 °C, 321.64 °C and 327.2 °C respectively, at full load.

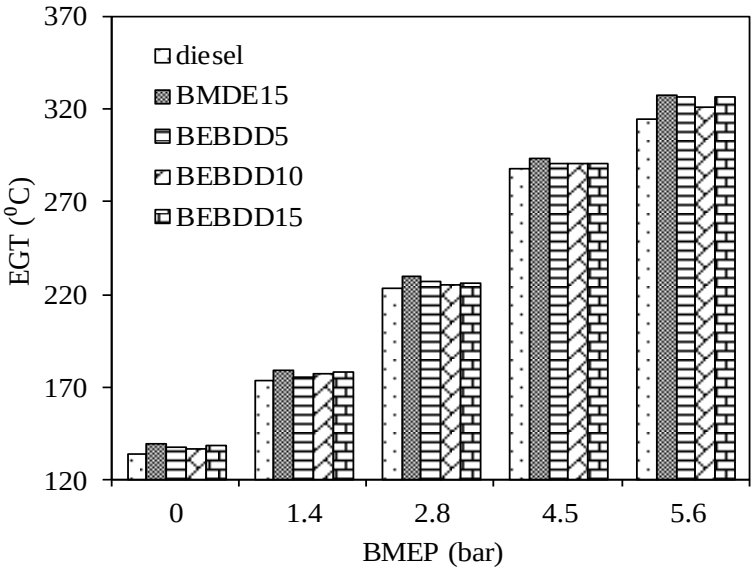

Fig. 6.67 Variation of EGT with BMEP

The BMDE15 emulsion exhibits the highest EGT among all the fuels tested in this study. The prolonged combustion as a result of longer ignition delay may be the reason for this. The reduction of EGT is found to be in the range of 1 to 7 °C for bioethanol-biodiesel-diesel blends, compared to that of the BMDE15 operation, at full load. The EGT for BEBDD15 is found to high compared to those of BEBDD5 and BEBDD10. High EGT can results from high fuel density, as dense fuels have shorter ignition delay leading to a higher cylinder pressure and cylinder temperature in the power stroke, which is also evident from the P-θ diagram.

6.7.2.3 Thermal energy balance

The variation of the thermal energy balance for diesel, BMDE15 and the bioethanol-biodiesel-diesel operation is depicted in Fig. 6.68. From the figure, it is noticed that the heat carried out by the lubricating oil for bioethanol-biodiesel-diesel operation is found to be decreased compared to that of BMDE15. This is due to lubricity property of fuel. The heat

carried out by the lubricating oil for diesel, BMDE15, BEBDD5, BEBDD10 and BEBDD15 is found to be 15.9%, 19.3%, 17.7%, 16.1%, and 16.7% respectively, at full load.

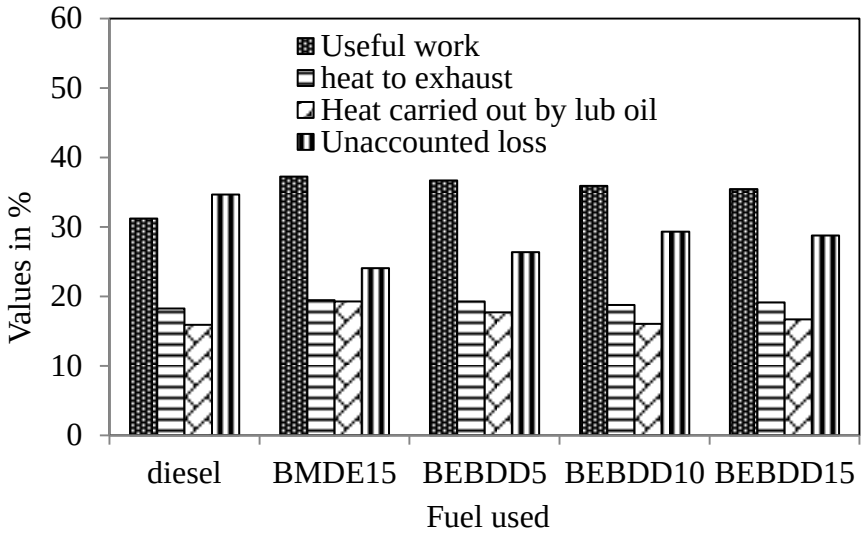

Fig. 6.68 Variation of thermal energy balance for diesel, BMDE15 and the bioethanol-biodiesel-diesel operation at full load

The useful work is found to be increased for both BMDE15 and bioethanol-biodiesel-diesel operation compared to that of diesel at full load.

6.7.3 Emission analysis

6.7.3.1 BSHC emission

The variation of BSHC emission for diesel, BMDE15 and the bioethanol-biodiesel-diesel blends is depicted in Fig. 6.69. The BSHC emission is observed to be lower for the bioethanol-biodiesel-diesel blends due to the more complete combustion, as a result of the oxygen availability and lower viscosity of the fuels. The higher BSHC emission for BMDE15 is due to flame quenching due to high latent heat of vaporisation than those of diesel and bioethanol-biodiesel-diesel blends. The values of BSHC emission for diesel, BMDE15, BEBDD5, BEBDD10 and BEBDD15 are 0.04, 0.045, 0.034, 0.033 and 0.038 g/kWh respectively at full load. The BSHC emissions for BEBDD5, BEBDD10 and BEBDD15 are lower by about 4%, 5.2% and 4.8% than those of diesel at full load. They are also lower by about 3.2%, 4.3% and 4.1% respectively, than that of BMDE15 at full load.

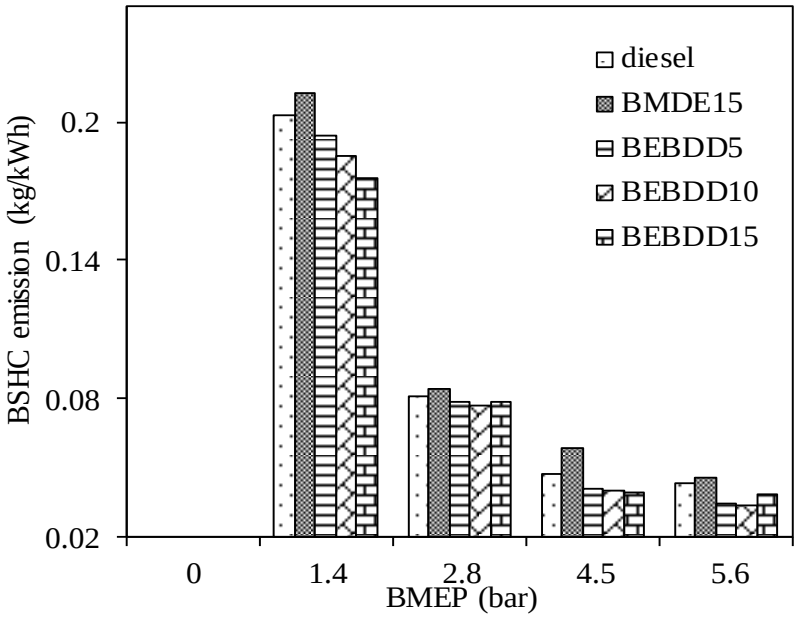

Fig. 6.69 Variation of BSHC emission with BMEP

With the bioethanol-biodiesel-diesel blends, more complete combustion is achieved due to the oxygen availability and proper mixture formation.

6.7.3.2 BSCO emission

The variation of BSCO emission with BMEP for diesel, BMDE15 and the bioethanol-biodiesel-diesel blends is shown in Fig. 6.70. The BSCO emission exhibits a declining trend for all the fuels tested in this study, as expected.

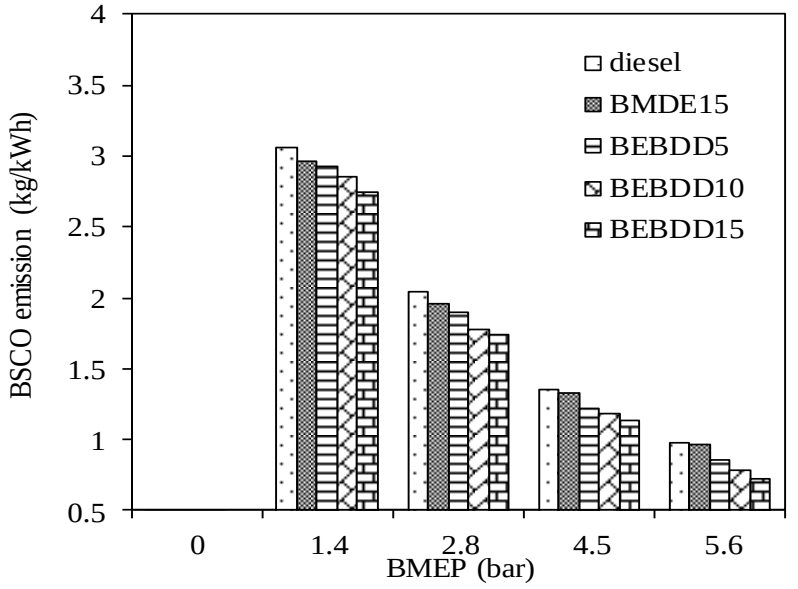

Fig. 6.70 Variation of BSCO emission with BMEP

The CO emission is due to the unavailability of oxygen and poor mixture formation. As bioethanol and biodiesel contain more oxygen content, there is more complete combustion of fuel. For a given input, increasing the biodiesel percentage in the bioethanol-biodiesel-diesel mixture reduces the BSCO emission at full load. The BSCO emission for BMDE15, BEBDD5, BEBDD10, and BEBDD15 are lower by about 2%, 3.1%, 4.2% and 6.3% than that of diesel, at full load.

6.7.3.3 BSNO emission

The BSNO emission variation recorded in the diesel, BMDE15 and the bioethanol-biodiesel-diesel operations with BMEP is plotted in Fig. 6.71.

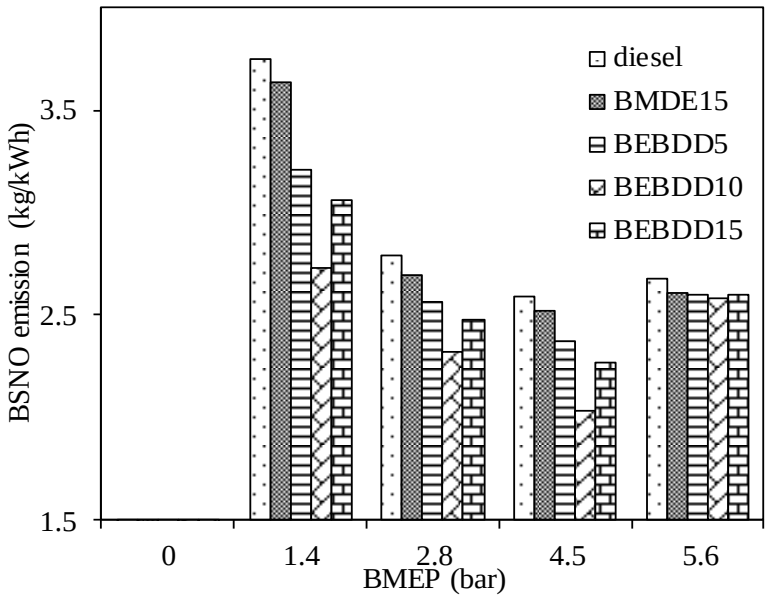

Fig. 6.71 Variation of BSNO emission with BMEP

For a given power output, the NO emission decreases with an increase in the load for all the fuels tested in this study. The NO emission is the highest for diesel, among all the fuels tested in this study in the entire load spectrum. The diesel curve is followed by the BMDE15 emulsion in the entire engine operation. The latent heat of vaporisation of BMDE15 is higher than that of diesel. In spite of more fuel being accumulated in the delay period with the BMDE15, the time taken for fuel evaporation may be higher for the BMDE15 than that of diesel; hence, a lower NO emission is noticed. In the case of the bioethanol-biodiesel-diesel blends, the BSNO emission is found to decrease with an increase in the percentage of biodiesel content in the blend, throughout the engine operation. In this case also, the latent heat of vaporisation and cetane number of the blends play a dominant role in the premixed

combustion phase, than the oxygen available with the blends. As a result, the BSNO emission in the bioethanol-biodiesel-diesel operation is found to be lower, in comparison with the diesel and BMDE15 operations, throughout the load spectrum. The NO emission in the bioethanol-biodiesel-diesel operation is lower in the range of 11 to 2% from no load and 4 to 2% to full load, than that in diesel operation. Similar results are reported by Sukjit et al., when they conducted experiments with the ethanol-rapeseed methyl ester-diesel blends in a single engine [154]. This is also evidenced by the heat release curves, as shown in Fig.6.62.

6.7.3.4 Smoke emission

The variation of smoke emission for diesel, BMDE15 and the bioethanol-biodiesel-diesel blends is depicted in Fig. 6.72.

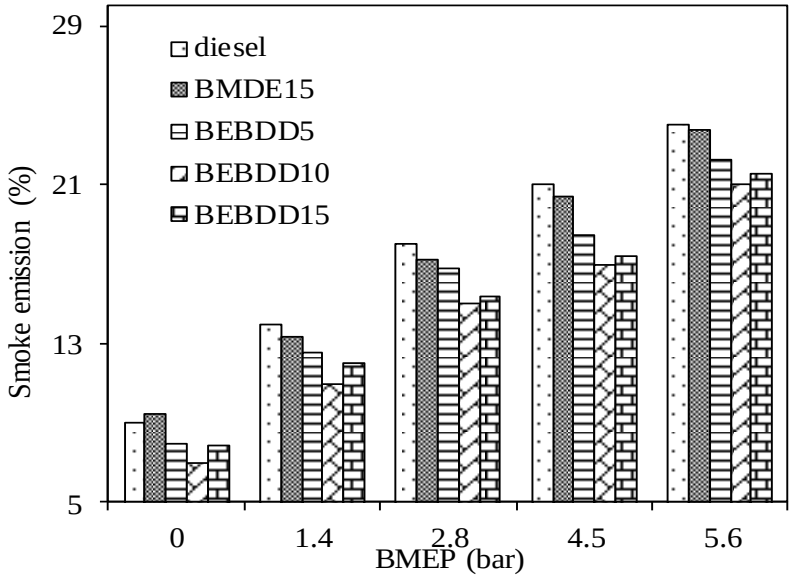

Fig. 6.72 Variation of smoke emission with BMEP

The smoke emission for the bioethanol-biodiesel-diesel blends and BMDE15 is found to be lower than that of diesel, throughout the load spectrum. As both the fuels have no aromatic content and low molecular weights, they result in lesser smoke emissions. The smoke values for diesel, BMDE15, BEBDD5, BEBDD10 and BEBDD15 at full load are 24, 23.8, 22.3, 21.02 and 21.6% opacity respectively. Slow combustion is the reason for the higher smoke in diesel operation. The reduction in the smoke emission for the bioethanol-biodiesel-diesel operation is about 2-4% at full load, than that of diesel operation. It is lower by about 1-3% than that of BMDE15. The highest and lowest smoke values for diesel are about 24% and 9%, respectively, at full load. The highest and lowest smoke values for BEBDD15 are about 20.6% and 6.2%, respectively, at full load.

6.7.4 Summary

The summary of the results obtained in the investigation are as follows,

The ignition delay and maximum cylinder pressure are closer to those of diesel for BEBDD10 blend, at full load. The BSEC and EGT are found to be lower by about 4% and 7 °C respectively, for BEBDD10 compared to that of BMDE15 at full load. The BSNO and smoke emission for is found to be decreased by about 4% and 21.1% respectively, at full load.

6.8 Durability issues of a diesel engine run on BMDE15 and BEBDD10

6.8.1 General

It is essential to conduct an endurance test in an engine, if a new alternative fuel is proposed and investigated. The main aim of the endurance test is to evaluate the wear characteristics of the components and change in the lubrication oil properties of the engine. This chapter presents the analysis of the results obtained for the wear characteristics and lubrication oil properties, from a single cylinder, four stroke, DI, diesel engine with two different fuels viz, (i) BMDE15 emulsion, and (ii) BEBDD10. A visual inspection was made for the analysis of the wear. The lubricating oil samples collected from the engine were analysed by Atomic Absorption Spectroscopy (AAS) for determining the different metal debris present in the lubricating oil due to the engine wear.

6.8.2 Analysis of carbon deposits on different engine components

6.8.2.1 Cylinder head and piston crown

As described in Chapter 5, the engine was run for 100 h to study the wear characteristics of the engine components, such as the cylinder head, piston crown and injector tip. The engine was subjected to run on the BMDE15 emulsion for 100 h, and the engine components were dismantled and studied. The engine components were visually inspected, and the dimensions of the components were measured before and after the endurance test. The engine was run with the BEBDD10 emulsion and the wear study was carried out in the same manner. Figures 6.73 a, b, and c show the photographic views of the cylinder head before and after the endurance test, carried out with the BMDE15 emulsion and BEBDD10 blend respectively. It is apparent from the three figures that more carbon deposits were observed with the BMDE15 emulsion than in the BEBDD10 operation. This may be due to the presence of diesel in the emulsion, whose carbon hydrogen ratio is higher and the presence of water in the emulsion. About 5 and 3.5 mg of carbon deposits were noticed in the cylinder head and combustion chamber. In the case of the BEBDD10 blend, small traces of carbon deposit are found, which is due to low soot formation and more complete combustion. Biodiesel is composed of several fatty acids and as it is an oxygen containing compound, it offers lubricity to the fuel. Hence, little traces are observed when the engine is operated with the BEBDD10 blend.

Description	Fresh engine components Before	BMDE15 After	BEBDD10 After
Cylinder head (a)	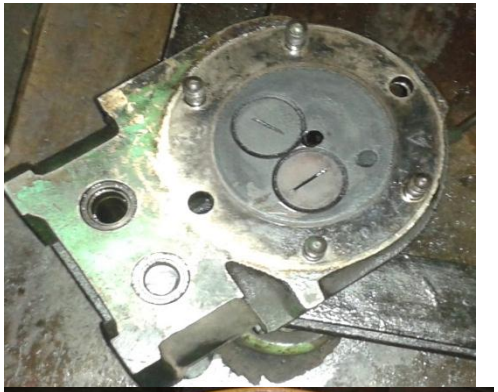	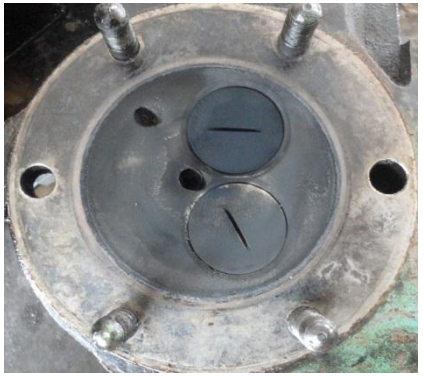	
Piston crown (b)			
Injector tip (c)	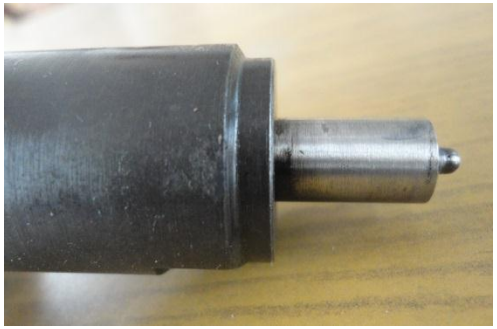		

Fig. 6.73 a, b and c Photographic view of the cylinder head, piston crown, and injector tip

The piston crown is also found with traces of carbon deposits, when the engine was run with the BMDE15 emulsion and the BEBDD10.

6.8.2.2 Fuel injector and its parts

The fuel injector components were dismantled after running the engine with the BMDE15 emulsion and after running with the BEBDD10 blend. Important parts like the needle and nozzle tip were visually inspected and analysed. The photographic views of the fuel injector parts before and after the endurance test are shown in Fig. 6.73 a, b, and c. The carbon deposits were found in the injector nozzle and in between the holes. A spray test was carried out in the nozzle with the nozzle testing equipment under room conditions. It was observed that the fuel spray of the BMDE15 emulsion and the BEBDD10 blend were observed to be distorted. This may be due to the blockage of the holes by small carbon deposits in the injector holes. The carbon content (wt%) was measured with the help of the weight balance, which is presented in Table 6.3.

Table 6.3 Carbon deposits (wt%) on different parts of the engine with both the fuels

	BMDE15	BEBDD10 blend
Carbon deposits on cylinder head (mg)	5	3
Carbon deposits on injector tip (mg)	3.5	2.1
Carbon deposit on piston crowns (mg)	4.3	3.2

6.8.2.3 Components of the fuel injection pump

Figures 6.74 (a), (b), (c) and (d) show the photographic views of the dismantled fuel injection pump components, which are considered for the wear analysis. It is observed that traces of wear were found in the plunger after the endurance test of engine, run with the BMDE15 emulsion. This may be due to the lower lubricity offered by the emulsion. In the case of the engine run with the BEBDD10 blend also, there are small traces of wear found in the fuel injection pump. The lower wear trace in comparison with that of BEBDD10 operation may be due to the improvement in the lubricity, that is offered by the addition of biodiesel. The wear in the fuel injection pump is considered as an important factor, because it may affect the ceiling between the plunger and the barrel, which may cause a pressure loss in the system and subsequently affect the injection.

Plunger (a)

Pump barrel (b)

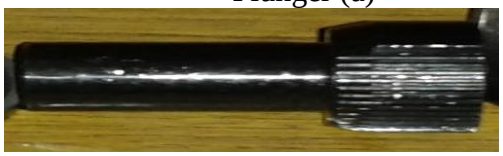

Pinion (c)

Spring (d)

Fig. 6.74 Photographic view of the dismantled fuel injection pump components

6.8.2.4 Wear measurements

The vital parts of injection pump and the injector were measured, before and after the engine fueled with the BMDE15 emulsion and subsequently with the BEBDD10 blend. An electronic balance was used to weigh the parts. The differences between the states, before and after the engine was run with the BMDE15 emulsion and BEBDD10, are tabulated in Table 6.4.

Table 6.4 Wear (wt%) amount on different components of the fuel injection pump

Sl. no	Component	BMDE15			BEBDD10	
		Before (g)	After (g)	Percentage change in weight	After (g)	Percentage change in weight
1	Plunger	252	249	-1.2%	250	-0.8%
2	Pump barrel	304	302	-0.65%	303	-0.33%
3	Pinion	180	176	-2.2%	179	-0.55%
4	Spring	210	206	-2%	209	-0.47%

The plunger is used to develop the pressure and inject the fuel into the nozzle. It reciprocates inside the barrel. Due to the low lubricity of the BMDE15, the top edge of the plunger is eroded more than that of the BEBDD10.

6.8.2.5 Lubrication oil analysis

Lubricating oil is composed of organic compounds with the additives of complex organo-metallic compounds. So, there is a lesser chance of the formation of inorganic carbon during the engine's running condition. It is essential, therefore, to analyse the total carbon present in the lubricating oil, to quantify the addition of soot for both the tested fuels after the durability

test. Figure 6.75 shows the percent change in the carbon content as a function of the lubricating oil usage for the BMDE15 emulsion and BEBDD10 blend. It is observed from Fig. 6.75 that the level of soot is found to be increased in the form of carbon levels for the BMDE15 operation compared to that of the BEBDD10 blend. This may reduce the efficiency of the lubricating oil, which in turn, increases the wear of different parts of the engine. The reduction in the soot of the BEBDD10 blend is due to more complete combustion.

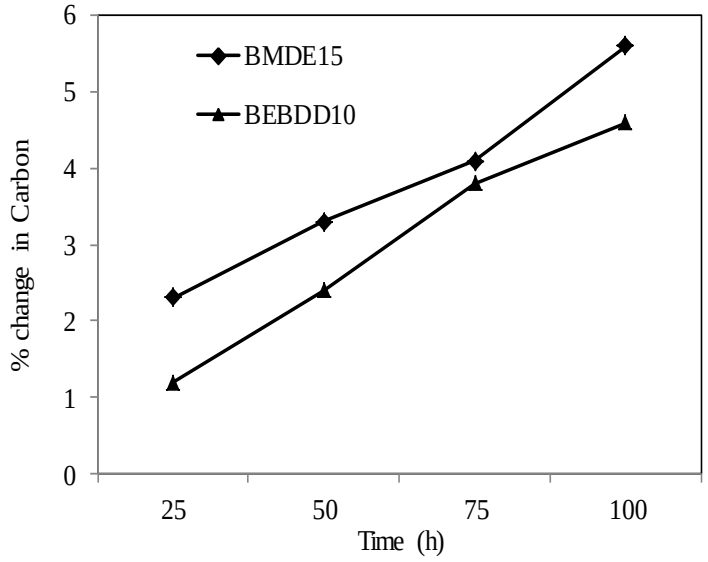

Fig. 6.75 Percent change in carbon content as a function of lubricating oil usage

Due to the wear between the engine components, the various metal debris of the engine components mixes with the lubricating oil and increases the contamination. The quantitative evaluation of the wear particles' presence in the oil gives the magnitude of the deterioration of engine components and the qualitative analysis determines its origin [155]. In this study, various metal elements present in the lubricating oil were determined using the AAS for both the BMDE15 emulsion and the BEBDD10 blend. The variations in the concentration wear metal debris including Fe, Cu, Zn, Mn, Ni, Cr in the used lubricating oil, are plotted and given in Figs. 6.76 a, b, and c.

Iron: This is resulted from the wear of the cylinder piston, liners, gears, rings, cam shaft, oil pump, crank shaft, bearing, etc. As the BMDE15 emulsion offers lower lubricity, the piston rings rub against the liner surface due to insufficient lubrication, or breakdown of the lubricating film during running conditions; hence, more iron was found in the lubricating oil of the BMDE15 operation, compared to that of the BEBDD10 operation.

Zinc: Generally, zinc is added to the lubricating oil as an anti-oxidant, corrosion inhibitor, anti-wear additive, detergent and extreme pressure additive. The concentration of the zinc gets reduced during 25 to 50 h operation of both the tested fuels. This may be due to the thermal stressing of oil, which may lead to the evaporation of zinc. The BMDE15 emulsion experiences more thermal stress due to higher frictional power and hence, more zinc is evaporated in this period. But, after a long term operation, the concentration of zinc is found to increase due to the wear of various moving parts of the engine and it is added to the lubricating oil. Figure 6.76a shows the presence of Zn, Fe and Cu in the lubricating oil with time

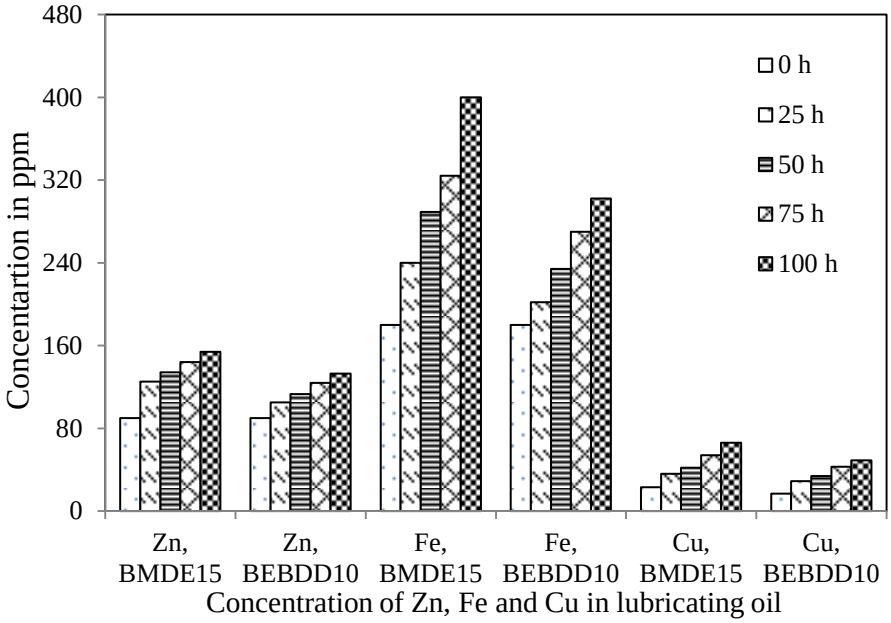

Fig. 6.76a Presence of Zn, Fe and Cu in the lubricating oil with time

Copper: The copper concentration in the lubricating oil increases with an increase in the operation of the engine for both the BMDE15 and BEBDD10 blends. The copper concentration originates from the wear of the bushings, injector shields, valve guides, connecting rods, piston rings, bearings and bearing cages.

Nickel: Nickel is added as an organo-metalllic additive to the lubricating oil, in a very small quantity. The nickel concentration in the oil is both due to engine wear and the oil itself. The wear of the bearings, valves, and gear planting may give rise to nickel in the oil.

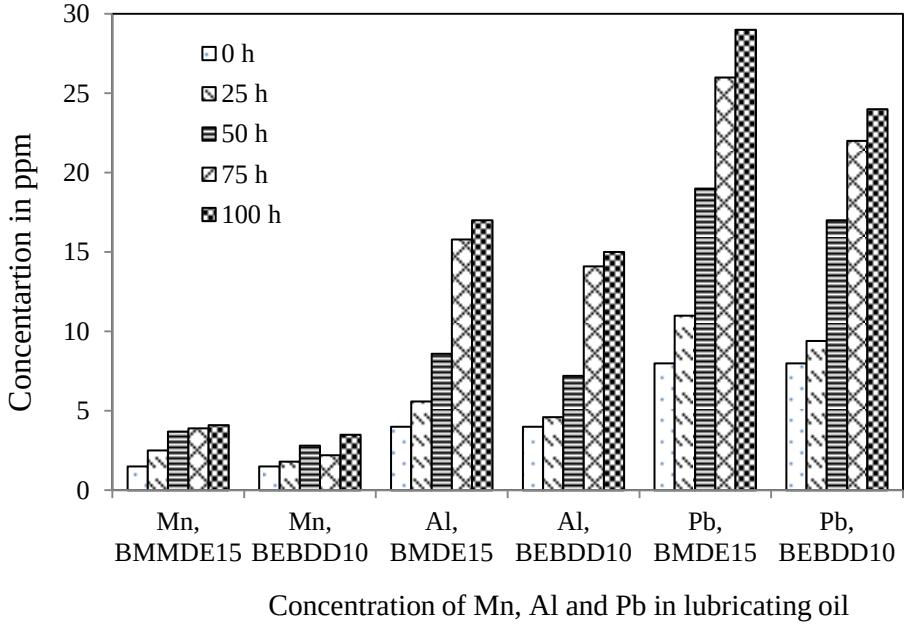

Fig. 6.76b Presence of Mn, Al and Pb in the lubricating oil with time

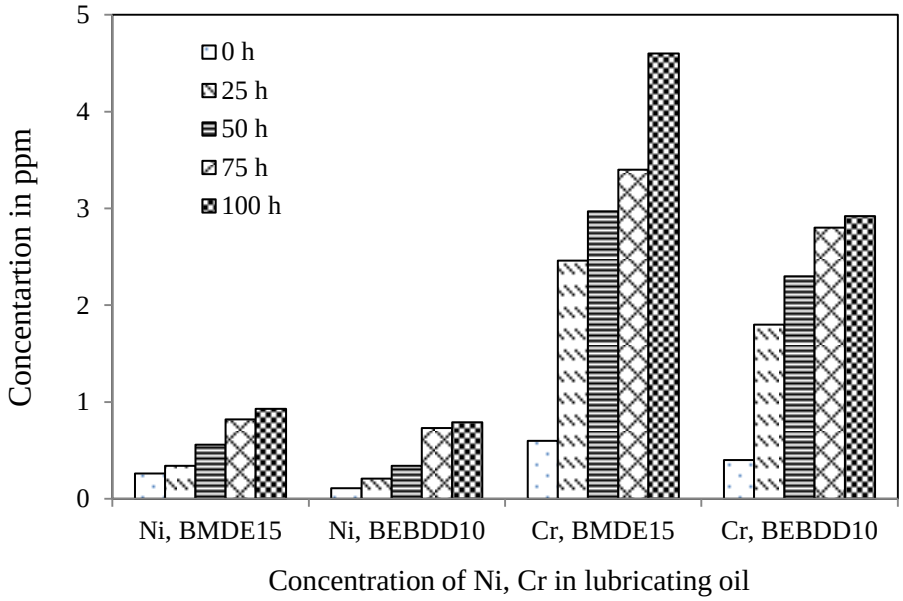

Fig. 6.76c Presence of Ni and Cr in the lubricating oil with time

Manganese: The concentration of manganese originates from the wear of the cylinder liner, valves, shafts etc. For 100 h operation of the engine, the manganese concentration is found to be increased for both the tested fuels.

Chromium: It results from the wear of the cylinder liner, compression rings, gears, crank shaft, bearing etc. The increase in the concentration of chromium is due to the high wear of the engine components during long term operation.

Aluminium: The concentration of aluminium in the oil is high for the BMDE15 emulsion compared to the BEBDD10 blend in a long term operation. This may be due to more wear of the piston, bearings, push rods, oil pump, gears etc.

Lead: It is added to the lubricating oil as an additive. It also results from the wear of the bearings.

6.8.3 Summary

After successful running of the engine with two different fuels, (i.e.), BMDE15 and BEBDD10 blends for 100 h, a visual inspection was carried out for the wear analysis. The results of the visual inspection of carbon deposits on different engine components imply, that there are traces of carbon deposits noticed in the cylinder head, combustion chamber and nozzle tip in the engine fueled with the BMDE15 emulsion; whereas little traces are noticed in the BEBDD10 operation. A marginal wear was also observed in the fuel injection pump. The lubricating properties were found to have deteriorated with both the fuels. The concentration of metals due to the wear of the engine was observed to be high with the BMDE15 emulsion compared to that of the BEBDD10 blend.

CHAPTER 7

CONCLUSION AND SCOPE FOR FURTHER RESEARCH

7.1 Conclusion

From the analysis of the combustion, performance and emission parameters of a single cylinder, four stroke, air cooled , DI diesel engine having a power output of 4.4 kW at a constant speed of 1500 rpm, run on bioethanol with diesel and adopting different techniques, the following conclusions are drawn;

7.1.1 Engine operated on the three different bioethanol-diesel emulsions

- The BMDE15 is found to be better than BMDE5 and BMDE10 based on the performance and emission parameters.
- The ignition delay of the bioethanol-diesel emulsions increased overall by about 1-3 ^{o}CA in comparison with diesel, which is due to a decrease in the cetane number of the emulsions.
- The NO emissions for the bioethanol-diesel emulsions are found to be lower with a maximum reduction of about 24% in comparison with diesel at full load.
- In comparison with diesel, the bioethanol-diesel operation exhibited lower smoke emissions with a maximum reduction of 21% with BMDE15, at full load, as a result of the lower carbon to hydrogen ratio, and more complete combustion.
- However, the HC emission with the bioethanol-diesel emulsions is found to be higher, as a result of the quench layer in comparison with diesel operation, though the CO emissions are found to be lower.

7.1.2 Addition of ignition improver with the bioethanol-diesel emulsion

- The DED1.5% emulsion shows a better performance and lower emissions compared to those of DED1%, DED2% and DED2.5% at full load.
- The BSCO, BSHC, BSNO and smoke emissions for DED1.5% are found to be reduced by about, 18%, 23%, 11.3% and 13.76% respectively, compared to that of diesel at full load.

7.1.3 Diethyl ether fumigation in the bioethanol engine

- Bioethanol can be used as an alternative fuel, by fumigated DEE at the intake manifold of the diesel engine. The bioethanol operation with 180 g/h flow rate of DEE

provides a shorter ignition delay, and higher cylinder pressure compared to 60 g/h, 120 g/h flow rates of DEE and diesel at full load.

- The BSNO and smoke emissions are found to lower by about 22.2% and 16.6% compared to those of diesel at full load.

7.1.4 Bioethanol in the dual fuel mode

- The bioethanol fumigation at the flow rate of 0.48 kg/h provides a better performance and lower emissions than the other flow rates. For Φ=0.88, this flow rate gave an increase in thermal efficiency of about 3% compared to diesel.

- The BSNO and smoke emissions for the 0.48 kg/h flow rate are found to be lower by about 24.2% and 5.5% respectively, than those of diesel operation at full load.

- The BSHC and BSCO emissions for the 0.48 kg/h flow rate are found to be higher by about 1.8% and 4.4% with ethanol fumigation, than those of diesel operation.

7.1.5 Mathematical analysis of the experimental results

- The spray pattern of BMDE15 is found to be better compared to that of diesel. The better atomization and vaporization of fuel is achieved with BMDE15 due to its lower density.

- The experimental results of the combustion, performance and emission parameters of BMDE15 are validated with the simulation data.

7.1.6 Engine operated with different bioethanol-biodiesel-diesel blends

The improvements in lubricity of the engine operated with the different bioethanol-biodiesel-diesel blends are also summarized and given below;

- The friction power with the BEBDD10 blend is found to be lower by about 8.5% compared to that of BMDE15 at full load.

- The BSNO and smoke emission for BEBDD10 are found to decrease by about 12% and 21.02% respectively, compared to those of diesel at full load.

7.1.7 Comparative study of the endurance test

For long term use of the BMDE15 emulsion and BEBDD10 blend, an endurance test is conducted for 100 h in the diesel engine and the results are given as follows:

- The carbon deposits on the cylinder head, piston crown and injector tip are observed to be more, in the case of the BMDE15 emulsion compared to that of the BEBDD10 blend.

- Also, the concentration of the metal debris in the lubricating oil is found to increase with the BMDE15 emulsion than with the BEBDD10 blend.

7.2 Scope for further research

The following points are suggested for future work, for the investigations of the use of bioethanol in diesel engines:

- An improvement in the lubricity properties of neat bioethanol with DEE operation needs to be carried out for long term use.
- A detailed study of the cyclic variability of the engines run on neat bioethanol and DEE can be done.
- Bioethanol can be run in the HCCI mode and low temperature combustion (LTC) mode.

Appendix A1

Technical specifications of the engine

Type	Kirloskar TAF1 Vertical diesel engine
No. of cylinder	1
Type of injection	Direct
Rated power at 1500 rpm, kW	4.41
Bore, mm	87.5
Stroke, mm	110
Compression ratio	17.5
Method of cooling	Air cooled with radial fan
Displacement volume, litres	0.662
Fuel injection timing bTDC, °CA	23
Number of injector nozzle holes	3
Nozzle-hole diameter, mm	0.25
Inlet valve opening bTDC, °CA	4.5
Inlet valve closing aBDC, °CA	35.5
Exhaust valve opening bBDC, °CA	35.5
Exhaust valve closing aTDC, °CA	4.5
Weight, kg	163
Type of fuel injection	Pump-line-nozzle injection system
Connecting rod length, mm	220

Appendix A2

Specifications of the exhaust gas analyser

Exhaust gas analyser model	AVL 444DiGas
Dimension (W × D × H), mm^3	270 × 320 × 85
Weight, kg	4.5 (net weight without accessories)
Interfaces	RS 232 C, pick up, oil temperature probe
Power consumption and voltage supply, W and V DC	25, 11-22
Response time, s	$t_{95} \leq 15$
Operating temperature, °C	5-45
Relative humidity, %	≤95, non-condensing
Connector CAL. Gas, l/h	60-140, max. overpressure 450 hPa
Connector Gas in, l/h	180, max. overpressure 450 hPa
Storage temperature, °C	0-50

Appendix A3

Specifications of the smoke meter

Instrument model and company	AVL 437C smoke meter
Dimension (W × D × H), mm^3	600 × 260× 370
Weight, kg	24
Measuring range, % opacity	0-100
Accuracy and repeatability, % of full scale	±1
Resolution, %	0.1
Application	For free-acceleration test only
Linearity check, % or m^{-1}	48.4-53.1 or 1.54-1.76 of measurement range
Smoke inlet	Through a control valve
Smoke temperature at entrance, °C	250 (maximum)
Measuring chamber length and heating, mm	430±5 and thermostatically controlled
Light source (Halogen lamp), V and W	12 and 5
Sensor	Selenium photocell (diameter 45 mm)
Power supply, V AC or V DC, Hz, A	190-240 or 11.5-36, 50-60, 2.5
Ambient temperature, °C	0-50
Ambient humidity, % at 50 °C	90% (non-condensing)

Appendix A4

Technical specification of the pressure transducer and charge amplifier

Make and model	Kistler and 5395A Piezotron® Quartz pressure sensor
Pressure range, bar	0-100
Type	Piezoelectric
Material	Quartz
Sensitivity, mV/bar	25
Cooling	Air cooled
Supply voltage, V DC	7-32
Supply current, mA	6
Output impedance, Ω	100
Operating temperature range, °C	-50-350

Appendix A5

Heat release rate calculation

The analysis of heat release rate describes the conversion of fuel chemical energy into heat energy with respect to time or rate of fuel burning in a diesel engine combustion process. The heat release rate determination procedure is based on the processing of the cylinder pressure (indicator) diagram. The heat release rate can be analysed with the help of the first law of thermodynamics for an open system which is at quasi static (homogeneous mixture, uniform pressure and temperature) state. The first law for an open system is given as,

$$\frac{dQ_n}{dt} = \frac{dU}{dt} + p\frac{dv}{dt} \quad \text{(A5.1)}$$

Where, $\frac{dQ_n}{dt}$ = Apparent net heat release rate which is the difference between gross heat release rate and heat transfer rate to the walls

$\frac{dU}{dt}$= Change in internal energy of the system

$p\frac{dv}{dt}$ =Rate at which work is done on the piston

The change in internal energy is, $dU=mC_vdT$

Then, the contents of the cylinder can be modelled as an ideal gas and can be written as,

$$\frac{dQ_n}{dt} = mC_v\frac{dT}{dt} + p\frac{dv}{dt} \quad \text{(A5.2)}$$

From the ideal gas law, $pv = mRT$ (A5.3)

Where, p=Cylinder pressure, v= Volume, m=Mass of the mixture, R=Gas constant, T=Temperature

$$p\frac{dv}{dt} + v\frac{dp}{dt} = mR\frac{dT}{dt}$$

$$\frac{dT}{dt} = \frac{1}{mR}\left[p\frac{dv}{dt} + v\frac{dp}{dt}\right] \quad \text{(A5.4)}$$

By substituting the value of equation A5.4 in A5.2, the heat release rate is,

$$\frac{dQ_n}{dt} = \left(1 + \frac{C_v}{R}\right)p\frac{dv}{dt} + \frac{C_v}{R}v\frac{dp}{dt} \quad \text{(A5.5)}$$

$$\frac{dQ_n}{dt} = \frac{\gamma}{\gamma-1}p\frac{dv}{dt} + \frac{1}{\gamma-1}v\frac{dp}{dt} \quad \text{(A5.6)}$$

In terms of crank angle, the apparent heat release rate can be written as,

$$\frac{dQ_n}{dt} = \frac{\gamma}{\gamma-1} p \frac{dv}{d\theta} + \frac{1}{\gamma-1} v \frac{dp}{d\theta} \quad \text{(A5.7)}$$

Where, C_v=Specific heat at constant volume

γ=Ratio of specific heat of mixture, for diesel engine γ=1.3-1.35

θ=Crank angle

Appendix A6

BSEC=(BSFC×Calorific value)/1000

HC emissions in g/kWh,

HC (g/kWh)= [(M_f+M_a)/(29*1000)*HC (in ppm)*13/BP]

CO emissions in g/kWh,

CO (g/kWh)= [((M_f+M_a)/29)*10*CO (in %vol)*28/BP]

NO emissions in g/kWh,

NO (g/kWh)= [(M_f+M_a)/(29*1000)*NO (in ppm)*32.4/BP]

Appendix A7

The range, accuracy and percentage uncertainty of the instruments

Instrument	Range	Accuracy	Percentage uncertainties
Load indicator, W	250–6000	±10	0.2
Temperature indicator, °C	0-900	±1	0.15
Speed sensor, rpm	0-10000	±10	1
Burette, cc	1-30	±0.2	1.5
Exhaust gas analyser			
NO, ppm	0-5000	±50	1
HC, ppm	0-20000	±10	0.5
CO, %Vol	0-10	±0.03	1
Smoke meter, %	0-100	±1	1
Pressure transducer, bar	0-110	±1	0.15
Crank angle encoder, °CA		±1	0.2

Appendix A8

Procedure for uncertainty analysis

The uncertainty or margin of error of a measurement is stated by giving a range of values likely to enclose the true value. It is a measure of the goodness of the result. The estimated standard uncertainty (U or U(Y)) of the mean is calculated by using the following formula []:

$$U \text{ or } U(Y) = \frac{s}{\sqrt{n}} \tag{A7.1}$$

where n is the number of measurements in the set. The standard deviation (s) for a series of n measurements can be expressed mathematically as:

$$s = \left(\frac{\sum_{i=1}^{n} (x_i - \bar{x})^2}{(n-1)} \right)^{\frac{1}{2}} \tag{A7.2}$$

where x_i is the result of the i^{th} measurement and $\bar{x}$ is the arithmetic mean of the n results. Evaluations of some unknown uncertainties from known physical quantities were obtained using the following general equation (Coleman and Steele 1989).

$$\frac{U_Y}{Y} = \left[\sum_{i=1}^{n} \left(\frac{1}{Y} \frac{\partial Y}{\partial x_i} U_{x_i} \right)^2 \right]^{1/2} \tag{A7.3}$$

In the equation cited, Y is the physical parameter that is dependent on the parameters x_i. The symbol U_Y denotes the uncertainty in Y. By using the above equation the uncertainty of the experiment was obtained as ±2.57%.

Annexure I

Uncertainty of the instruments used for the measurement of fuel properties

Properties	Instrument used	Uncertainty of the instrument
Specific gravity	Hydrometer	±0.05%
Lower heating value	Bomb calorimeter	±3%
Flash point	closed-cup flash and pour point analyser	±1%
Pour point	-do-	±1%
Cold filter plugging point	KLA-4 automatic cold filter plugging point system	±1.5%
Kinematic viscosity	Automated viscometers	±0.02%
Carbon residue	Conradson apparatus	±0.05%

Annexure II

An Algorithm for the Function of the Electronically Controlled Injector

Program for Bioethanol Fumigation

```
/*
  Program to control the amount of fuel injected into the air inlet.

 It uses a switch statement to interact with the computer through serial communication and
control the timing of injector relay.

        The switch
 statement allows one to choose from among a set of discrete values
 of a variable.  It's similar to a series of if statements.

  The circuit:
 * Input of a motor driver is attached to digital pin 3 of the microcontroller.

 Fuel motor pump is connected directly to the 12volt power supply.

 */
Int dutycycle =0;

Int dutycycle1 = 10;

Int dutycycle2 = 20;

Int dutycycle3 = 30;

Int dutycycle4 = 40;

Int dutycycle5 = 50;

Int dutycycle6 = 60;

Int dutycycle7 = 70;

Int dutycycle8 = 80;

Int dutycycle9 = 90;

Int dutycycle10 = 100;


void setup() {
  // initialize serial communication:

  Serial.begin(9600);
   // initialize the injector pin:
              pinMode(3, OUTPUT);
```

```
      }
}
void loop() {
  // read the sensor:
  if (Serial.available() > 0) {
    int inByte = Serial.read();
    // do something different depending on the character received.
    // The switch statement expects single number values for each
case;
    // the controller to get the ASCII value for the
character.  For
    // example 'a' = 97, 'b' = 98, and so forth:
    switch (inByte) {
    case 'a':
     dutycycle = dutycycle1;

      Serial.Println(" Duty cycle 10% initiated");
       break;
   case 'b':
      Serial.Println(" Duty cycle 20% initiated");

     dutycycle = dutycycle2;
      break;
    case 'c':
      Serial.Println(" Duty cycle 30% initiated");

     dutycycle = dutycycle3;
      break;
    case 'd':
      Serial.Println(" Duty cycle 40% initiated");

     dutycycle = dutycycle4;
      break;
    case 'e':
      Serial.Println(" Duty cycle 50% initiated");

     dutycycle = dutycycle5;
      break;

     case 'f':
      Serial.Println(" Duty cycle 60% initiated");

     dutycycle = dutycycle6;
      break;

     case 'g':
      Serial.Println(" Duty cycle 70% initiated");

     dutycycle = dutycycle7;
      break;
```

```
      case 'h':
       Serial.Println(" Duty cycle 80% initiated");

      dutycycle = dutycycle8;
       break;

      case 'i':
       Serial.Println(" Duty cycle 90% initiated");

      dutycycle = dutycycle9;
       break;

      case 'j':
       Serial.Println(" Duty cycle 100% initiated");

      dutycycle = dutycycle10;
       break;

case 'k':
       Serial.Println(" Duty cycle 0% initiated");

      dutycycle = 0;
       break;

          default:
    }

      digitalWrite(3,HIGH);

      // Switch on the injector.

      delay(dutycycle);

      // give a suitable delay to keep the injector valve open for a
specified time period.

      digitalWrite(3,LOW);

      //turn off the injector valve.

      delay(100 - dutycycle);

      //adjust the time period of the wave

    Serial.Print(" Current Duty cycle:  ");

      Serial.Println(dutycycle);

      // give the feedback to the computer about the current
dutycycle.

  }
}
```

Annexure III

Program for Spray Characteristics

```
k=1.19*10^9; %bulk modulus
densityL= 809; %density
L=.7;  %Length
N=1500;  %input done
Ns =1500; %input
n=10; %input
Fpump = .00025; %input check
Fnozzle = 0.05*10^-6; %input
Cd = .39;  %input
Dn = 0.25*10^-3; %input
Mftot =1.18*10^-5;%input
psi = 1.0; %modify while executing
z=3;
densityA=1.1;
vL=1.95*10^-2;
sig=0.02;
vA=20.76*10^-6;
t=1;
Ln=.364*(10^-3);
xs=zeros(20,20);
ys=zeros(20,20);

     Cpump = [ .0047, .0047, .0047, .0047, .0047, .0047, .0047, .0047,
.0047, 0.0047,0.0047,0,0,0,0,0,0,0,0,0,0,0,0,0,0,0,0,0,0,0];
    Pinj = zeros(100,1);
    Uinj = zeros(100,1);
    Mfinj = zeros(100,1);
    Mfz=zeros(100,1);
    Reinj = zeros(100,1);
    Weinj=zeros(100,1);
    Dsm1=zeros(100,1);
    Dsm2=zeros(100,1);
    Dsmm=zeros(100,1);
    Rmid=zeros(100,1);
    Umid=zeros(100,1);
    thetaZ=zeros(20,14,7);
    Uz=zeros(20,14,7);
    Cswz=zeros(20,14,7);
    Dsm=zeros(20,14,7);
    Ndrop=zeros(20,14,7);
    Uzs=zeros(20,14,7);
    Maz=zeros(20,14,7);
    phi=zeros(20,14,7);
    thetaZS=zeros(20,14,7);
    x=zeros(20,14,7);
    y=zeros(20,14,7);
    Rz=zeros(20,14,7);
    RZimp=zeros(20,14,7);
    thetaZSimp=zeros(20,14,7);
    thetaZROT=zeros (20,14,7);
    AFst= 14.2;
    c=0;
    p=0;
   cop=zeros(20,20);
        Pinja = 0;
```

```
        As = sqrt( k/densityL);   %velocity of sound
        psiID= (L/As)*N*6;        %injection delay
     %all will be in a giant for loop which runs the crank angle

       for i=2:11
            Pinj(i) = As*densityL*Cpump(i)*(Fpump/Fnozzle);%injection
pressure
            Pinja = Pinja + (Pinj(i)/n);%avg injection pressure

       end
       Pinja= 200*10^5;

        Uinja = Cd*sqrt((2*Pinja)/densityL);    %mean jet velocity from
each nozzle hole
        Mfinja = (pi*Dn*Dn/4)*densityL*Uinja/(6*N); %fuel injection rate
per jet
        psiI = (Mftot/z)/Mfinja; %z is number of nozzle holes

        Tbr = 28.61*densityL*Dn/sqrt(Pinja*densityA);
        Sbr= Uinja*Tbr;

        Rs = Ns/N;  %introducing swirl is equal to 1 id no swirl
        Sbrs = Sbr/(1 + (pi*Rs*N*Sbr/(30*Uinja)));
        Tbrs =  Sbrs*Tbr/Sbr;

        Ac = 3 + 0.28*(Ln/Dn);

        %theta = 4*atan((4*pi*sqrt(densityA/densityL)*sqrt(3))/(Ac*6));
        theta=.25;
        j=1;

      for k=2:11

        imax = psiI/double(psi);


                Uinj(k)= .39*sqrt(2*Pinj(k)/densityL);
                Mfinj(k) = (pi*Dn*Dn/4)*densityL*Uinj(k)/(6*N);


                jmax =imax/2;

                %there is a statemnt for cummulative fuel injected
                %all arrays after this have to be initialized and allocated
                %memory

                Mfz(k)= (Mfinj(k))/((jmax));
                Reinj(k) = Uinj(k)*Dn/vL;
                Weinj(k) = Uinj(k)*Uinj(k)*Dn*densityL/sig; %define sigma
                Dsm1(k) = 0.38*power(Reinj(k),0.25)*power(Weinj(k),-
.32)*power(vL/vA,0.37)*power(densityL/densityA,-.47)*Dn;%choose the maximum
of the 2 values
                Dsm2(k) = 0.38*power(Reinj(k),0.12)*power(Weinj(k),-
.75)*power(vL/vA,0.54)*power(densityL/densityA,.18)*Dn;

                jmid= (jmax/2) + 1;
```

```
                if(Dsm1(k)<Dsm2(k))
                    Dsmm(k)= Dsm2(k);
                else
                    Dsmm(k) = Dsm1(k);
                end

                    beta=.50;

               for i = 2:k
                    Umid(i) =
2*2.95*beta*power(Pinj(k)/densityL,0.25)*sqrt(Dn)/(power(i*1.11*(10^-4),1-
beta));
                  for j= 1:5

                       alpha=4.5*4.5;
                       thetaZ(k,i,j) = -(theta/2) + ((j-1)*theta/5) +
((theta)/(2*5));
                       Uz(k,i,j) = Umid(i)*(2.7^(-
alpha*thetaZ(k,i,j)*thetaZ(k,i,j)));%check
                       Cswz(k,i,j)= 1;

                       w=5; %assign w between 5-10
                       Dsm(k,i,j)= (1-1/w)*Dsmm(k)*(j-1)/(jmid-1);

                       Ndrop(k,i,j) =
Mfz(k)/((pi/6)*power(Dsm(k,i,j),3)*densityL);

                       Uzs(k,i,j)=Uz(k,i,j)/(Cswz(k,i,j));
                       Maz(k,i,j)= Mfz(k)*(Uinj(k) -
Uzs(k,i,j)*cos(thetaZ(k,i,j)))/(Uzs(k,i,j)*cos(thetaZ(k,i,j)));

                       %air equivalence ratio in each zone
                       phi(k,i,j) = (Mfz(k)/Maz(k,i,j))/(1/(AFst));
                       if(j<jmid)
                           thetaZS(k,i,j) =
(thetaZ(k,i,j))*power((Cswz(k,i,j)),2);
                       else if (j>jmid)
                           thetaZS(k,i,j)= thetaZ(k,i,j) +
thetaZS(k,i,int64(jmid));
                           else
                            thetaZS(k,i,int64(jmid))=
0.5*thetaZ(k,i,int64(jmid)) + .5*thetaZS(k,i,int64(jmid-1));


                           end
                       end
                        Rmid(k)=sqrt(power(x(k,i,3),2)+
power(y(k,i,3),2));

                       %all the following statement needs to be corrected

                       if(Rz(k,i-1,j)<=45)
```

```
                                x(k,i,j) = x(k,i-1,j) +
(Uzs(k,i,j))*cos(thetaZS(k,i,j))/(6*N)*10^3;
                                y(k,i,j) = y(k,i-1,j) +
(Uzs(k,i,j)*sin(thetaZS(k,i,j)))/(6*N)*10^3;
                                Rz(k,i,j) = sqrt(power(x(k,i,j),2)+
power(y(k,i,j),2));

                                RZimp = Rz(k,i-1,j);
                                thetaZSimp= thetaZS(k,i,j);

                        else



                                if (j<jmid)
                                thetaZROT(k,i,j) = thetaZROT(k-1,i,j) +
(Uzs(k,i,j)/(RZimp*6*N));
                                else
                                thetaZROT(k,i,j) = thetaZROT(k-1,i,j) -
(Uzs(k,i,j)/(RZimp*6*N));

                                end

                                thetaZS(k,i,j) = thetaZSimp +
thetaZROT(k,i,j);
                                x(k,i,j)=RZimp*cos(thetaZS(k,i,j));
                                y(k,i,j) = RZimp*sin(thetaZS(k,i,j));

                        end
                        xs(i-1,j)= x(11,i,j);
                        ys(i-1,j)=y(11,i,j);
                        cop(i-1,j)=Uzs(11,i,j);

                    end

                end

        end
```

Annexure IV

Program for Combustion and Emission model

```
%Fuel Injection alock

z=3; %numaer of nozzles
Mftot =1.18*2.8e-3/170;%input for total fuel input in the engine for 3
nozzles.
Matot = 14.2*Mftot/3; %mass of air
Mftot1= Mftot/z; %input for fuel injection per nozzle
Minjp =[0.1485136,  2.279569,  3.036051,3.42156,  3.741282, 3.908897,
12.11944,  25.21904,  38.43114,  51.38495,  62.85519,  72.4708, 80.32899,
86.64405, 91.58, 95.39, 98.39,  100 ];
N = 1500; %RPM
%value needs to be edited. Fuel injected in 53 0CA

Dn= 0.25*10^-3;
densityL=809;
Uinja=zeros(20);
Pinj= zeros(20);
Utot=0;
for i=2:18
    Uinja(i) = ((Minjp(i)-Minjp(i-
1))*Mftot1*6*N/100)/((pi*Dn*Dn/4)*densityL);
    Utot=Utot + Uinja(i);
    Pinj(i)=power(Uinja(i)/.39,2)*densityL/2;
end

Uavg = Utot/18;
CA= zeros(400);
t=zeros(400);
p=zeros(400);
v=zeros(400);

  %defining initial temperature pressure and volume
rc=17.5; %compression ratio
R= 3.5;
Vc= 3.7*(10^-5);
CA(1)=-180;
t(1)=350;
p(1)=1.655e5;
v(1)=Vc*(1 + .5*(rc-1)*(R+1 - cos(3.14*CA(1)/180) - sqrt(R*R-
sin(3.14*CA(1)/180)*sin(3.14*CA(1)/180))));
densityA = 1.618;
E = zeros(400);
E(1) = Matot*1000*(.3 * ienergy(t(1), .446, .3098, -.123, .227, -.1552, -
.489) + .78*ienergy(t(1), .289, .1515, -.57235, .99807, -.6522, -.90586 ) +
.21*ienergy(t(1), .362, .736, -.196, .362, -.289, -.120));



%fuel breai up time
Tbr = 28.61*densityL*Dn/sqrt(200*10^5*densityA);

%fuel spray angle
Ac=4.9;
theta = 2*atan((4*pi*sqrt(densityA/densityL)*sqrt(3))/(Ac*6));
gamma=1.35;
W=zeros(400);
```

```
E1=zeros(400);
hr=zeros(400); %heat release
for i=2: 157
    %Compression starts after suction
    CA(i)=CA(i-1)+1;
    v(i)=Vc*(1+.5*(rc-1)*(R+1 - cos(3.14*CA(i)/180) - sqrt(R*R-
sin(3.14*CA(i)/180)*sin(3.14*CA(i )/180))));
    c=power(v(i-1)/v(i),.35);



    t(i)= t(i-1)*c;
    p(i)=p(i-1)*(v(i-1)/v(i))*(t(i)/t(i-1));

   for j=1:10 %newton raphson method needs correction correct values not
shown.
    E(i) = Matot*1000*(.3 * ienergy(t(i), .446, .3098, -.123, .227, -.1552,
-.489) + .78*ienergy(t(i), .289, .1515, -.57235, .99807, -.6522, -.90586 )
+ .21*ienergy(t(i), .362, .736, -.196, .362, -.289, -.120));

    W(i)= 0.5*(p(i)+p(i-1))*(v(i)-v(i-1));
    Q=heatL(t(i));
    f= E(i)-E(i-1) + W(i) -Q;
    Q1=heatL1(t(i));
    E1(i) = Matot*1000*(.3 * ienergy1(t(i), .446, .3098, -.123, .227, -
.1552) + .78*ienergy1(t(i), .289, .1515, -.57235, .99807, -.6522 ) +
.21*ienergy1(t(i), .362, .736, -.196, .362, -.289));
    E1(i-1) = Matot*1000*(.3 * ienergy1(t(i-1), .446, .3098, -.123, .227, -
.1552) + .78*ienergy1(t(i-1), .289, .1515, -.57235, .99807, -.6522 ) +
.21*ienergy1(t(i-1), .362, .736, -.196, .362, -.289));
    f1= E1(i)-E1(i-1) + W(i) - Q1;
    t(i)=t(i) - f/f1;
   end
    hr(i)=Q;
end



%Sauter Mean Diameter
vL=1.95*10^-2;
sig=0.02;
vA=20.76*10^-6;
Reinj = zeros(20);
Weinj=zeros(20);
Dsm1=zeros(20);
Dsm2=zeros(20);
Dsmm=zeros(20);
imax = 52;
jmax= 26;
jmid= 5;
Rmid =  zeros(20,20);
x= zeros(20,20,20);
y= zeros(20,20,20);
Umid = zeros(20,20);
thetaZ = zeros(20,20,20);
Uz = zeros(20,20,20);
Dsm = zeros(20,20,20);
Ndrop= zeros(20,20,20);
phi= zeros(20,20,20);
Maz= zeros(20,20,20);
thetaZS= zeros(20,20,20);
Rz=zeros(22,18,20);
```

```
Rzimp = zeros(20,20,20);
thetaZSimp=zeros(20,20,20);
thetaZROT = zeros(20,20,20);
xs=zeros(20,20);
ys=zeros(20,20);
cop=zeros(20,20);
sh=zeros(20);
rd=zeros(20);
vA=20.76*10^-6;
Mfz=zeros(20,20);
for k=2:18 %23 deg BTDC
for i=2:k

    %fuel development
     Reinj(k) = Uinja(k)*Dn/vL;
     Weinj(k) = Uinja(k)*Uinja(k)*Dn*densityL/sig;
     Dsm1(k) = 0.38*power(Reinj(k),0.25)*power(Weinj(i),-
.32)*power(vL/vA,0.37)*power(densityL/densityA,-.47)*Dn;%choose the maximum
of the 2 values
     Dsm2(k) = 0.38*power(Reinj(k),0.12)*power(Weinj(i),-
.75)*power(vL/vA,0.54)*power(densityL/densityA,.18)*Dn;

                    if(Dsm1(k)<Dsm2(k))
                        Dsmm(k)= Dsm2(k);
                    else
                        Dsmm(k) = Dsm1(k);
                    end


       Rmid(k,i)=sqrt(power(x(k,i,5),2)+ power(y(k,i,5),2));
       beta = .57;
       Umid(k,i) =
2.95*beta*power(Pinj(k)/densityA,0.25)*sqrt(Dn)/(power(i*1.11*(10^-4),1-
beta));%mid zone velocity
        Mfz(k) = (Minjp(i)-Minjp(i-1))*Mftot1/9;
                    for j=2:9

                        alpha=4.5*4.5;
                        thetaZ(k,i,j) = -(theta/2) + ((j-1)*theta/9) +
((theta)/(2*9));

                        Uz(k,i,j) = Umid(k,i)*(2.7^(-
alpha*thetaZ(k,i,j)*thetaZ(k,i,j)));

                        w=7.5; %assign w between 5-10
                        Dsm(k,i,j)= (1-1/w)*Dsmm(k)*(j-1)/(jmid-1);

                        Ndrop(k,i,j) =
Minjp(k)*Mftot1/((pi/6)*power(Dsm(k,i,j),3)*densityL);

                        Maz(k,i,j)= Minjp(k)*Mftot1*(Uinja(k) -
Uz(k,i,j)*cos(thetaZ(k,i,j)))/(Uz(k,i,j)*cos(thetaZ(k,i,j)));



                        %air equivalence ratio in each zone
                        phi(k,i,j) =
(Minjp(k)*Mftot1/Maz(k,i,j))/(1/(14.2));
```

```
                        if(j<jmid)
                            thetaZS(k,i,j) = (thetaZ(k,i,j));
                        else if (j>jmid)
                            thetaZS(k,i,j)= thetaZ(k,i,j) +
thetaZS(k,i,jmid);
                        else
                            thetaZS(k,i,jmid)= 0.5*thetaZ(k,i,jmid) +
.5*thetaZS(k,i,jmid-1);

                            end
                        end


                        if(Rz(k-1,i,j)<40)

                                x(k,i,j) = x(k-1,i,j) +
(Uz(k,i,j))*cos(thetaZS(k,i,j))/(6*N)*10^3;
                                y(k,i,j) = y(k-1,i,j) +
(Uz(k,i,j)*sin(thetaZS(k,i,j)))/(6*N)*10^3;

                                Rz(k,i,j) = sqrt(power(x(k,i,j),2)+
power(y(k,i,j),2));
                                if (Rz(k,i,j)>40)

                                    x(k,i,j)=x(k-1,i,j);
                                    y(k,i,j) = y(k-1,i,j);
                                end

                                RZimp = 46;
                                thetaZSimp= thetaZS(k,i,j);

                        end
                        if(Rz(k-1,i,j)>=40)
                                if (j<jmid)
                                thetaZROT(k,i,j) = thetaZROT(k,i,j) +
(Uz(k,i,j)*1000/(46*6*N));
                                end
                                if(j>=jmid)
                                thetaZROT(k,i,j) = thetaZROT(k,i,j) -
(Uz(k,i,j)*1000/(46*6*N));

                                end

                                thetaZS(k,i,j) = thetaZSimp +
thetaZROT(k,i,j);

                                x(k,i,j)=RZimp*cos(thetaZS(k,i,j));
                                if(j<jmid)
                                y(k,i,j) = -RZimp*sin(thetaZS(k,i,j));
                                end
                                if(j>=jmid)
                                y(k,i,j) = -RZimp*sin(thetaZS(k,i,j));
                                end

                        end
                        xs(i-1,j)= x(18,i,j);
                        ys(i-1,j)=y(18,i,j);
                        cop(19-i,j)=Uz(18,i,j);
```

```
                        %evaporation model
                        Ua(k,i,j) = (2*3.14*N/60)*Rz(k,i,j);
                        urel(k,i,j)=sqrt(Uz(k,i,j)^2 + Ua(k,i,j)^2);
                        Madrop= Maz(k,i,j)/Ndrop(k,i,j);
                        Re=Dsm(k,i,j)*Urel*vA;

                        Dfa = 8.1*(10^-
6)*power(t(157+k)/399),1.5)/(p(157+k)/101325);
                        Sc=vA,/Dfa;%database required
                        Sh=2 + .6*(Re^.5)*(Sc^.333);
                        Y= densityFV/densityA;
                        Ys = Mftot1/(Mftot1 + Matot*(p(157+k)/pv)-1);
                        B=(Ys-Y)/(1-Ys);
                        rd(k,i,j)= rd(k-1,i,j)-
((densityA/densityL)*(Dfa/Dsm)*Sh*log(1+B)*2.303;



                        Mev(i,j)=Mfz(i)*2*rd(18,i,j)/Dsm(18,i,j);
                        phiE(i,j) = (Mev(i,j)/Maz(18,i,j))/(i/14.2);


                        %ignition delay
                        I(k,i,j) = I(k-1,i,j)+ 1/(Kpr*power(p(k+157),-
.757)*exp(618840/(CN+25)*8.314*T(k+257)));
                        %enter CN and Kpr
                    end


end


end

T2u = T2;
T2k= T2;
V2u= v(157);
V2k=v(157);
bn1 = 6.1*10^-3);%CO
bn2 =5.7*(10^-1);%CO2
bn3 = 9.7*(10^-5);%H
bn4 = 1.5*(10^-4); %H2
bn5 = 1.0*(10^-1);%H2O
bn6 = 1*(10^-5);%N
bn7=5*(10^-6);%NO
bn8= 1.5*(10^-2);%NO
bn9 =6.9*(10^-1);%N2
bn10=8.6*(10^-1);%O
bn11 = 2.2*(10^-2);%OH
bn12 = 2.3*(10^-2);%O2
Tbulk1=0;
Tbulk2=0;
T1u=t(157);
T1k=t(157);
for i=157:360
```

```
    v(i)=Vc*(1+.5*(rc-1)*(R+1 - cos(3.14*CA(i)/180) - sqrt(R*R-
sin(3.14*CA(i)/180)*sin(3.14*CA(i )/180))));
    p(i)=p(i-1)*power(v(i-1)/v(i),1.35);


    Tbulk1= ((bn1 + bn2 +bn3 + bn4 +bn5 + bn6+bn7 + bn8 +bn9 + bn10 +bn11 +
bn12)*T1u +   (bn1k + bn2k +bn3k + bn4k +bn5k + bn6k+bn7k + bn8k +bn9k +
bn10k +bn11k + bn12k)*T1k)/((bn1 + bn2 +bn3 + bn4 +bn5 + bn6+bn7 + bn8 +bn9
+ bn10 +bn11 + bn12) + ((bn1k + bn2k +bn3k + bn4k +bn5k + bn6k+bn7k + bn8k
+bn9k + bn10k +bn11k + bn12k));
    Tbulk2=((an1 + an2 +an3 + an4 +an5 + an6+an7 + an8 +an9 + an10 +an11 +
an12)*T2u +   (an1k + an2k +an3k + an4k +an5k + an6k+an7k + an8k +an9k +
an10k +an11k + an12k)*T2k)/((an1 + an2 +an3 + an4 +an5 + an6+an7 + an8 +an9
+ an10 +an11 + an12) + ((an1k + an2k +an3k + an4k +an5k + an6k+an7k + an8k
+an9k + an10k +an11k + an12k));

    qu= heatLI((Tbulk1+Tbulk2)/2))*((bn1 + bn2 +bn3 + bn4 +bn5 + bn6 + bn7
+ bn8 +bn9 + bn10 +bn11 + bn12)*T1u + (an1 + an2 +an3 + an4 +an5 + an6+an7
+ an8 +an9 + an10 +an11 + an12)*T2u/((bn1 + bn2 +bn3 + bn4 +bn5 + bn6+bn7 +
bn8 +bn9 + bn10 +bn11 + bn12)T1u + ((bn1k + bn2k +bn3k + bn4k +bn5k +
bn6k+bn7k + bn8k +bn9k + bn10k +bn11k + bn12k)*T1k + (an1 + an2 +an3 + an4
+an5 + an6+an7 + an8 +an9 + an10 +an11 + an12)T12u + ((an1k + an2k +an3k +
an4k +an5k + an6k+an7k + an8k +an9k + an10k +an11k + an12k)*T2k);
    qk=heatLI((Tbulk1+Tbulk2)/2))*((bn1 + bn2 +bn3 + bn4 +bn5 + bn6 + bn7 +
bn8 +bn9 + bn10 +bn11 + bn12)*T1k + (an1 + an2 +an3 + an4 +an5 + an6+an7 +
an8 +an9 + an10 +an11 + an12)*T2k/((bn1 + bn2 +bn3 + bn4 +bn5 + bn6+bn7 +
bn8 +bn9 + bn10 +bn11 + bn12)T1u + ((bn1k + bn2k +bn3k + bn4k +bn5k +
bn6k+bn7k + bn8k +bn9k + bn10k +bn11k + bn12k)*T1k + (an1 + an2 +an3 + an4
+an5 + an6+an7 + an8 +an9 + an10 +an11 + an12)T12u + ((an1k + an2k +an3k +
an4k +an5k + an6k+an7k + an8k +an9k + an10k +an11k + an12k)*T2k);
    w1u=bn1 + bn2 +bn3 + bn4 +bn5 + bn6+bn7 + bn8 +bn9 + bn10 +bn11 + bn12;
    for k=1:18
        for j=1:9
            if (I(i-156,k,j)<1)%zone not burning

                E(i) = Matot*1000*(.3 * ienergy(T1u), .446, .3098, -.123,
.227, -.1552, -.489) + .78*ienergy(T1u), .289, .1515, -.57235, .99807, -
.6522, -.90586 ) + .21*ienergy(T1u), .362, .736, -.196, .362, -.289, -
.120));

                W(i-1)= 0.5*(p(i-1)+p(i-2))*(v(i-1)-v(i-2));
                Q=heatL(T1u);
                f= E(i)-E(i-1) + W(i) -Q;
                V1u = Mftot*w1u*8.314*T1u/p(i-1);
                w2u= (Matot - (Maz(i-156,k,j)/Ma)/Mftot; %Ma molecular
weight of air
                wloss=w1u-w2u;
                an1=bn1;
                an2=bn2;
                an3=bn3;
                an4=bn4;
                an7=bn7;
                an8=bn8;
                an9=bn9;
                an10=bn10;
                an11=bn11;
                an12=bn12;
                an5=bn5-.21*wloss;
                an6=bn6 - .79*wloss;
```

```
                c=power(v(i-1)/v(i),.35);


                 T2u= T1u*c;
                 V2u= Mftot*W2u*8.314*T2u/p(i);
                 W(i)= 0.5*(p(i)+p(i-1))*(v(i)-v(i-1));
                 %newton Raphson to be applied



            else %zone burning

                wg= ((Maz(i-155)-Maz(i-156)/Ma)/Mftot;
                bn1km = bn1k;
                bn2km = bn2k;
                bn3km = bn3k;
                bn4km = bn4k;
                bn8km = bn8k;
                bn9km = bn9k;
                bn10km = bn10k;
                bn11km = bn11k;
                bn12km = bn12k;

                bn5km = bn5k + 0.21*wg;
                bn6km = bn6k + .79*wg;
                bn7km = bn7k + ((Mev(i-156,k,j)/Mf)/Mftot;

                w1km= bn1km + bn2km +bn3km +bn4km +bn5km +bn6km +bn7km
+bn8km +bn9km +bn10km +bn11km +bn12km ;
                po = p(i-1)*(b5km)/w1km;
                %enthalpy of 12 elements
                %enthalpy of air entered of wg
                T1km = (w1km*T1k + wg*T1u)/(w1km + wg);
                v1km = (w1km*v1k + wg*v1u)/(w1km + wg);

                if (Mev(i-156,k,j) - Mfb(i-156,k,j) < Maz(i-156,k,j) -
14.2*Mfb(i-156,k,j))
                dmfb = Kbu*(p(i-1)^.757)*((Mev(i-156,k,j) - Mfb(i-
156,k,j))*power(2.7,-5000/t(i-1));
                else
                     dmfb = Kbu*(p(i-1)^.757)*((Maz(i-156,k,j) - 14.2*Mfb(i-
156,k,j))*power(2.7,-5000/t(i-1));
                end
                Mfb(i-156,k,j) = Mfb(i-156,k,j)-dmfb;

                T2k = T1km*power(p(i)/p(i-1), (gamma-1/gamma))-
dfmb*Qc/(Mftot*w1km*Cv); ;
                V2k = Mftot*w1km*8.314*T2k/p(i);
                W1 = 0.5*(p(i-1) - p(i))*(V2k - V1k);

                %NO sub model
                k1f = 3.1*(10^10)*exp(-160/T2k);
                k2f =6.4*(10^6)*exp(-3125/T2k);
                k3f=4.2*(10^10);
                R1= k1f*bn6k*bn7k;
                R2= k2f*bn6k*bn12k;
                R3= k3f*bn6k*bn11k;
                alpha = bn7k/bn7;
                bn7k = 2*(i-alpha^2)*(R1/(1+ alpha/(R2+R3)));
```

```
                %soot submodel
                msf = power(Mev-Mfb, 0.8)*(p^0.5)*power(2.71,-
Esf/8.314*t(i));
                msc= msn(i-1)*(Po(i)/p(i))*power(p,1.8)*power(2.71,-
Esc/8.314*t(i));
                msn(i)= msf - msc;


            end

        end
    end
end
```

REFERENCES

[1] Energy supply and demand, Chevron. http://www.chevron.com/globalissues /energy supply/demand/ [accessed on 15.04.2014]

[2] List of countries by energy consumption per capita. http://en.wikipedia.org/wiki/List of countries by energy consumption per capita. [accessed on 6.04.2014]

[3] Energy statistics 2013 (twentieth issue), Central statistics office, Ministry of statistics and programme implementation Govt. of India, New Delhi, pp-41.

[4] Global energy observatory, last update is 2014. http://globalenergyobservatory.org/list. php?db=PowerPlants&type=Oil. [accessed on 15.04.2014]

[5] List of power stations in India. http:/en.wikipedia.org/wiki/List_of_power_stations_in_ India. [accessed on 6.04.2014]

[6] Daniel and Deborah Gordon. 2009. Two billion cars: driving toward sustainability. Oxford University Press, New York. pp. 4 and 13.ISBN 978-0-19-537664-7. See Chapter 1, Note 1, pp. 261.

[7] Natural gas vehicle statistics: summary data 2010. http://www.iangv.org/current-ngv-stats/. [accessed on 15.04.2014]

[8] International organization of motor vehicle manufacturers (OICA). 2012 Production statistics. http://www.oica.net/2012-production-statistics/OICA. [accessed on 16.04.2014]

[9] Thipse SS. Allternative fuel for IC engines. Jaico Publishing House, 1st edition, 2010.

[10] World fuel ethanol production, renewable fuels association. http://ethanolrfa.org /pages/World-Fuel-Ethanol-Production [accessed on 5.9.2014]

[11] Leite RCC, Leal MRLV, Cortez LAB, Barbosa LA, Griffin WM and Scandiffio MIG. Can Brazil replace 5% of the 2025 gasoline world demand with ethanol? Energy 2009; 34: 655–61.

[12] Macedo IC, Seabra JEA and Silva JEAR. Greenhouse gases emissions in the production and use of ethanol from sugarcane in Brazil: the 2005/2006 averages and a prediction for 2020. Biomass and Bioenergy 2008; 32: 582-95.

[13] Icoz E, Tugrul MK, Saral A and Icoz E. Research on ethanol production and use from sugar beet in Turkey. Biomass and Bioenergy 2009; 33: 1-7.

[14] Ogbonna JC, Mashima H and Tanaka H. Scale up of fuel ethanol production from sugar beet juice using loofa sponge immobilized bioreactor. Bioresource Technology 2001; 76: 1-8.

[15] Yu J, Xuzhang and Tan T. Ethanol production by solid state fermentation of Sweet Sorghum using thermo-tolerant yeast strain. Fuel Processing Technology 2008; 89: 1056-9.

[16] Prasad S, Singh A, Jain N and Joshi HC. Ethanol production from Sweet Sorghum syrup for utilization as automotive fuel in India. Energy and Fuel 2007; 21: 2415-20.

[17] Mamma D, Christakopoulos P, Koullas D, Kekos D, Macris BJ and Kouki E. An alternative approach to the bioconversion ff sweet sorghum carbohydrates to ethanol. Biomass and Bioenergy 1995; 8: 99-103.

[18] Dragone G, Mussatto SI, Oliveira JM and Teixeira JA. Characterisation of volatile compounds in an alcoholic beverage produced by whey fermentation. Food Chemistry 2009; 112: 929-35.

[19] Silveira WB, Passos FJV, Mantovani HC and Passos FML. Ethanol production from cheese whey permeate by Kluyveromyces marxianus UFV-3: a flux analysis of oxido-reductive metabolism as a function of lactose concentration and oxygen levels. Enzyme and Microbial Technololgy 2005; 36: 930–6.

[20] Gnansounou E, Dauriat A and Wyman CE. Refining sweet sorghum to ethanol and sugar: economic trade-offs in the context of North China. Bioresources Technology 2005; 96: 985-1002.

[21] Domingues L, Lima N and Teixeira JA. Alcohol production from cheese whey permeate using genetically modified flocculent yeast cells. Biotechnology and Bioengineering 2001; 72: 507-14.

[22] Roukas T. Ethanol production from non-sterilized beet molasses by free and immobilized *Saccharomyces cerevisiae* cells using fed-batch culture. Journal of Food Enginering 1996; 27: 87-96.

[23] Persson T, Garcia A, Paz J, Jones J and Hoogenbooma G. Maize ethanol feedstock production and net energy value as affected by climate variability and crop management practices. Agricultural Systems 2009; 100: 11-21.

[24] Gaspar M, Kálmán G and Réczey K. Corn fiber as a raw material for hemicellulose and ethanol production. Process Biochemistry 2007; 42: 1135-9.

[25] Nigam JN. Ethanol production from wheat straw hemicellulose hydrolysate by Pichia stipitis. Journal of Biotechnology 2001; 87: 17-27.

[26] Kosugi A, Kondo A, Ueda M, Murata Y, Vaithanomsat P and Thanapase W. Production of ethanol from cassava pulp via fermentation with a surface-engineered yeast strain displaying glucoamylase. Renewable Energy 2009; 34: 1354-8.

[27] Rattanachomsri U, Tanapongpipat S, Eurwilaichitr L and Champreda V. Simultaneous non-thermal saccharification of cassava pulp by multi-enzyme activity and ethanol fermentation by Candida tropicalis. J Biosci Bioeng 2009; 107: 488-93.

[28] Amutha R and Gunasekaran P. Production of ethanol from liquefied cassava starch using co-immobilized cells of Zymomonas mobilis and *Saccharomyces* diastaticus. Journal of Bioscience Bioengineering 2001; 92: 560-4.

[29] Ballesteros M, Oliva JM, Negro MJ, Manzanares P and Ballesteros I. Ethanol from lignocellulosic materials by a simultaneous saccharification and fermentation process (SFS) with Kluyveromyces marxianus CECT 10875. Process Biochemistry 2004; 39: 1843-8.

[30] Silva JPA, Mussatto SI and Roberto IC. The influence of initial xylose concentration, agitation, and aeration on ethanol production by Pichia stipitis from rice straw hemicellulosic hydrolysate. Applied Biochemistry and Biotechnology 2010; doi:10.1007/s12010-009-8867-6.

[31] Huang CF, Lin TH, Guo GL and Hwang WS. Enhanced ethanol production by fermentation of rice straw hydrolysate without detoxification using a newly adapted strain of Pichia stipitis. Bioresource Technology 2009; 100: 3914-20.

[32] Lin Y and Tanaka S. Ethanol fermentation from biomass resources: current state and prospects. Applied Microbial Biotechnology 2006; 69: 627-42.

[33] Hahn-Hägerdal B, Galbe M, Gorwa-Grauslund MF, Lidén G and Zacchi G. Bio-ethanol-the fuel of tomorrow from the residues of today. Trends in Biotechnology 2006; 24: 549-56.

[34] Mussatto SI, Dragone G, Guimarães PMR, Silva JPA, Carneiro LM, Roberto IC, Vicente A, Domingues L and Teixeira JA. Technological trends, global market, and challenges of bio-ethanol production- Research review paper. Biotechnology Advances 2010; 28: 817-30.

[35] Badger PC. Reprinted from: Trends in new crops and new uses. ASHS Press, Alexandria, VA, 2002.

[36] Demirbas A. Bioethanol from cellulosic materials: a renewable motor fuel from biomass. Energy Sources 2005; 27: 327-37.

[37] Bastos VD. Etanol, alcoolquímica e biorrefinarias. BNDES Setorial 2007; 25: 5-38.

[38] Cardona CA and Sánchez J. Fuel ethanol production: process design trends and integration opportunities-Review. Bioresource Technology 2007; 98: 2415-57.

[39] Ling KC. Whey to ethanol. Is there a biofuel role for dairy cooperatives? Rural Cooperatives; 2008. http://www.rurdev.usda.gov/rbs/pub/ mar08/whey.htm. [accessed on 15.07.2014]

[40] Guimarães PMR, François J, Parrou JL, Teixeira JA and Domingues L. Adaptive evolution of a lactose-consuming *Saccharomyces cerevisiae* recombinant. Applied Environmental Microbiology 2008; 74: 1748-56.

[41] David Pimentel and Patzek Tad W. Ethanol production using corn, switchgrass, and wood; biodiesel production using soybean and sunflower natural resources research, Vol. 14, No. 1, March 2005; (C -2005) DOI: 10.1007/s11053-005-4679-8.

[42] Demirbas MF, Balat M and Balat H. Potential contribution of biomass to the sustainable energy development. Energy Conversion Management 2009; 50: 1746-60.

[43] Bothast RJ. New technologies in biofuel production. Agricultural outlook forum, 2005; http://ageconsearch.umn.edu/bitstream/32873/1/fo05bo02.pdf.[accessed on 15.07.2014]

[44] Mielenz JR. Ethanol production from biomass: technology and commercialization status. Current Opinion in Microbiology 2001; 4: 324-29.

[45] Chipman DC. Hybrid thermochemical/biological processing of biomass for the production of polyhydroxy alkanoates and hydrogen gas from Rhodospirillum rubrum cultured on synthesis gas 2009; Graduate Theses and Dissertations. Paper 10945.

[46] Sun Y and Cheng J. Hydrolysis of lignocellulosic materials for ethanol production: a review. Bioresource Technology 2002; 83: 1-11.

[47] Galbe M and Zacchi G. Simulation of ethanol production processes based on enzymatic hydrolysis of woody biomass. Computers and Chemical Engineering 1994; 18: 687-91.

[48] Palmqvist E, Hahn-Ha¨gerdal B, Szengyel Z, Zacchi G and Re`czey K. Simultaneous detoxification and enzyme production of hemicellulose hydrolysates obtained after steam pretreatment. Enzyme and Microbial Technology 1997; 20: 286-93.

[49] Mes-Hartree M, Hogan CM and Saddler JN. Recycle of enzymes and substrate following enzymatic hydrolysis of steam-pretreated aspen wood. Biotechnology and Bioengineering 1987; 30: 558-64.

[50] Nguyen QA, Keller FA, Tucker MP, Lombard CK, Jenkins BM, Yomogida DE and Tiangco VM. Bioconversion of mixed solids waste to ethanol. Applied Biochemistry and Biotechnology 1999; 77-9: 455-72.

[51] Sánchez OJ and Cardona CA. Trends in biotechnological production of fuel ethanol from different feedstocks. Bioresource Technology 2008; 99: 5270-95.

[52] Swain MR, Kar S, Sahoo SK and Ray RC. Ethanol fermentation of mahula (Madhuca latifolia L.) flowers using free and immobilized yeast *Saccharomyces cerevisiae*. Microbiological Research 2007; 162: 93-8.

[53] Mohanty SK, Behera S, Swain MR and Ray RC. Bioethanol production from mahula (Madhuca latifolia L.) flowers by solid-state fermentation. Applied Energy 2009; 86: 640-4.

[54] Benerji DSN, Rajini K, Rao BS, Benerjee DRN, Rani KS, Rajkumar G and Ayyanna C. Studies on physico-chemical and nutritional parameters for the production of ethanol from mahua flower (madhuca indica) using *saccharomyces cerevisiae* – 3090 through

submerged fermentation (smf). Journal of microbial & Biochemical technology, Volume 2010; 2(2): 046-07-050.

[55] Behera S, Kar S, Mohanty RC and Ray RC. Comparative study of bio-ethanol production from mahula (Madhuca latifolia L.) flowers by *Saccharomyces cerevisiae* cells immobilized in agar agar and Ca-alginate matrices. Applied Energy 2010; 87: 96-100.

[56] Behera S, Ray RC and Mohanty RC. Comparative study of bioethanol production from mahula (Madhuca latifolia L.) flowers by immobilized cells of *Saccharomyces cerevisiae* and Zymomonas mobilis in calcium alginate beads. Journal of Scientific & Industrial Research, June 2010; vol.69: 472-5.

[57] Behera S, Mohanty RC and Ray RC. Comparative study of bioethanol production from mahula (Madhuca latifolia L.) flowers by *Saccharomyces cerevisiae* and Zymomonas mobilis. Applied Energy 2010; 87: 2352-5.

[58] Behera S, Mohanty RC and Ray RC. Ethanol production from mahula (Madhuca latifolia L.) flowers with immobilized cells of *Saccharomyces cerevisiae* in Luffa cylindrica L. sponge discs. Applied Energy 2011; 88: 212-5.

[59] Ecklund EE, Bechtold RL, Timbario TJ and McCallum PW. State-of-theart report on the use of alcohols in diesel engines. SAE Technical Paper 840118, 1984; 1684 - 1702.

[60] Strait J, Boedicker JJ, and Johanson KC. Diesel oil and ethanol mixtures for diesel powered farm tractors. Final report to the State of Minneasota Energy Agency from the Agricultural Engineering Department, University of Minnesota, St. Paul, 1978.

[61] Wrage KE and Goering CE. Technical feasibility of diesohol. ASAE (American Society of Agricultural Engineers) Paper No. 79·1052, MI 49085, 1979.

[62] Moses CA, Ryan TW and Likos WE. Experiments with alcohol/diesel fuel blends in compression–ignition engines. In: VI International Symposium on Alcohol Fuels Technology, Guaruja, Brazil, 1980.

[63] Baker QA. Use of alcohol-in-diesel fuel emulsions and solutions in a medium-speed diesel engine. SAE Technical Paper 810254, 1981.

[64] Hardenberg HO and Schaefer AJ. The use of ethanol as a fuel for compression–ignition engines. SAE Technical Paper 811211, 1981.

[65] Hardenberg HO and Ehnert ER. Ignition quality determination problems with alternative fuels for compression ignition engines. SAE Technical Paper 811212, 1981.

[66] Schaefer AJ and Hardenberg HO. Ignition improvers for ethanol fuels. SAE Technical Paper 810249, 1981.

[67] Boruff PA, Schwab AW, Goering CE, and Pryde EH. Evaluation of diesel fuel-ethanol Microemulsions. Transaction of ASAE (American Society of Agricultural Engineers) 1982; 25(1): 47-53.

[68] Letcher TM. Diesel blends for diesel engines. South African Journal of Science 1983; 79(1): 4-7.

[69] Battelle. Flammability limits for ethanol/diesel blends. Final report prepared by Battelle, Columbus, OH, USA, 1998.

[70] Gerdes KR and Suppes GJ. Miscibility of ethanol in diesel fuels. Industrial Engineering Chemistry Resource 2001; 40 (3): 949-56.

[71] Satge de Caro P, Mouloungui Z, Vaitilingom G and Berge JC. Interest of combining an additive with diesel and ethanol blends for use in diesel engines. Fuel 2001; 80: 565-74.

[72] Hansen AC, Zhang Q and Lyne W. Peter Ethanol-diesel fuel blends-A review. Bioresource Technology 2005; 96: 277-85.

[73] Lapuerta M, Armas O and Garcia-Contreras R. Stability of diesel-bioethanol blends for use in diesel engines. Fuel 2007; 86: 1351-57.

[74] Rakopoulos DC, Rakopoulos CD, Kakaras EC and Giakoumis EG. Effects of ethanol-diesel fuel blends on the performance and exhaust emissions of heavy duty DI diesel engine. Energy Conversion Management 2008; 49: 3155-62.

[75] Li D, Zhen H, Xingcai L, Wu-Gao Z, Jian-Guang Y. Physicochemical properties of ethanol–diesel blend fuel and its effect on performance and emissions of diesel engines. Renewable Energy 2005; 30 (6):967-76.

[76] Kumar C, Athawe M, Aghav YV, Babu MKG, Das LM. Effects of ethanol addition on performance, emission and combustion of DI diesel engine running at different injection pressures. SAE paper no. 2007-01-0626; 2007.

[77] Arapatsakos C. Application of diesel–ethanol mixtures in tractor engine. International Journal of Energy and Environment 2009; 3(2): 77-84.

[78] Huang J, Wang Y, Li S, Roskilly AP, Hongdong Y, Li H. Experimental investigation on the performance and emissions of a diesel engine fuelled with ethanol–diesel blends. Applied Thermal Engineering 2009; 29(11– 12): 2484-90.

[79] Ganesh RS, Kumar SS, Dinesh S. Effect of ethanol addition on performance, emission and combustion characteristics of a diesel engine at various injection angles. Frontiers in Automobile and Mechanical Engineering 2010; 27: 108-12.

[80] Song C, Zhao Z, Lv G, Song J, Liu L, Zhao R. Carbonyl compound emissions from a heavy-duty diesel engine fueled with diesel fuel and ethanol–diesel blend. Chemosphere 2010; 79: 1033-39.

[81] Banugopan VN, Prabhakar S, Annamalai K, Jayaraj S, Sentilkumar P. Experimental investigation on DI diesel engine fuelled by ethanol diesel blend with varying inlet air temperature. Frontiers in Mechanical Engineering 2010; 25(27): 128–34.

[82] Jilin Lei, Yuhua Y, Shen L. Performance and emission characteristics of diesel engine fueled with ethanol-diesel blends in different altitude regions. Journal of Biomedicine and Biotechnology 2011. http://dx.doi.org/10.1155/ 2011/417421.

[83] Lyford-Pike EJ, Neves FC, Zulino AC and Duggal VK. Development of a commercial cummins nt series engine to burn ethanol alcohol. VII International Symposium on Alcohol Fuels. Paris. 1986; 331-6.

[84] Hodgson N. Performance evaluation of methanol and ethanol in Otto and diesel cycled engines derived from the same base-line engine. IX International Symposium on Alcohol Fuels. Firenze. 1991; Vol. II, 491-6.

[85] Cai LX, Guang YJ, Gao ZW and Zhen H. Effect of cetane number improver on heat release rate and emissions of high speed diesel engine fueled with ethanol-diesel blend fuel. Fuel 2004; 83: 2013-20.

[86] Ren Y, Huang ZH, Jiang DM, Li W, Liu B and Wang XB. Effects of the addition of ethanol and Cetane number improver on the combustion and emission characteristics of a compression ignition engine. Proceedings of the Institution of Mechanical Engineers, Part D: Journal of Automobile Engineering 2008; 222: 1077.

[87] Pidol L, Lecointe B, Starck L and Jeuland N. Ethanol-biodiesel-diesel fuel blends: performances and emissions in conventional diesel and advanced low temperature combustions. Fuel 2012; 93: 329-38.

[88] Can O, Celikten I, Usta N. Effects of ethanol blended diesel fuel on exhaust emissions from a diesel engine. Pamukkale University Journal of Engineering Sciences 2005;11(2):219–24.

[89] Ashok MP. Identification of best additive using the selected ratio of ethanol-diesel based emulsified fuel. International Journal of Sustainable Energy 2012; 31(3): 203-12.

[90] Ashok MP. Effect of best emulsified fuel: with and without water addition for the reduction of automobile CO and NOX emissions in human life. International Journal of Sustainable Energy 2012; 31(5): 327-35.

[91] Padala S, Woo C, Kook S and Hawkes HR. Ethanol utilisation in a diesel engine using dual-fuelling technology. Fuel 2013; 109: 597-607.

[92] Britto Jr. RF and Martins CA. Experimental analysis of a diesel engine operating in diesel-ethanol dual-fuel mode. Fuel 2014; 134: 140-150.

[93] Britto Jr. RF and Martins CA. Emission analysis of a diesel engine operating in diesel-ethanol dual-fuel mode. Fuel 2015; 148:191-201.

[94] Ajav EA, Singh B and Bhattacharya TK. Performance of a stationary diesel engine using vaporized ethanol as supplementary fuel. Biomass Bioenergy 1998; 15(6): 493-02.

[95] Surawski NC, Miljevic B, Roberts BA, Modini RL, Situ R, Brown RJ, Bottle SE and Ristovski ZD. Particle emissions, volatility, and toxicity from an ethanol fumigated compression ignition engine. Environmental Science & Technology 2010; 44: 229-35.

[96] Heisey JB and Lestz SS. Aqueous alcohol fumigation of a single cylinder DI diesel engine. SAE Technical paper 1981; 81128: DOI: 10.4271/811208.

[97] Surawski NC, Ristovski ZD, Brown RJ and Situ R. Gaseous and particle emissions from an ethanol fumigated compression ignition engine. Energy Conversion and Management 2012; 54: 145-151.

[98] Chauhan BS, Kumar N, Pal SS and Jun YD. Experimental studies on fumigation of ethanol in a small capacity diesel engine. Energy 2011; 36: 1030-38.

[99] Bodisco T and Brown RJ. Inter-cycle variability of in-cylinder pressure parameters in an ethanol fumigated common rail diesel engine. Energy 2013; 52: 55-65.

[100] Lopez AF, Cadrazco M, Agudelo AF, Corredor LA, Velez JA, Agudelo JR. Impact of n butanol and hydrous ethanol fumigation on the performance and pollutant emissions of an automotive diesel engine. Fuel 2015; 153: 483-91.

[101] Sahin Z, Durgun O and Kurt M. Experimental investigation of improving diesel combustion and engine performance by ethanol fumigation-heat release and flammability analysis. Energy Conversion and Management 2015; 89: 175-87.

[102] Hilger U, Jain G and Pischinger F. Development of a DI methanol engine for passenger car application. IX International Symposium on Alcohol Fuels, Firenze, 1991; Vol. II. 479-84.

[103] Nagalingam B, Sridhar BL, Panchapakesan NR, Gopalakrishnan KV and Murthy BS. Surface ignition initiated combustion of alcohol in diesel engines-a new approach. SAE Technical Paper 800262, 1980; doi:10.4271/800262.

[104] Kapus P and Zelenka P. Development and dynamic optimisation of glow plug assisted di/tc methanol engine for passenger cars and light duty vehicles. IX International Symposium on Alcohol Fuels, Firenze. 1991; Vol. II: 391-97.

[105] Johns RA, Henham AWE and Newnham S. Spark-assisted ethanol fuelled diesel engine. 2nd International Conference on Small Engines and their Fuels for Developing Countries, Reading, 1987.

[106] Newnham SKC. The combustion of ethanol in a sparkassisted diesel engine. PhD Thesis. Department of Mechanical Engineering, University of Surrey, 1990.

[107] Shi X, Yu Y, He H, Shuai S, Wang J and Li R. Emission characteristics using methyl soyate-ethanol-diesel fuel blends on a diesel engine. Fuel 2005; 84: 1543-1549.

[108] Kwanchareon P, Luengnaruemitchai A and Jai-In S. Solubility of a diesel-biodiesel-ethanol blend, its fuel properties, and its emission characteristics from diesel engine. Fuel 2007; 86: 1053-61.

[109] Chen H, Shuai SJ and Wang JX. Study on combustion characteristics and PM emission of diesel engines using ester–ethanol–diesel blended fuels. Proceedings of the Combustion Institute 2007; 31: 2981-89.

[110] Chotwichien A, Luengnaruemitchai A and Jai-In S. Utilization of palm oil alkyl esters as an additive in ethanol–diesel and butanol–diesel blends. Fuel 2009; 88: 1618-24.

[111] Rahimi H, Ghobadian B, Yusaf T, Najafi G and Khatamifar M. Diesterol: An environment-friendly IC engine fuel. Renewable Energy 2009; 34: 335-42.

[112] Subramanian R, Rajendiran G, Venkatachalam R, Nedunchezhian N and Mayilsamy K. Experimental investigation on performance, emission and combustion analysis of multicylinder diesel engine using diesel-ethanol-vegetable oil as fuel. SAE Technical Paper 2011-26-0009, 2011, doi:10.4271/2011-26-0009.

[113] Yilmaz N. Comparative analysis of biodiesel-ethanol-diesel and biodiesel-methanol-diesel blends in a diesel engine. Energy 2012; 40: 210-13.

[114] Sukjit E, Herreros JM, Dearn KD, García-Contreras R and Tsolakis A. The effect of the addition of individual methyl esters on the combustion and emissions of ethanol and butanol-diesel blends. Energy 2012; 42: 364-74.

[115]Di Y, Cheung CS, Huang Z. Comparison of the effect of biodiesel-diesel and ethanol-diesel on the gaseous emission of a direct-injection diesel engine. Atmospheric Environment 2009; 43(17): 2721-30.

[116]Tse H, Leung CW and Cheung CS. Investigation on the combustion characteristics and particulate emissions from a diesel engine fueled with diesel biodiesel-ethanol blends. Energy 2015; 83: 343-50.

[117]Oliveira A, Morais AM, Valente OS and Sodre JR. Combustion characteristics, performance and emissions from a diesel power generator fuelled by B7-ethanol blends. Fuel Processing Technology 2015; 139: 67-72.

[118] Madhuca Indica. The new source of biodiesel. [http://www.jatrophabiodiesel. Org/Madhuca%20Indica/index.php] [accessed on dt. 3.7.2014]

[119] Introduction to Fourier transform infrared spectroscopy.Thermo nicolet corporation, 2001. [http://mmrc.caltech.edu/FTIR/FTIRintro.pdf] [accessed on dt. 1.7.2014]

[120] Hites RA. Gas Chromatography Mass Spectrometry, a Handbook of Instrumental Techniques for Analytical Chemistry.

[121] Lee S, Speight GJ and Loyalka SK. Handbook of alternative fuel technology. 2nd ed. Page 481.

[122] Ganesan V. Internal combustion engine, The McGraw-Hill companies, 3rd ed. 2008.

[123] Shanmuga P, Sivakumar V, Sridhar G and Venkatesh S. Performance and exhaust emissions of a diesel engine using hybrid fuel with an ANN. Modern Applied Science 2009; 3: 32-7.

[124] Exhaust gas analysis. ftp://ftp.energia.bme.hu/pub/Measurements_in_Thermal_ Engineering_BMEGEENMWM1/GasAnalysis.pdf [accessed on dt. 9.08. 2014]

[125] Cambustion. http://www.cambustion.com/products/hfr500/fast-fid-principles [accessed on dt. 9.08. 2014]

[126] Electrochemical sensor. http://www.intlsensor.com/pdf/electrochemical.pdf [accessed on dt. 9.08. 2014]

[127] Holman JP. Experimental techniques. Tata McGraw Hill publications, 2003.

[128] Heywood JB. Internal combustion engine fundamentals. Tata McGraw Hill publications, 1998.

[129] Swami Nathan S, Mallikarjuna JM and Ramesh A. An experimental study of the biogas diesel HCCI mode of engine operation. Energy Conversion and Management, 2010; 51: 1347 - 53.

[130]Mendera KZ, Spyra A, Smereka M. Mass fraction burned analysis. Journal of KONES Internal Combustion Engines 2002, No. 3-4 ISSN 1231-4005.

[131] Arai M, Tabata M, Hiroyasu H, Shimizu M. Disintegration process and spray characterization of fuel jet injected by a Diesel nozzle. SAE Technical Paper no. 840275, 1984.

[132] Dent JC, Derham JA. Air motion in a four-stroke direct injection Diesel engine. Proceedings of Institue of Mechanical Engineering 1974; 188: 269-80.

[133] Rakopoulos CD, Rakopoulos DC, Kyritsis DC. Development and validation of a comprehensive two-zone model for combustion and emissions formation in a DI Diesel engine. Energy Resources 2003; 27: 1221-49.

[134] Rakopoulos CD, Rakopoulos DC, Giakoumis EG and Kyritsis DC. Validation and sensitivity analysis of a two-zone Diesel engine model for combustion and emissions prediction. Energy Conversion Management 2004; 45: 1471-95.

[135] Reitz RD and Bracco FV. On the dependence of spray angle and other spray parameters on nozzle design and operating conditions. SAE Technical Paper no. 790494, 1979.

[136] Hiroyasu H, Arai M and Tabata M. Empirical equations for the Sauter mean diameter of a Diesel spray. SAE Technical Paper no. 890464, 1989.

[137] Whitehouse ND and Way RJB. A simple method for the calculation of heat release rates in Diesel engines based on the fuel injection rate. SAE Technical Paper no. 710134, 1971.

[138] Ramadhas AS, Jayaraj S and Muraleedharan C. Theoretical modeling and experimental studies on biodiesel-fueled engine- Technical note. Renewable Energy 2006; 31: 1813-1826.

[139] Annand WJD. Heat transfer in the cylinders of reciprocating internal combustion engines. Proceedings of Institue of Mechanical Engineering 1963; 177: 973-90.

[140] Gogoi TK and Baruah DC. A cycle simulation model for predicting the performance of a diesel engine fuelled by diesel and biodiesel blends. Energy 2010; 35: 1317-1323.

[141] Way RJB. Methods for determination of composition and thermodynamic properties of combustion products for internal combustion engine calculations. Proceedings of Institue of Mechanical Engineering 1977; 190(60/76): 687-97.

[142] Lavoie GA, Heywood JB and Keck JC. Experimental and theoretical study of nitric oxide formation in internal combustion engines. Combustion Science and Technology 1970; 1: 313-26.

[143] Hiroyasu H, Kadota T and Arai M. Development and use of a spray combustion modeling to predict Diesel engine efficiency and pollutant emissions. Bull Japan Society of Mechanical Engineers 1983; 26 (214): 569.

[144] Rakopoulos DC, Rakopoulos CD, Giakoumis EG, Papagiannakis RG and Kyritsis DC. Experimental-stochastic investigation of the combustion cyclic variability in HSDI diesel engine using ethanol–diesel fuel blends. Fuel 2008; 87: 1478-91.

[145] Ajav EA, Singh B and Bhattacharya TK. Thermal balance of a single cylinder diesel engine operating on alternative fuels. Energy Conversion & Management 2000; 41: 1533-41.

[146] Chen H, Wang J, Shuai S and Chen W. Study of oxygenate biomass fuel blends on a diesel engine. Fuel 2008; 87: 3462-8.

[147] Corkwell KC, Jackson MM, and Daly DT. Review of exhaust emissions of compression ignition engines operation on E-diesel fuel blends. SAE paper no. 01-3283, 2003.

[148] Agarwal AK. Biofuels (alcohols and biodiesel) applications as fuels in internal combustion engines. Progress in Energy Combustion Science 2007; 32: 233-71

[149] Chacartegui CM and GLopez GE. Blending ethanol in diesel engine. Final report for Lot 3b of the Bioscopes project, EC project TREN/D2/44-LOT 3/S07.54848, May 2007.

[150] Cinar C, Can O, Sahin F and Yucesu HS. Effects of premixed diethyl ether (DEE) on combustion and exhaust emissions in a HCCI-DI diesel engine. Applied Thermal Engineering 2010; 30: 360-65.

[151] Nagarajan G, Rao AN and Renganarayanan S. Emission and performance characteristics of neat ethanol fueled DI diesel engine. International Journal of Ambient Energy 2002; 23(3): 149-58.

[152] Abu-Qudais M, Haddad O and Qudaisat M. The effect of alcohol fumigation on diesel engine performance and emissions. Energy Conversion and Management 2000; 41(4): 389-99.

[153] Ekholm K, Karlsson M, Tunestål P and Johansson R. et al. Ethanol-diesel fumigation in a multi-cylinder engine. SAE International Journals of Fuels and Lubricants 2009; 1(1): 26-36: DOI:10.4271/2008-01-0033.

[154] Sukjit E, Herreros JM, Dearn KD, Contreras RG and Tsolakis A. The effect of addition of individual methyl esters on the combustion and emissions of ethanol and butanol diesel blends, Energy, Vol.42, 2012.

[155] Singh SK, Agarwal AK and Sharma M. Experimental investigations of heavy metal addition in lubricating oil and soot deposition in an EGR operated engine. Applied Thermal Engineering 2006; 26: 259-266.

BIODATA

Mrs. Dulari Hansdah, graduated in Mechanical Engineering from Indira Gandhi Institute of Technology, Dhenkanal in the year 2008. She did her postgraduate study in Mechanical Engineering with specialization in Thermal Engineering at National Institute of Technology Rourkela. Immediately after completion of M.Tech in 2011, she did her Ph.D. at National Institute of Technology Rourkela in the Department of Mechanical Engineering.

List of Publications:

(a) International Journals

[1] **DulariHansdah**, S. Murugan and L.M. Das. Experimental Studies on a DI Diesel Engine Fueled with Bioethanol-Diesel Emulsions. Alexandria Engineering Journal, 2013 (52), pp. 267-276.

[2] **Dulari Hansdah** and S. Murugan. Bioethanol Fumigation in a DI Diesel Engine. Fuel, 2014 (130), pp. 324-333.

[3] **Dulari Hansdah** and S. Murugan. Comparative Studies of a Bioethanol Fueled DI Diesel Engine with Cetane Improver. International Journal of Oil, Gas and Coal Technology, Inderscience Publications (Accepted)

(b) List of International Conferences

[1] **Dulari Hansdah**, B.Suna and S.Mururgan. Experimental Analysis of Diesel Engine Fuelled with E-diesel Produced from Madhuca Indica Flowers with the Addition of an Ignition Improver, SAE World Congress, Paper No-2013-01-1700, 2013.

[2] **Dulari Hansdah** and S. Murugan. Performance and Emission Characteristics of a DI Diesel Engine Fuelled with Bioethanol Produced from Madhuca Indica Flower, MNIT, Jaipur, ICAFICE 2013, 6-8 February 2013.

[3] **Dulari Hansdah** and S. Murugan. Studies on Characterization and Utilization of Bioethanol in a DI Diesel Engine, Nirma university, Ahmedabad, NUiCONE 2013, 28-30 November, 2013.

[4] N. Kumar, A. Behera, **Dulari Hansdah** and S.Murugan. Combustion Behaviour of Bioethanol Fumigated DI Diesel Engine, CV Raman College of Engineering, BBSR, ICETRE 2013, 27-28 December, 2013.

[5] N. Kumar, A. Behera, **Dulari Hansdah** and S.Murugan. Effect of Diethyl Ether (DEE) Fumigation on Engine Performance and Emissions in a Bioethanol Fueled Diesel Engine, SAE World Congress, paper no-2014-01-1466, 2014.